SORBONNE UNIVERSITÉ

Thèse de doctorat de Sorbonne Université

École doctorale « Sciences mathématiques de Paris Centre »
Laboratoire Jacques-Louis Lions

Development of efficient multiscale methods and extrapolation techniques for multiphysics molecular chemistry

Développement de méthodes multiéchelles efficaces et de techniques d'extrapolation pour des modèles multiphysiques en chimie moléculaire

Présentée par

Étienne Polack

Pour obtenir le grade de
Docteur de Sorbonne Université

Spécialité
Mathématiques appliquées

Soutenue publiquement le 11 janvier 2022 devant le jury composé de

M. Éric Cancès	*Professeur*	Président du jury
Mme Virginie Ehrlacher	*Chargée de recherche*	Rapporteure
Mme Laura Grigori	*Directrice de recherche*	Examinatrice
M. Filippo Lipparini	*Maître de conférences*	Examinateur
M. Yvon Maday	*Professeur*	Directeur de thèse
M. Andreas Savin	*Directeur de recherche*	Examinateur
M. Reinhold Schneider	*Professeur*	Rapporteur
Mme Katharina Schratz	*Professeure*	Examinatrice

Development of efficient multiscale methods and extrapolation techniques for multiphysics molecular chemistry

Étienne Polack

Front matter

Abstract / Résumé

Abstract

Development of efficient multiscale methods and extrapolation techniques for multiphysics molecular chemistry

In this work, we are interested in developing new methods for molecular chemistry, in particular for classical or quantum molecular dynamics. These methods are developed either in order to increase the efficiency of the computations or in order to improve the description of the chemical systems considered. We are interested in describing in a pedagogical way methods of algorithmic complexity in $\mathcal{O}(N \log N)$ using Ewald's method of summation for the calculation of the energy of classical chemical systems. We also present a modification of the fast multipole method (of algorithmic complexity in $\mathcal{O}(N)$), allowing its use with polarizable force fields describing the density up to quadrupoles. We will also introduce the multiscale method QM/AMOEBA, which allows to describe efficiently and precisely chemical systems containing tens of thousands of atoms. Finally, we will look at how to improve the description and the efficiency of quantum computations by developing extrapolation methods.

Keywords: quantum mechanics, molecular mechanics, continuum solvation, molecular dynamics, force field, high-performance computing

Résumé

Développement de méthodes multiéchelles efficaces et de techniques d'extrapolation pour des modèles multiphysiques en chimie moléculaire

Dans ce travail, nous nous intéressons à développer de nouvelles méthodes pour la chimie moléculaire, en particulier pour la dynamique moléculaire classique ou quantique. Ces méthodes sont développées soit dans le but d'augmenter l'efficacité des calculs ou dans le but d'améliorer la description des systèmes chimiques considérés. Nous nous intéresserons à décrire de façon pédagogique des méthodes de complexité algorithmique en $\mathcal{O}(N \log N)$ utilisant la sommation d'Ewald pour le calcul de l'énergie d'un système moléculaire chimique classique. Dans ce même contexte, nous présenterons une modification de la méthode multipolaire rapide (de complexité algorithmique en $\mathcal{O}(N)$), permettant son utilisation avec des champs de force polarisables décrivant la densité jusqu'au quadrupôles. Nous nous introduirons aussi la méthode multiéchelle QM/AMOEBA, qui permet de décrire de manière efficace et précise des systèmes chimiques contenant plusieurs dizaines de milliers d'atomes. Enfin, nous regarderons comment améliorer la description et l'efficacité de calculs quantiques en développant des méthodes d'extrapolation.

Mots-clés : mécanique quantique, mécanique classique, solvatation implicite, dynamique moléculaire, champs de force, calcul haute performance

Contents

List of Figures

List of Tables

Chapter I

General introduction

I.A Context

Chemistry is the science of matter and of its elements. It covers a range of fields that can go from physics with its laws that govern the world as we experience it to biology, that studies living organisms. Chemistry is everywhere in everyday life: synthesis of plastics from petroleum, of drugs such as the acetylsalicylic acid — the aspirin, or the removal of contaminants from wastewater in sewage treatment plants, to name a few. By learning how the building blocs of matter interact with one another, we are able to understand subtle mechanism in life science, and possibly act on these by, *e.g.*, synthesise an ever growing catalog of compounds.

However, synthesising and evaluating physical properties of new compounds can be costly. Thousands of molecules may have to be created to be able to find the one that works as expected. Hence the common thread linking the difficulties we want to tackle in this work: given the myriad of possibilities of compounds that we can synthesise for a given target, how can we improve some existing method to help and select a small subset that seems the most promising for evaluation?

For instance, in Chapters II to IV we will be mostly interested in having a better understanding of existing methods (respectively about particle–mesh method, quantum mechanics/molecular mechanics descriptions and the fast multipole method) and how to develop or improve them to tackle complex molecular simulations. In Chapters V and VI we will look at ways to develop new tools that could be used to replace current approaches: In the first by trying to learn from the behaviour of families of operators, while in the second by using the geometry behind density matrices to predict its values.

I.A.I Mathematical chemistry

Mathematics is ubiquitous in chemistry: from differential equations that govern chemical kinetics to combinatorics that is used for modelling crystals. Chemists have embraced mathematical tools to model evolution of chemical systems. However, the field of chemistry has long been a mostly uncharted territory for applied mathematicians.

As long as the available computing power was *small*, mathematicians with their bottom-up approach were more inclined to look at theoretical physics. They developed tools to facilitate the expressions of physical laws, showing that equations were indeed well-posed and sometimes finding analytical solutions. This is a way to make theories more robust, and when gaps are found, to make them more consistent.

On the other hand, chemists, with their top-down approach, seemed to make egregious simplifications: sometimes using ill-posed problems or oversimplified equations. And rightly so: the alternative would have been not having usable results. Moreover, their knowledge of expected physical results also allowed them to develop predictive tools out of *a priori* non-rigorous approaches. It was useful for developing intuition when used critically, but the class of problems they looked at seemed too constrained and too much tinkering was involved.

However, since the 2000s and the democratisation of supercomputers, chemists have been able to complexify simulations and use the same mix of intuition and computation to bigger and bigger applications. And the results are impressive: in quantum mechanics using only a few Gaussian basis functions that may exhibit linear dependency issues, they can predict quickly and with remarkable accuracy physical properties of molecular systems; in molecular mechanics they can simulate viruses of millions of atoms to be able to fine-tune molecular inhibitors, etc [Kar14; Lev14; War14; El +21].

These results are too impressive to be ignored. However, there is room from improvement: in the choice of algorithms used to solve some problems, in the efficient use of clusters of computers, in removing tinkering for the choice of basis functions for quantum mechanics or the manual

approach to fix some parameters in molecular mechanics, in providing error bounds on results, etc.

I.A.2 Modelling matter accurately at a small scale

We make sense of the way natural phenomena occurs through scientific laws. At a molecular level, the interactions are best explained through quantum mechanics (see Section I.D); in particular by the SCHRÖDINGER equation, or its approximation with HARTREE–FOCK, post-HARTREE–FOCK or density functional theory methods [HJO00]. At this scale, it is possible to describe electrons, which enables the method to give predictive results on par with physical experimentation. Albeit extremely precise and self-contained — without the need of empirical quantities, it becomes computationally prohibitive to use as the size of the system increases.

Another theory, less precise and less computationally intensive is through NEWTON's law of motion with molecular mechanics (see Section I.E). At this scale, electrons cannot be described explicitly and are replaced by a notion of chemical bonds.

At a still larger scale, we can average physical properties in space, and look at the physical laws through a continuum, with the use of continuum mechanics methods (see Section I.F).

Choosing among these scales, or possibly a combination of them, and different methods to describe molecular interactions depends on the objectives or quantities of interest, and can even be a matter of personal choice. It depends on a delicate balance between needed accuracy and computational cost. We are interested with the present work in broadening that choice for molecular dynamics simulations.

To understand the different issues we want to tackle, it is useful to have in mind a problem that can make use of the method we developed; it is why we describe in details in the next section the case of drug design. In particular, methods in Chapters II to IV and VI are applicable to the example we develop in the next section, although they are actually more general.

I.B Drug design as a practical application of molecular simulations

When considering new lubricant oils for mechanics, we may be interested to the viscosity indices for a range of temperatures. When considering soaps and shampoos, we may look at tuning wetting additives to increase the penetration speed of active ingredients [Lee+20]. When doing drug design, we may want to compare the ligand efficiencies of molecules against a target, a virus' enzyme for instance, to find drugs able to inhibit processes in the virus that renders it infectious.

What all the previous cases have in common is the need to extract and predict physical properties from molecular systems, which we may want to do with computer simulations. As we have said previously, in the current section, we will show tropism towards drug design and will be mostly describing works needed for the latter example. We assume that biologists or chemists are able to provide a list of compounds to be tested. That in itself is by no means easy and is the field of chemical engineering. They have to use their knowledge of chemical processes to propose a catalog of possible compounds that should react with the intended target.

Before the advances of computing power, they would have needed to synthesise these compounds, and have laboratory experiments to extract the desired physical properties *in vitro*. Only then could they be able to discard the ones that show the least potential. The cost in time and material of this way can be overwhelming; forcing scientists to discard molecules that they think might work, but seem less inclined to or ones that are the more complicated and costly to synthesis.

This has begun to change: With easy access to astounding computing power, we can hope to automatise the discovery of list of compounds worthy of synthesis for further testing with what is sometimes called *in silico* methods. However, we are nowhere near being able to replace the complete procedure for drug design: that would require being able to model *in vivo* reactions, the ones inside a living organism such as the human. But this goal does not seem nowadays as far fetched as it used to.

I.B.1 Molecular docking

At a supramolecular scale, chemical systems may bond with each other to form complex assembled structures. For example, the human immunodeficiency virus 1 is able to infect cells of the human immune system. On the most external shell of the human immunodeficiency virus 1, are proteins that can attach to human cells, the first step in the process of infecting them [BRD13].

If the human immunodeficiency virus 1 has attached a human cell, we say that it has docked it: there is a stable bond between a *receptor* on the surface of the human cell and a *ligand* on the surface of the virus. A pharmacologist when doing drug design may want to use the same process against the virus by finding adequate ligands against virus receptors (that may have had the role of ligands when considering the docking to human cells) on the virus surface to prevent the infection to process.

On a macroscopic level, all of this is a question of geometry: how well a ligand is able to *fit* a receptor to activate. The same way a door can be unlocked with the correct key (an analogy first made by Fischer [Fis94]). This means having the geometry of both the ligand and the receptor. At this scale, the problem of drug design can be seen as how to increase the *contact* between two molecules.

We note that this implies deep understanding of the infection process, as well as to be able to know which are the *active sites* involved in this process and the geometry in which the compounds will present themselves to each other.

Let us recapitulate some major steps of drug design for a target:

(i) Identify the processes and its active sites in which the target is involved;

(ii) Choose adequate ligands that may bind with receptors on the target;

(iii) Evaluate the ligands' affinities to pick the ones that show the most promises.

I.B.2 Know your enemy

When considering *in silico* research, Item (i) may be the most difficult step of all. As can be seen in the years that took the quest to understand how the human immunodeficiency virus 1 worked: By first isolating the virus, then showing that it was responsible of the acquired immune deficiency syndrome and finally how it can infect human cells. Even if in this particular case, the research took place in the 1980s, it is still a difficult enterprise nowadays, as is seen in the current worldwide effort to understand the coronavirus disease 2019 for example.

This is a difficult [Sny+05; Yee+05] and mandatory step, because having the sequence of atoms in a molecule is often not enough. The number of different geometries becomes a combinatorial hell as the number of atoms increases. And ferreting through all the possible combinations with a computer to extract the most probable combinations seems too remote for the moment; even for relatively small compounds of a few thousands atoms, and much less so for viruses with millions of them. We note however that some methods using machine learning seem promising, as can be seen in the results of the *AlphaFold* method by Senior et al. [Sen+20], where the authors are able to predict with remarkable accuracy the three-dimensional conformations of large proteins.

So for this part, a lot of laboratory experiments and input from experienced biologists and chemists is necessary. And no matter how much computing power is thrown at the problem, we are still a long way to being able brute-force our way out of this issue. We need to have access to as few geometries for the target, or at least to some of its active site, as possible as a starting point.

Once the geometry of the target is available and active sites to which we want to bind have been identified, we have to tackle Item (II). As it was the case for the previous item, it is still mostly done by hand. Scientists have to mobilise their knowledge of existing ligands and similar situations to tune some aspects of the ligands to apply to the current situation. Computational tools may help to augment the space of configurations to be tried [Boe11].

Items (I) and (II) require deep knowledge of chemistry and is hardly accessible to outsiders. Thankfully for the author, that it not the case for Item (III):

If we think of chemical interactions as rigid bodies, getting back to the key-lock analogy by Fischer [Fis94], this means we have to [Rog11]: (I) Search for the possible conformations of the ligands with respect to the receptor (*i.e.*, have different keys to test); (II) Evaluate how probable the ligand is to find itself close to the receptor (*i.e.*, how probable is it for the key to unlock the door) [Ain+15]. This is is the role of scoring functions, which are often classified in three classical categories (empirical, knowledge-based and theoretical), with a fourth containing machine-learning based approach.

In this work, we will be interested in theoretical — or physically-based — methods, which can tackle those two steps at the same time when doing molecular dynamics.

I.C Multiscale problems

To improve accuracy of *in silico* methods, we can look at developing new methods (Chapter V). Or we can look at issues related to modelling scale or computational scales (Chapters II to IV and VI).

I.C.I Modelling scale

The first question we have to answer is at which scale to model matter. As we have previously said, quantum mechanics is the only method able to accurately account for electrons. Hence for high accuracy at active sites, we would like to use quantum mechanics methods. However, even for methods that treat nuclei classically and which have some parameterisation to speedup computations — such as density functional theory, we cannot hope to model systems having more than a few thousands atoms [Bur12]. This is not enough for most systems of interest, not to mention molecular systems such as viruses with millions of atoms.

At the other end of the scale, we know that solvent has an effect on molecular interactions, and should be modelled to have accurate simulations [TP94; Amo+98]. But if we have to also model enough solvent around the system of interest, we also face the problem of having to model very large systems, so we may want to use a coarser description of the physics using continuum mechanics. This is a difficult conundrum to solve; hence the idea to develop multiphysics methods, where different physical laws can be used together to model complex systems.

In the case of drug design, it is possible to use quantum mechanics to model atoms near the active sites, where the *magic* happens, then use molecular mechanics to model atoms at some distance, where we do not need to account with high accuracy the effects of electrons. Molecular mechanics can be used to model other atoms *linked* in some way to the quantum mechanics system, or solvent molecules — such as water or acetone.

We developed methods in Chapters III and IV with such multiphysics in mind.

I.C.2 Computational scale

Once we have chosen the physics we want to use, we can improve accuracy by increasing the size of the molecular system, for example taking into account more solvent molecules. Or we may want to simulate the evolution of the system for a longer period of time. This can be done by taking advantage of the possibility to use cluster of computers, for which we need to have methods that scale with the added computational power. That may force to change parts of a method, or to develop a new method altogether. This is what we look at in Chapters II to IV. In Chapter VI, we look at how to speedup computations to allow for longer simulations.

I.D Quantum mechanics and Hartree–Fock theory

To be able to perform molecular dynamics simulations, we need access to an energy functional $\mathcal{E}$ that depends on the configuration of the molecular system, is regular with respect to the positions of the atoms and which may require to solve a complex problem. Hence, in the remaining of this part, we introduce general notions — in particular the energy functionals we use, which will be useful for the reader in the forthcoming chapters. Namely, we introduce quantum mechanics in this section, molecular mechanics and force fields in Section I.E and continuum mechanics in Section I.F. In this section, we will abundantly use results from Helgaker, Jørgensen, and Olsen [HJO00] and Cancès, Bris, and Maday [CBM06], and we do not consider particles' spins.

The quantum mechanics energy comes from the deceptively innocent looking Schrödinger's equation that is in the time-independent version

$$\mathcal{H}\psi = \mathcal{E}\psi, \tag{IV.1}$$

where the operator $\mathcal{H}$ is the Hamiltonian of the system, ψ is an eigenfunction called the wave function and $\mathcal{E}$ is a real, the energy associated to ψ. We will give the explicit expression for this Hamiltonian, but we start first with some generalities about the Schrödinger equation.

I.D.1 Time-independent Schrödinger equation

We consider a molecular system composed of M nuclei of charge Z_i at positions R_i, for $i \in [\![1 \,..\, M]\!]$ and N electrons of charge -1 in atomic units. Under the Born–Oppenheimer approximation [MH09], the nuclei are treated as classical particles that obey Newton's law of motion. The electrons are described by a wave function $\psi \in \mathsf{L}^2(\mathbf{R}^{3N}, \mathbf{C})$. This approximation can be done because the nuclei have a much bigger mass — by three orders of magnitude, than the electrons and are thus more localised in space.

Moreover, an axiom of quantum mechanics states that electrons must be indiscernible from each other and are fermionic particles. This means that for any permutation $\sigma \in \mathfrak{S}_N$ of $[\![1 \,..\, N]\!]$,

$$\psi(x_1, \dots, x_N) = \varepsilon(\sigma)\psi(x_{\sigma(1)}, \dots, x_{\sigma(N)}), \tag{IV.2}$$

where $\varepsilon(\sigma)$ is the signature of σ. This means that ψ is an antisymmetric function, and that in particular $\psi(x_1, \dots, x, \dots, x, \dots, x_N) = 0$, with which we recover Pauli's exclusion principle that two electrons cannot be at the same position. We denote the space of antisymmetric functions to which ψ belongs

$$\mathsf{L}^2_a(\mathbf{R}^{3N}, \mathbf{C}) := \bigwedge_1^N \mathsf{L}^2(\mathbf{R}^3, \mathbf{C}), \tag{IV.3}$$

where $\bigwedge$ is the antisymmetric tensor product.

It is of particular interest to find what is called a ground state of the system. That is to find a minimiser of the problem

$$\inf\{\langle\psi, \mathcal{H}\psi\rangle \mid \psi \in \mathsf{L}^2_a(\mathbf{R}^{3N}, \mathbf{C}),\ |\psi| = 1\}, \tag{IV.4}$$

where the Hamiltonian is

$$\mathcal{H} = -\sum_{i=1}^{N} \frac{1}{2}\Delta_{x_i} + \sum_{i=1}^{N} V(x_i) + \sum_{1\le i<j\le N} \frac{1}{|x_i - x_j|}, \tag{IV.5}$$

with

$$V(x) := -\sum_{k=1}^{M} \frac{Z_k}{|x - R_k|} \tag{IV.6}$$

the potential created by the nuclei to the electrons.

I.D.2 HARTREE–FOCK method

To simplify the overwhelming cost of the SCHRÖDINGER's equation, several methods have been proposed. One of particular interest, and on which we will rely a lot, is the HARTREE–FOCK method. We note that we will only consider the restricted setting, where all orbitals are doubly occupied by electrons.

In the HARTREE–FOCK method, we consider wave functions that can be written as a single SLATER determinant of monoelectronic orthonormal functions, called *orbitals*. For N orbitals $\phi_i \in \mathsf{L}^2(\mathbf{R}^3, \mathbf{C})$, we look for a normalised ψ that solves Eq. (IV.4) under the form

$$\psi = \frac{1}{\sqrt{N!}} \det\left(\phi_i(x_j)\right)_{i,j}. \tag{IV.7}$$

Physically, with the HARTREE–FOCK method we make the assumption that electrons act independently from each other, so that there is no correct correlation between them.

The first term represents the kinetics energy, the second the attractive interaction energy between the nuclei and the electrons, the third the repulsive Coulombic energy between electrons.

We should also remark that we have omitted the kinetics energy of nuclei and the repulsive Coulombic energy between them. As the nuclei are treated classically, the computation of those terms does not pose any difficulty. However they should be included to have the correct total energy.

We now define the space

$$\mathcal{W}_N := \left\{\Phi := (\phi_1, \dots, \phi_N) \in \mathsf{L}^2(\mathbf{R}^3, \mathbf{C})^N \,\middle|\, \langle\phi_i, \phi_j\rangle = \delta_{ij}, 1 \le i, j \le N\right\}, \tag{IV.8}$$

which can be rewritten if we introduce the Gram matrix

$$\operatorname{Gram}\Phi := \left(\langle\phi_i, \phi_j\rangle\right)_{ij} \tag{IV.9}$$

as

$$\mathcal{W}_N = \{\Phi \in \mathsf{L}^2(\mathbf{R}^3, \mathbf{C})^N \mid \operatorname{Gram}\Phi = \mathrm{Id}_N\}. \tag{IV.10}$$

If we define the space of SLATER determinants as

$$\begin{aligned} \mathcal{S}_N &= \left\{\psi \in \mathsf{L}^2_a(\mathbf{R}^{3N}, \mathbf{C}) \,\middle|\, \psi = \frac{1}{\sqrt{N!}} \det\left(\phi_i(x_j)\right)_{i,j}\right\} \\ &= \left\{\psi \in \mathsf{L}^2_a(\mathbf{R}^{3N}, \mathbf{C}) \,\middle|\, \exists\Phi \in \mathcal{W}_N,\ \psi = \frac{1}{\sqrt{N!}} \det\left(\phi_i(x_j)\right)_{i,j}\right\}, \end{aligned} \tag{IV.11}$$

then the Hartree–Fock method corresponds to looking for solution of Eq. (IV.4) in this space

$$\inf\{\langle\psi, \mathcal{H}\psi\rangle \mid \psi \in \mathcal{S}_N\}. \tag{IV.12}$$

Moreover, when ψ is a Slater determinant, there holds

$$\langle\psi, \mathcal{H}\psi\rangle = \mathcal{E}^{\mathrm{HF}}(\Phi), \tag{IV.13}$$

where

$$\mathcal{E}^{\mathrm{HF}}(\Phi) = \sum_{i=1}^{N} \frac{1}{2}\int_{\mathbf{R}^3} |\nabla\phi_i|^2 + \int_{\mathbf{R}^3}\left(\sum_{i=1}^{N}|\phi_i|^2\right)V + \frac{1}{2}\int_{\mathbf{R}^3}\int_{\mathbf{R}^3} \frac{\left(\sum_{i=1}^{N}|\phi_i(x)|^2\right)\left(\sum_{i=1}^{N}|\phi_i(x')|^2\right)}{|x-x'|}\,\mathrm{d}x\,\mathrm{d}x' - \frac{1}{2}\int_{\mathbf{R}^3}\int_{\mathbf{R}^3} \frac{\left|\sum_{i=1}^{N}\phi_i(x)\phi_i(x')\right|^2}{|x-x'|}\,\mathrm{d}x\,\mathrm{d}x'. \tag{IV.14}$$

If we define respectively the density matrix and the electronic density as

$$\gamma_\Phi(x,x') := \sum_{i=1}^{N}\phi_i(x)\phi_i(x'), \quad \text{and} \quad \rho_\Phi(x) := \gamma_\Phi(x,x) = \sum_{i=1}^{N}|\phi_i(x)|^2, \tag{IV.15}$$

then we can rewrite $\mathcal{E}^{\mathrm{HF}}(\Phi)$ as

$$\mathcal{E}^{\mathrm{HF}}(\Phi) = \sum_{i=1}^{N} \frac{1}{2}\int_{\mathbf{R}^3} |\nabla\phi_i|^2 + \int_{\mathbf{R}^3}\rho_\Phi V + \frac{1}{2}\int_{\mathbf{R}^3}\int_{\mathbf{R}^3} \frac{\rho_\Phi(x)\rho_\Phi(x')}{|x-x'|}\,\mathrm{d}x\,\mathrm{d}x' - \frac{1}{2}\int_{\mathbf{R}^3}\int_{\mathbf{R}^3} \frac{|\gamma_\Phi(x,x')|^2}{|x-x'|}\,\mathrm{d}x\,\mathrm{d}x'. \tag{IV.16}$$

The first term represents the kinetics energy, the second the attractive interaction energy between the nuclei and the electrons, the third the repulsive Coulombic energy between electrons and the fourth term is called the *exchange* term, and is a correction due to the antisymmetry of the wave function.

We have also that $\gamma_\Phi \in \mathsf{L}^2(\mathbf{R}^3\times\mathbf{R}^3, \mathbf{C})$ is the kernel of a density operator $\mathcal{D}_\Phi$, that is

$$\forall\psi \in \mathsf{L}^2(\mathbf{R}^3), \quad (\mathcal{D}_\Phi\psi)(x) = \int_{\mathbf{R}^3}\gamma_\Phi(x,x')\psi(x')\,\mathrm{d}x' = \sum_{i=1}^{N}\langle\phi_i,\psi_i\rangle\phi_i. \tag{IV.17}$$

Thus, the density operator is the orthogonal projector on $\mathrm{Span}(\phi_1,\dots,\phi_N)$ in $\mathsf{L}^2(\mathbf{R}^3,\mathbf{C})$. It is often written

$$\mathcal{D}_\Phi = \sum_{i=1}^{N}|\phi_i\rangle\langle\phi_i|. \tag{IV.18}$$

Moreover, the Hartree–Fock energy has the property to be invariant by rotations. Indeed, for any $U \in \mathrm{U}_N$,

$$\mathcal{E}^{\mathrm{HF}}(U\Phi) = \mathcal{E}^{\mathrm{HF}}(\Phi), \quad \gamma_{U\Phi}(x,y) = \gamma_\Phi(x,y), \quad \text{and} \quad \mathrm{Gram}\,U\Phi = \mathrm{Id}_N\,. \tag{IV.19}$$

This is consistent with the indiscernibility properties of electrons. Hence, what matters is not the orbitals ϕ_i as much as the linear spaces generated from them.

By completing the N orthogonal functions ϕ_i to be a basis of $\mathsf{L}^2(\mathbf{R}^3, \mathbf{C})$, we can also write the kinetics part of the energy from the density matrix with

$$\sum_{i=1}^{N} \frac{1}{2} \int_{\mathbf{R}^3} |\nabla \phi_i|^2 = \frac{1}{2} \operatorname{Tr}(\Delta \gamma_\Phi), \tag{IV.20}$$

then the energy can be seen as a function of the density operator

$$\mathcal{E}^{\mathrm{HF}}(\Phi) = \mathcal{E}^{\mathrm{HF}}(\mathcal{D}_\Phi). \tag{IV.21}$$

Finally, the problem can be written as

$$\inf\{\mathcal{E}^{\mathrm{HF}}(\mathcal{D}) \mid \mathcal{D} \in \mathcal{P}_N\}, \tag{IV.22}$$

where $\mathcal{P}_N$ is the set of orthogonal projectors of rank N in $\mathsf{L}^2(\mathbf{R}^3, \mathbf{C})$

$$\mathcal{P}_N := \{\mathcal{D} \in \mathcal{L}^1 \mid \operatorname{Span}(\mathcal{D}) \subset \mathsf{L}^2(\mathbf{R}^3, \mathbf{C}),\ \mathcal{D}^2 = \mathcal{D},\ \mathcal{D}^\dagger = \mathcal{D},\ \operatorname{Tr}(\mathcal{D}) = N\}, \tag{IV.23}$$

with $\mathcal{L}^1$ the set of trace operators onto $\mathsf{L}^2(\mathbf{R}^3, \mathbf{C})$ [RS81], and where

$$\mathcal{E}^{\mathrm{HF}}(\mathcal{D}) := \operatorname{Tr}(h\mathcal{D}) + \frac{1}{2} \operatorname{Tr}(\mathcal{G}(\mathcal{D}) \cdot \mathcal{D})\mathcal{D} \in \mathcal{P}_N, \tag{IV.24}$$

$$h := -\frac{1}{2}\Delta + V, \quad \text{and} \quad (\mathcal{G}(\mathcal{D}) \cdot \phi)(x) := \left(\rho_{\mathcal{D}} * \frac{1}{|\cdot|}\right)(x)\phi(x) - \int_{\mathbf{R}^3} \frac{\gamma_{\mathcal{D}}(x, x')}{|x - x'|}\phi(x')\,\mathrm{d}x', \tag{IV.25}$$

where $\gamma_{\mathcal{D}}$ is the kernel of $\mathcal{D}$ and $\rho_{\mathcal{D}}(x) = \gamma_{\mathcal{D}}(x, x)$.

We can define the Fock operator as

$$\mathcal{F}(\mathcal{D}) := h + \mathcal{G}(\mathcal{D}). \tag{IV.26}$$

The first term is the one-electron operator and the second the (non-linear) two-electron operator.

I.D.3 Discretisation with Gaussian-type functions

To solve computationally the Hartree–Fock problem, we can use a Galerkin approximation, where the problem is solved in a finite-dimensional subspace $\mathcal{V}$ of $\mathcal{W}_N$. If the subspace $\mathcal{V}$ is spanned by elements of a complete basis of $\mathcal{W}_N$, then we have a systematic way to construct an increasing family as $k \to +\infty$ of subspaces $\mathcal{V}_k$ such that the error done by discretising the problem goes to zero as $k \to +\infty$. This enables the possibility to solve the problem for any accuracy.

A lot of work has been done by chemists to optimise the basis to have as few functions as possible to diminish the computational cost, while providing accurate enough results. In doing so, most chemistry codes do not use systematic and mathematically complete basis.

A common technique is the linear combination of atomic orbitals, where the orbitals are expanded into a set of simple one-electron functions

$$\phi_i(r) = \sum_{\mu} C_\mu \chi_\mu(r - R_i), \tag{IV.27}$$

which is a linear combination of atomic orbitals that are centred around nuclei positions of the system R_i. The atomic orbitals can be chosen as Gaussian-type functions under the form

$$\chi_\mu(r) := |r|^{2(n-\ell-1)} \exp(-\alpha r^2) Y_{\ell m}(r), \tag{IV.28}$$

where $Y_{\ell m}$ are the spherical harmonics, n is a strictly positive integer called the principal quantum number, $\ell < n$ is the angular–momentum quantum number, and m is such that $|\ell| \geq m$.

This particular family of functions is complete for fixed α, but non-orthogonal. However, the families are often chosen with different α, to speedup the computations, doing this we may lose the completeness property of the basis.

A common choice of basis are the complex spherical-harmonics Gaussian-type orbitals given by

$$\chi^{\mathrm{GTO}}_{\alpha\ell m}(\rho,\theta,\varphi) := R^{\mathrm{GTO}}_{\ell}(\alpha,\rho)Y_{\ell m}(\theta,\varphi), \tag{IV.29}$$

where

$$R^{\mathrm{GTO}}_{\ell}(\alpha,\rho) := \frac{2(2\alpha)^{3/4}}{\pi^{1/4}}\sqrt{\frac{2^{\ell}}{(2\ell+1)!!}}\left(\sqrt{2\alpha}\rho\right)^{\ell}\exp(-\alpha r^2), \tag{IV.30}$$

$r = (\rho,\theta,\varphi)$ in spherical coordinates and $\alpha > 0$ is the orbital exponent. The choice of the Gaussian functions is essentially due to the separation of variables that simplifies greatly the computation of integrals.

To further speedup the computations, contracted Gaussian-type orbitals are often used. They are a fixed linear combinations of Gaussian-type orbitals

$$R^{\mathrm{CGTO}}_{a\ell}(r) := \sum_i d_{ia} R^{\mathrm{GTO}}_{\ell}(\alpha_i, r), \tag{IV.31}$$

where the d_{ia} are the contraction coefficients. The coefficients are optimised to decrease the number of basis functions that have to be used to obtain accurate results.

In this work, we will always assume to use Gaussian-type orbitals.

I.D.4 Discrete Hartree–Fock problem

We now look at the discrete Hartree–Fock problem. We assume that a suitable basis $\{\chi_\mu\}_{\mu=1}^{N_b}$ has been chosen that generates some space $\mathcal{V}$. We thus look at the problem with functions on the restricted space $\mathcal{W}_N(\mathcal{V})$, where

$$\mathcal{W}_N(\mathcal{V}) := \{\Phi \in \mathrm{L}^2(\mathbf{R}^3,\mathbf{C})^N \mid \phi_i \in \mathcal{V},\ \mathrm{Gram}\,\Phi = \mathrm{Id}_N\}. \tag{IV.32}$$

If we introduce the overlap matrix

$$S := \left(\int_{\mathbf{R}^3} \chi_\mu \chi_\nu\right)_{\mu\nu}, \tag{IV.33}$$

the condition that $\mathrm{Gram}\,\Phi = \mathrm{Id}_N$ can be rewritten as $C^{\mathsf{T}}SC = \mathrm{Id}_N$, where C is the matrix of coefficients of the ϕ_i in the basis χ_μ

$$\phi_i(x) = \sum_{\mu=1}^{N_b} C_{\mu i}\chi_\mu(x). \tag{IV.34}$$

If we denote by h the matrix

$$h := \left(\left\langle \chi_\mu, h\chi_\nu \right\rangle\right)_{\mu\nu}, \tag{IV.35}$$

then we have the equality

$$\sum_{i=1}^{N}\frac{1}{2}\int_{\mathbf{R}^3}|\nabla\phi_i|^2 + \int_{\mathbf{R}^3}\rho_\Phi V = \mathrm{Tr}(hCC^{\mathsf{T}}). \tag{IV.36}$$

Moreover, defining

$$(\mu\nu|\kappa\lambda) := \int_{\mathbf{R}^3}\int_{\mathbf{R}^3} \frac{\chi_\mu(x)\chi_\nu(x)\chi_\kappa(x')\chi_\lambda(x')}{|x-x'|}\,\mathrm{d}^3x\,\mathrm{d}^3x', \tag{IV.37}$$

we have $G := J - K$ where J and K are defined for any matrix $D \in \mathbf{R}^{N_b\times N_b}$ with

$$J(D) := \left(\sum_{\kappa,\lambda=1}^{N_b}(\mu\nu|\kappa\lambda)D_{\kappa\lambda}\right)_{\mu\nu} \quad \text{and} \quad K(D) := \left(\sum_{\kappa,\lambda=1}^{N_b}(\mu\lambda|\kappa\nu)D_{\kappa\lambda}\right)_{\mu\nu}, \tag{IV.38}$$

then we have the identities

$$\int_{\mathbf{R}^3}\int_{\mathbf{R}^3} \frac{\rho_\Phi(x)\rho_\Phi(x')}{|x-x'|}\,\mathrm{d}x\,\mathrm{d}x' = \mathrm{Tr}\left(J(CC^\mathsf{T})CC^\mathsf{T}\right), \tag{IV.39}$$

and

$$\int_{\mathbf{R}^3}\int_{\mathbf{R}^3} \frac{|\gamma_\Phi(x,x')|^2}{|x-x'|}\,\mathrm{d}x\,\mathrm{d}x' = \mathrm{Tr}\left(K(CC^\mathsf{T})CC^\mathsf{T}\right). \tag{IV.40}$$

With all this, we can rewrite the discrete HARTREE–FOCK problem as

$$\min\{\mathcal{E}^{\mathrm{HF}}(CC^\mathsf{T}) \mid C \in \mathcal{W}_N(\mathbf{R}^{N_b\times N})\}, \tag{IV.41}$$

where

$$\mathcal{E}^{\mathrm{HF}}(D) := \mathrm{Tr}\left(hD + \frac{1}{2}G(D)D\right), \tag{IV.42}$$

and

$$\mathcal{W}_N(\mathbf{R}^{N_b\times N}) := \{C \in \mathbf{R}^{N_b\times N} \mid C^\mathsf{T}SC = \mathrm{Id}_N\}. \tag{IV.43}$$

We also have the equality of the sets

$$\begin{aligned}\mathcal{W}_N(\mathbf{R}^{N_b\times N}) &:= \{CC^\mathsf{T} \mid C \in \mathbf{R}^{N_b\times N},\ C^\mathsf{T}SC = \mathrm{Id}_N\}\\ &= \{D \in \mathbf{R}^{N_b\times N_b} \mid D^\mathsf{T} = D,\ DSD = D,\ \mathrm{Tr}(SD) = N\} =: \tilde{\mathcal{P}}_N.\end{aligned} \tag{IV.44}$$

So, with a change of variables $D \to S^{1/2}D$, we can also work on the space

$$\mathcal{P}_N := \{D \in \mathbf{R}^{N_b\times N_b} \mid D^\mathsf{T} = D,\ D^2 = D,\ \mathrm{Tr}(D) = N\}, \tag{IV.45}$$

which includes orthogonal projectors onto the space spanned by the N orbitals, which is bijective to some smooth manifold, the GRASSMANN manifold $\mathcal{G}r(N, N_b)$. This will be of importance in Chapter VI and we refer the reader to this chapter for more details.

I.D.5 Solving the problem with the self-consistent field algorithm

We are now interested in solving the discrete HARTREE–FOCK problem

$$\min\left\{\mathcal{E}^{\mathrm{HF}}(D) \,\middle|\, D \in \tilde{\mathcal{P}}_N\right\}. \tag{IV.46}$$

This problem is often solved using a fixed-point type algorithm referred globally as the self-consistent field method. It contains for instance the ROOTHAAN algorithm [Roo51] for closed shell systems with an linear combination of atomic orbitals basis set, its damped version by ZERNER and HEHENBERGER [ZH79] as well as the level-shifting algorithm from SAUNDERS and HILLIER [SH73]. A mathematical study of these algorithms was done by CANCÈS and BRIS [CB00].

We introduce the symmetric matrix Λ of Lagrange multipliers, and the Lagrangian function

$$\mathcal{L}(\Lambda, C) := \mathcal{E}^{\mathrm{HF}}(CC^{\mathsf{T}}) - \langle \Lambda, C^{\mathsf{T}}SC - \mathrm{Id}_N \rangle \tag{IV.47a}$$
$$= \mathcal{E}^{\mathrm{HF}}(CC^{\mathsf{T}}) - \mathrm{Tr}\left(\Lambda^{\mathsf{T}}(C^{\mathsf{T}}SC - \mathrm{Id}_N)\right). \tag{IV.47b}$$

Then, using the properties that $\mathrm{Tr}(G(D)D') = \mathrm{Tr}(G(D')D)$ for any D and D' in $\mathbf{R}^{N_b \times N_b}$ and that Λ is symmetric,

$$\nabla_C \mathcal{L}(\Lambda, C) = 2F(D)C - 2SC\Lambda, \tag{IV.48}$$

where

$$F(D) := h + G(D). \tag{IV.49}$$

Hence, to solve the discrete Hartree–Fock problem, we may look at solving the system

$$\begin{cases} \nabla_C \mathcal{L}(\Lambda, C) = 0 \\ \nabla_\Lambda \mathcal{L}(\Lambda, C) = 0 \end{cases} \Leftrightarrow \begin{cases} F(D)C = SC\Lambda \\ C^{\mathsf{T}}SC = \mathrm{Id}_N \\ D = CC^{\mathsf{T}} \end{cases}. \tag{IV.50}$$

Moreover, if C is a critical point, then for any orthogonal matrix U, CU is also a critical point. We can thus diagonalise Λ and solve

$$\begin{cases} F(D)C = SCE \\ C^{\mathsf{T}}SC = \mathrm{Id}_N \\ D = CC^{\mathsf{T}} \end{cases}, \tag{IV.51}$$

where $E := \mathrm{Diag}(\varepsilon_1, \dots, \varepsilon_N)$.

This system can be solved using a fixed-point algorithm. We first chose an initial guess matrix C_0. Then we solve the system iteratively to find a sequence of points C_n such that $|C_{n-1} - C_n|$ converges to zero and verifies the system

$$\begin{cases} F(D_{n-1})C_n = SC_nE_n \\ C_n^{\mathsf{T}}SC_n = \mathrm{Id}_N \\ D_n = C_nC_n^{\mathsf{T}} \end{cases}, \tag{IV.52}$$

where E_n is diagonal. This is the gist of the self-consistent field method. Modifications to improve the convergence are often related on how the C_n matrices are updated at each iteration.

I.D.6 Density functional theory

Hartree–Fock is the building block of even more accurate methods, that are often referred as post-Hartree–Fock methods. However, those methods have a computational complexity of at least the one for Hartree–Fock in $\mathcal{O}(N^4)$. This is an issue for molecular dynamics simulations, as it greatly limits the size of the systems that can be considered, as well as the simulations lengths. An alternative is to use density functional theory, which has a computational complexity in $\mathcal{O}(N^3)$ or $\mathcal{O}(N^4)$, depending on the approximation, but with greater accuracy. It works by introducing some heuristic quantity in the form of an energy functional.

At our level, we can consider this to be a black box algorithm that replaces Hartree–Fock. However, as this is the method that was used for computations in Chapters III and V, and partially in Chapter VI, we will give a brief description.

The first theoretical justification for density functional theory was proposed by Hohenberg and Kohn [HK64], and later generalised by Lieb [Lie83]. It is often referred as the Hohenberg–Kohn

theorem, and posits the existence of a density functional F with which the Schrödinger's equation can be rewritten as finding a density ρ that minimises

$$\inf_{\rho}\left\{F(\rho)+\int \rho V \;\middle|\; \rho \geq 0,\ \rho^{1/2} \in \mathsf{H}^1(\mathbf{R}^3),\ \int \rho = N\right\}. \tag{IV.53}$$

This is an existence theorem, and the expression of the functional is not know in general. However, chemists have proposed different expressions that work remarkably well in practice. In this work, the functional used will often be supposed to be the one introduced by Kohn and Sham [KS65].

In Chapter v, we look at how to obtain physical properties by looking at families of equations, where the Coulomb operator was damped by some function. In Chapter vi, we are interested in fastening molecular dynamics when using Hartree–Fock or density functional theory by reducing the number of Fock matrices evaluations.

I.E Molecular mechanics and force fields

As with the Born–Oppenheimer's approximation in quantum mechanics, atoms are represented in classical mechanics by point charges. However, we lose laws to describe electrons of the system. Hence, nuclei interact with each other through an empirical potential energy $\mathcal{E}$, which require parameters that are tuned with respect to experiments or quantum mechanics computations. The choice of representation is often called a force field in the molecular mechanics community.

Force fields make abundant use of notions of covalent bonds between atoms to be able to describe strong electronic interactions. Moreover, in most force fields, covalent bonds between atoms cannot be broken and are less flexible than the molecular system as a whole. Hence, potential energies can be split in bounded and unbounded parts, which include respectively covalent (or intramolecular) and non-covalent (or intermolecular) contributions

$$\mathcal{E} := \mathcal{E}_{\text{intra}} + \mathcal{E}_{\text{inter}}. \tag{V.1}$$

In this work, we will be mostly interested in long-range interactions represented through the intermolecular contribution to the energy $\mathcal{E}_{\text{inter}}$. The notion of density in quantum mechanics is represented at first-order by point charges that are often placed at the positions of the nuclei. To take into account the anisotropic properties of molecular systems, point multipoles can also be used instead of only point charges. Those force fields are known as classical force field.

However, in most classical force fields those point charges or multipoles are permanent and do not change with respect to the geometry of the molecular system as a all. This can make it difficult to account for some properties such as hydrogen bonds. To solve this shortcoming, we can add a notion called polarisation at second order, whose goal is to mimic more accurately the behaviour of quantum mechanics density. The force fields making use of this description are commonly referred as second generation or polarisable force fields.

Our work with molecular mechanics is mostly centred around the amoeba polarisable force field and its implementation in the software `TINKER` [Pon+10].

I.E.I Classical force fields

In classical force fields implementations, pioneered with software such as `AMBER` [WK81] and `CHARMM` [Bro+83], the atoms (or sometimes a functional group) are represented by point multipoles. The multipoles are invariant during a simulation, and can be seen as an approximation of molecular orbitals in quantum mechanics. For example, point charges would mimic the s molecular orbitals.

In the following, we will consider all-atomic force fields where the smallest and only fragments are the atoms. We also introduce the notion of topological distance. A molecule is represented as a graph, where atoms are linked between each other through covalent bonds, or edges. The topological distance between two atoms in a same molecule is thus the shortest number of edges between the two.

Covalent terms

We often find three main types of interactions for the covalent potential energy:

- Two-body *stretching* terms, represented by an harmonic oscillator between two atoms separated by a covalent bond. It is used to discriminate against a distance far from some value at an equilibrium. They are under the form

$$\mathcal{E}_{\text{stretch}} := \sum_{e_{ij}} k^s_{e_{ij}} (\ell(e_{ij}) - \ell_0)^2, \tag{V.2}$$

  where $k^s_{e_{ij}} \in \mathbf{R}$ are the oscillator parameters and $\ell(e_{ij})$ is the length of the bond e_{ij}.

- Three-body *bending* terms, represented by an harmonic oscillator between two atoms at a topological distance of two. It increases the cost for the two ends to be planar. They are under the form

$$\mathcal{E}_{\text{bending}} := \sum_{e_{ijk}} k^b_{e_{ijk}} (\theta(e_{ijk}) - \theta_0)^2, \tag{V.3}$$

  where $k^b_{e_{ijk}} \in \mathbf{R}$ are the oscillator parameters and $\theta(e_{ijk})$ is the angle of the bond e_{ijk}.

- Four-body *dihedral* terms between four consecutive atoms. It increases the cost for the bond to rotate around the middle of the bond between the two atoms at the centre. They are under the form

$$\mathcal{E}_{\text{dihedral}} := \sum_{e_{ijkl}} \sum_{n=1}^{N} k^d_{e_{ijkl},n} \Big(1 + n \cos(\phi(e_{ijkl}) - \phi_0)\Big), \tag{V.4}$$

  where $k^d_{e_{ijkl}} \in \mathbf{R}$ are the dihedral parameters and $\phi(e_{ijkl})$ is the angle of the chain e_{ijkl}.

The intramolecular energy is the sum of all those contributions

$$\mathcal{E}_{\text{intra}} := \mathcal{E}_{\text{stretch}} + \mathcal{E}_{\text{bending}} + \mathcal{E}_{\text{dihedral}}, \tag{V.5}$$

and its computation is local and of no difficulty, as its computational complexity grows linearly with the number of particles.

Moreover, the more terms we add, the better we can hope to accurately represent the physics. So some force fields may add three-body Urey–Bradley terms or four-body improper dihedral terms, etc. However the more terms we add, the more work as to be done to parameterise them, and the more we risk to overfit the model. In the AMOEBA force field for example, there are five intramolecular terms.

Non-covalent terms

The non-covalent contributions often include two-body Van der Waals and electrostatic potentials and are between all atoms of the simulation

$$\mathcal{E}_{\text{inter}} := \mathcal{E}_{\text{VdW}} + \mathcal{E}_{\text{elec}}. \tag{V.6}$$

Both of them decrease in intensity as a power of the inverse of the distance between each pairs of atoms in the system.

Van der Waals potential The Van der Waals potential includes a repulsive term, which describes the Pauli repulsion: two atoms cannot get too close to each other. It may also include a less physical attractive term that helps in the accuracy of the force field. Its quick decrease makes it negligible when atoms are at some distance, and thus can be considered only locally. This means that the computational complexity to compute Van der Waals potentials may grow linearly with the number of atoms.

They are often referred to in the form n–m, where n is the inverse power of the repulsive term and m the inverse power of the attractive term. A well-known Van der Waals potential is the 12–6 Lennard–Jones potential. In the case of amoeba a distance-buffered 14–7 potential is used [Hal92]. It is of the form

$$\mathcal{E}_{\text{VdW}} := \sum_{i,j} k^v_{i,j} \left(\frac{1}{r_{ji}^{14}} - \frac{1}{r_{ji}^{7}} \right), \tag{V.7}$$

where $k^v_{i,j}$ are real parameters for the Van der Waals potential.

Coulomb potential The second term, the electrostatic potential, is attractive and follows Coulomb's law. It decreases slowly as the inverse of the distance between atoms. Hence, to have accurate simulations, it may be important to compute it for all pairs of atoms. It is of the form

$$\mathcal{E}_{\text{elec}} := \sum_{i,j} k^c_{i,j} \frac{1}{r_{ji}}, \tag{V.8}$$

where $k^c_{i,j}$ are real parameters for the Coulomb potential.

In the case where all two-body order interactions are considered, the computation of the electrostatic potential grows quadratically with the number of particles. Hence, there is a need to find accurate and less expensive ways to do the computations. In Chapters II and IV, we look at how to speedup the computation of this term, which is a bottleneck in force fields. Chapter II describe the method of choice for number of molecular mechanics software using periodic boundary conditions, while Chapter IV describes a method often applied in the physics community for non-periodic boundary conditions case, but rarely for chemical applications.

I.E.2 amoeba polarisable force field

With polarisable force fields, the description of the atoms is further enriched by considering polarisation. It is a way to take into account the fact that at a quantum mechanics level, the density changes with the geometry.

In biological applications, this term is of major importance. Several methods have been proposed:

- the fluctuating charge model [RG91], where the values of the point charges are modified during the simulation;
- the Drude oscillator model [LR03], where a point charge is introduced near atoms with an harmonic oscillator;
- the induced dipole model [ACF72], where point dipoles are added to the invariant multipoles at atomic sites.

The amoeba force field uses an induced dipole model for polarisation

$$\mathcal{E}^{\text{AMOEBA}}_{\text{inter}} := \mathcal{E}_{\text{VdW}} + \mathcal{E}_{\text{elec}} + \mathcal{E}_{\text{ipol}}, \tag{V.9}$$

where $\mathcal{E}_{\text{ipol}}$ is the energy associated to the induced dipoles. The polarisation term is evaluated using an iterative procedure. However, for most of what we present, it can be understood as a simple additional contribution to the permanent point dipole. As we did not work on polarisation but with it, we will only give a description in the following, as it plays a central part in the AMOEBA force field on which we often rely in this work.

Generalities about AMOEBA

The AMOEBA [PC03; Pon+10] force field differs from most classical force fields in two main ways. It uses (static) point multipoles up to quadrupoles in order to approximate the electrostatic properties of a molecule, and it is polarisable in the sense that each atomic site is additionally (with respect to the static multipoles) equipped with an induced dipole that is determined by minimising a polarisation energy for each new atomic configuration. Therefore, these induced dipoles are degrees of freedom which are determined on the fly by the resolution of a linear system (the polarisation equation) at each time-step and are not empirically fitted like the static multipoles.

Of course, it shall be reminded that the force field still contains the covalent-terms and the VAN DER WAALS-terms, but the emphasis is shed on the (computationally) costly part due to the long-range electrostatic interaction. Indeed, the quick decrease of the VAN DER WAALS-terms means that we can use a simple cutoff method to take them into account, which is not the case for the electrostatic interaction.

Most force fields make use of *damping* or *screening* to modify the interactions between close-by atoms. However the distinction between the two may not be always clear-cut. In this text, we will distinguish between screening and damping in the following way: Screening will apply to terms that are corrected due to a topological distance — that is a distance that depends only on the bonds between atoms, whereas damping will apply to terms that are corrected due to the physical distance between atoms. Screening and damping will be grouped together into the scaling term.

The AMOEBA energy functional is a sum of all those term

$$\mathcal{E}^{\text{AMOEBA}} := \mathcal{E}_{\text{intra}} + \mathcal{E}_{\text{VdW}} + \mathcal{E}_{\text{elec}} + \mathcal{E}_{\text{ipol}}. \tag{V.10}$$

Description of a force field based on static point quadrupoles

We first introduce the static (or permanent) part of the electrostatic contribution to the force field. The polarisability is discussed in the upcoming section.

Let $\underline{r}^{\{N\}}$ be a system composed of N atoms at positions $\{r_i\}_{1\leq i\leq N}$ in $\mathbf{R}^3$. Each point r_i is associated to a static point multipole operator

$$\hat{\mathrm{L}}_i := \mathrm{M}_{0i} + \mathrm{M}_{1i} \cdot \mathrm{D}_i + \mathrm{M}_{2i} \cdot \mathrm{D}_i^2, \tag{V.11}$$

where $\cdot$ is the point-wise product, M_{di} is a tensor of dimension 3^d describing the point 2^d-pole and D_i^d is the matrix of d-order partial derivatives with respect to atom coordinates i. Note that for $k = 1$, the operator D_r (respectively D_i) is equivalent to the usual ∇ notation, and acts on the variable r (respectively r_i).

Hence, for any $r \in \mathbf{R}^3$, the density associated to the point multipole $\hat{\mathrm{L}}_i$ is

$$\rho_i(r) := \hat{\mathrm{L}}_i \delta(r - r_i) \in \mathbf{R}, \tag{V.12}$$

where δ is the DIRAC function. This represents a generalisation of a more classical density only composed on point charges $\mathrm{M}_{0i} \in \mathbf{R}$ at positions r_i which are given by $\mathrm{M}_{0i}\delta(r - r_i)$.

In particular, for any $r \in \mathbf{R}^3$, the electric potential, electric field, gradient of the field and Hessian of the field created by the point multipole i are then respectively

$$\phi_i(r) := \hat{\mathrm{L}}_i\left(\frac{1}{|r - r_i|}\right), \tag{V.13a}$$

$$\mathrm{E}_i(r) := -\,\mathrm{D}_r\phi_i(r) = -\,\mathrm{D}_r\left(\hat{\mathrm{L}}_i\frac{1}{|r - r_i|}\right), \tag{V.13b}$$

$$[\mathrm{D}_r\mathrm{E}_i(r)]^{\gamma\gamma'} := -\,\partial^\gamma\,\partial^{\gamma'}\hat{\mathrm{L}}_i\left(\frac{1}{|r - r_i|}\right), \tag{V.13c}$$

$$[\mathrm{D}_r^2\mathrm{E}_i(r)]^{\alpha\beta\gamma} := -\,\partial^\alpha\,\partial^\beta\,\partial^\gamma\hat{\mathrm{L}}_i\left(\frac{1}{|r - r_i|}\right). \tag{V.13d}$$

Moreover, the electrostatic (interaction) energy of the system is

$$\mathcal{E}(\underline{r}^{\{N\}}) := \frac{1}{2}\sum_{\substack{1\le i,j\le N\\ j\neq i}}\hat{\mathrm{L}}_j\phi_i(r_j) = \frac{1}{2}\sum_{\substack{1\le i,j\le N\\ j\neq i}}\hat{\mathrm{L}}_i\hat{\mathrm{L}}_j\left(\frac{1}{|r_i - r_j|}\right). \tag{V.14}$$

Indeed, the potential at r_j created by all other multipoles $i \neq j$ is given by

$$\phi_{\mathrm{int},j}(r_j) := \sum_{\substack{1\le i\le N\\ j\neq i}}\phi_i(r_j). \tag{V.15}$$

As is it the case for most force fields, scaling factors are used for some specific interactions, in particular the interaction between closed atomic sites. In the AMOEBA force field, those are used to screen 1–n atoms interactions, where $n \in [\![1\,..\,5]\!]$ (*i.e.*, interaction between atomic sites that can be reached by less than six bonds). Hence, the energy of the system is in fact

$$\mathcal{E}^{\mathrm{AMOEBA}}_{\mathrm{stat}}(\underline{r}^{\{N\}}) := \frac{1}{2}\sum_{1\le i\neq j\le N} s_{ij}\hat{\mathrm{L}}_i\hat{\mathrm{L}}_j\left(\frac{1}{|r_i - r_j|}\right), \tag{V.16}$$

for some scaling factors s_{ij}. Or equivalently, the energy $\mathcal{E}(\underline{r}^{\{N\}})$ has to be corrected by the energy

$$\mathcal{E}^{\mathrm{AMOEBA}}_{\mathrm{stat,corr}}(\underline{r}^{\{N\}}) := \frac{1}{2}\sum_{1\le i\le N}\sum_{j\in\mathsf{M}_{\mathrm{stat}}(i)}(1 - s_{ij})\hat{\mathrm{L}}_i\hat{\mathrm{L}}_j\left(\frac{1}{|r_i - r_j|}\right), \tag{V.17}$$

where $\mathsf{M}_{\mathrm{stat}}(i)$ contains the interactions with atom i that have to be scaled.

Description of a polarisable force field

For an introductory lecture to polarisation, we refer to PÉREZ, CARLES, and FLECKINGER [PCF01] and KITTEL [Kit95]. For a more detailed support, the book from BÖTTCHER [Böt73] has also a discussion about multipoles.

As anticipated earlier, the electrostatic description of the molecular system is completed by induced dipoles, using the APPLEQUIST model [ACF72]. The energy due to polarisation, which decreases as $\mathscr{O}(|r|^{-3})$, can have a major impact on molecular systems; in particular for the water model, where hydrogen bonds have a large impact. Indeed, molecules such as water, that have a permanent dipolar moment provokes displacements of electrons in neighbouring molecules, which leads to the emergence of a dipolar moment in the all system. This cascade effect is called *polarisation*. This effect is important with molecules that have π bounds, and between systems with permanent dipolar moments.

For each atomic site i at location r_i, the induced dipole is described by the unknown dipole-moment μ_i and the total multipole operator for the site i is therefore given by

$$\mathrm{L}_i := \mu_i \cdot \mathrm{D}_i + \hat{\mathrm{L}}_i = \mathrm{M}_{0i} + (\mathrm{M}_{1i} + \mu_i) \cdot \mathrm{D}_i + \mathrm{M}_{2i} \cdot \mathrm{D}_i^2. \tag{V.18}$$

We should repeat that the moments M_{di} are static and fixed once and for all. The total electrostatic energy

$$\tilde{\mathcal{E}}_{\mathrm{tot}}(\underline{r}^{\{N\}}) := \frac{1}{2} \sum_{\substack{1 \le i,j \le N \\ j \neq i}} \mathrm{L}_i \mathrm{L}_j \left(\frac{1}{|r_i - r_j|} \right) \tag{V.19}$$

can then be decomposed into the static part $\mathcal{E}(\underline{r}^{\{N\}})$ and a part involving the induced dipoles

$$\mathcal{E}_{\mathrm{tot}}(\underline{r}^{\{N\}}) := \mathcal{E}(\underline{r}^{\{N\}}) + \mathcal{E}_{\mathrm{ipol}}(\underline{r}^{\{N\}}). \tag{V.20}$$

The polarisation energy $\mathcal{E}_{\mathrm{ipol}}(\underline{r}^{\{N\}})$ is defined as the minimum of a functional $\mathcal{E}_{\mathrm{ipol}}(\underline{r}^{\{N\}}, \mu)$ with respect to the induced dipoles μ

$$\mathcal{E}_{\mathrm{ipol}}(\underline{r}^{\{N\}}) = \inf_{\mu \in \mathbf{R}^{3N}} \mathcal{E}_{\mathrm{ipol}}(\underline{r}^{\{N\}}, \mu) = -\mathrm{E}_{\mathrm{stat}} \cdot \mu_m + \frac{1}{2} \mu_m \cdot T \mu_m, \tag{V.21}$$

where

$$\mathcal{E}_{\mathrm{ipol}}(\underline{r}^{\{N\}}, \mu) := -\mathrm{E}_{\mathrm{stat}} \cdot \mu + \frac{1}{2} \mu \cdot T \mu. \tag{V.22}$$

Here we use a compact notation where the set of induced dipoles μ_i and electric fields $\mathrm{E}_{\mathrm{i,stat}}(r_i)$ are collected in global $\mathbf{R}^{3N}$ vectors μ and $\mathrm{E}_{\mathrm{stat}}$. The symmetric matrix T denotes the $3N \times 3N$-matrix with off-diagonal block entries $-T_{ij} \in \mathbf{R}^{3\times 3}$ and the block-diagonal given by $T_{ii} = \alpha_i^{-1} \in \mathbf{R}^{3\times 3}$, where the α_i are the so-called polarisability tensors. The coefficients $[T_{ij}]^{\gamma\gamma'}$ of the off-diagonal ($i \neq j$) blocks T_{ij} with $i, j \in [\![1 \,..\, N]\!]$ are explicitly given by

$$[T_{ij}]^{\gamma\gamma'} := \partial^\gamma \, \partial^{\gamma'} \left(\frac{1}{|r_{ij}|} \right) = \partial^\gamma \left(-\frac{[r_{ij}]^{\gamma'}}{|r_{ij}|^3} \right) = 3 \frac{[r_{ij}]^\gamma \, [r_{ij}]^{\gamma'}}{|r_{ij}|^5} - \frac{\delta_{\gamma\gamma'}}{|r_{ij}|^3}, \tag{V.23}$$

with

$$r_{ij} = r_i - r_j = \left([r_{ij}]_x, [r_{ij}]_y, [r_{ij}]_z \right)^{\mathsf{T}}. \tag{V.24}$$

We note that the diagonal part involving the polarisabilities in Eq. (V.21) can be thought as the energetic cost for the polarisation to happen [BGS87].

The minimiser μ_m of Eq. (V.21) verifies the first-order optimality condition

$$T \mu_m = \mathrm{E}_{\mathrm{stat}}, \tag{V.25}$$

which is called the polarisation equation. Moreover, we note that the induced energy is always negative; this is because induction is always favorable to the molecular system. This equation can be solved by directly inverting the T matrix, if it is of small dimension. However in general, it is solved using an iterative algorithm that stops when a residue is smaller than a desired threshold.

Scaling terms in the case of AMOEBA

THOLE damping It appears that in some cases, the polarisation energy $\mathcal{E}_{\text{ipol}}(\underline{r}^{\{N\}}, \mu)$ is unbounded from below in μ; the often-called *polarisation catastrophe*. Indeed, at a mathematical level, this is translated to the fact that the polarisation matrix T is no longer positive definite and has at least one negative eigenvalue. This typically arises when two atoms become close. Hence the idea is to damp certain interactions when atoms are close and one of the most commonly used (and empirical) scheme is the THOLE damping [Tho81]. It consists of introducing the atom dependent quantity

$$\lambda(u_{ij}) = 1 - \exp\left(-a u_{ij}^2\right), \tag{V.26}$$

where a is some positive parameter,

$$u_{ij} = \frac{9\, r_{ij}}{\text{Tr}(\alpha_i)\,\text{Tr}(\alpha_j)}, \tag{V.27}$$

α is the polarisability tensor and Tr is the trace operator.

The off-diagonal part ($i \neq j$) of the polarisation matrix T with components $[T_{ij}]^{\gamma\gamma'}$ is then replaced by the damped polarisation matrix

$$[T_{\text{Thole},ij}]^{\gamma\gamma'} = \partial^{\gamma}\left(-\lambda(u_{ij})\frac{[r_{ij}]^{\gamma'}}{r_{ij}^3}\right). \tag{V.28}$$

Screening A particularity of the AMOEBA force field is that it uses two sets of electric fields, called the direct and polar fields which are noted respectively E_d and E_p. They differ by the fact that the static electric field is screened [PC03] by two different sets of parameters $s_{ij}^{\{d,p\}}$, as mentioned in Section I.E.2. This leads to two different sets of minimising induced dipoles (see Eq. (V.21)) μ_d and μ_p given by

$$\mu_d = T_{\text{Thole}}^{-1}\text{E}_d \quad \text{and} \quad \mu_p = T_{\text{Thole}}^{-1}\text{E}_p. \tag{V.29}$$

The AMOEBA polarisation energy is then defined as

$$\mathcal{E}_{\text{ipol}}^{\text{AMOEBA}}(\underline{r}^{\{N\}}) = -\frac{1}{2}\mu_d \cdot \text{E}_p. \tag{V.30}$$

The AMOEBA energy Combining the static electrostatic energy, the scaling and the polarisation energy yields the AMOEBA energy

$$\mathcal{E}_{\text{tot}}^{\text{AMOEBA}}(\underline{r}^{\{N\}}) = \mathcal{E}_{\text{stat}}^{\text{AMOEBA}}(\underline{r}^{\{N\}}) + \mathcal{E}_{\text{ipol}}^{\text{AMOEBA}}(\underline{r}^{\{N\}}). \tag{V.31}$$

The periodic case formalism using EWALD's sums was introduced by NYMAND and LINSE [NL00]. The expression with particle mesh EWALD was described by TOUKMAJI et al. [Tou+00], and then optimised by WANG and SKEEL [WS05]. We refer the reader to Chapter II for more information about this.

Forces

Computing the energy of the system is of course not the only quantity of interest. In contrast, computing the force that acts on each atomic site is indispensable for a molecular dynamics simulation.

The forces at site i is defined by

$$F_i(r_i) = -\,\text{D}_i\mathcal{E}_{\text{tot}}^{\text{AMOEBA}}(\underline{r}^{\{N\}}). \tag{V.32}$$

Hence, for molecular dynamics we need to compute the matrices of third order partial derivatives of the potentials, as well as the potential itself, the field, its gradient and its Hessian (see Eq. (V.13)).

I.F Continuum solvation and the COSMO model

To limit the need to represent every single solvent molecule, we may also use an implicit description with a continuum solvation model, such as the polarisable COSMO model [KS93; TP94]. Instead of having explicit molecules, the solvent is modelled as a continuum medium with the bulk dielectric permittivity of the solvent. The electrostatic solvent–solute interaction can then be computed by solving an integral equation on the solute cavity-surface. The ddCOSMO algorithm [CMS13] is a discretisation of the COSMO model that takes advantage of the SCHWARZ domain decomposition method to efficiently compute solution to this model.

This model can be coupled with a quantum mechanics method or a polarisable force field and its complexity grows linearly with the number of quantum mechanics or molecular mechanics atoms. Methods we developed in Chapters III and IV were thought to allow for the possibility to couple them with this continuum mechanics model, to be able to take into account a large bulk of solvent.

We will only give a brief overview of the method, as we only make use of this model which thus can be think as a black-box method that allows for more solvent to be described.

I.F.1 Coupling with variational polarisable force field

We define a variational polarisable force field as a force field whose energy can be written as the minimum of an energy functional depending on the induced dipoles.

$$\mathcal{E}_{\text{var}} := \min_{\mu \in \mathbf{R}^n} \mathcal{E}_{\text{var}}(\mu) = \min_{\mu \in \mathbf{R}^n} \left(\mathcal{E}_{\text{inter}} + \mathcal{E}_{\text{VdW}} + \mathcal{E}_{\text{elec}} + \mathcal{E}_{\text{ipol}}(\mu) \right). \tag{VI.1}$$

The coupling between ddCOSMO and a variational polarisable force field with induced dipoles can be done by looking for the minimum of the functional [Lip+15]

$$\mathcal{E}_{\text{pol}}(\underline{r}^{\{N\}}, \mu) := -\mathrm{E}_{\text{stat}} \cdot \mu + \frac{1}{2} \mu \cdot T\mu + \frac{1}{2} f(\varepsilon) \langle \psi(\mu) | X(\mu) \rangle, \tag{VI.2}$$

where $f(\varepsilon)$ is an empirical quantity that depends on the dielectric constant of the solvent, $\psi(\mu)$ is a vector representing the solute's molecular charge density distribution and $X(\mu)$ is a vector representing the solvent polarisation. We have the notation

$$\langle a | b \rangle := \sum_{1 \leq i \leq N} \sum_{1 \leq \ell \leq L} \sum_{|m| \leq \ell} [a_i]_\ell^m [b_i]_\ell^m, \tag{VI.3}$$

where the $[\cdot]_\ell^m$ are the spherical harmonics expansion on the cavity with maximum angular momentum L.

The solution of Eq. (VI.2) is given by solving the first-order optimality equation of the form

$$T\mu + \frac{1}{2} f(\varepsilon) [AX(\mu) + BS(\mu)] = \mathrm{E}_{\text{stat}}, \tag{VI.4}$$

where $X(\mu)$ and $S(\mu)$ are solution of the following linear systems

$$LX(\mu) = g(\mu), \tag{VI.5a}$$
$$L^* S(\mu) = \psi(\mu). \tag{VI.5b}$$

For more details, we refer to Section 2 of LIPPARINI et al. [Lip+15].

I.F.2 Coupling with AMOEBA

Due to the form of the polarisation energy functional given by Eq. (V.30), AMOEBA is not a variational force field. However it is possible to write the functional as a sum of three variational terms [Lip+15]

$$\mathcal{E}_{\text{pol}}(\underline{r}^{\{N\}}) = \mathcal{E}_{\text{pol}}(\underline{r}^{\{N\}}, \mu_d + \mu_p) - \mathcal{E}_{\text{pol}}(\underline{r}^{\{N\}}, \mu_d) - \mathcal{E}_{\text{pol}}(\underline{r}^{\{N\}}, \mu_p) \tag{VI.6}$$

In Chapter III, we use insight from this method to be able to couple molecular mechanics using the AMOEBA force field and quantum mechanics, which open paths for fully polarisable molecular dynamics on three different scales of physics.

I.G Sailing instructions

This work is being exposed in two part. The first one is directed at multiscale problems and applications, with different physics scales: quantum, classical or continuous and different scales of the computation. We will see how to accommodate for bigger and bigger problems, either on one computer or on a network of them.

In Chapter II we dwell into polarisable classical molecular dynamics and in particular EWALD's method of summation for periodic systems.

In Chapter III we look at multiscale physics simulation of a molecular system using quantum mechanics, molecular mechanics and possibly continuum solvation.

In Chapter IV we look at a way to improve the efficiency in the computing of the long-range Coulombic potential when multipoles are used.

In the second part, we take some distance from applications, and look at the theories underlying theoretical chemistry by looking at extrapolation methods for quantum mechanics.

In Chapter V we explore a way to use reduced-order models to quicken the computation of the energy.

In Chapter VI we look at density matrices from a differential geometry point of view to quicken the self-consistent field method in quantum mechanics.

I.H References

[ACF72] Applequist, Jon, Carl, James R., and Fung, Kwok-Kueng. "Atom Dipole Interaction Model for Molecular Polarizability. Application to Polyatomic Molecules and Determination of Atom Polarizabilities". In: *Journal of the American Chemical Society* 94.9 (May 1, 1972), pp. 2952–2960. ISSN: 0002-7863 (cit. on pp. 15, 17).

[Ain+15] Ain, Qurrat Ul et al. "Machine-Learning Scoring Functions to Improve Structure-Based Binding Affinity Prediction and Virtual Screening". In: *WIREs Computational Molecular Science* 5.6 (2015), pp. 405–424. ISSN: 1759-0884 (cit. on p. 5).

[Amo+98] Amovilli, Claudio et al. "Recent Advances in the Description of Solvent Effects with the Polarizable Continuum Model". In: *Advances in Quantum Chemistry*. Ed. by Löwdin, Per-Olov. Vol. 32. Academic Press, Jan. 1, 1998, pp. 227–261 (cit. on pp. 5, 69).

[BGS87] Berendsen, H. J. C., Grigera, J. R., and Straatsma, T. P. "The Missing Term in Effective Pair Potentials". In: *The Journal of Physical Chemistry* 91.24 (Nov. 1, 1987), pp. 6269–6271. ISSN: 0022-3654 (cit. on p. 18).

[Boe11] Boehm, Markus. "Virtual Screening of Chemical Space: From Generic Compound Collections to Tailored Screening Libraries". In: *Virtual Screening*. Ed. by Sotriffer, Christoph. Methods and Principles in Medicinal Chemistry. Weinheim, Germany: John Wiley & Sons, Ltd, 2011, pp. 1–33. ISBN: 978-3-527-63332-6 (cit. on p. 5).

[Böt73] Böttcher, Carl Johan Friedrich. "Theory of Electric Polarization, Volume 1: Dielectrics in Static Fields". 2nd ed. Elsevier, Jan. 1973. ISBN: 978-0-444-41019-1 (cit. on p. 17).

[BRD13] Barré-Sinoussi, Françoise, Ross, Anna Laura, and Delfraissy, Jean-François. "Past, Present and Future: 30 Years of HIV Research". In: *Nature Reviews Microbiology* 11.12 (12 Dec. 2013), pp. 877–883. ISSN: 1740-1534 (cit. on p. 4).

[Bro+83] Brooks, Bernard R. et al. "CHARMM: A Program for Macromolecular Energy, Minimization, and Dynamics Calculations". In: *Journal of Computational Chemistry* 4.2 (1983), pp. 187–217. ISSN: 1096-987X (cit. on p. 13).

[Bur12] Burke, Kieron. "Perspective on Density Functional Theory". In: *The Journal of Chemical Physics* 136.15 (Apr. 21, 2012), p. 150901. ISSN: 0021-9606 (cit. on p. 5).

[CB00] Cancès, Eric and Bris, Claude Le. "On the Convergence of SCF Algorithms for the Hartree-Fock Equations". In: *ESAIM: Mathematical Modelling and Numerical Analysis* 34.4 (4 July 1, 2000), pp. 749–774. ISSN: 0764-583X (cit. on p. 11).

[CBM06] Cancès, Eric, Bris, Claude Le, and Maday, Yvon. "Méthodes Mathématiques En Chimie Quantique. Une Introduction". Mathématiques et Applications. Berlin Heidelberg: Springer-Verlag, 2006. ISBN: 978-3-540-30996-3 (cit. on pp. 6, 68).

[CMS13] Cancès, Eric, Maday, Yvon, and Stamm, Benjamin. "Domain Decomposition for Implicit Solvation Models". In: *The Journal of Chemical Physics* 139.5 (2013), p. 054111 (cit. on pp. 20, 104).

[El +21] El Ahdab, Dina et al. "Interfacial Water Many-Body Effects Drive Structural Dynamics and Allosteric Interactions in SARS-CoV-2 Main Protease Dimerization Interface". In: *The Journal of Physical Chemistry Letters* 12.26 (July 8, 2021), pp. 6218–6226 (cit. on p. 2).

[Fis94] Fischer, Emil. "Synthesen in Der Zuckergruppe II". In: *Berichte der deutschen chemischen Gesellschaft* 27.3 (1894), pp. 3189–3232. ISSN: 1099-0682 (cit. on pp. 4, 5).

[Hal92] Halgren, Thomas A. "The Representation of van Der Waals (vdW) Interactions in Molecular Mechanics Force Fields: Potential Form, Combination Rules, and vdW Parameters". In: *Journal of the American Chemical Society* 114.20 (Sept. 1992), pp. 7827–7843. ISSN: 0002-7863 (cit. on p. 15).

[HJO00] Helgaker, Trygve, Jørgensen, Poul, and Olsen, Jeppe. "Molecular Electronic-Structure Theory". John Wiley & Sons, Aug. 2000. ISBN: 978-0-471-96755-2 (cit. on pp. 3, 6).

[HK64] Hohenberg, P. and Kohn, W. "Inhomogeneous Electron Gas". In: *Physical Review* 136 (3B Nov. 9, 1964), B864–B871. ISSN: 0031-899X (cit. on p. 12).

[Kar14] Karplus, Martin. "Development of Multiscale Models for Complex Chemical Systems: From H+H2 to Biomolecules (Nobel Lecture)". In: *Angewandte Chemie International Edition* 53.38 (2014), pp. 9992–10005. ISSN: 1521-3773 (cit. on pp. 2, 69).

[Kit95] Kittel, Charles. "Introduction to Solid State Physics". 7th ed. John Wiley & Sons, Aug. 1995. ISBN: 978-0-471-11181-8 (cit. on p. 17).

[KS65] Kohn, W. and Sham, L. J. "Self-Consistent Equations Including Exchange and Correlation Effects". In: *Physical Review* 140 (4A Nov. 15, 1965), A1133–A1138 (cit. on p. 13).

[KS93] Klamt, A. and Schuurmann, G. "COSMO: A New Approach to Dielectric Screening in Solvents with Explicit Expressions for the Screening Energy and Its Gradient". In: *Journal of the Chemical Society, Perkin Transactions 2* 5 (1993), pp. 799–805 (cit. on pp. 20, 104).

[Lee+20] Leermakers, Frans A. M. et al. "Turning Autophobic Wetting on Biomimetic Surfaces into Complete Wetting by Wetting Additives". In: *Soft Matter* 16.20 (May 27, 2020), pp. 4823–4839. ISSN: 1744-6848 (cit. on p. 3).

[Lev14] Levitt, Michael. "Birth and Future of Multiscale Modeling for Macromolecular Systems (Nobel Lecture)". In: *Angewandte Chemie International Edition* 53.38 (2014), pp. 10006–10018. ISSN: 1521-3773 (cit. on pp. 2, 69).

[Lie83] Lieb, Elliott H. "Density Functionals for Coulomb Systems". In: *International Journal of Quantum Chemistry* 24.3 (1983), pp. 243–277. ISSN: 1097-461X (cit. on p. 12).

[Lip+15] Lipparini, Filippo et al. "Polarizable Molecular Dynamics in a Polarizable Continuum Solvent". In: *Journal of Chemical Theory and Computation* 11.2 (Feb. 10, 2015), pp. 623–634. ISSN: 1549-9618 (cit. on pp. 20, 21).

[LR03] Lamoureux, Guillaume and Roux, Benoît. "Modeling Induced Polarization with Classical Drude Oscillators: Theory and Molecular Dynamics Simulation Algorithm". In: *The Journal of Chemical Physics* 119.6 (July 24, 2003), pp. 3025–3039. ISSN: 0021-9606 (cit. on p. 15).

[MH09] Marx, Dominik and Hutter, Jürg. "Ab Initio Molecular Dynamics: Basic Theory and Advanced Methods". Cambridge: Cambridge University Press, 2009. ISBN: 978-0-521-89863-8 (cit. on pp. 6, 112).

[NL00] Nymand, Thomas M. and Linse, Per. "Ewald Summation and Reaction Field Methods for Potentials with Atomic Charges, Dipoles, and Polarizabilities". In: *The Journal of Chemical Physics* 112.14 (Mar. 30, 2000), pp. 6152–6160. ISSN: 0021-9606 (cit. on p. 19).

[PC03] Ponder, Jay W. and Case, David A. "Force Fields for Protein Simulations". In: *Protein Simulations*. Ed. by Daggett, Valerie. Vol. 66. Advances in Protein Chemistry. Academic Press, 2003, pp. 27–85 (cit. on pp. 16, 19, 57, 69).

[PCF01] Pérez, José-Philippe, Carles, Robert, and Fleckinger, Robert. "Électromagnétisme, Fondements et Applications". 4th ed. Dunod, Nov. 2001. ISBN: 978-2-10-005574-6 (cit. on pp. 17, 31).

[Pon+10] Ponder, Jay W. et al. "Current Status of the AMOEBA Polarizable Force Field". In: *Journal of Physical Chemistry B* 114.8 (2010), pp. 2549–2564 (cit. on pp. 13, 16, 71, 93).

[RG91] Rappe, Anthony K. and Goddard, William A. "Charge Equilibration for Molecular Dynamics Simulations". In: *The Journal of Physical Chemistry* 95.8 (Apr. 1, 1991), pp. 3358–3363. ISSN: 0022-3654 (cit. on p. 15).

[Rog11] Rognan, Didier. "Docking Methods for Virtual Screening: Principles and Recent Advances". In: *Virtual Screening*. Ed. by Sotriffer, Christoph. Methods and Principles in Medicinal Chemistry. Weinheim, Germany: John Wiley & Sons, Ltd, 2011, pp. 153–176. ISBN: 978-3-527-63332-6 (cit. on p. 5).

[Roo51] Roothaan, C. C. J. "New Developments in Molecular Orbital Theory". In: *Reviews of Modern Physics* 23.2 (Apr. 1, 1951), pp. 69–89 (cit. on p. 11).

[RS81] Reed, Michael and Simon, Barry. "I: Functional Analysis". Academic Press, Feb. 23, 1981. 417 pp. ISBN: 978-0-08-057048-8 (cit. on p. 9).

[Sen+20] Senior, Andrew W. et al. "Improved Protein Structure Prediction Using Potentials from Deep Learning". In: *Nature* 577.7792 (7792 Jan. 2020), pp. 706–710. ISSN: 1476-4687 (cit. on p. 4).

[SH73] Saunders, V. R. and Hillier, I. H. "A "Level–Shifting" Method for Converging Closed Shell Hartree–Fock Wave Functions". In: *International Journal of Quantum Chemistry* 7.4 (1973), pp. 699–705. ISSN: 1097-461X (cit. on p. 11).

[Sny+05] Snyder, David A. et al. "Comparisons of NMR Spectral Quality and Success in Crystallization Demonstrate That NMR and X-ray Crystallography Are Complementary Methods for Small Protein Structure Determination". In: *Journal of the American Chemical Society* 127.47 (Nov. 30, 2005), pp. 16505–16511. ISSN: 0002-7863 (cit. on p. 4).

[Tho81] Thole, B. T. "Molecular Polarizabilities Calculated with a Modified Dipole Interaction". In: *Chemical Physics* 59.3 (Aug. 1, 1981), pp. 341–350. ISSN: 0301-0104 (cit. on p. 19).

[Tou+00] Toukmaji, Abdulnour et al. "Efficient Particle-Mesh Ewald Based Approach to Fixed and Induced Dipolar Interactions". In: *The Journal of Chemical Physics* 113.24 (Dec. 13, 2000), pp. 10913–10927. ISSN: 0021-9606 (cit. on p. 19).

[TP94] Tomasi, Jacopo and Persico, Maurizio. "Molecular Interactions in Solution: An Overview of Methods Based on Continuous Distributions of the Solvent". In: *Chemical Reviews* 94.7 (Nov. 1994), pp. 2027–2094. ISSN: 0009-2665 (cit. on pp. 5, 20).

[War14] Warshel, Arieh. "Multiscale Modeling of Biological Functions: From Enzymes to Molecular Machines (Nobel Lecture)". In: *Angewandte Chemie International Edition* 53.38 (2014), pp. 10020–10031. ISSN: 1521-3773 (cit. on pp. 2, 69).

[WK81] Weiner, Paul K. and Kollman, Peter A. "AMBER: Assisted Model Building with Energy Refinement. A General Program for Modeling Molecules and Their Interactions". In: *Journal of Computational Chemistry* 2.3 (1981), pp. 287–303. ISSN: 1096-987X (cit. on p. 13).

[WS05] Wang, Wei and Skeel, Robert D. "Fast Evaluation of Polarizable Forces". In: *The Journal of Chemical Physics* 123.16 (Oct. 22, 2005), p. 164107. ISSN: 0021-9606 (cit. on p. 19).

[Yee+05] Yee, Adelinda A. et al. "NMR and X-ray Crystallography, Complementary Tools in Structural Proteomics of Small Proteins". In: *Journal of the American Chemical Society* 127.47 (Nov. 30, 2005), pp. 16512–16517. ISSN: 0002-7863 (cit. on p. 4).

[ZH79] Zerner, Michael C. and Hehenberger, Michael. "A Dynamical Damping Scheme for Converging Molecular Scf Calculations". In: *Chemical Physics Letters* 62.3 (Apr. 15, 1979), pp. 550–554. ISSN: 0009-2614 (cit. on p. 11).

Face A

Multiscale problems and applications

Chapter II

Polarisable classical molecular dynamics

Overview

Modified software TINKER

APIs • OpenMP • MPI

Visit RWTH Aachen University (Aachen, three days, Apr. 2017) with Benjamin Stamm

Papers

- [Lag+15] Lagardère, Louis et al. "Scalable Evaluation of Polarization Energy and Associated Forces in Polarizable Molecular Dynamics: II. Toward Massively Parallel Computations Using Smooth Particle Mesh Ewald". In: *Journal of Chemical Theory and Computation* 11.6 (June 9, 2015), pp. 2589–2599. ISSN: 1549-9618
- [Nar+16] Narth, Christophe et al. "Scalable Improvement of SPME Multipolar Electrostatics in Anisotropic Polarizable Molecular Mechanics Using a General Short-Range Penetration Correction up to Quadrupoles". In: *Journal of Computational Chemistry* 37.5 (2016), pp. 494–506. ISSN: 1096-987X

Collaborators

• Louis Lagardère • Yvon Maday • Christophe Narth • Jean-Philippe Piquemal • Benjamin Stamm

II.A Problem statement

As we have briefly seen in Chapter I, the energy associated to the electrostatic potential poses a particular challenge. It is an N-body problem: For a system of N particles, we want to describe how the system evolves when each particle is interacting with every other ones

$$\mathcal{E}_{\text{elec}} := \sum_{1 \leqslant i \neq j \leqslant N} \frac{k^e_{i,j}}{|r_j - r_i|}, \tag{I.1}$$

where r_i is the position of the i-th particle, and $k^e_{i,j}$ are real parameters that we will explicit below.

The naive way to solve this by doing the explicit summation is of quadratic computational complexity $\mathcal{O}(N^2)$, which quickly becomes insurmountable as the number of particles increases. To speedup the computations, a simple method is to use cutoffs, where interactions farther than a certain radius are truncated. However, neglecting parts of the Coulombic interaction — the long-range effects, comes at the cost of less exploitable numerical results, as was shown by York et al. [Yor+94].

In this chapter, we are interested in a particular class of methods to decrease the quadratic computational cost of the electrostatic potential, namely the Ewald's summation technique. Ironically, the method works by considering an infinite periodic system in three dimensions. The complexity then grows as $N \log N$, as we are able to use fast Fourier transforms.

We will present a full derivation of this method, starting with basic axioms of molecular mechanics, in the case of the amoeba polarisable force field. This chapter contains a pedagogical overview of results for this method, with no new result, except a derivation for any multipole order for what is commonly referred as the self-terms in Section II.D.2.

We will see that using periodic boundary conditions comes at a cost, as the law that describes the potential energy, the Coulomb's law, forces us to manipulate Madelung sums. This implies

that the order of summation should be taken into account, which is not straightforward.

The periodic boundary conditions problem has been extensively studied in crystallography, as crystals can be thought at a first-order approximation as a two- or three-dimensional periodic systems. And the Ewald's summation method was first developed for these cases. Nonetheless, this model has also been successfully applied for interactions between chemical systems, even for ones that do not seem to have any reason to be treated in a periodic way. That seems to be explained by the extreme importance of the solvent, for example water molecules. That is a reason why a huge part of the work by Ponder for the amoeba force field [RP03] was dedicated to have an accurate model for water.

Indeed, when we consider molecular systems with periodicity, there may not be any reason for them to *feel* the presence of their periodic images. We thus have to surround the systems with enough water so it can evolve as if they were *alone* among the solvent. This is at the cost of computational complexity. But without this, we may not be able to accurately compute physical quantities for the system.

II.B Derivation of Ewald's summation method

II.B.1 Electrostatic field

In this section, we use notation and formalism of Pérez, Carles, and Fleckinger [PCF01]. We may also, instead of referring to a particle of index i at position r_i with charge q_i, use only one of those properties as a shortcut to describe the particle.

We first start with the fundamental law that describes the interaction between charged particles.

Axiom II.B.1 (Coulomb's law). — We consider a system of two immobile point charges q_1 and q_2 in a vacuum.

- The magnitude of the electrostatic force that has a point charge q_1 on another q_2 is inversely proportional to the square of the distance between the two charges.
- The vector goes from the charge q_1 to q_2.

We thus have the equality

$$\mathrm{F}_{1\to 2} = \frac{g(q_1, q_2)}{|r_{21}|^2} e_{21}, \tag{II.1}$$

where $r_{21} := r_2 - r_1$, e_{21} is the unit vector $r_{21}/|r_{21}|$, and $g(q_1, q_2)$ is a scalar.

Experiments show that $g(q_1, q_2) = k q_1 q_2$, where k is a constant. In the following, we will use atomic units, where $k \equiv 1$, as is customary in crystallography.

Definition II.B.1 (Electrostatic field). — The electrostatic field created at a fictitious charge q at r by a charge q_i at r_i is

$$\mathrm{E}_i(r) := \frac{\mathrm{F}_{i\to q}}{q} = \frac{q_i}{|r - r_i|^2} e_i \quad \text{where} \quad e_i := \frac{r - r_i}{|r - r_i|}. \tag{II.2}$$

If we consider a (not necessarily continuous) charge distribution (or density) $r \mapsto \rho(r)$ in a volume V, the field is

$$\mathrm{E}(r) := \int_V \frac{r - r'}{|r - r'|^3} \rho(r')\, \mathrm{d}r'. \tag{II.3}$$

We note that this definition implies a discontinuity of the electrostatic field at the positions of the charges.

We will also make use of the Maxwell–Gauss' law. We note that this law still holds when the charges are not stationary.

Axiom II.B.2 (Maxwell–Gauss' law)**.—** With the previous notation, we have the differential form identity

$$\nabla \cdot \mathrm{E} = 4\pi\rho. \tag{II.4}$$

We note that the 4π factor is due to the use of atomic units.

The differential form can be rewritten as an integral form using Stokes' theorem.

Theorem II.B.1 (Stokes)**.—** Let E be a vector field on $\mathbf{R}^3$. Then for all volume V of $\mathbf{R}^3$,

$$\int_{\partial V} \mathrm{E} \cdot n \, \mathrm{d}\sigma = \int_V \nabla \cdot \mathrm{E} \, \mathrm{d}\tau, \tag{II.5}$$

where n is the normal vector pointing to the exterior.

Admitted proof: This is a classical theorem of analysis; see, *e.g.*, the third volume of the series about analysis from Godement [God01, chap. IX]. □

Theorem II.B.2 (Gauss)**.—** With the previous notation,

$$\frac{1}{4\pi} \int_{\partial V} \mathrm{E} \cdot n \, \mathrm{d}\sigma = \int_V \rho \, \mathrm{d}\tau. \tag{II.6}$$

Proof: It is a direct consequence of Axiom II.B.2 using Stokes' theorem. ■

II.B.2 Electrostatic potential energy

Let E be an electrostatic field

$$\mathrm{E}(r) = \sum_{i=1}^{N} q_i \frac{r - r_i}{|r - r_i|^3}. \tag{II.7}$$

The Coulomb force being conservative, there is a function $\mathcal{E}$, such that for a fictitious charge q at r

$$\mathrm{F} = q\mathrm{E} = -\nabla\mathcal{E} \quad \text{with} \quad \mathcal{E}(r) = q \sum_{i=1}^{N} \frac{q_i}{|r - r_i|} + c, \tag{II.8}$$

where c is a scalar. By having $|r| \to +\infty$, we can chose a convention where $c \equiv 0$. The function $\mathcal{E}$ is called the electrostatic potential energy of interaction, and $\phi := \mathcal{E}/q$ is called the electrostatic potential.

Definition II.B.2.— The difference of electrostatic potential energy — often shortened as electrostatic energy — at (q, r) due to the force F is

$$E(r) := \mathcal{E}(r) - \mathcal{E}(r_{\mathrm{ref}}) = -\int_r^{r_{\mathrm{ref}}} \mathrm{F}(r') \, \mathrm{d}r'. \tag{II.9}$$

With the convention $\mathcal{E}(r_{\text{ref}} \equiv +\infty) = 0$, we have

$$E(r) = \mathcal{E}(r) = q\phi(r). \tag{II.10}$$

To simplify the notations, we will use the following convention.

Notation. — The vectors $r_j - r_i$ and $r_j - r_i + n$ can be shortened respectively by r_{ji} and r_{jin}.

We can now define the electrostatic potential energy for a system of N point charges.

Definition II.B.3 (Electrostatic potential energy). — For N point charges $\underline{r}^{\{N\}} := (r_1, \dots, r_N)$, the electrostatic potential energy is

$$\mathcal{E}_0(\underline{r}^{\{N\}}) := \sum_{1 \le i < j \le N} \frac{q_i q_j}{|r_j - r_i|} = \frac{1}{2} \sum_{i=1}^{N} \sum_{\substack{j=1 \\ j \neq i}}^{N} \frac{q_i q_j}{|r_j - r_i|} = \frac{1}{2} \sum_{i=1}^{N} q_i \phi^i(r_i), \tag{II.11}$$

where

$$\phi^i(r) := \sum_{\substack{j=1 \\ j \neq i}}^{N} \frac{q_j}{|r_j - r|}. \tag{II.12}$$

There is an *equivalent* to the Maxwell–Gauss' law for the electrostatic potential. It is given by the Poisson equation.

Theorem II.B.3 (Poisson equation). — Let ϕ be an electrostatic potential and ρ its charge distribution. Then we have

$$\Delta\phi = -4\pi\rho. \tag{II.13}$$

Proof: By using Axiom II.B.2 and the fact that the force is conservative, we have

$$\Delta\phi \overset{\text{def.}}{=} \nabla \cdot \left(\frac{\nabla \mathcal{E}}{q} \right) = \nabla \cdot \frac{-\mathrm{F}}{q} \overset{\text{def.}}{=} -\nabla \cdot \mathrm{E} = -4\pi\rho. \tag{II.14}$$

■

Of particular interest for us are the potentials due to the point charge density $\rho^i(r)$ and to the Gaussian density $\rho_g^i(r)$. The densities

$$\rho^i(r) := q_i \delta(r - r_i) \quad \text{and} \quad \rho_g^i(r) := q_i \left(\frac{\alpha}{\pi} \right)^{3/2} \exp(-\alpha |r - r_i|^2),$$

have respective potentials

$$\phi^i(r) = \frac{q_i}{|r - r_i|} \quad \text{and} \quad \phi_g^i(r) = \frac{q_i}{|r - r_i|} \operatorname{erf}(\alpha^{1/2} |r - r_i|),$$

where α is a strictly positive parameter and the error function erf is defined next.

Definition II.B.4 (Error function). — Let V be the volume of the primitive unit cell U, and U^* its dual. The error function erf is defined on $\mathbf{R}$ by

$$\operatorname{erf}(r) := \frac{2}{\sqrt{\pi}} \int_0^r \exp(-t^2)\, \mathrm{d}t, \tag{II.15}$$

and the complementary error function erfc by $1 \equiv \operatorname{erf} + \operatorname{erfc}$. See Fig. II.2a Page 40 for a plot

of these two functions.

II.B.3 Periodic particle distribution

From Eq. (II.11), we see that the computational cost of the electrostatic energy quickly increases: quadratically in the number of point charges. However, if we consider a periodic system — a Bravais lattice, we can then use the Ewald's summation method to reduce the computational complexity of numerical results.

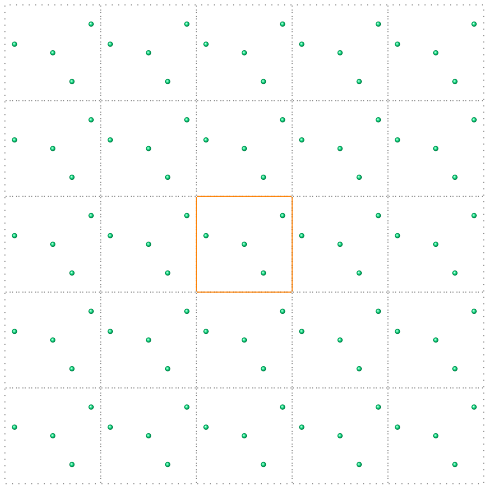

Figure II.1: Schematic two-dimensional lattice with a primitive unit cell at the centre

In this section, we will introduce the concepts for the electrostatic energy in a periodic system. This method has mostly been developed in crystallography, hence the vocabulary that is used. However Ewald's summation method can be used for any Coulombic periodic system. In Fig. II.1, we give a schematic description for a two-dimensional lattice, where a primitive unit cell is highlighted in the centre.

In the following, we will use notation from Darden [Dar08]. Moreover, we first only introduce the problem for point charge distribution. We will present the case of multipoles up to quadrupoles, which are used by the amoeba force field, in Section II.D.

Definition II.B.5. — We note $\underline{r}^{\{\infty\}}$ an infinite lattice of point charges in $\mathbf{R}^3$.

- A unit cell is a compact subspace without charge on its border, such that a lattice can be described by translation of the unit cell with a set of linearly independent vectors — called primitive vectors;
- a primitive unit cell is a unit cell that has the least number of point charges.

Next, we introduce notation for the lattice and its dual. They will be used throughout this chapter, in particular when we will refer to the direct and reciprocal sums.

Notation. — Let (a^1, a^2, a^3) be a basis of primitive vectors, and (a_1^*, a_2^*, a_3^*) its dual basis. That is $a_i^* \cdot a^j = \delta_{ij}$ for $i, j \in \{1, 2, 3\}$. If we note $V := \det(a^1, a^2, a^3)$ the volume of the unit cell and $\wedge$ the exterior product, we have

$$a_1^* = \frac{a^2 \wedge a^3}{V}, \quad a_2^* = \frac{-a^1 \wedge a^3}{V} \quad \text{and} \quad a_3^* = \frac{a^1 \wedge a^2}{V}. \tag{II.16}$$

This dual basis will be of intensive use when using Fourier transforms later on.

We will also use the notation

$$n := n_1 a^1 + n_2 a^2 + n_3 a^3, \quad m := m^1 a_1^* + m^2 a_2^* + m^3 a_3^*, \quad \text{and} \quad r := s_1 a^1 + s_2 a^2 + s_3 a^3, \tag{II.17}$$

where for $\gamma = 1, 2, 3$, n_γ and m^γ are integers, and s_γ are reals. The vectors n are points on the lattice and the covectors m points on the dual lattice.

The cells in the dual space are known as the Brillouin zones; the primitive unit cell in the dual space is known as the first Brillouin zone.

Let U be a unit cell that we will copy in every direction in the space. The total energy for such a system can be defined as the sum of the energy $\mathcal{E}_0$ of the primitive unit cell and the energies between the primitive unit cell and its copies. We have the following definition.

Definition II.B.6. — Let $\underline{r}^{\{N\}}$ be the lattice in a primitive unit cell, we then define the energy of the periodic system by

$$\mathcal{E}(\underline{r}^{\{N\}}) := \frac{1}{2}{\sum_n}' \sum_{1 \le i,j \le N} \frac{q_i q_j}{|r_j - r_i + n|}, \tag{II.18}$$

where the prime indicates that we should exclude the indices $i = j$ when $n = 0$. When we do not precise the summation — as it is the case here for the sum over n, it should be assumed that the sum is for all boxes in $\mathbf{R}^3$ (*i.e.*, $n \in \mathbf{Z}^3$ for a unit cubic cell).

Let U be a unit cell composed of N point charges q_i, for $i \in [\![1 \,..\, N]\!]$. We will look at the condition for the previous sum to converge. For this, we introduce $Q := \sum_{i=1}^N q_i$ the total charge of the unit cell U and $\mathrm{D} := \sum_{j=1}^N q_j r_j$ its dipolar moment.

To look at the convergence, we first do a Taylor expansion of the inverse function with respect to the cells.

Proposition II.B.1. — There exist two vectorial constants such that for any integers i and j, and with $C^1 = C^1(i,j)$ and $C^2 = C^2(i,j)$ such that asymptotically as $|n| \to +\infty$

$$\frac{1}{|r_j - r_i + n|} = \frac{1}{|n|} + \sum_{1 \le \gamma \le 3} C^1_\gamma \frac{n_\gamma}{|n|^3} + \sum_{1 \le \gamma, \gamma' \le 3} C^2_{\gamma,\gamma'} \frac{3 n_\gamma n_{\gamma'} - \delta_{\gamma\gamma'} |n|^2}{|n|^5} + \mathscr{O}\left(\frac{1}{|n|^4}\right). \tag{II.19}$$

Proof: Let $\bar{r} := \frac{1}{N} \sum_{1 \le i \le N} r_i$ and $\bar{r}_n := \bar{r} + n$ be respectively the centre of mass for the primitive unit cell U and its image by the vector n.

Then, using the notation $\Delta r_i \overset{\text{def.}}{=} r_i - \bar{r}$, $\Delta r_j \overset{\text{def.}}{=} r_j - \bar{r}$ and $\Delta_{ij} = \Delta \overset{\text{def.}}{=} \Delta r_i - \Delta r_j$, we have

$$\frac{1}{|r_j - r_i + n|} = \frac{1}{|(r_j - \bar{r}) + (\bar{r} - \bar{r}_n) + (\bar{r}_n - r_{in})|} = \frac{1}{|n - \Delta|} = \frac{1}{\sqrt{\sum_{\gamma=1}^3 (n_\gamma - \Delta_\gamma)^2}}. \tag{II.20}$$

If we now omit the sum on γ, to lighten the notations, we have

$$\frac{1}{|r_j - r_i + n|} = \frac{1}{\sqrt{(n_\gamma - \Delta_\gamma)\, \delta^{\gamma\gamma'} (n_{\gamma'} - \Delta_{\gamma'})}} = \frac{|n|^{-1}}{\sqrt{1 - 2\frac{n_\gamma \delta^{\gamma\gamma'} \Delta_{\gamma'}}{|n|^2} + \frac{\Delta_\gamma \delta^{\gamma\gamma'} \Delta_{\gamma'}}{|n|^2}}}. \tag{II.21}$$

Finally, we find by a Taylor expansion as $|n| \to +\infty$ that

$$\begin{aligned}\frac{1}{|r_j - r_i + n|} &= \frac{|n|^{-1}}{1 - \frac{n_\gamma \delta^{\gamma\gamma'} \Delta_{\gamma'}}{|n|^2} + \frac{1}{2}\left(\frac{\Delta_\gamma \delta^{\gamma\gamma'} \Delta_{\gamma'}}{|n|^2} - \frac{n_\gamma \delta^{\gamma\gamma'} \Delta_{\gamma'} n_\upsilon \delta^{\upsilon\upsilon'} \Delta_{\upsilon'}}{|n|^4}\right) + \mathcal{O}\left(|n|^{-3}\right)} \\ &= \frac{1}{|n|} + \frac{n_\gamma \delta^{\gamma\gamma'} \Delta_{\gamma'}}{|n|^3} - \frac{1}{2}\left(\frac{\Delta_\gamma \delta^{\gamma\gamma'} \Delta_{\gamma'}}{|n|^3} - \frac{n_\gamma \delta^{\gamma\gamma'} \Delta_{\gamma'} n_\upsilon \delta^{\upsilon\upsilon'} \Delta_{\upsilon'}}{|n|^5}\right) + \left(\frac{n_\gamma \delta^{\gamma\gamma'} \Delta_{\gamma'}}{|n|^{5/2}}\right)^2 + \mathcal{O}\left(|n|^{-4}\right) \\ &= \frac{1}{|n|} + \frac{n_\gamma \delta^{\gamma\gamma'} \Delta_{\gamma'}}{|n|^3} + \frac{3 n_\gamma n_\upsilon \delta^{\gamma\gamma'} \delta^{\upsilon\upsilon'} - \delta^{\upsilon'\gamma'} |n|^2}{2|n|^5} \Delta_{\gamma'} \Delta_{\upsilon'} + \mathcal{O}\left(|n|^{-4}\right).\end{aligned} \tag{II.22}$$

This concludes the proof of this proposition. ■

From this result we can deduce the following proposition.

Proposition II.B.2. — There is a vectorial constant C such that for all vector $n \in \mathbf{R}^3 \setminus \{0\}$

$$\sum_{1 \le i,j \le N} \frac{q_i q_j}{|r_j - r_i + n|} = \frac{Q^2}{|n|} + \sum_{1 \le \gamma, \gamma' \le 3} \frac{3 n_\gamma n_{\gamma'} - \delta_{\gamma\gamma'} |n|^2}{|n|^5} \left(Q C_{\gamma,\gamma'} - \mathrm{D}_\gamma \mathrm{D}_{\gamma'}\right) + \mathcal{O}\left(\frac{1}{|n|^4}\right). \tag{II.23}$$

Proof: This result is a direct consequence of the previous proposition. ■

This result implies the series from Eq. (II.18) can only converge with respect to n if the primitive unit cell is neutral, *i.e.*, $Q = 0$. Moreover, even in this case it will only be conditionally convergent in most cases because $r \mapsto 1/|r|^3$, which is present in the second term of the sum, is not integrable on $\mathbf{R}^3$. We will explain in the following the notion of conditional convergence.

We note that when $Q \neq 0$, even as the energy series diverges, the problem may still be of interest, as explained by Wolf et al. [Wol+99].

Definition II.B.7. — We introduce different notion of convergence for series.

(I) A series $\sum_{n \in \mathbf{N}} a_n$ is convergent if the limit $\lim_{N \to +\infty} \sum_{0 \le n \le N} a_n$ exists and is finite.

(II) A series is absolutely convergent if the series $\sum_{n \in \mathbf{N}} |a_n|$ is convergent.

(III) A series is conditionally convergent if it is convergent but not absolutely convergent.

A conditionally convergent series makes the computation of its sum more difficult due to the following theorem.

Theorem II.B.4 (Riemann series theorem). — Let (a_n) be a conditionally convergent series. Then, for all $\ell_1, \ell_2 \in \mathbf{R} \cup \{-\infty, +\infty\}$, there exists a permutation σ of $\mathbf{N}$ such that

$$\ell_1 = \liminf_{N \to +\infty} \sum_{n=0}^{N} a_{\sigma(n)} \quad \text{and} \quad \ell_2 = \limsup_{N \to +\infty} \sum_{n=0}^{N} a_{\sigma(n)}. \tag{II.24}$$

Admitted proof: See for example the book of Ponnusamy [Pon12]. □

Thus, in addition to the geometry of the primitive cell, the order in which we do the summation is essential.

As it is often the case in literature, in the following we will assume that the primitive unit cell U is cubic and such that

$$U = \left\{ r = s_1 a^1 + s_2 a^2 + s_3 a^3 \;\middle|\; -\frac{1}{2} \leq s_\gamma \leq \frac{1}{2},\ \gamma = 1,2,3 \right\}. \tag{II.25}$$

This choice does not change the underlying results, but may change the values of some quantities that we will compute, such as the *surface term* that can be seen as the representation of the distribution of charges on the macroscopic surface of the system. Regarding the summation, it is usual in the literature to use sums in spheres of radius $N \in \mathbf{N}$ (such that $|n|^2 \leq N$) or cubes of length $2N$ (for which $\max_{\gamma\in\{1,2,3\}}|n_\gamma| \leq N$). We refer the reader to Section II.D.1 for a more detailed discussion about this point.

II.B.4 EWALD's summation

Definition and convergence

EWALD [Ewa21] proposed a method of summation in 1921 to rewrite the computation of the periodic boundary conditions electrostatic energy as the sum of two series that converge quickly. One of them, the direct sum, only consists on summations for a small number of particles; often the ones in the primitive unit cell. The second, the reciprocal sum, has a function regular enough for its FOURIER transform to also converge quickly.

This technique however consists in reordering the sum, so it is equivalent only if the sum is absolutely convergent, which is the case only if the dipolar moment of the primitive unit cell U is zero.

The separation of the energy by EWALD into two sums is done by using the error function, and this is what we present here. However, we could have considered other functions, see for example [HE88].

Definition II.B.8 (EWALD energy). — We will call EWALD energy the quantity

$$\mathcal{E}_{\text{Ewald}}(\underline{r}^{\{N\}}) := \frac{1}{2}{\sum_n}' \sum_{1\leq i,j\leq N} q_i q_j \frac{\operatorname{erfc}(\alpha^{1/2}|r_{jin}|)}{|r_{jin}|} - \left(\frac{\alpha}{\pi}\right)^{1/2} \sum_{j=1}^{N} q_j^2 + \frac{1}{2\pi V} \sum_{m\neq 0} \frac{\exp(-\pi^2|m|^2/\alpha)}{|m|^2} |S(m)|^2, \tag{II.26}$$

where the structure factor $S(m)$ is defined as

$$S(m) := \sum_{j=1}^{N} q_j \exp(2i\pi m \cdot r_j), \tag{II.27}$$

and α is a positive real called *EWALD coefficient*. The third term of the sum is called *reciprocal energy* and noted $\mathcal{E}_r$. The quantity $\mathcal{E}_d := \mathcal{E}_{\text{Ewald}} - \mathcal{E}_r$ is the direct energy. The constant term of the direct energy is sometimes called self-term, and noted $\mathcal{E}_{\text{self}}$. It has no physical meaning, and is a side effect of the reordering of the sum.

As we will show in the following, the two series converge quickly. But first, we need the following theorem of comparison between series and integrals.

Theorem II.B.5. — Let $f\colon \mathbf{R}_+ \to \mathbf{R}_+$ be a decreasing function. Then, the integral $\int_0^{+\infty} f$ and the series $\sum_{n\in\mathbf{N}} f(n)$ have the same kind of convergence.

ADMITTED PROOF: This is a classical theorem on series. See for example the lecture of ARNAUDIÈS and FRAYSSE [AF93, chap. VIII]. □

Proposition II.B.3. — The series of the EWALD energy are absolutely convergent.

PROOF: To show this, it is sufficient to show that each of the two series are absolutely convergent. Using the previous theorem of comparison, this is true if the associated functions are integrable at infinity.

First, for the reciprocal sum, it suffices to notice that the function $r \mapsto \exp(-\pi^2|r|^2/\alpha)/|r|^2$ is integrable for all $\alpha \in \mathbf{R}_+^*$

$$\int_{\mathbf{R}^3} \frac{\exp(-\pi^2|r|^2/\alpha)}{|r|^2}\,\mathrm{d}^3r = 4\pi\int_0^{+\infty} \exp(-\pi^2 r^2/\alpha)\,\mathrm{d}r = 2\alpha^{1/2}\sqrt{\pi}. \tag{II.28}$$

We do the same for the direct sum. Let $\alpha \in \mathbf{R}_+^*$ and $\mathbf{B}^3 \subset \mathbf{R}^3$ be the unit ball, then we have

$$\begin{aligned}
\int_{\mathbf{R}^3\setminus\mathbf{B}^3} \frac{\operatorname{erfc}(\alpha^{1/2}|r|)}{4\pi|r|}\,\mathrm{d}^3r &= \int_1^{+\infty} r\cdot\operatorname{erfc}(\alpha^{1/2}r)\,\mathrm{d}r = \left[\frac{r^2}{2}\operatorname{erfc}(\alpha^{1/2}r)\right]_1^{+\infty} - \int_1^{+\infty}\frac{r^2}{2}\left(-\frac{2}{\sqrt{\pi}}\alpha^{1/2}e^{-\alpha r^2}\right)\mathrm{d}r \\
&= \frac{-\operatorname{erfc}(\alpha^{1/2})}{2} + \frac{1}{\sqrt{\pi}}\int_1^{+\infty} r\cdot\alpha^{1/2}re^{-\alpha r^2}\,\mathrm{d}r \\
&= \frac{-\operatorname{erfc}(\alpha^{1/2})}{2} + \frac{1}{\sqrt{\pi}}\left[-r\frac{e^{-\alpha r^2}}{2\alpha^{1/2}}\right]_1^{+\infty} + \frac{1}{\sqrt{\pi}}\int_1^{+\infty}\frac{e^{-\alpha r^2}}{2\alpha}\,\mathrm{d}r \\
&= \frac{1-2\alpha}{4\alpha}\operatorname{erfc}(\alpha^{1/2}) + \frac{\exp(-\alpha)}{2\alpha^{1/2}\sqrt{\pi}}.
\end{aligned} \tag{II.29}$$

Hence, we have the result. ■

We notice a singularity in the direct sum as the EWALD coefficient α goes to zero. This is consistent with the fact that the series of $\mathcal{E}(\underline{r}^{\{N\}})$ is in general conditionally convergent.

Moreover, as will be shown just below, the function erfc has the same behaviour as the function $\exp(-\cdot^2)$. Hence, increasing the EWALD coefficient *crushes* exponentially quickly the direct energy, whereas the increase in the reciprocal sum is sub-linear.

Proposition II.B.4. — We have the equivalence

$$\operatorname{erfc}(\alpha^{1/2}) \sim \frac{\exp(-\alpha)}{\alpha^{1/2}\sqrt{\pi}}, \tag{II.30}$$

as α goes to infinity.

Proof: Let $\alpha > 0$ be a strictly positive number. Then using the property that the product of any polynomial function with $\exp(-\cdot^2)$ is integrable on $\mathbf{R}$, we have

$$\begin{aligned}\operatorname{erfc}(\alpha^{1/2}) &= \frac{\int_\alpha^{+\infty} t^{-1/2} e^{-t}\,\mathrm{d}t}{\sqrt{\pi}} = e^{-\alpha}\int_0^{+\infty} \frac{e^{-t^2}}{\sqrt{\alpha+t^2}}\,\mathrm{d}t = \frac{2e^{-\alpha}}{\alpha^{1/2}\sqrt{\pi}}\int_0^{+\infty} t\left(1-\frac{t^2}{2\alpha^{1/2}}+\mathscr{O}\left(\alpha^{-1}\right)\right)e^{-t^2}\,\mathrm{d}t \\ &= \frac{e^{-\alpha}}{\alpha^{1/2}\sqrt{\pi}}+\mathscr{O}\left(\alpha^{-1}\right).\end{aligned} \tag{II.31}$$

This concludes the proof. ■

Hence, the Ewald coefficient is a parameter that influences the cost of computing the direct or reciprocal sum in the evaluation of the energy. We also note that when $\alpha \to 0$, we recover the naive summation. In the literature, when doing molecular dynamics for molecular systems, α is often chosen such that the point charges further than 9 ångströms can be neglected in the direct sum.

Electrostatic energy of a periodic system

We now look at how to derive the Ewald energy by splitting the inverse function in two using the error function. The first demonstration is due to Smith [Smi81] in 1981, who used Legendre transforms. Here, we follow the proof of Darden [Dar08].

Lemma II.B.1. — For all non-zero vector r, we have the identity

$$\frac{1}{|r|} = \frac{\operatorname{erfc}(\alpha^{1/2}|r|)}{|r|} + \frac{1}{\pi}\sum_m \int_{U^*} \frac{\exp(-\pi^2|v+m|^2/\alpha)}{|v+m|^2}\exp(-2i\pi(v+m)\cdot r)\,\mathrm{d}^3v, \tag{II.32}$$

where the sum for m is on all covectors of which we will omit the indices.

We note the existence of an analogue formula for any function $r \mapsto 1/|r|^p$, for all $p > 0$. We refer to the articles of Essmann et al. [Ess+95] and of Darden [Dar08]. This enables the use of the same method for other energies, such as the Van der Waals energy. However, due to the quick decrease of such energies, this splitting is in practice only done for the electrostatic energy.

The proof is as follow.

Proof: Let Γ be the gamma function. We have [Col21b]

$$\sqrt{\pi} = \Gamma(1/2) = \int_0^{+\infty} t^{-1/2}e^{-t}\,\mathrm{d}t = \lambda^{1/2}\int_0^{+\infty} t^{-1/2}e^{-\lambda t}\,\mathrm{d}t. \tag{II.33}$$

Hence, if we replace λ with $|r|^2$,

$$\begin{aligned}\frac{1}{|r|} &= \frac{1}{\sqrt{\pi}}\left(\int_\alpha^{+\infty}+\int_0^\alpha\right)t^{-1/2}\exp(-|r|^2t)\,\mathrm{d}t \\ &= \frac{1}{\sqrt{\pi}}\int_\alpha^{+\infty} t^{-1/2}e^{-|r|^2t}\,\mathrm{d}t + \frac{1}{\sqrt{\pi}}\int_0^\alpha t^{-1/2}\left(\frac{\pi}{t}\right)^{3/2}\int_{\mathbf{R}^3} e^{-\pi^2|u|^2/t}e^{-2i\pi u\cdot r}\,\mathrm{d}^3v\,\mathrm{d}t.\end{aligned} \tag{II.34}$$

By using Fubini's theorem [Col21a], and after a change of variables, we obtain

$$\begin{aligned}\frac{1}{|r|} &= \frac{1}{\sqrt{\pi}} \int_{\alpha^{1/2}|r|}^{+\infty} \frac{2}{|r|} e^{-s^2} \,\mathrm{d}s + \pi \int_{\mathbf{R}^3} \int_{\pi|u|/\alpha^{1/2}}^{+\infty} \frac{2s}{\pi^2|u|^2} e^{-s^2} e^{-2i\pi u\cdot r} \,\mathrm{d}s \,\mathrm{d}^3u \\ &= \frac{\operatorname{erfc}(\alpha^{1/2}|r|)}{|r|} + \frac{\pi}{\alpha} \int_{\mathbf{R}^3} e^{-2i\pi u\cdot r} \frac{e^{-\pi^2|u|^2/\alpha}}{\pi^2|u|^2/\alpha} \,\mathrm{d}^3u \\ &\underset{\text{Fubini}}{=} \frac{\operatorname{erfc}(\alpha^{1/2}|r|)}{|r|} + \frac{1}{\pi} \sum_m \int_{U^*} \frac{\exp(-\pi^2|v+m|^2/\alpha)}{|v+m|^2} \exp\left(-2i\pi(v+m)\cdot r\right) \mathrm{d}^3v.\end{aligned} \tag{II.35}$$

We notice that the sum is well defined, as the function under the integral is integrable on U^* for $m = 0$, because $v \mapsto |v|^{-2} \in \mathrm{L}^1_{\mathrm{loc}}(\mathbf{R}^3)$. Hence, we obtain the lemma. ■

We refer to Figs. II.2 and II.3 for respectively one- and two-dimensional examples of the splitting of the inverse function using the error function.

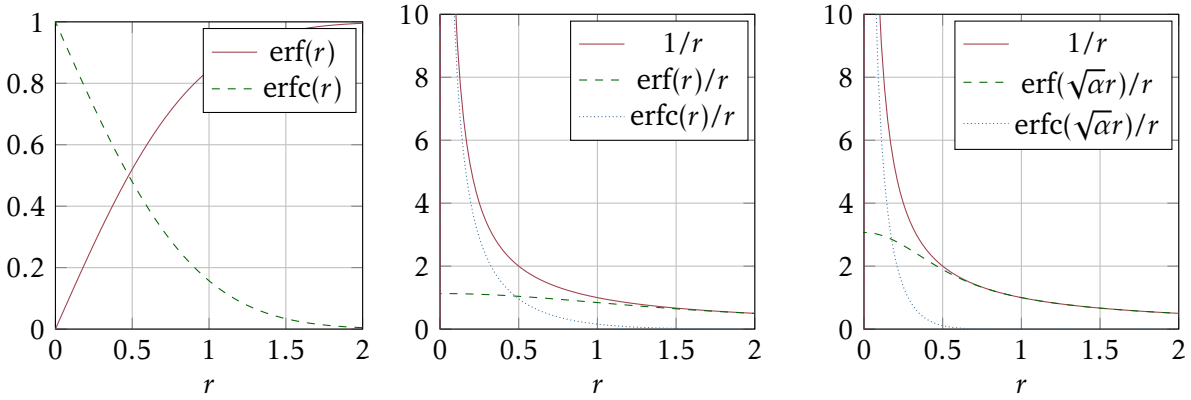

(a) Error function and its complementary

(b) Range separation with $\alpha = 1$

(c) Range separation with $\alpha = 7.42$ for a truncation at 1.0 ångström

Figure II.2: Range separation in 1D

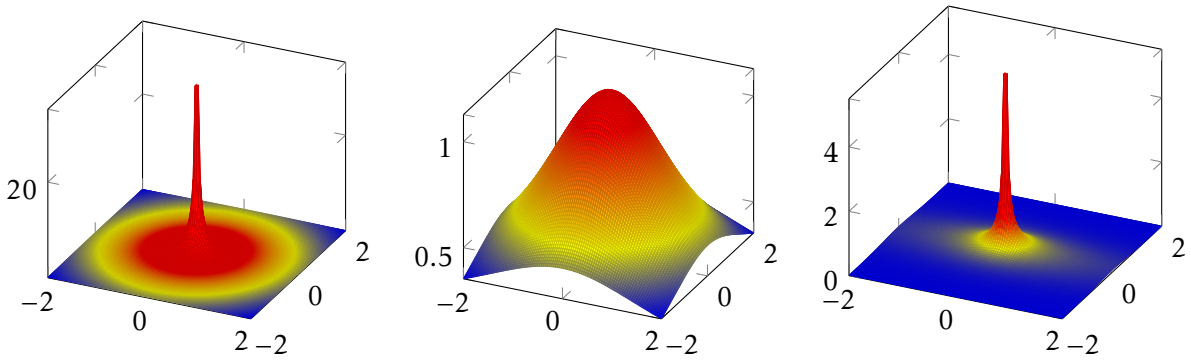

(a) Function $r \mapsto 1/r$

(b) Function $r \mapsto \operatorname{erf}(r)/r$

(c) Function $r \mapsto \operatorname{erfc}(r)/r$

Figure II.3: Range separation in 2D

Physically, what we have done is to split the potential in two using the identity $\operatorname{erf} + \operatorname{erfc} \equiv 1$. The function $r \mapsto \operatorname{erfc}(r)/r$ decreases quickly and can thus be truncated when r is large enough. In the reciprocal sum, we can see the Fourier transform of $v \mapsto \frac{\exp(-\pi^2|v+m|^2/\alpha)}{|v+m|^2}$. This will enable

us to use fast Fourier transforms, which will decrease the computational complexity required to compute the electrostatic energy of a periodic boundary conditions molecular system.

This explains that in the literature, the direct energy is often said to take into account particles that are close together and the reciprocal energy the long-range interactions. However, the reciprocal energy also includes Fourier modes of short-range interactions.

To account for the order of summation, which can be thought as the macroscopic shape of the system, we introduce the following notation.

Notation. — For a set $P \subset \mathbf{R}^3$ and a strictly positive integer K, we define the set

$$\Omega(P,K) := \left\{ n = \sum_{1\leq\gamma\leq 3} n_\gamma a_\gamma \;\middle|\; \begin{array}{c} (n_\gamma)_{1\leq\gamma\leq 3} \in \mathbf{Z}^3 \\ |n|/K \in P \end{array} \right\}. \tag{II.36}$$

The energy $\mathcal{E}_{P,K}$ of a lattice $\underline{r}^{\{N\}}$ in the volume $\Omega(P,K)$ is defined as

$$\mathcal{E}_{P,K}(\underline{r}^{\{N\}}) := \frac{1}{2} {\sum_{n\in\Omega(P,K)}}' \sum_{1\leq i,j\leq N} \frac{q_i q_j}{|r_j - r_i + n|}, \tag{II.37}$$

and $J(\mathrm{D},P,K)$ is the quantity

$$\frac{J(\mathrm{D},P,K)}{2\pi} := \sum_{n\in\Omega(P,K)} \int_{U^*} \frac{(v\cdot \mathrm{D})^2}{|v|^2} \exp(-2i\pi v\cdot n)\,\mathrm{d}^3 v. \tag{II.38}$$

We have now all the tools to show the central result for the Ewald's summation method.

Theorem II.B.6 (Smith). — Let P be a symmetric compact subset of $\mathbf{R}^3$, that is $r \in P$ if and only if $-r \in P$. Then for any lattice $\underline{r}^{\{N\}}$,

$$\mathcal{E}_{P,K}(\underline{r}^{\{N\}}) = \mathcal{E}_{\mathrm{Ewald}}(\underline{r}^{\{N\}}) + J(\mathrm{D},P,K) + \varepsilon(K), \tag{II.39}$$

where $\varepsilon(K) \underset{K\to+\infty}{\longrightarrow} 0$.

As for the previous lemma, we use the proof of Darden [Dar08], which is less general than this one originally proposed by Smith [Smi81]. We will use the classical Dirichlet's theorem.

Theorem II.B.7 (Dirichlet's theorem). — Let f be a periodic and locally integrable function, $\mathscr{C}^1$ by parts, *i.e.*, $f \in \mathrm{L}^1_{\mathrm{loc}}(\mathbf{R}/\mathbf{Z}) \cap \mathscr{C}^1_{\mathrm{pm}}$. Then, for any $t \in \mathbf{R}/\mathbf{Z}$,

$$\lim_{n\to\infty} \sum_{k=-n}^{n} \mathcal{F}(f)(k) \exp(2i\pi k t) = \frac{f(t^-) + f(t^+)}{2}, \tag{II.40}$$

where

$$f(t^\pm) = \lim_{s\to t^\pm} f(t). \tag{II.41}$$

Admitted proof. □

Proof of Theorem II.B.6: First, we introduce the notation $h_{m,r}$ for the second term of the

equality in Eq. (II.32) as

$$h_{m,r}(v) \overset{\text{def.}}{=} \frac{\exp(-\pi^2|v+m|^2/\alpha)}{|v+m|^2}\exp(-2i\pi(v+m)\cdot r). \tag{II.42}$$

We want to reorder the terms of the sum to simplify it as a sum of $h_{m,r}(0)$. However, for $m = 0$, the function is not well defined.

This term is what will result in what is called the *surface term*. As it corresponds to the zeroth Fourier mode of the expression of the Gaussian potential in Fourier, it cannot be known using the Poisson equation in Fourier. This explains its absence in the derivations of the Ewald sum: it was arbitrarily set to zero. We will come back to it later.

We notice that for any relative integers n and m, we have $\exp(-2i\pi m\cdot n) = 1$, so with V the volume of the unit cell

$$\begin{aligned} I &\overset{\text{def.}}{=} \sum_n \sum_{m\neq 0} \int_{U^*} h_{m,r}(v)\exp(-2i\pi(v+m)\cdot n)\,\mathrm{d}^3v = \frac{1}{V}\sum_n\sum_{m\neq 0}\mathcal{F}\left(h^p_{m,r}\right)(n) \\ &\underset{\text{Fubini}}{=} \frac{1}{V}\sum_{m\neq 0}\sum_n \mathcal{F}\left(h^p_{m,r}\right)(n)\exp(2i\pi 0\cdot n) \\ &\underset{\text{Thm. II.B.7}}{=} \frac{1}{V}\sum_{m\neq 0} h_{m,r}(0). \end{aligned} \tag{II.43}$$

Moreover, at $v = 0$, the Taylor expansion with respect to v is

$$h_{0,r}(v) = \frac{1-2i\pi v\cdot r - 2\pi^2(v\cdot r)^2}{|v|^2} - \frac{\pi^2}{\alpha} + \theta(v), \tag{II.44}$$

where the θ function is smooth, bounded for any order of derivation and $\theta(0) = 0$.

Thus, if $r \neq 0$, using Lemma II.B.1, we find that

$$\begin{aligned} \zeta(r) &\overset{\text{def.}}{=} \sum_{n\in\Omega(P,K)} \frac{1}{|r+n|} \\ &= \sum_n \frac{\operatorname{erfc}(\alpha^{1/2}|r+n|)}{|r+n|} + \frac{I}{\pi} + \frac{1}{\pi}\sum_{n\in\Omega(P,K)}\int_{U^*} h_{0,r}(v)\exp(-2i\pi v\cdot n)\,\mathrm{d}^3v + \varepsilon_{1,r}(\alpha,K), \end{aligned} \tag{II.45}$$

with $\varepsilon_{1,r} = o(1)$ the error made by doing in the first term above the summation on all terms, and not only on $n \in \Omega(P,K)$. Hence, we have

$$\begin{aligned} \zeta(r) = \sum_n \frac{\operatorname{erfc}(\alpha^{1/2}|r+n|)}{|r+n|} - \frac{\pi}{\alpha V}\sum_{n\in\Omega(P,K)}\delta(n) \\ + \frac{1}{\pi V}\sum_{m\neq 0}\frac{\exp(-\pi^2|m|^2/\alpha)}{|m|^2}\exp(-2i\pi m\cdot r) + \frac{1}{\pi}H_{P,K}(r) + \varepsilon_{2,r}(\alpha,K), \end{aligned} \tag{II.46}$$

where

$$H_{P,K}(r) \overset{\text{def.}}{=} \sum_{n\in\Omega(P,K)}\int_{U^*}\frac{1-2i\pi v\cdot r - 2\pi^2(v\cdot r)^2}{|v|^2}\exp(-2i\pi v\cdot n)\,\mathrm{d}^3v, \tag{II.47}$$

and

$$\varepsilon_{2,r}(\alpha,K) \overset{\text{def.}}{=} \varepsilon_{1,r}(\alpha,K) + \frac{1}{\pi V}\sum_{n\in\Omega(P,K)}\mathcal{F}(\theta^p)(n) = o(1). \tag{II.48}$$

Finally, we obtain

$$\zeta(r) = \sum_n \frac{\operatorname{erfc}(\alpha^{1/2}|r+n|)}{|r+n|} - \frac{\pi}{\alpha V} + \frac{1}{\pi V}\sum_{m\neq 0}\frac{\exp(-\pi^2|m|^2/\alpha)}{|m|^2}\exp(-2i\pi m\cdot r) + \frac{1}{\pi}H_{P,K}(r) + \varepsilon_{2,r}(\alpha,K). \quad \text{(II.49)}$$

To compute $\mathcal{E}_{P,K}$, we can use the function

$$\widetilde{\phi}(r) \overset{\text{def.}}{=} \sum_{i=1}^{N} q_i \zeta(r-r_i). \quad \text{(II.50)}$$

As the sum in the ζ function is for all n, to get the potential at $i=j$, we have to substract its own contribution — which will gives the self-energy. This gives us

$$\begin{aligned}\phi(r_j) &= \lim_{r\to r_j}\left(\widetilde{\phi}(r) - \frac{q_j}{|r-r_j|}\right)\\ &= \sum_{\substack{1\leq i\leq N\\ n\neq 0}} q_i\frac{\operatorname{erfc}(\alpha^{1/2}|r_{jin}|)}{|r_{jin}|} + \sum_{\substack{1\leq i\leq N\\ i\neq j}} q_i\frac{\operatorname{erfc}(\alpha^{1/2}|r_{ji}|)}{|r_{ji}|} - \lim_{r\to r_j}\left(q_j\frac{\operatorname{erf}(\alpha^{1/2}|r-r_j|)}{|r-r_j|}\right)\\ &\quad + \frac{1}{\pi V}\sum_{m\neq 0}\frac{\exp(-\pi^2|m|^2/\alpha)}{|m|^2}\exp(-2i\pi m\cdot r_j)S(m)\\ &\quad + \sum_{1\leq i\leq N} q_i\frac{\pi}{\alpha V} + \frac{1}{\pi}\sum_{1\leq i\leq N} q_i H_{P,K}(r-r_i) + \sum_{1\leq i\leq N} q_i\varepsilon_{2,r_{ji}}(\alpha,K).\end{aligned} \quad \text{(II.51)}$$

As we assume the primitive unit cell to be neutral, the fifth term in the previous equation is null and there is a simplification on the last, which means that we can rewrite the previous quantity as

$$\begin{aligned}\phi(r_j) &= {\sum_{\substack{1\leq i\leq N\\ n}}}' q_i\frac{\operatorname{erfc}(\alpha^{1/2}|r_{jin}|)}{|r_{jin}|} - 2q_j\left(\frac{\alpha}{\pi}\right)^{1/2} + \frac{1}{\pi V}\sum_{m\neq 0}\frac{\exp(-\pi^2|m|^2/\alpha)}{|m|^2}\exp(-2i\pi m\cdot r_j)S(m)\\ &\quad + \sum_{\substack{n\in\Omega(P,K)\\ 1\leq i\leq N}} q_i\int_{U^*}\frac{2iv\cdot r_i - 2\pi(v\cdot(r_j-r_i))^2}{|v|^2}\exp(-2i\pi v\cdot n)\,\mathrm{d}^3v + \sum_{1\leq i\leq N} q_i\varepsilon_{2,r_{ji}}(\alpha,K).\end{aligned} \quad \text{(II.52)}$$

Finally, we notice that

$$\begin{aligned}C &\overset{\text{def.}}{=} \sum_{1\leq i,j\leq N} q_iq_j(v\cdot r_j - v\cdot r_i)^2 = 2\sum_{1\leq i\leq N} q_i\sum_{1\leq j\leq N} q_j(v\cdot r_j)^2 - 2(v\cdot \mathrm{D})^2\\ &= -2(v\cdot\mathrm{D})^2,\end{aligned} \quad \text{(II.53)}$$

and the theorem is proven, taking

$$\varepsilon := \sum_{1\leq i,j\leq N} q_iq_j\varepsilon_{2,v_{ji}}. \quad \text{(II.54)}$$

■

This proof also gives a sound derivation of the *surface term* which takes into account the geometry of the unit cell and the order of summation. It is defined as follow.

Notation (Surface term). — In the following, we use if it exists, $J(\mathrm{D}, P)$ the limit

$$J(\mathrm{D}, P) := \lim_{K \to +\infty} J(\mathrm{D}, P, K). \tag{II.55}$$

It is called the *surface term*.

As we have already observed, the electrostatic energy is unambiguously defined when the sums are absolutely convergent, which can be seen by the cancellation of the surface term when the dipolar moment is null. When this is not the case, it is possible to cancel the surface term by considering that the system is embedded in a medium of infinite vacuum permittivity, the tinfoil model. This method, evoked in the article of de Leeuw et al. [dLee+80], and is developed in Section II.D.1.

In Fig. II.4, we show different summations, that impact the computations of the surface term. In particular, we should not confuse spherical summation with spherical truncation.

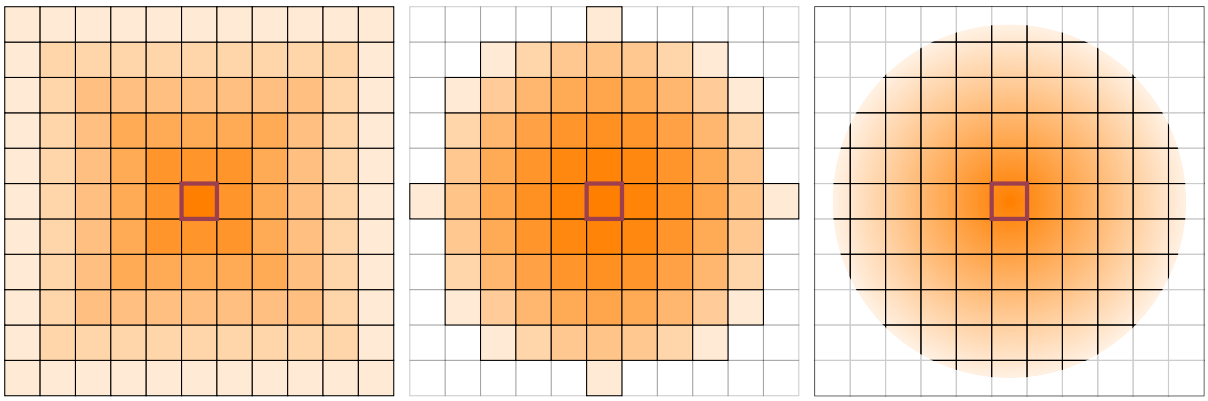

(a) Square summation with $N = 5$

(b) Spherical summation with $N = 5^2$ corresponding to the domain $\Omega(\mathbf{B}^3, 5)$

(c) Spherical truncation with $R = 5$ boxes

Figure II.4: Different methods of summation. We only sum particles inside the orange domain.

As we can observe in Eq. (II.26), there is no restriction for the choice of Ewald coefficient α. The bigger it is, the more terms of the reciprocal series have to be computed for a given precision. The optimum coefficients highly depend on the size and the homogeneity of the system that we consider. For instance, Saunders et al. [Sau+92] have obtained good results with $\alpha = 2^8/V^{2/3}$. An interesting case is due to Perram, Petersen, and De Leeuw [PPD88], where they have shown that by chosing an adequate α, they were able to decrease the computational complexity for the computation of the energy to $N^{3/2}$.

We insist on the fact that an optimal coefficient is highly dependent on the system we look at and some considerations are purely empirical. For a detailed discussion on the subject, we refer to the article from Kolafa and Perram [KP92].

In practice, for molecular dynamics of molecular systems, the Ewald coefficient is often chosen to respect the *minimum image convention*. That is to only have to compute interactions between particles that are at a distance smaller than the length of the unit cell.

By using a *neighbour list* that is updated at each step in a molecular dynamics, this enables the computation of the direct sum to have a linear computational complexity in the numbers of particles of the primitive unit cell.

In the following section, we will look at methods that decrease the computational cost for the reciprocal sum, using fast Fourier transforms.

II.C Efficient evaluation of reciprocal sum

We present three different methods to compute the reciprocal sum with algorithms of computational complexity in $N\log(N)$, where N is the number of particles in a primitive unit cell. All the methods build on fast FOURIER transforms, where either the potential or the density is split.

Those methods use a mesh of the primitive unit cell of size which depends mostly on its density. Hence to be more accurate, in three dimensions, the computational complexity is in $K_1K_2K_3\log(K_1K_2K_3)$, where K_i, for $i \in \{1, 2, 3\}$ is the inverse of the length of the mesh in each direction of primitive vectors. At constant particles density, the more atoms there are in a unit cell, the thinner the mesh has to be to have comparable accuracy.

In molecular simulations, the size of the mesh is often chosen around 1 ångström, which empirically gives a density of less than one atom per cube of the mesh. We refer to Fig. II.5 for an extrapolation of the mesh size based on this observation.

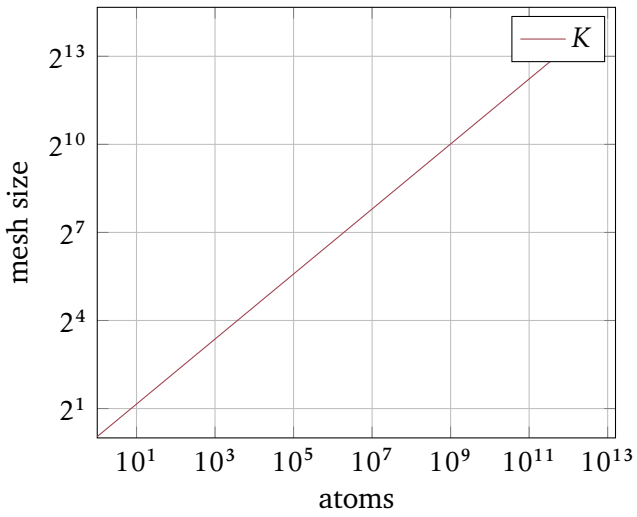

Figure II.5: Extrapolation of the mesh size for a density of 0.91 atom/Å^3

Under those conditions, for one billion particles, we would need a mesh of 1024^3, which is easily accessible on personal computers. This nice property comes from the smoothness of the reciprocal sum, which enables the use of a coarse mesh to accurately compute it with fast FOURIER transforms.

At the heart of all those methods is work from EASTWOOD, HOCKNEY, and LAWRENCE [EHL79] in the 1970s and 1980s, which we briefly describe in the next section.

II.C.1 Particle-particle–particle-mesh

The particle-particle–particle-mesh method, published in 1979 by EASTWOOD, HOCKNEY, and LAWRENCE [EHL79] is one of the first to try to approximate the full electrostatic potential from a density of charges, and not to rely on a cutoff of the electrostatic potential energy. The method is extensively described in the book of HOCKNEY and EASTWOOD [HE88].

The method improves on the *particle-mesh* method of HOCKNEY, GOEL, and EASTWOOD [HGE73], which consists in computing the electrostatic energy at the nodes of a mesh for particles. Hence, to be able to accurately compute close interactions, a fine mesh has to be used, as only the variations bigger than the size of the mesh can be well described.

With particle-particle–particle-mesh, the energy of close charges is computed exactly. As in the case for the EWALD's summation method, a function has to be chosen to split the potential. In

their work, Eastwood, Hockney, and Lawrence use a function that corresponds to a continuous potential with compact support in a sphere.

Other functions are mentioned, although no derivation is done, such as a uniformly charged sphere and another that we used for the Ewald's summation method we presented: the Gaussian density. According to Pollock and Glosli [PG96], those different functions do not seem to have advantage over each other.

The sketch of the method is to (I) assign charges to grid points from the density; (II) solve the Poisson equation at the nodes of the grid; (III) compute the forces at the nodes; (IV) interpolate back the forces at the particles positions.

II.C.2 Interpolation of the energy

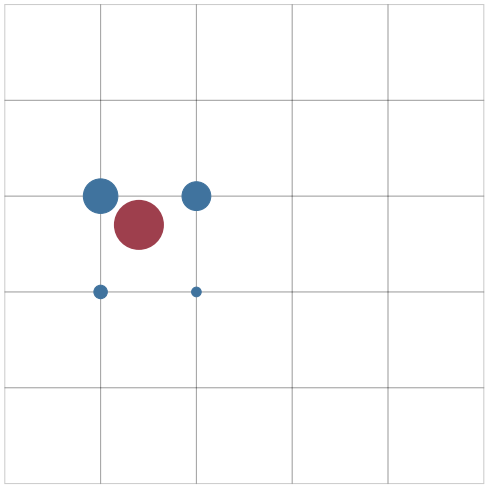

Figure II.6: Schematics for the interpolation in two dimensions on four points. The charge is in red, and the interpolated points are shown in blue.

The most commonly used method in chemistry for molecular dynamics simulations of molecular systems is the smooth particle mesh Ewald [Ess+95], that we will describe in details below. It is easy to implement and provides by default energy conservation, which may explain why it is often the method of reference.

The method builds on the particle mesh Ewald [DYP93] method from the same authors, which as we will see in the following section had some limitations that had to be addressed for molecular dynamics.

The main difference between the methods presented in this section is that while the particle-particle–particle-mesh interpolates the forces, the particle mesh Ewald and smooth particle mesh Ewald methods interpolate the energy.

Particle mesh Ewald

The particle mesh Ewald method proposed by Darden, York, and Pedersen [DYP93] in 1993, uses the same idea of particle-particle–particle-mesh to use a grid and perform fast Fourier transforms on it.

The Lagrange interpolation method is applied to the exponential function. After some manipulations, we can reformulate the reciprocal sum to obtain discrete Fourier transforms to be able to quickly compute the structure factor, which is the costly term to evaluate.

Proposition II.C.1 (Particle mesh EWALD). — There is a smooth by parts function Q and a smooth function ψ_r such that

$$\mathcal{E}_r(K) = \frac{1}{2}\sum_{m_1=0}^{K_1-1}\sum_{m_2=0}^{K_2-1}\sum_{m_3=0}^{K_3-1} Q(m)\cdot(\psi_r * Q)(m) + \varepsilon(K), \tag{III.1}$$

where $\varepsilon(K) \underset{K\to+\infty}{\longrightarrow} 0$.

PROOF: First, we look at the interpolation of the exponential in the one-dimensional case.

Let K be a strictly positive integer and $r \in \mathbf{R}$. We will do the interpolation at the nodes of a grid of constant length $1/K$. Let $\left(\ell^k_{p,K}\right)_{k=0,\dots,2p-1}$ be the LAGRANGE interpolation polynomials of order $2p$ associated to the points

$$\left(\frac{0}{K},\dots,\frac{2p-1}{K}\right), \tag{III.2}$$

with the convention that $\ell^k_{p,K} \equiv 0$ if $k<0$ or $k \geq 2p$.

Introducing $k_{p,K}(r) \overset{\text{def.}}{=} \lfloor Kr \rfloor - p + 1$, then for any $k \in \mathbf{Z}$ we denote

$$\theta_{p,K}(r,k) \overset{\text{def.}}{=} \ell^{k-k_{p,K}(r)}_{p,K}\left(r - \frac{k_{p,K}(r)}{K}\right). \tag{III.3}$$

This corresponds to doing an interpolation at the $(p-1)$-points of the grids before the point r and at the $p+1$ next, by translating the Lagrangian interpolants.

So there is a function $\varepsilon_{p,m}(K) = o(1)$ such that for all $m, r \in \mathbf{R}$,

$$\exp(2i\pi mr) = \sum_{k\in\mathbf{Z}} \theta_{p,K}(r,k)\exp\left(2i\pi m\frac{k}{K}\right) + \varepsilon_{p,m}(K). \tag{III.4}$$

For the error estimates of the method, we refer to the article of DARDEN [Dar08].

Hence, in three dimensions, with $(K_1,K_2,K_3) \in \mathbf{N}^3 \setminus \{0\}$, we have

$$\begin{aligned} S(m) &= \sum_{1\leq j\leq N} q_j \exp(2i\pi m\cdot r_j) = \sum_{\substack{1\leq j\leq N\\ k_1,k_2,k_3\in\mathbf{Z}}} q_j \prod_{1\leq\gamma\leq 3}\theta_{p,K_\gamma}(s_{j\gamma},k_\gamma)\exp\left(2i\pi m_\gamma\frac{k_\gamma}{K_\gamma}\right) + o(K)\\ &= \sum_{k_1=0}^{K_1-1}\sum_{k_2=0}^{K_2-1}\sum_{k_3=0}^{K_3-1} Q(k_1,k_2,k_3)\prod_{1\leq\gamma\leq 3}\exp\left(2i\pi m_\gamma\frac{k_\gamma}{K_\gamma}\right) + o(K)\\ &= \mathcal{F}_d(Q)(m_1,m_2,m_3) + o(K), \end{aligned} \tag{III.5}$$

where $\mathcal{F}_d(Q)$ is the discrete FOURIER transform of

$$Q(k_1,k_2,k_3) := \sum_{\substack{1\leq j\leq N\\ n_1,n_2,n_3\in\mathbf{Z}}} q_j \prod_{1\leq\gamma\leq 3}\theta_{p,K_\gamma}(s_{j\gamma},k_\gamma + n_\gamma K_\gamma). \tag{III.6}$$

Hence, denoting

$$\psi_r(n_1,n_2,n_3) \overset{\text{def.}}{=} \frac{1}{\pi V}\sum_{m\neq 0}\frac{\exp(-\pi^2|m|^2/\alpha)}{|m|^2}\exp\left(2i\pi\left(\frac{m_1n_1}{K_1}+\frac{m_2n_2}{K_2}+\frac{m_3n_3}{K_3}\right)\right), \tag{III.7}$$

and because (in one dimension to simplify) for all $m \in \mathbf{R}$

$$\begin{aligned}
\mathcal{F}_d^{-1}(\psi_r)(m) &= \frac{1}{K}\sum_{n=0}^{K-1}\psi_r(n)\exp\left(-2i\pi m\frac{n}{K}\right) = \frac{1}{K}\sum_{n=0}^{K-1}\frac{1}{\pi V}\sum_{q\neq 0}\frac{e^{-\pi^2q^2/\alpha}}{q^2}\exp\left(-2i\pi(m-q)\frac{n}{K}\right)\\
&= \frac{1}{\pi V}\sum_{q\neq 0}\frac{\exp(-\pi^2q^2/\alpha)}{q^2}\delta_m(q \mod K)\\
&= \begin{cases}\dfrac{1}{\pi V}\displaystyle\sum_{n\in\mathbf{Z}}\frac{\exp(-\pi^2(m+nK)^2/\alpha)}{(m+nK)^2} & \text{if } m\neq 0\\ \dfrac{1}{\pi V}\displaystyle\sum_{n\in\mathbf{Z}^*}\frac{\exp(-\pi^2(nK)^2/\alpha)}{(nK)^2} & \text{else}\end{cases},
\end{aligned} \tag{III.8}$$

we have

$$\mathcal{E}_r(K) \approx \frac{1}{2\pi V}\sum_{m\neq 0}\frac{\exp(-\pi^2|m|^2/\alpha)}{|m|^2}\mathcal{F}_d(Q)(m_1,m_2,m_3)\mathcal{F}_d(Q)(-m_1,-m_2,-m_3) + \varepsilon(K) \tag{III.9a}$$

$$\begin{aligned}
&= \frac{1}{2}\sum_{m_1=0}^{K_1-1}\sum_{m_2=0}^{K_2-1}\sum_{m_3=0}^{K_3-1}\mathcal{F}_d^{-1}(\psi_r)(m_1,m_2,m_3)\mathcal{F}_d(Q)(m_1,m_2,m_3)\mathcal{F}_d^{-1}(Q)(m_1,m_2,m_3) \qquad \text{(III.9b)}\\
&\qquad\qquad \times \mathcal{F}_d(Q)(m_1,m_2,m_3)K_1K_2K_3\mathcal{F}_d^{-1}(Q)(m_1,m_2,m_3+\varepsilon(K))\\
&= \frac{K_1K_2K_3}{2}\sum_{m_1=0}^{K_1-1}\sum_{m_2=0}^{K_2-1}\sum_{m_3=0}^{K_3-1}Q(m_1,m_2,m_3)\mathcal{F}_d\left(\mathcal{F}_d^{-1}(\psi_r\cdot\mathcal{F}_d^{-1}(Q))\right)(m_1,m_2,m_2)+\varepsilon(K). \qquad \text{(III.9c)}
\end{aligned}$$

Hence, we have the property. ■

Due to the use of Lagrange interpolation, the function Q is continuous and only regular by parts, which is not enough to be able to have accurate molecular dynamics. Thus, we have to interpolate the forces on their own, which means that we cannot have the energy conservation property.

However, the symmetry in the interpolation means that we do verify the second law of Newton to machine precision. That is for our isolated system

$$\sum_i\sum_j \mathrm{F}_{j\to i} = \sum_i m_i\frac{\mathrm{d}^2r_i}{\mathrm{d}t^2} = 0. \tag{III.10}$$

By using fast Fourier transform to compute Eq. (III.9a), we have a method of $\mathcal{O}(N\log N)$ computational complexity. Indeed, as Q is a real valued function, we have

$$\mathcal{E}_r(K) = \frac{1}{2\pi V}\sum_{m\neq 0}\frac{\exp(-\pi^2|m|^2/\alpha)}{|m|^2}|\mathcal{F}_d(Q)|^2(m) + \varepsilon(K). \tag{III.11}$$

The convergence of this series is quick with respect to m and we can truncate it to approximate the reciprocal energy.

The energy is written as in Proposition II.C.1, so the formula can be used again for the computations of the forces. Indeed, the ψ_r function does not depend on the positions of the particles and so the derivative of the convolution product with respect to the atoms positions is zero and the only difference between the computation of the energy and the forces will be in the expression of the function Q.

In Fig. II.7 we give a schematic representation of the interpolation scheme presented here, which explains graphically why the functions $\theta_{p,K}$ are in general only continuous.

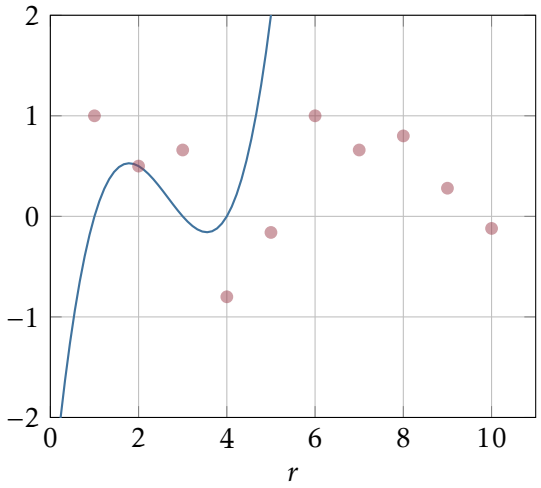

(a) Lagrangian interpolation of order 3 of the second point

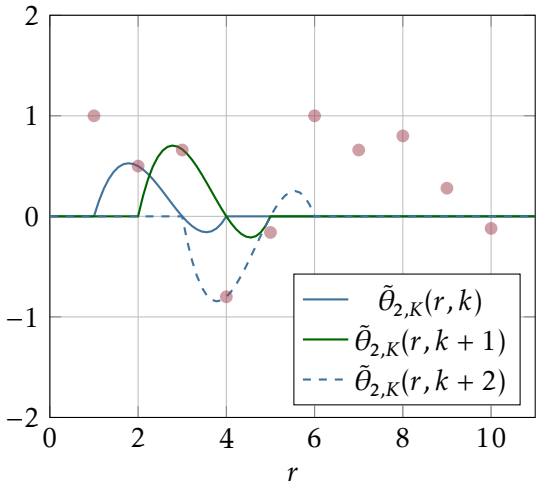

(b) Truncated interpolation function. These are similar to the functions $\theta_{2,K}$.

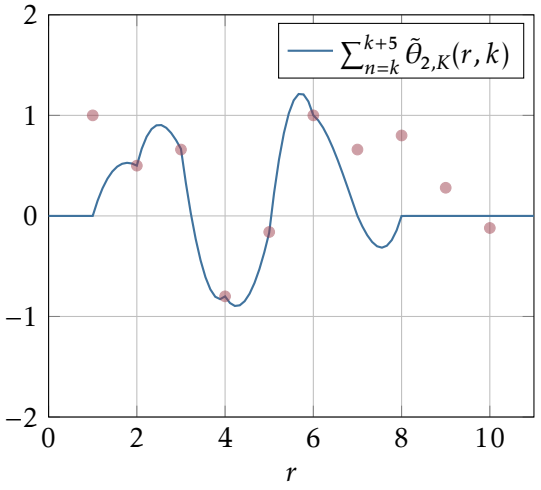

(c) Sum of five functions similar to $\theta_{2,K}$

Figure II.7: Graphical explanation of the interpolation scheme for particle mesh Ewald. The dots in red are the values to interpolate.

Smooth particle mesh Ewald

The smooth particle mesh Ewald method from Essmann et al. [Ess+95] improves on the particle mesh Ewald. It is a more regular interpolation of the exponential at the nodes of the grid (see Fig. II.7c) using *B-splines* — linear combination of regular polynomials. This enables the direct derivation of the reciprocal energy formulation, an important condition to have accurate molecular dynamics.

Proposition II.C.2 (Smooth particle mesh Ewald)**.—** For any $n \in \mathbf{N}$, there exists a $n-2$-times derivable function Q, a smooth function θ_r such that

$$\mathcal{E}_r(K) = \frac{1}{2}\sum_{m_1=0}^{K_1-1}\sum_{m_2=0}^{K_2-1}\sum_{m_3=0}^{K_3-1} Q(m)\cdot(\theta_r * Q)(m) + \varepsilon(K), \tag{III.12}$$

where $\varepsilon(K) \underset{K\to+\infty}{\longrightarrow} 0$.

Proof: To have regular functions $\theta_{p,K}$ in r we will interpolate the exponential function with a linear combination of regular polynomials functions, the B-splines.

We use the same notation as in Proposition II.C.1. For any integer $n \geq 2$, we can approximate the 1D exponential function with

$$\exp(2i\pi mr) = b(m)\sum_{k\in\mathbf{Z}} B_k^n(r)\exp\left(2i\pi m\frac{k}{K}\right) + o(1), \tag{III.13}$$

where

$$b(m) := \frac{\exp(2i\pi m(n-1)/K)}{\sum_{0\leq k\leq n-2} B_0^n(k+1)\exp(2i\pi mk/K)}, \tag{III.14}$$

and where the B_j^n are $(n-2)$-times derivable functions with compact support in $[0\,;n]$.

We can approximate the structure factor with

$$S(m) \approx \prod_{1\leq\gamma\leq 3} b(m_\gamma)\mathcal{F}_d(Q)(m), \tag{III.15}$$

where

$$Q(k) := \sum_{\substack{1\leq j\leq N\\ n\in\mathbf{Z}^3}} q_j \prod_{1\leq\gamma\leq 3} B^n_{k_\gamma+n_\gamma K_\gamma}(s_{j\gamma}). \tag{III.16}$$

If we define

$$B(m) \overset{\text{def.}}{=} \prod_{1\leq\gamma\leq 3} |b(m_\gamma)|^2, \tag{III.17}$$

then

$$\begin{aligned}\mathcal{E}_r(K) &= \frac{1}{2\pi V}\sum_{m\neq 0}\frac{\exp(-\pi^2|m|^2/\alpha)}{|m|^2}B(m)\cdot\mathcal{F}_d(Q)(m)\cdot\mathcal{F}_d(Q)(-m) + \varepsilon(K)\\ &= \frac{1}{2}\sum_{m_1=0}^{K_1-1}\sum_{m_2=0}^{K_2-1}\sum_{m_3=0}^{K_3-1} Q(m)\cdot(\theta_{\text{rec}} * Q)(m) + \varepsilon(K),\end{aligned} \tag{III.18}$$

where

$$\theta_{\text{rec}} = \mathcal{F}_d\left(B\cdot\mathcal{F}_d^{-1}(\psi_{\text{rec}})\right). \tag{III.19}$$

■

Due to the regularity of the function Q, we can immediately derive the forces from Eq. (III.12), by noticing that the θ_{rec} functions do not depend on the positions of the particles

$$\mathrm{F}_i = -\nabla_i \mathcal{E}_r = \frac{1}{2} \sum_{m_1=0}^{K_1-1} \sum_{m_2=0}^{K_2-1} \sum_{m_3=0}^{K_3-1} \nabla_i Q(m) \cdot (\theta_r * Q)(m) + \tilde{\varepsilon}(K). \tag{III.20}$$

This means that we can now have energy conservation up to machine precision during molecular dynamics. However, this comes at the cost of losing the symmetry property during the computation of the forces, hence the second law of Newton is not satisfied. The centre of gravity of the system is thus moving from a random quantity of the order of magnitude the error on the computations of the forces. To prevent this phenomenon, it may be necessary during a molecular dynamics to shift, at least for some time-steps, the forces [Ess+95].

In the case of higher order multipoles, for example when using the amoeba force field that requires multipoles up to quadrupoles, we also need higher derivatives of the energy function. However, as it consists only in using a new Q function, this does not increase the computational complexity of the method.

II.C.3 Splitting of the density

In 1994, York and Yang [YY94] presented an alternative to particle mesh Ewald, the fast Fourier–Poisson. Their idea was to split the density, which leads to an integral where the terms can be approximated directly on a grid adapted for the fast Fourier transform. This bypass the need for interpolation.

We recall that Ewald's clever idea was to mask the point charge potential ϕ by the one due to a Gaussian charge, giving two terms ϕ_d and ϕ_r, which leads to two absolute convergent sums. In this method, it is the density that is split using the equality for any $r \in \mathbf{R}^3$

$$\rho(r) = \Big(\rho(r) - \rho_g(r)\Big) + \rho_g(r). \tag{III.21}$$

Proposition II.C.3 (Fast Fourier–Poisson)**.—** The energy of a periodic system $\underline{r}^{\{N\}}$ is

$$\mathcal{E}(\underline{r}^{\{N\}}) = \frac{1}{2}{\sum_n}' \sum_{1 \le i,j \le N} q_i q_j \frac{\operatorname{erfc}(\alpha^{1/2}|r_{jin}|/\sqrt{2})}{|r_{jin}|} - \left(\frac{\alpha}{\pi}\right)^{1/2} \sum_{j=1}^{N} q_j^2 - \frac{1}{2} \int_{\mathbf{R}^3} \rho_g(r')\phi_g(r')\,\mathrm{d}^3 r' + J(\mathrm{D}, P). \tag{III.22}$$

Proof: We can rewrite the reciprocal energy $\mathcal{E}_r$ under an integral form

$$\mathcal{E}_r = \frac{1}{2} \int_{\mathbf{R}^3} \rho(r')\phi_g(r')\,\mathrm{d}r' = \frac{1}{2} \int_{\mathbf{R}^3} \Big(\rho(r') - \rho_g(r')\Big)\phi_g(r') + \rho_g(r')\phi_g(r')\,\mathrm{d}^3 r', \tag{III.23}$$

and I as

$$\begin{aligned} I &\overset{\text{def.}}{=} \int_{\mathbf{R}^3} \Big(\rho(r') - \rho_g(r')\Big)\,\phi_g(r')\,\mathrm{d}^3 r' \\ &= \frac{1}{\pi V} \sum_{\substack{1 \le i,j \le N \\ m \ne 0}} q_i q_j \frac{e^{-\pi^2|m|^2/\alpha}}{|m|^2} e^{-2i\pi m \cdot r_i} \int_{\mathbf{R}^3} \left(\delta(r' - r_j) - \left(\frac{\alpha}{\pi}\right)^{3/2} e^{-\alpha|r'-r_j|^2}\right) e^{2i\pi m \cdot r'}\,\mathrm{d}^3 r' \\ &= \frac{1}{\pi V} \sum_{\substack{1 \le i,j \le N \\ m \ne 0}} q_i q_j \frac{e^{-\pi^2|m|^2/\alpha}}{|m|^2} e^{2i\pi m \cdot r_{ji}} \int_{\mathbf{R}^3} \left(\delta(r') - \left(\frac{\alpha}{\pi}\right)^{3/2} e^{-\alpha|r'|^2}\right) e^{2i\pi m \cdot r'}\,\mathrm{d}^3 r'. \end{aligned} \tag{III.24}$$

We notice in the integral I a difference between

$$\mathcal{F}^{-1}(\delta) = 1 \tag{III.25}$$

and

$$\mathcal{F}^{-1}\left(r \mapsto \left(\frac{\alpha}{\pi}\right)^{3/2} e^{-\alpha|r|^2}\right) = e^{-\pi^2|m|^2/\alpha}. \tag{III.26}$$

Hence, we obtain

$$\begin{aligned} I &= \sum_{\substack{1\leq i,j\leq N \\ m\neq 0}} \frac{q_i q_j}{\pi V}\left(\frac{e^{-\pi^2|m|^2/\alpha}}{|m|^2} - \frac{e^{-2\pi^2|m|^2/\alpha}}{|m|^2}\right) e^{2i\pi m\cdot r_{ji}} \\ &= \sum_{\substack{1\leq i,j\leq N \\ n}}{}' q_i q_j \left(\frac{\operatorname{erf}(\alpha^{1/2}|r_{jin}|)}{|r_{jin}|} - \frac{\operatorname{erf}(\alpha^{1/2}|r_{jin}|/\sqrt{2})}{r_{jin}}\right), \end{aligned} \tag{III.27}$$

which concludes the proof. ∎

To compute the force, we have to differentiate the potential energy with respect to r_i

$$\mathrm{F}_i = -\nabla_i \mathcal{E}(\underline{r}^{\{N\}}). \tag{III.28}$$

With a straightforward computation, we have $\nabla_i\nabla_i\phi_g = 4\pi\rho_g^i$. Thus, using Theorem II.B.3, we have

$$\begin{aligned} \nabla_i\left(\int_{\mathbf{R}^3}\rho_g\phi_g\right) &= \nabla_i\left(\frac{1}{4\pi}\int_{\mathbf{R}^3} -\Delta\phi_g\phi_g\right) = \nabla_i\left(\frac{1}{4\pi}\int_{\mathbf{R}^3}\nabla\phi_g\nabla\phi_g\right) = \frac{1}{2\pi}\int_{\mathbf{R}^3}\nabla_i\nabla\phi_g\nabla\phi_g \\ &= 2\int_{\mathbf{R}^3}\rho_g^i\nabla\phi_g. \end{aligned} \tag{III.29}$$

Finally, we have

$$\begin{aligned} \frac{\mathrm{F}_i}{q_i} = -\sum_n{}' \sum_{j=1}^N q_j \left(\left(\frac{2\alpha}{\pi}\right)^{1/2}\frac{\exp(-\alpha|r_{jin}|^2/2)}{|r_{jin}|} - \frac{\operatorname{erf}\left(\alpha^{1/2}|r_{jin}|/\sqrt{2}\right)}{|r_{jin}|^2}\right)\cdot e_{jin} \\ - \int_{\mathbf{R}^3}\rho_g^i(r')\nabla\phi_g(r')\,\mathrm{d}^3r' - \nabla_i J(\mathrm{D}, P). \end{aligned} \tag{III.30}$$

Knowing ρ_g and ϕ_g and its gradient at the nodes of the grid, we can evaluate the integrals for the force and the energy by using a fast Fourier transform from the equation

$$\int_{\mathbf{R}^3}\rho_g(r)\phi_g(r)\,\mathrm{d}^3r = \int_{\mathbf{R}^3}\mathcal{F}(\rho_g)(-u)\cdot\mathcal{F}(\phi_g)(u)\,\mathrm{d}^3u. \tag{III.31}$$

II.C.4 particle mesh Ewald and particle-particle–particle-mesh

In 1999, Sagui and Darden [SD99] have shown that the particle mesh Ewald method could be modified to recover the particle-particle–particle-mesh method. In fact, with particle-particle–particle-mesh, Eastwood, Hockney, and Lawrence were interested in interpolating the charges on a grid in a way that would minimise the error on the forces. With particle mesh Ewald, Darden, York, and Pedersen only cared about interpolating the charges for the computation of the energy. In doing so, the error on the energy is minimised. But by changing the interpolation function, Sagui and Darden were able to link the two methods.

The reverse has been done by Ballenegger et al. [Bal+08] to modify the particle-particle–particle-mesh method to minimise the error on the energy rather than on the forces. Moreover, it has been shown in [BCH12] that it was possible to transform the error estimates of particle-particle–particle-mesh into the ones of particle mesh Ewald and *vice-versa*.

II.D Generalisations for the AMOEBA force field

What we have presented so far cannot be used for the AMOEBA force field. Indeed, we have still left unresolved the computation of the surface term, and we have not introduced the EWALD's summation method in the case where we have point multipoles and not only point charges. This section is here to remedy this.

II.D.1 Surface term

In this section, we will derive some explicit formulæ for the surface term. It should be remembered that the results continue to depend on the shape of the primitive unit cell; which is still assumed to be a cubic one.

Shape of the lattice

First, we give the expression of the surface term in some common cases. We will use results from de LEEUW et al. [dLee+80], SMITH [Smi81], and van EIJCK and KROON [vEK97], as well as notation from DARDEN [Dar08].

To prove the results, we will need the following classical lemma of RIEMANN integration.

Lemma II.D.1. — For any continuous function f

$$\lim_{K\to+\infty} \sum_{n\in\Omega(P,K)} \frac{f(n/K)}{K^3} = \frac{1}{V}\int_P f(r)\,\mathrm{d}^3r. \tag{IV.1}$$

ADMITTED PROOF: This is a classic property of RIEMANN integration. □

Theorem II.D.1. — With the same notation as in Theorem II.B.6, we have

$$J(\mathrm{D},P) = \frac{2\pi}{V}\int_{\mathbf{R}^3}\frac{(w\cdot\mathrm{D})^2}{|w|^2}\int_P \exp(-2i\pi w\cdot r)\,\mathrm{d}^3r\,\mathrm{d}^3w. \tag{IV.2}$$

PROOF: By definition of the surface term and after a change of variables, we have

$$\begin{aligned}\frac{J(\mathrm{D},P,K)}{2\pi} &= \int_{KU^*}\frac{(w\cdot\mathrm{D})^2}{|w|^2}\sum_{n\in\Omega(P,K)}\frac{e^{-2i\pi w\cdot n/K}}{K^3}\,\mathrm{d}^3w \\ &\underset{\text{Lem. II.D.1}}{=} \frac{1}{V}\int_{KU^*}\frac{(w\cdot\mathrm{D})^2}{|w|^2}\int_P \exp(-2i\pi w\cdot r)\,\mathrm{d}^3r\,\mathrm{d}^3w + \varepsilon(K),\end{aligned} \tag{IV.3}$$

where $\varepsilon(K) \underset{K\to+\infty}{\longrightarrow} 0$. This concludes the proof. ■

Corollary II.D.1. — Let $\mathbf{B}^3$ the (compact) unit ball of $\mathbf{R}^3$. Then

$$J(\mathrm{D},\mathbf{B}^3) = \frac{2\pi|\mathrm{D}|^2}{3V}. \tag{IV.4}$$

Proof: We can see with a change of variables that the second integral of the previous theorem is a radial function of w, hence if we note for any $w \in \mathbf{R}^3$

$$g(|w|) \overset{\text{def.}}{=} q \int_{\mathbf{B}^3} \exp(-2i\pi w \cdot u)\, \mathrm{d}^3 u, \tag{IV.5}$$

we find

$$\begin{aligned} J(\mathrm{D}, \mathbf{B}^3) &= \frac{2\pi}{V} \int_{\mathbf{R}^3} \frac{(w \cdot \mathrm{D})^2}{|w|^2} g(|w|)\, \mathrm{d}^3 w \\ &= \frac{2\pi}{V} \int_0^{\pi} \int_0^{2\pi} \int_0^{+\infty} \frac{(w\cos(\varphi) M)^2}{w^2} g(w) w^2 \sin(\varphi)\, \mathrm{d}w\, \mathrm{d}\theta\, \mathrm{d}\varphi, \end{aligned} \tag{IV.6}$$

if the *up* axis is taken as parallel to w. Thus

$$\begin{aligned} J(\mathrm{D}, \mathbf{B}^3) &= \frac{2\pi |\mathrm{D}|^2}{3V} \int_{\mathbf{R}^3} g(|w|)\, \mathrm{d}^3 w \\ &\underset{\text{Fubini}}{=} \frac{2\pi |\mathrm{D}|^2}{3V} \int_{\mathbf{B}^3} \int_{\mathbf{R}^3} \exp(-2i\pi w \cdot u)\, \mathrm{d}^3 w\, \mathrm{d}^3 u. \end{aligned} \tag{IV.7}$$

We have the results by noticing that the integral is equivalent to the Dirac function δ_u. ■

Proposition II.D.1.— Let P a compact of $\mathbf{R}^3$ that contains the unit ball $\mathbf{B}^3$. Then, we have

$$J(\mathrm{D}, P) = \frac{1}{2V} \int_{r \in \partial P} \frac{\mathrm{M}_1 \cdot r}{|r|^3} * \mathrm{D} \cdot \mathrm{d}\sigma. \tag{IV.8}$$

Proof: We can decompose for any $K > 0$

$$\mathcal{E}_{P,K}(\underline{r}^{\{N\}}) = \mathcal{E}_{\mathbf{B}^3,K}(\underline{r}^{\{N\}}) + \mathcal{E}_{P,K}(\underline{r}^{\{N\}}) - \mathcal{E}_{\mathbf{B}^3,K}(\underline{r}^{\{N\}}). \tag{IV.9}$$

Hence, we obtain using Proposition II.B.2

$$\begin{aligned} \mathcal{E}_{P\setminus\mathbf{B}^3,K}(\underline{r}^{\{N\}}) &= \frac{1}{2} \sum_{n \in \Omega(P\setminus\mathbf{B}^3)} \left(\frac{|\mathrm{D}|^2}{|n|^3} - 3\frac{(\mathrm{D}\cdot n)^2}{|n|^5} \right) + \mathscr{O}(|n|^{-4}) \\ &\underset{\text{Lem. II.D.1}}{=} \frac{1}{2V} \int_{P\setminus\mathbf{B}^3} \left(\frac{|\mathrm{D}|^2}{|r|^3} - 3\frac{(\mathrm{D}\cdot r)^2}{|r|^5} \right) \mathrm{d}^3 r + \varepsilon(K) + \mathscr{O}(|n|^{-4}) \\ &\underset{\text{Thm. II.B.1}}{=} \frac{1}{2V} \int_{\partial(P\setminus\mathbf{B}^3)} \frac{\mathrm{D}\cdot r}{|r|^3} \mathrm{D}\cdot n\, \mathrm{d}\sigma + \varepsilon(K) + \mathscr{O}(|n|^{-4}), \end{aligned} \tag{IV.10}$$

where $\varepsilon(K) \underset{K\to+\infty}{\longrightarrow} 0$. Moreover, we have $n \to +\infty$ when K goes to infinity.

And by a simple calculation, we find

$$\frac{1}{2V} \int_{\partial\mathbf{B}^3} \frac{\mathrm{D}\cdot r}{|r|^3} \mathrm{D}\cdot n\, \mathrm{d}\sigma = \frac{2\pi|\mathrm{D}|^2}{3V} = J(\mathrm{D}, \mathbf{B}^3), \tag{IV.11}$$

which concludes the proof of the property. ■

Cancellation of the surface term

In this section we will see that under certain conditions it is possible to have a null surface term. This happens due to polarisation that emerges if we embed the system in a medium of infinite permittivity ϵ.

Theorem II.D.2. — Let $\mathbf{B}^3$ the unit ball of $\mathbf{R}^3$ surrounded by a medium of dielectric permittivity ϵ. Then

$$J_\epsilon(\mathrm{D}, \mathbf{B}^3) = \frac{2\pi}{V} \cdot \frac{|\mathrm{D}|^2}{2\epsilon + 1}. \tag{IV.12}$$

This result is a generalisation of the equivalent in the previous section, where the dielectric permittivity was the one of vacuum ϵ_0, which is equal to one. For the proof of this result, we use the one of SMITH [Smi94].

For the proof, we will use the following definition for spherical harmonics.

Definition II.D.1 (Spherical harmonics). — Let Γ be the set defined as

$$\Gamma := \{(n, m) \in \mathbf{N} \times \mathbf{Z} \mid -n \leq m \leq n\}. \tag{IV.13}$$

Then we define for any $(n, m) \in \Gamma$ and $\hat{r} = (\theta, \varphi) \in \mathbf{S}^3$ such that $\theta \in [0\,;\pi]$ and $\varphi \in [0\,;2\pi[$ the spherical harmonic of order m and degree n as

$$Y_n^m(\hat{r}) := \sqrt{\frac{2n+1}{4\pi}\frac{(n-m)!}{(n+m)!}} P_n^m(\cos\theta)\exp(im\varphi). \tag{IV.14}$$

We will also denote by $Y_n^{m*} := Y_n^{-m}$ the conjugate of Y_n^m.

PROOF OF THEOREM II.D.2: Let K be a strictly positive scalar. We consider the ball $B := K \cdot \mathbf{B}^3$, the ball of radius K in $\mathbf{R}^3$, which is embedded in a medium of dielectric permittivity ϵ. We note that the ball B itself has the same dielectric permittivity as vacuum ϵ_0. We refer to Fig. II.8 for a representation.

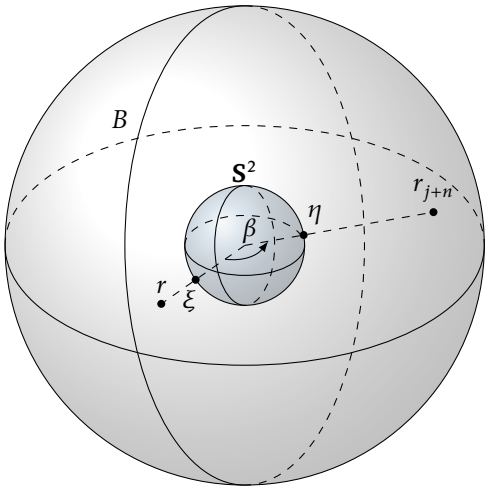

Figure II.8: Ball B embedded in a medium with dielectric permittivity ϵ

We will compute the potential due to polarisation, and conclude by the superposition principle. The polarisation happens because a charge q_j polarises the medium outside of the ball B of dielectric permittivity ϵ, which induces a potential in B that acts on all other charges.

We will use spherical harmonics. For any non-zero r of $\mathbf{R}^3$ and any $(\ell, m) \in \mathbf{Z} \times \mathbf{N}$ such that $-\ell \leq m \leq \ell$, we note $\phi_\ell^m(r) \overset{\text{def.}}{=} |r|^\ell Y_\ell^m(\hat{r})$, where $\hat{r} \overset{\text{def.}}{=} r/|r|$ and the Y_ℓ^m functions are the spherical harmonics of order m and degree ℓ. Then, the potential at $r \in U$ due to a charge $r_{j+n} \in B$

is [Smi94]

$$\phi_{j+n}(r) = -\sum_{\substack{\ell\in\mathbf{N}\\|m|\leq\ell}} \frac{4\pi}{2\ell+1}\frac{(\ell+1)(\epsilon-1)}{\epsilon(\ell+1)+\ell}\frac{\phi_\ell^m(r)\phi_\ell^{m*}(r_j+n)}{K^{2\ell+1}}. \tag{IV.15}$$

Hence, we find that the polarisation potential due to the lattice $\underline{r}^{\{N\}}$ is for any $r \in U$

$$\begin{aligned}\phi_{\mathbf{B}^3,K}(r) &\overset{\text{def.}}{=} \sum_{\substack{1\leq j\leq N\\ n\in\Omega(\mathbf{B}^3,K)}} q_j\phi_{j+n}(r) = -\sum_{\substack{l\in\mathbf{N}\\|m|\leq l}}(-1)^m\frac{C_\ell}{K^{2l+1}}\sum_{\substack{1\leq j\leq N\\ n\in\Omega(\mathbf{B}^3,K)}} q_j\phi_l^m(r)\phi_l^{-m}(r_j+n)\\ &\underset{\mathcal{Q}=0}{=} -\sum_{\substack{l\in\mathbf{N}\\|m|\leq l}}(-1)^m\frac{C_\ell}{K^{l+1}}\phi_l^m(r)\sum_{\substack{1\leq j\leq N\\ n\in\Omega(\mathbf{B}^3,K)}} q_j\left(\phi_l^{-m}\left(\frac{r_j+n}{K}\right)-\phi_l^{-m}\left(\frac{n}{K}\right)\right)\\ &\underset{\text{Lem. II.D.1}}{=} -\sum_{\substack{l\in\mathbf{N}\\|m|\leq l}}(-1)^m\frac{C_\ell}{K^{l-1}}\phi_l^m(r)\sum_{1\leq j\leq N}\underbrace{\frac{K}{V}\int_{\mathbf{B}^3}\left(\phi_l^{-m}\left(\frac{r_j}{K}+r\right)-\phi_l^{-m}(r)\right)\mathrm{d}^3r}_{=:\,I},\end{aligned} \tag{IV.16}$$

where C_ℓ are the first two fractions in the previous sum of Eq. (IV.15)

Moreover, a Taylor expansion gives us that

$$V\cdot I = r_j\cdot\int_{\mathbf{B}^3}\nabla\phi_\ell^{-m}(r)+\mathscr{O}(K^{-1})\,\mathrm{d}^3r. \tag{IV.17}$$

Thus, we have the equality

$$\phi_{\mathbf{B}^3,K}(r) = -\frac{1}{V}\sum_{\substack{\ell\in\mathbf{N}\\|m|\leq\ell}}(-1)^m\frac{C_\ell}{K^{\ell-1}}\phi_\ell^m(r)\mathrm{D}\cdot\int_{\mathbf{B}^3}\nabla\phi_\ell^{-m}(r')\,\mathrm{d}^3r'+\varepsilon(K), \tag{IV.18}$$

where $\varepsilon(K)\underset{K\to+\infty}{\longrightarrow}0$.

As we want the behaviour when K goes to infinity, only the case when $\ell = 0$ or 1 is unclear. To study this, we introduce the spherical basis, which is such that

$$e_{-1}\overset{\text{def.}}{=}\frac{1}{\sqrt{2}}(1,i,0)\quad e_0\overset{\text{def.}}{=}(0,0,1)\quad e_1\overset{\text{def.}}{=}-\frac{1}{\sqrt{2}}(1,-i,0) \tag{IV.19}$$

in the canonical basis. We remark that we have $e_m^* = e_{-m}$.

Then, we have

$$\int_{\mathbf{B}^3}\nabla\phi_\ell^{-m}(r')\,\mathrm{d}^3r' = \sqrt{\frac{4\pi}{3}}\,\delta_{\ell 1}\,e_m^*. \tag{IV.20}$$

Moreover, a direct calculation gives

$$\begin{aligned}\phi_{\mathbf{B}^3,K} &= \frac{4\pi}{3}\cdot\frac{2(\epsilon-1)}{2\epsilon+1}\cdot\sqrt{\frac{4\pi}{3}}\,\mathrm{D}\cdot|r|\left(-Y_1^{-1}(\hat{r})e_{-1}+Y_0^0(\hat{r})e_0-Y_1^1(\hat{r})e_1\right)+\varepsilon(K)\\ &= \frac{4\pi}{3}\cdot\frac{2(\epsilon-1)}{2\epsilon+1}\mathrm{D}\cdot|r|\hat{r}+o_K(1).\end{aligned} \tag{IV.21}$$

So, for the lattice $\underline{r}^{\{N\}}$, we have

$$\phi_S(r_j)\overset{\text{def.}}{=}\lim_{K\to+\infty}\phi_{\mathbf{B}^3,K}(r_j) = -\frac{4\pi}{3V}\cdot\frac{2(\epsilon-1)}{2\epsilon+1}q_jr\cdot\mathrm{D}. \tag{IV.22}$$

Thus, the polarisation energy is

$$\frac{1}{2}\sum_{1\leq j\leq N} q_j\phi_S(r_j) = -\frac{4\pi}{3V}\cdot\frac{\epsilon-1}{2\epsilon+1}|\mathrm{D}|^2. \tag{IV.23}$$

Finally, because

$$\frac{2\pi|\mathrm{D}|^2}{3V} - \frac{4\pi}{3V}\cdot\frac{\epsilon-1}{2\epsilon+1}|\mathrm{D}|^2 = \frac{2\pi}{V}\cdot\frac{|\mathrm{D}|^2}{2\epsilon+1}, \tag{IV.24}$$

we deduce the result. ■

This result implies that the surface term disappears in the limit where ϵ goes to infinity. This is — often implicitly — the case in which we consider periodic systems in molecular dynamics. This enables the absolute convergence of the series, and hence we do not have to worry about the order of summation.

II.D.2 Generalised EWALD's summation method for multipoles

Up to now, we have neglected all interactions other than point charges. It is thus impossible to precisely model some interactions that are best described with multipoles up to quadrupoles [WR84]. In particular, using only the previous results, it would not be possible to implement the AMOEBA force field [PC03].

The development that we describe here is due to a 1982 paper that was reedited in 1998 by [Smi98]. We will explain how to obtain the energy $\mathcal{E}(\underline{r}^{\{N\}})$ as EWALD's sums up to quadrupoles. The method has been applied by SAGUI, PEDERSEN, and DARDEN [SPD04] in 2004 for the smooth particle mesh EWALD method. The development here is done for Cartesian coordinates. We refer to the work of SIMMONETT et al. [Sim+14] for the EWALD's summation method using spherical harmonics.

First, we rewrite the energy $\mathcal{E}(\underline{r}^{\{N\}})$ to take into account multipolar moments up to order p.

Definition II.D.2. — Let $p\in\mathbf{N}$ be the maximum order of multipoles that we consider. Then, for $i\in[\![1\,..\,N]\!]$ we denote by M_{di} the 3^d tensor representing the 2^d-order multipole at position r_i. We call multipolar operator the quantity

$$\hat{\mathrm{L}}_i := \sum_{0\leq d\leq p} \mathrm{M}_{di}\cdot\mathrm{D}_i^d, \tag{IV.25}$$

where $\cdot$ is the point-wise product, and D_i^d is the matrix of d-order partial derivatives with respect to atomic coordinates i. We note that we have replaced in this section the notation q_i by M_{0i}.

The potential $\phi(r_i)$ at position r_i is then

$$\phi(r_i) = \sum_{0\leq d\leq p}(-1)^d\mathrm{M}_{dj}\cdot\mathrm{D}_i^d\left(\frac{1}{|r_{ji}|}\right), \tag{IV.26}$$

and the associated energy is

$$\mathcal{E}(\underline{r}^{\{N\}}) = \frac{1}{2}{\sum_n}'\sum_{1\leq i,j\leq N}\hat{\mathrm{L}}_i\hat{\mathrm{L}}_j\left(\frac{1}{|r_j-r_i+n|}\right). \tag{IV.27}$$

If we consider multipoles up to dipoles, the previous series is explicitly

$$\sum_{i,j=1}^{N}\left(\frac{\mathrm{M}_{0i}\mathrm{M}_{0j}}{|r_{jin}|} + \frac{(\mathrm{M}_{0j}\mathrm{M}_{1i}-\mathrm{M}_{0i}\mathrm{M}_{1j})\cdot r_{jin}+\mathrm{M}_{1i}\cdot\mathrm{M}_{1j}}{|r_{jin}|^3} - 3\frac{\mathrm{M}_{1j}\cdot r_{jin}\mathrm{M}_{1i}\cdot r_{jin}}{|r_{jin}|^5}\right), \tag{IV.28}$$

With the same notation as for Eq. (II.20) and by developing the scalar products in the previous equation we get the asymptotic behaviour for the absolute value of the second term of the series

$$\frac{1}{|n|^3}\left(-2Q\sum_{1\le i\le N} r_i^2 + Q^2 + 3|\mathrm{D}|^2\right), \tag{IV.29}$$

and in the third term, the only term in $O(|n|^{-3})$ is

$$3\frac{(\mathrm{D}\cdot n)^2}{|n|^5}. \tag{IV.30}$$

We thus have absolute convergence of the infinite sum with the same conditions as for point charges, that is $Q = 0$ and $\mathrm{D} = 0$.

When considering higher order multipoles, it is necessary that the quadrupoles are also zero. Indeed, in this case we only have terms that decrease as $|n|^4$ which belongs to $\mathrm{L}^1_{\mathrm{loc}}(\mathbf{R}^3)$. We refer the reader to articles from Harris [Har75] and Saunders et al. [Sau+92] for discussions on this case.

We can now introduce the Ewald's summation method for arbitrary multipoles.

Proposition – Definition II.D.1. — For any $m \in \mathbf{R}^3$, we denote by

$$\tilde{S}(m) := \sum_{1\le j\le N} \mathcal{F}(\hat{\mathrm{L}}_j)(m)\exp(2i\pi m\cdot r_j) \tag{IV.31}$$

the multipolar structure factor. The multipolar electrostatic Ewald energy of the lattice $\underline{r}^{\{N\}}$ is

$$\tilde{\mathcal{E}}_{\mathrm{Ewald}}(\underline{r}^{\{N\}}) = \frac{1}{2}{\sum_{1\le i,j\le N}}' \hat{\mathrm{L}}_i\hat{\mathrm{L}}_j\left(\frac{\operatorname{erfc}(a^{1/2}|r_{jin}|)}{|r_{jin}|}\right) - \mathcal{E}_{\mathrm{self}} + \frac{1}{2\pi V}\sum_{m\neq 0}\frac{\exp(-\pi^2|m|^2/\alpha)}{|m|^2}|\tilde{S}(m)|^2, \tag{IV.32}$$

where the self-energy $\mathcal{E}_{\mathrm{self}}$ is a term that we will explain in the next section, in particular in Proposition II.D.4.

As it is the case for the point charges, the two series of Eq. (IV.32) are absolutely convergent. The proof is similar to the one for point charges.

Proof: The result is straightforward once we have noticed that for every $m \in \mathbf{R}^3$

$$\begin{aligned}\mathcal{F}(\nabla_j)(m) &= \int_{\mathbf{R}^3}\nabla_j\exp(-2i\pi m\cdot r_j)\,\mathrm{d}^3r_j = -(2i\pi m)\int_{\mathbf{R}^3}\exp(-2i\pi m\cdot r_j)\,\mathrm{d}^3r_j\\ &= -(2i\pi m)\,\delta_{r_j}(m),\end{aligned} \tag{IV.33}$$

hence

$$\mathcal{F}(\hat{\mathrm{L}}_j)(m) = \sum_{0\le d\le p}(2i\pi)^d\mathrm{M}_{dj}\cdot m^{\otimes d}. \tag{IV.34}$$

We can then redo the proof of Proposition II.C.1. ∎

Self-energy term

The self-energy term has two be computed case by case, in the same way that for interaction between point charges. In this section, we give a proof for its expression for multipoles of arbitrary order. We are not aware of similar development in the literature.

For the expression of the self-energy, we will need the following results.

Proposition II.D.2. — For any $\alpha > 0$, the function $r \mapsto \operatorname{erf}(\alpha^{1/2} r)/r$ has the following power series expansion

$$\frac{\operatorname{erf}(\alpha^{1/2} r)}{r} = 2\sqrt{\frac{\alpha}{\pi}} \sum_{k \in \mathbf{N}} (-1)^k \frac{\alpha^k}{(2k+1)k!} r^{2k} \tag{IV.35}$$

on $\mathbf{R}$.

PROOF: We can show this using the definition of the error function and expanding the exponential inside the integral, and then applying FUBINI's theorem. ■

Lemma II.D.2. — For any $n \in \mathbf{N}$, we have the equality

$$\sum_{1 \leq k \leq n} \frac{(-2)^k}{(2k+1)\mathsf{i}} \frac{n!}{(n-k)!} = -\frac{2n}{2n+1}, \tag{IV.36}$$

where $(2k+1)\mathsf{i} = (2k+1) \times \cdots \times 3 \times 1$ and $(2k)\mathsf{i} = (2k) \times \cdots \times 2$.

PROOF: We show the (stronger) result with recursion

$$\sum_{1 \leq k \leq n} \frac{(-2)^k}{(2k+\nu)\mathsf{i}} \frac{n!}{(n-k)!} = -\frac{2n}{\nu\mathsf{i}(2n+\nu)}, \tag{IV.37}$$

where ν is an odd integer. Indeed, the result is clearly true for $n = 1$. At rank $n+1$, we have

$$\begin{aligned} S &\overset{\text{def.}}{=} \sum_{1 \leq k \leq n+1} \frac{(-2)^k}{(2k+\nu)\mathsf{i}} \frac{(n+1)!}{(n+1-k)!} = (n+1) \sum_{1 \leq k \leq n} \frac{(-2)^{k+1}}{(2(k+1)+\nu)\mathsf{i}} \frac{n!}{(n-k)!} - \frac{2(n+1)}{(2+\nu)\mathsf{i}} \\ &= -2(n+1)\left(-\frac{2n}{(2+\nu)\mathsf{i}(2(n+1)+\nu)} + \frac{1}{(2+\nu)\mathsf{i}}\right) = -\frac{2(n+1)}{\nu\mathsf{i}(2(n+1)+\nu)}. \end{aligned} \tag{IV.38}$$

Hence, the result is verified for $n+1$. ■

Lemma II.D.3. — For any $n \in \mathbf{N}$, every $\alpha > 0$ and all $r > 0$, we have the identity

$$\sum_{k=0}^{n-1} \frac{(-1)^k \alpha^k}{k!} \left(\frac{1}{2\alpha} \sum_{\ell=1}^{n-k} \frac{(4\alpha)^\ell \ell!}{(2\ell)!} r^{2(\ell-1)} - \frac{1}{2k+1} \right) r^{2k} = 0. \tag{IV.39}$$

PROOF: To use the previous lemma, we can rewrite the sum as

$$\begin{aligned}
&\sum_{k=0}^{n} \frac{(-1)^k \alpha^k}{k!} \left(\frac{1}{2\alpha} \sum_{\ell=1}^{n+1-k} \frac{(4\alpha)^\ell \ell!}{(2\ell)!} r^{2(\ell-1)} - \frac{1}{2k+1} \right) r^{2k} \\
&\quad = \sum_{k=0}^{n-1} \frac{(-1)^k \alpha^k}{k!} \left(\frac{1}{2\alpha} \sum_{\ell=1}^{n-k} \frac{(4\alpha)^\ell \ell!}{(2\ell)!} r^{2(\ell-1)} - \frac{1}{2k+1} + \frac{2^{2(n-k)+1} \alpha^{n-k} (n+1-k)!}{(2(n+1-k))!} r^{2(n-k)} \right) r^{2k} \\
&\qquad\qquad + \frac{(-\alpha)^n}{n!} \frac{2n}{2n+1} r^{2n} \\
&\quad = \frac{(-\alpha)^n r^{2n}}{n!} \left(\sum_{k=0}^{n-1} \frac{(-1)^{n-k} 2^{2(n-k)+1} (n+1-k)! n!}{k! (2(n+1-k))!} + \frac{2n}{2n+1} \right).
\end{aligned} \tag{IV.40}$$

By noticing that for every integer k we have

$$\frac{2^k k!}{(2k)!} = \frac{1}{(2k-1)\mathrm{i}}, \tag{IV.41}$$

we can conclude using the previous lemma after a change of index. ■

With the same method used by SMITH [Smi98], we introduce the functions B_n with values on $\mathbf{R}_+$ defined by the reccurence relations for all $(n, r) \in \mathbf{N} \times \mathbf{R}_+$

$$B_0(r) \overset{\text{def.}}{=} -\frac{\operatorname{erf}(\alpha^{1/2} r)}{r}, \qquad B_n(r) \overset{\text{def.}}{=} \frac{1}{r^2} \left((2n-1) B_{n-1}(r) + \frac{(2\alpha)^n}{\alpha^{1/2} \sqrt{\pi}} \exp(-\alpha r^2) \right). \tag{IV.42}$$

These functions verify for all $n \in \mathbf{N}$

$$\frac{\mathrm{d}B_n}{\mathrm{d}r}(r) = -r B_{n+1}(r), \tag{IV.43}$$

which implies

$$\mathrm{D}_i B_n(|r_{jin}|) = r_{jin} B_{n+1}(|r_{jin}|). \tag{IV.44}$$

We recall that for point charges, we had to look at the limit

$$\lim_{r \to r_j} \left(\mathrm{M}_{0j} \frac{\operatorname{erf}(\alpha^{1/2} |r_j - r|)}{|r_j - r|} \right), \tag{IV.45}$$

which corresponds to

$$\lim_{r_i \to r_j} \mathrm{M}_{0j} B_0(|r_{ji0}|). \tag{IV.46}$$

To generalise for any multipoles, we thus have to study the existence of the functions B_n at the origin. This is what the following propositions gives.

Proposition II.D.3.— For every integer n, the function B_n is defined on $\mathbf{R}_+$ and

$$\lim_{r \to 0} B_n(r) = B_n(0) = -\frac{\alpha^{n+1/2}}{\sqrt{\pi}} \frac{2^{n+1}}{2n+1}. \tag{IV.47}$$

PROOF: It is clear that the function B_n is defined for all $r > 0$. It remains to show the result at the origin. With a simple recurrence, we show that for every $r > 0$ and all $n \geq 1$

$$B_n(r) = \frac{\exp(-\alpha r^2)}{\alpha^{1/2}\sqrt{\pi} r^2} \sum_{k=0}^{n-1} \frac{(2\alpha)^{n-k}}{r^{2k}} \frac{(2n-1)\mathrm{i}}{(2(n-k)-1)\mathrm{i}} - (2n-1)\mathrm{i}\frac{\operatorname{erf}(\alpha^{1/2} r)}{r^{2n+1}}. \tag{IV.48}$$

Thus, using the power series expansion of the error function using Proposition II.D.2 and of the exponential, we have that for all $r > 0$

$$\begin{aligned} B_n(r) = -(2n-1)\mathrm{i}\frac{2\alpha^{1/2}}{\sqrt{\pi}} \sum_{k=0}^{+\infty} \frac{(-\alpha)^k}{(2k+1)k!} r^{2(k-n)} \\ + \frac{1}{\alpha^{1/2}\sqrt{\pi}} \sum_{\ell=0}^{+\infty} \sum_{k=0}^{n-1} \frac{(-1)^\ell 2^{n-k} \alpha^{n+\ell-k} (2n-1)\mathrm{i}}{\ell!(2(n-k)-1)\mathrm{i}} r^{2(\ell-k-1)}. \end{aligned} \tag{IV.49}$$

It clearly appears in the latter expression that we have to study the terms for which $k - n$ and $\ell - k - 1$ are negatives. Indeed, when strictly positive, these terms goes to zero when r goes to zero.

We begin with introducing Σ and Σ' defined by

$$\begin{aligned} \Sigma &\overset{\text{def.}}{=} \frac{B_n(r)\sqrt{\pi}}{2\alpha^{1/2}(2n-1)\mathrm{i}} \\ &= \sum_{k=0}^{n-1} \left(-\frac{(-\alpha)^k}{(2k+1)k!} r^{2(k-n)} + \sum_{l=0}^{k} \frac{(-1)^\ell 2^{2(n-k)-1} \alpha^{n-k+\ell-1} (n-k)!}{\ell!(2(n-k))!} r^{2(\ell-k-1)} \right). \end{aligned} \tag{IV.50}$$

With a change of variables, we are have

$$r^{2n}\Sigma = \sum_{k=0}^{n-1} \frac{(-\alpha)^k}{k!} \left(\frac{1}{2\alpha} \sum_{\ell=1}^{n-k} \frac{(4\alpha)^\ell \ell!}{(2\ell)!} r^{2(\ell-1)} - \frac{1}{2k+1} \right) r^{2k}, \tag{IV.51}$$

which is defined at zero by Proposition – Definition II.D.1, because it is equal to zero.

It remains to study the constant term, that is

$$\Upsilon \overset{\text{def.}}{=} 2(2n-1)\mathrm{i}\sqrt{\frac{\alpha}{\pi}}(-\alpha)^n \left(\frac{-1}{(2n+1)n!} + \frac{1}{2} \sum_{k=0}^{n-1} \frac{(-1)^{n-k-1} 2^{2(n-k)} (n-k)!}{(k+1)!(2(n-k))!} \right), \tag{IV.52}$$

which gives after a change of variables

$$\Upsilon = -2(2n-1)\mathrm{i}\sqrt{\frac{\alpha}{\pi}}(-\alpha)^n \left(\frac{1}{(2n+1)n!} + \frac{1}{2} \sum_{k=1}^{n} \frac{(-4)^k k!}{(n-k+1)!(2k)!} \right). \tag{IV.53}$$

By recurrence, we then show that

$$\frac{1}{(2n+1)} + \frac{1}{2} \sum_{k=1}^{n} \frac{(-4)^k k! n!}{(n-k+1)!(2k)!} = \frac{(-4)^n n!^2}{(2n+1)!}. \tag{IV.54}$$

Indeed, the result is clear at rank $n = 1$, and at rank $n + 1$ we have

$$\begin{aligned} S &\overset{\text{def.}}{=} \frac{1}{2n+3} + \frac{1}{2} \sum_{k=1}^{n+1} \frac{(-2)^k (n+1)!}{(2k-1)\mathrm{i}(n+2-k)!} = \frac{1}{2n+3} - \sum_{k=0}^{n} \frac{(-2)^k (n+1)!}{(2k+1)\mathrm{i}(n+1-k)!} \\ &= \frac{1}{2n+3} - \sum_{k=1}^{n+1} \frac{(-2)^k (n+1)!}{(2k+1)\mathrm{i}(n+1-k)!} + \frac{(-2)^{n+1}(n+1)!}{(2n+3)\mathrm{i}} - 1 \underset{\text{Lem. II.D.2}}{=} \frac{(-2)^{n+1}(n+1)!}{(2n+3)\mathrm{i}} \\ &= \frac{(-4)^{n+1}(n+1)!^2}{(2n+3)!}, \end{aligned} \tag{IV.55}$$

hence the result at rank $n+1$, and thus for all $n \geq 1$.

Finally, for every integer n strictly positive,

$$\Upsilon = -\frac{\alpha^{n+1/2}}{\sqrt{\pi}} \frac{2^{n+1}}{2n+1}. \tag{IV.56}$$

With the convention $(-1)!! = 1$, we notice that when $n = 0$ in the previous expression, we recover the potential of the self-energy for charges. The formula is thus defined for all $n \in \mathbf{N}$. ■

We now have everything that is necessary to have the general expression of the self-energy.

Proposition II.D.4 (Self-energy). — The self-energy is well defined for any multipole order. In particular, for interactions up to quadrupoles, we have

$$\mathcal{E}_{\text{self}} = -\sqrt{\frac{\alpha}{\pi}} \sum_{j=1}^{N} \left(\mathrm{M}_{0j}^2 + \frac{2\alpha}{3} \left(|\mathrm{M}_{1j}|^2 - 2\mathrm{M}_{0j} \operatorname{Tr}(\mathrm{M}_{2j}) \right) + \frac{4\alpha^2}{5} \left(2\mathrm{M}_{2j} \cdot \mathrm{M}_{2j} + (\operatorname{Tr}(\mathrm{M}_{2j}))^2 \right) \right), \tag{IV.57}$$

where Tr is the trace operator on matrices.

Proof: To keep the proof simple, we will give the results in the most common setting, when the matrix of quadrupoles is symmetric with zero trace.

The j-th self-potential ϕ_{self} at an arbitrary point r in a neighborhood of r_j writes as

$$\begin{aligned} \phi_{\text{self}}^j(r) &= -\hat{\mathrm{L}}_j \frac{\operatorname{erf}(\alpha^{1/2}|r-r_j|)}{|r-r_j|} = -\hat{\mathrm{L}}_j B_0(|r-r_j|) \\ &= -\mathrm{M}_{0j} B_0(|r-r_j|) - \mathrm{M}_{1j} \cdot \mathrm{D}_j^1 B_0(|r-r_j|) - \mathrm{M}_{2j} \cdot \mathrm{D}_j^2 B_0(|r-r_j|) \\ &= -\mathrm{M}_{0j} B_0(|r-r_j|) + B_1(|r-r_j|) \mathrm{M}_{1j} \cdot (r-r_j) - B_2(|r-r_j|) \mathrm{M}_{2j} \cdot \left((r-r_j)^{\mathsf{T}} (r-r_j) \right). \end{aligned} \tag{IV.58}$$

Then, the evaluation of the self-potential at $r = r_j$ is then given by

$$\phi_{\text{self}}^j(r_j) = \lim_{r \to r_j} \phi_{\text{self}}(r) = -\mathrm{M}_{0j} B_0(0) = \mathrm{M}_{0j} 2 \frac{\alpha^{1/2}}{\sqrt{\pi}}, \tag{IV.59}$$

which does not depend anymore on r_j, only depends on the charge M_{0j} and is well-defined. This formula is of course valid for any kind of multipolar distribution and not restricted to orders to up to quadrupoles only.

Finally, the self-energy as defined above writes as

$$\begin{aligned} \mathcal{E}_{\text{self}}(\underline{r}^{\{N\}}) &= \frac{1}{2} \sum_{1 \leq j \leq N} \left(\hat{\mathrm{L}}_j \phi_{\text{self}}^j(r) \right)\Big|_{r=r_j} = -\frac{1}{2} \sum_{1 \leq j \leq N} \left(\mathrm{M}_{0j} \cdot \mathrm{M}_{0j} B_0(0) + \mathrm{M}_{1j} \cdot \mathrm{M}_{1j} B_1(0) + 2\mathrm{M}_{2j} \cdot \mathrm{M}_{2j} B_2(0) \right) \\ &= -\sqrt{\frac{\alpha}{\pi}} \sum_{1 \leq j \leq N} \left(\mathrm{M}_{0j} \cdot \mathrm{M}_{0j} + \frac{2\alpha}{3} \mathrm{M}_{1j} \cdot \mathrm{M}_{1j} + \frac{8\alpha^2}{5} \mathrm{M}_{2j} \cdot \mathrm{M}_{2j} \right). \end{aligned} \tag{IV.60}$$

This concludes the proof. ■

The expression of the self-potential in the proof also gives us that the self-field at $r = r_j$

$$\mathrm{E}_{\text{self}}^j(r) = -\lim_{r \to r_j} (\mathrm{D}_r \phi_{\text{self}}(r)) = \lim_{r \to r_j} \left(\mathrm{D}_r \hat{\mathrm{L}}_j B_0(|r-r_j|) \right) = -\mathrm{M}_{1j} B_1(0) = \mathrm{M}_{1j} \frac{\alpha^{3/2}}{\sqrt{\pi}} \frac{4}{3}, \tag{IV.61}$$

which only depends on the dipole moment at site j and is also valid for any kind of multipolar distribution.

Finally, we add a small remark on the surface term. It can be shown by using the same technique of Section II.D.1, that for multipoles of any order, the surface term in the case of spherical summation when surrounded by a medium of dielectric permittivity ϵ is

$$J_\epsilon(\mathrm{D}, \mathrm{M}, \mathbf{B}^3) = \frac{2\pi}{(2\epsilon + 1)V} |\mathrm{D} + \mathrm{M}|^2, \tag{IV.62}$$

where $\mathrm{M} := \sum_{j=1}^{N} \mathrm{M}_{1\,i}$.

We recall that the results of this sections are general for any order of multipoles, which gives a systematic way to derives quantities associated to the EWALD's summation method. This concludes the overview on the particle-mesh methods of summation.

II.E References

[AF93] Arnaudiès, Jean-Marie and Fraysse, Henri. "Cours de Mathématiques. Tome 2. Analyse". Dunod, Mar. 1993 (cit. on p. 38).

[Bal+08] Ballenegger, Vincent et al. "The Optimal p3m Algorithm for Computing Electrostatic Energies in Periodic Systems". In: *Journal of Chemical Physics* 128.3, 034109 (2008), pp. 1–13 (cit. on p. 52).

[BCH12] Ballenegger, Vincent, Cerdà, Juan J., and Holm, Christian. "How to Convert spme to p3m: Influence Functions and Error Estimates". In: *Journal of Chemical Theory and Computation* 8.3 (2012), pp. 936–947 (cit. on p. 52).

[Col21a] Collective. *Fubini's Theorem*. In: *Wikipedia*. Ed. by Wikipedia. Mar. 3, 2021 (cit. on p. 40).

[Col21b] Collective. *Gamma Function*. In: *Wikipedia*. Ed. by Wikipedia. Apr. 2, 2021 (cit. on p. 39).

[Dar08] Darden, Thomas A. "Extensions of the Ewald Method for Coulomb Interactions in Crystals". In: *Reciprocal Space*. Ed. by Shmueli, Uri. 3rd ed. Vol. B. International Tables for Crystallography. John Wiley & Sons, Aug. 2008, pp. 458–481 (cit. on pp. 34, 39, 41, 47, 53).

[dLee+80] De Leeuw, S. W. et al. "Simulation of Electrostatic Systems in Periodic Boundary Conditions. I. Lattice Sums and Dielectric Constants". In: *Proceedings of the Royal Society of London. A. Mathematical and Physical Sciences* 373.1752 (Oct. 31, 1980), pp. 27–56 (cit. on pp. 44, 53).

[DYP93] Darden, Tom, York, Darrin, and Pedersen, Lee. "Particle Mesh Ewald: An N□log(N) Method for Ewald Sums in Large Systems". In: *The Journal of Chemical Physics* 98.12 (June 15, 1993), pp. 10089–10092. issn: 0021-9606 (cit. on pp. 46, 52).

[EHL79] Eastwood, James W., Hockney, Roger W., and Lawrence, D. N. "p3m3dp – The Three-Dimentional Periodique Particle-Particle/Particle-Mesh Program". In: *Computer Physics Communications* 19 (1979), pp. 215–261 (cit. on pp. 45, 46, 52).

[Ess+95] Essmann, Ulrich et al. "A Smooth Particle Mesh Ewald Method". In: *The Journal of Chemical Physics* 103.19 (Nov. 15, 1995), pp. 8577–8593. issn: 0021-9606 (cit. on pp. 39, 46, 50, 51).

[Ewa21] Ewald, P. P. "Die Berechnung Optischer Und Elektrostatischer Gitterpotentiale". In: *Annalen der Physik* 369.3 (1921), pp. 253–287. issn: 1521-3889 (cit. on p. 37).

[God01] Godement, Roger. "Analyse Mathématique iii. Fonctions Analytiques, Différentielles et Variétés, Surfaces de Riemann". Springer, Nov. 2001 (cit. on p. 32).

[Har75] Harris, Frank E. "Hartree-Fock Studies of Electronic Structures of Crystalline Solids*". In: *Theoretical Chemistry*. Ed. by Eyring, HENRY and Henderson, DOUGLAS. Vol. 1. Theoretical Chemistry. Elsevier, Jan. 1, 1975, pp. 147–218 (cit. on p. 58).

[HE88] Hockney, Roger W. and Eastwood, James W. "Computer Simulation Using Particles". Adam Higler, 1988. isbn: 978-0-85274-392-8 (cit. on pp. 37, 45).

[HGE73] Hockney, Roger W., Goel, S. P., and Eastwood, James W. "A 10000 Particle Molecular Dynamics Model with Long Range Forces". In: *Chemical Physics Letters* 21.3 (1973), pp. 589–591 (cit. on p. 45).

[KP92] Kolafa, Jiří and Perram, John W. "Cutoff Errors in the Ewald Summation Formulae for Point Charge Systems". In: *Molecular Simulation* 9.5 (1992), pp. 351–368 (cit. on p. 44).

[Lag+15] Lagardère, Louis et al. "Scalable Evaluation of Polarization Energy and Associated Forces in Polarizable Molecular Dynamics: II. Toward Massively Parallel Computations Using Smooth Particle Mesh Ewald". In: *Journal of Chemical Theory and Computation* 11.6 (June 9, 2015), pp. 2589–2599. ISSN: 1549-9618 (cit. on p. 30).

[Nar+16] Narth, Christophe et al. "Scalable Improvement of SPME Multipolar Electrostatics in Anisotropic Polarizable Molecular Mechanics Using a General Short-Range Penetration Correction up to Quadrupoles". In: *Journal of Computational Chemistry* 37.5 (2016), pp. 494–506. ISSN: 1096-987X (cit. on p. 30).

[PC03] Ponder, Jay W. and Case, David A. "Force Fields for Protein Simulations". In: *Protein Simulations*. Ed. by Daggett, Valerie. Vol. 66. Advances in Protein Chemistry. Academic Press, 2003, pp. 27–85 (cit. on pp. 16, 19, 57, 69).

[PCF01] Pérez, José-Philippe, Carles, Robert, and Fleckinger, Robert. "Électromagnétisme, Fondements et Applications". 4th ed. Dunod, Nov. 2001. ISBN: 978-2-10-005574-6 (cit. on pp. 17, 31).

[PG96] Pollock, E. L. and Glosli, Jim. "Comments on P3M, FMM, and the Ewald Method for Large Periodic Coulombic Systems". In: *Computer Physics Communications* 95.2–3 (1996), pp. 93–110 (cit. on p. 46).

[Pon12] Ponnusamy, S. "Foundations of Mathematical Analysis". Boston, MA: Birkhäuser Boston, 2012. ISBN: 978-0-8176-8292-7 (cit. on p. 36).

[PPD88] Perram, John W., Petersen, Henrik G., and De Leeuw, Simon W. "An Algorithm for the Simulation of Condensed Matter Which Grows as the 3/2 Power of the Number of Particles". In: *Molecular Physics* 65.4 (Nov. 1, 1988), pp. 875–893. ISSN: 0026-8976 (cit. on p. 44).

[RP03] Ren, Pengyu and Ponder, Jay W. "Polarizable Atomic Multipole Water Model for Molecular Mechanics Simulation". In: *The Journal of Physical Chemistry B* 107.24 (2003), pp. 5933–5947 (cit. on p. 31).

[Sau+92] Saunders, V.r. et al. "On the Electrostatic Potential in Crystalline Systems Where the Charge Density Is Expanded in Gaussian Functions". In: *Molecular Physics* 77.4 (Nov. 1, 1992), pp. 629–665. ISSN: 0026-8976 (cit. on pp. 44, 58).

[SD99] Sagui, Celeste and Darden, Thomas A. "P3M and PME: A Comparison of the Two Methods". In: *Simulation and Theory of Electrostatic Interactions in Solution*. Ed. by Proceedings, AIP Conference. Vol. 492. 1999, pp. 104–113 (cit. on p. 52).

[Sim+14] Simmonett, Andrew C. et al. "An Efficient Algorithm for Multipole Energies and Derivatives Based on Spherical Harmonics and Extensions to Particle Mesh Ewald". In: *Journal of Chemical Physics* 140.18, 184101 (2014), pp. 1–7 (cit. on p. 57).

[Smi81] Smith, E. R. "Electrostatic Energy in Ionic Crystals". In: *Proceedings of the Royal Society of London. A. Mathematical and Physical Sciences* 375.1763 (Apr. 13, 1981), pp. 475–505 (cit. on pp. 39, 41, 53).

[Smi94] Smith, Edgar R. "Calculating the Pressure in Simulations Using Periodic Boundary Conditions". In: *Journal of Statistical Physics* 77.1–2 (1994), pp. 449–472 (cit. on pp. 55, 56).

[Smi98] Smith, W. "Point Multipoles in the Ewald Summation (Revisited)". In: *CCP5 Newsletter* 46 (1998), pp. 18–30 (cit. on pp. 57, 60).

[SPD04] Sagui, Celeste, Pedersen, Lee G., and Darden, Thomas A. "Towards an Accurate Representation of Electrostatics in Classical Force Fields: Efficient Implementation of Multipolar Interactions in Biomolecular Simulations". In: *The Journal of Chemical Physics* 120.1 (Jan. 1, 2004), pp. 73–87. ISSN: 0021-9606 (cit. on p. 57).

[vEK97] Van Eijck, Bouke .P. and Kroon, Jan. "Coulomb Energy of Polar Crystals". In: *Journal of Physical Chemistry B* 101.6 (1997), pp. 1096–1100 (cit. on p. 53).

[Wol+99] Wolf, D. et al. "Exact Method for the Simulation of Coulombic Systems by Spherically Truncated, Pairwise R−1 Summation". In: *The Journal of Chemical Physics* 110.17 (Apr. 22, 1999), pp. 8254–8282. ISSN: 0021-9606 (cit. on p. 36).

[WR84] Warshel, Arieh and Russell, Stephen T. "Calculations of Electrostatic Interactions in Biological Systems and in Solutions". In: *Quarterly Reviews of Biophysics* 17.3 (Aug. 1984), pp. 283–422. ISSN: 0033-5835 (cit. on pp. 57, 69).

[Yor+94] York, D. M. et al. "Atomic-Level Accuracy in Simulations of Large Protein Crystals". In: *Proceedings of the National Academy of Sciences* 91.18 (Aug. 30, 1994), pp. 8715–8718. ISSN: 0027-8424 (cit. on p. 30).

[YY94] York, Darrin M. and Yang, Weitao. "The Fast Fourier Poisson Method for Calculating Ewald Sums". In: *Journal of Chemical Physics* 101.4 (1994), pp. 3298–3300 (cit. on p. 51).

Chapter III

Multiscale ab-initio molecular dynamics

Overview

Programming languages • `Fortran` • `Bash`

APIs • OpenMP • MPI

Modified software • `Gaussian` • `TINKER`

Visit Università di Pisa (Pisa, three weeks, Mar. 2015) with Stefano Caprasecca, Filippo Lipparini, Daniele Loco and Benedetta Mennucci

Presentation LCT Seminar (talk, Paris, May 2015)

Paper

[Loc+16] Loco, Daniele et al. "A QM/MM Approach Using the AMOEBA Polarizable Embedding: From Ground State Energies to Electronic Excitations". In: *Journal of Chemical Theory and Computation* 12.8 (Aug. 9, 2016), pp. 3654–3661. ISSN: 1549-9618

Collaborators • Stefano Caprasecca • Louis Lagardère • Filippo Lipparini • Daniele Loco • Benedetta Mennucci • Jean-Philippe Piquemal

III.A Problem setting

We have presented in Chapter II a method to do efficient molecular dynamics simulations with a classical polarisable force field. With its computational complexity of $\mathcal{O}(N \log N)$, the Ewald's method of summation to perform computations for a large number of particles. Molecular dynamics for millions of atoms can be considered, thus allowing to accurately take into account the environment of systems of interest.

However, classical methods are inherently limited by the fact they cannot describe electrons. As such, effects such as fluorescence, which can be explained by excited states in quantum mechanics, or even seemingly simple concepts such as the creation and destruction of molecular bonds cannot be modeled. Alas, quantum methods are much more computationally intensive, with computational complexity in $\mathcal{O}(N^4)$ for Hartree–Fock, between $\mathcal{O}(N^3)$ and $\mathcal{O}(N^4)$, depending on the approximation of the model, for density functional theory and even higher for post-Hartree–Fock methods [CBM06]. Such methods are thus limited to modeling a few thousand atoms, which is not big enough to describe most proteins; and even less so to describe them with a complex environment.

Thankfully, quantum mechanics precision may not be needed everywhere. For example in drug design, biologists often have insights in the processes that can take place, and hence know particular sites of proteins where the description should be precise; what can be referred as active sites.

In this chapter, we look at how to model large chemical systems by developing multiscale — or multiphysics — methods. Some parts of the molecular system will be described with quantum mechanics, while others will be described with molecular mechanics or continuum solvation. By mixing the two, we can limit the computational complexity by having $\mathcal{O}(N_q^{\geq 3} + N_m \log N_m)$, where N_q is the number of quantum atoms and N_m is the number of classical atoms.

The idea to combine different physics is not new. For example, in quantum mechanics, chemists already make abundant use of hybrid functionals in density functional theory, for example through

range separation of the Coulombic potential [TCS04]. Multiphysics quantum mechanics/continuum solvation methods have also been developed, in particular with the polarisable continuum model [Amo+98].

For quantum mechanics/molecular mechanics methods, the most common description is done using *electrostatic embedding*, a method we will use in this chapter. This method was pioneered in the 1970s and 1980s by the work of the 2014 Nobel laureates Martin Karplus [Kar14], Michael Levitt [Lev14] and Arieh Warshell [War14]. This method takes into account an isolated quantum mechanics system and its interaction with the classical environment, represented as point charges on the positions of the molecular mechanics atoms. This limits the use of electrostatic embedding to small systems that can be fully computed with quantum methods. However, we should note that there are ways to overcome this limit, in particular through the use of pseudopotentials. However this goes beyond the scope of this chapter. We note that even at the beginning of the development of those methods, the authors were aware of the need to use point multipoles and polarisation for the molecular mechanics part; in particular to accurately describe water [WR84].

The present work started in collaboration with the group of Benedetta Menucci in Pisa, which was already developing a quantum mechanics/molecular mechanics [Cur+09] model, *mmpol*. The model uses the amber force field, with point charges and polarisation, and has been successfully coupled with polarisable continuum model models [CCM12] to have quantum mechanics/molecular mechanics/continuum solvation simulations. The aim of the present work was to develop the same kind of methods, but with the amoeba force field, which is singularly accurate in describing water, for example, and has a larger set of parameterisation [PC03], which makes it more suitable at simulating large and complex molecular systems.

In this chapter we will only give a bare-bones description of the proposed quantum mechanics/molecular mechanics method that we call qm/amoeba, and the ideas to use it for molecular dynamics. We refer the reader to the article Page 74 for more details.

III.B Method

We recall from Section I.E that the energy functional of the amoeba force field accounts for intramolecular energies, Van der Waals and Coulomb potentials as well as polarisation

$$\mathcal{E}_{\text{AMOEBA}}(\mu) := \mathcal{E}^{\text{intra}} + \mathcal{E}^{\text{VdW}} + \mathcal{E}^{\text{el}} + \mathcal{E}^{\text{pol}}(\mu), \tag{II.1}$$

where μ represents the induced dipoles.

We propose a global variational energy, compatible with the use of self-consistent field methods, depending on the quantum density D and the classical induced dipoles μ written as the sum of three terms

$$\mathcal{E}(D, \mu) := \mathcal{E}_{\text{QM}}(D) + \mathcal{E}_{\text{AMOEBA}}(\mu) + \mathcal{E}_{\text{coup}}(D, \mu), \tag{II.2}$$

of which we will give a brief description. The sum of the last two terms accounts for the energy due to the environment

$$\mathcal{E}_{\text{env}}(D, \mu) := \mathcal{E}_{\text{AMOEBA}}(\mu) + \mathcal{E}_{\text{coup}}(D, \mu). \tag{II.3}$$

The coupling term $\mathcal{E}_{\text{coup}}(D, \mu)$ accounts for the reaction of the classical induced dipoles to the electric field due to the quantum mechanics density as well as the Van der Waals and Coulomb energy between the quantum mechanics and molecular mechanics subsystems

$$\mathcal{E}_{\text{coup}}(D, \mu) := \mathcal{E}^{\text{pol}}_{\text{coup}}(D, \mu) + \mathcal{E}^{\text{VdW}}_{\text{coup}} + \mathcal{E}^{\text{el}}_{\text{coup}}(D). \tag{II.4}$$

The Van der Waals interactions are treated using the amoeba force field, using only the positions of the quantum atoms. This is due to the peculiar difficulty in having an efficient model for

dispersion and repulsion in quantum mechanics. Hence it makes sense to regroup them with the intramolecular energy functional, as none of those terms depends on either the quantum density or the induced dipoles. We will denote this new functional by $\mathcal{E}_{\text{FF}}$. Finally, if we merge the classical and coupling polarisation in the same functional $\tilde{\mathcal{E}}^{\text{pol}}(D,\mu)$, we can rewrite the environment functional as the sum of

$$\mathcal{E}_{\text{env}}(D,\mu) = \mathcal{E}_{\text{FF}} + \tilde{\mathcal{E}}^{\text{pol}}(D,\mu) + \mathcal{E}^{\text{el}}_{\text{coup}}(D), \tag{II.5}$$

where

$$\mathcal{E}_{\text{FF}} := \mathcal{E}^{\text{intra}} + \mathcal{E}^{\text{VdW}} + \mathcal{E}^{\text{VdW}}_{\text{coup}} + \mathcal{E}^{\text{el}}, \tag{II.6a}$$

$$\tilde{\mathcal{E}}^{\text{pol}}(D,\mu) := \mathcal{E}^{\text{pol}}_{\text{AMOEBA}}(\mu) - \frac{1}{2}(\mu_d + \mu_p)\mathrm{E}_{\text{QM}}(D), \tag{II.6b}$$

$$\mathcal{E}^{\text{el}}_{\text{coup}}(D) := qV_{\text{QM}}(D) - \mu_{\text{stat}}\mathrm{E}_{\text{QM}}(D) - \Theta\mathsf{G}_{\text{QM}}(D), \tag{II.6c}$$

and where q, μ_{stat} and Θ are matrices representing respectively the permanent charges, dipoles and quadrupoles at the positions of the classical atoms. The quantum potential and its first and second derivatives are evaluated at each classical atomic positions and have respectively the following expressions

$$V_{\text{QM}}(r_i, D) := \sum_{k=1}^{N_{\text{QM}}} \frac{Z_k}{|r_i - R_k|} + \sum_{\mu,\nu=1}^{N_b} D_{\mu\nu} V_{\mu\nu}(r_i), \tag{II.7a}$$

$$\mathrm{E}_{\text{QM}}(r_i, D) := \sum_{k=1}^{N_{\text{QM}}} \frac{Z_k(r_i - R_k)}{|r_i - R_k|^3} + \sum_{\mu,\nu=1}^{N_b} D_{\mu\nu} \mathrm{E}_{\mu\nu}(r_i), \tag{II.7b}$$

$$[\mathsf{G}_{\text{QM}}]^{\gamma\gamma'}(r_i, D) := \sum_{k=1}^{N_{\text{QM}}} Z_k \left(\frac{3(r_i^\gamma - R_k^\gamma)(r_i^{\gamma'} - R_k^{\gamma'})}{|r_i - R_k|^5} - \frac{\delta_{\gamma\gamma'}}{|r_i - R_k|^3} \right) + \sum_{\mu,\nu=1}^{N_b} D_{\mu\nu} \mathsf{G}_{\mu\nu}^{\gamma\gamma'}(r_i), \tag{II.7c}$$

where γ and γ' are placeholders for Cartesian coordinates x, y or z. The integrals $V_{\mu\nu}(r_i)$, $\mathrm{E}_{\mu\nu}(r_i)$ and $\mathsf{G}_{\mu\nu}^{\gamma\gamma'}(r_i)$ have the expressions

$$V_{\mu\nu}(r_i) := -\int_{\mathbf{R}^3} \frac{\chi_\mu(r)\chi_\nu(r)}{|r_i - r|}, \tag{II.8a}$$

$$\mathrm{E}_{\mu\nu}(r_i) := -\int_{\mathbf{R}^3} \frac{\chi_\mu(r)\chi_\nu(r)(r_i - r)}{|r_i - r|^3}, \tag{II.8b}$$

$$\mathsf{G}_{\mu\nu}^{\gamma\gamma'}(r_i) := -\int_{\mathbf{R}^3} \chi_\mu(r)\chi_\nu(r) \left(\frac{3(r_i^\gamma - r^\gamma)(r_i^{\gamma'} - r^{\gamma'})}{|r_i - r|^5} - \frac{\delta_{\gamma\gamma'}}{|r_i - r|^3} \right) \mathrm{d}^3 r, \tag{II.8c}$$

where the functions $r_i \mapsto \chi_\cdot(r_i)$ are the atomic orbitals (see Section I.D.3). Using a variational formulation, the Fock matrix is obtained as the derivative of the energy functional with respect to the density matrix

$$F(D,\mu) := \frac{\partial \mathcal{E}(D,\mu)}{\partial D} = F_{\text{QM}}(D) + F_{\text{env}}(D,\mu), \tag{II.9}$$

where F_{QM} is the standard Fock matrix for the quantum subsystem and

$$(F_{\text{env}})_{\mu\nu} := qV_{\mu\nu} - \mu_{\text{stat}}\mathrm{E}_{\mu\nu} - \Theta\mathsf{G}_{\mu\nu} - \frac{1}{2}(\mu_d + \mu_p)\mathrm{E}_{\mu\nu}. \tag{II.10}$$

We have split the terms with respect to the field produced by the quantum density in case the induced dipoles sites are different from the permanent multipoles sites.

To solve this, we can solve alternatively for the induced dipoles μ and for the density matrices D, hoping to achieve convergence. Which the algorithm does in practice; this is no small matter, due to the lack of repulsive model in quantum mechanics (see remark above regarding the VAN DER WAALS terms), which cannot prevent density from *spilling out* from the quantum mechanics part to the molecular mechanics part; especially if a positively charge part of the molecular mechanics comes close to the quantum mechanics subsystem.

The implementation of this method in `Gaussian` [Fri+09] and `TINKER` [Pon+10] was successful in computing properties for excited states (see supporting paper Page 74).

III.c Molecular dynamics

To be able to perform molecular dynamics, we need the gradients of the energy terms with respect to the atomic positions. The derivatives of $\mathcal{E}_{\text{QM}}(D)$ and $\mathcal{E}_{\text{AMOEBA}}(\mu)$ are already known from the models we have used. The new formulæ we need are for

$$\frac{\partial \tilde{\mathcal{E}}^{\text{pol}}}{\partial R_k}(D,\mu) = -\frac{1}{2}(\mu_d + \mu_p)\frac{\partial \mathrm{E}_{\text{QM}}}{\partial R_k}(D) \tag{III.1}$$

and

$$\frac{\partial \mathcal{E}^{\text{el}}_{\text{coup}}}{\partial R_k}(D) = q\frac{\partial V_{\text{QM}}}{\partial R_k}(D) - \mu_{\text{stat}}\frac{\partial \mathrm{E}_{\text{QM}}}{\partial R_k}(D) - \Theta\frac{\partial \mathsf{G}_{\text{QM}}}{\partial R_k}(D) \tag{III.2}$$

for all $k \in [\![1 \,..\, N_{\text{QM}}]\!]$. There holds for the potential, the field and its gradient

$$\frac{\partial V_{\text{QM}}}{\partial R_k^\alpha}(r_i, D) = \frac{Z_k(r_i^\alpha - R_k^\alpha)}{|r_i - R_k|^3} + \sum_{\mu,\nu=1}^{N_b} D_{\mu\nu}\frac{\partial V_{\mu\nu}}{\partial R_k^\alpha}(r_i) \tag{III.3a}$$

$$\frac{\partial (\mathrm{E}_{\text{QM}})^{\gamma'}_{\mu\nu}}{\partial R_k^\alpha}(r_i, D) = Z_k\left(\frac{3(r_i^\alpha - R_k^\alpha)(r_i^{\gamma'} - R_k^{\gamma'})}{|r_i - R_k|^5} - \frac{\delta_{\alpha\gamma'}}{|r_i - R_k|^3}\right) + \sum_{\mu,\nu=1}^{N_b} D_{\mu\nu}\frac{\partial \mathrm{E}^{\gamma'}_{\mu\nu}}{\partial R_k^\alpha}(r_i) \tag{III.3b}$$

$$\begin{aligned}\frac{\partial [\mathsf{G}_{\text{QM}}]^{\gamma\gamma'}_{\mu\nu}}{\partial R_k^\alpha}(r_i, D) = {} & 3Z_k\frac{(r_i^\alpha - R_k^\alpha)\,\delta_{\gamma\gamma'} + (r_i^\gamma - R_k^\gamma)\,\delta_{\alpha\gamma'} + (r_i^{\gamma'} - R_k^{\gamma'})\,\delta_{\alpha\gamma}}{|r_i - R_k|^5} \\ & - 15Z_k\frac{(r_i^\alpha - R_k^\alpha)(r_i^\gamma - R_k^\gamma)(r_i^{\gamma'} - R_k^{\gamma'})}{|r_i - R_k|} + \sum_{\mu,\nu=1}^{N_b} D_{\mu\nu}\frac{\partial G^{\gamma\gamma'}_{\mu\nu}}{\partial R_k^\alpha}(r_i).\end{aligned} \tag{III.3c}$$

We note that the gradients of the integrals in Eq. (II.8) are already computed by quantum mechanics codes, and do not need to be changed.

We also need the derivatives of $\tilde{\mathcal{E}}^{\text{pol}}$ and $\mathcal{E}^{\text{el}}_{\text{coup}}$ with respect to the positions of the classical nuclei. The formulæ are a bit simpler once we have noticed that the derivative of the potential is the electrostatic field, which we already have. The same is true for its gradient. The only new quantity that we have to write is the matrix of third derivatives of the potential

$$\begin{aligned}[O_{\text{QM}}]^{\alpha\beta\gamma}(r_i, D) := {} & -\sum_{k=1}^{N_{\text{QM}}} 3Z_k\frac{(r_i^\alpha - R_k^\alpha)\,\delta_{\beta\gamma} + (r_i^\beta - R_k^\beta)\,\delta_{\alpha\gamma} + (r_i^\gamma - R_k^\gamma)\,\delta_{\alpha\beta}}{|r_i - R_k|^5} \\ & - 15Z_k\frac{(r_i^\alpha - R_k^\alpha)(r_i^\beta - R_k^\beta)(r_i^\gamma - R_k^\gamma)}{|r_i - R_k|} + \sum_{\mu,\nu=1}^{N_b} D_{\mu\nu}O^{\alpha\beta\gamma}_{\mu\nu}(r_i),\end{aligned} \tag{III.4}$$

where

$$O_{\mu\nu}^{\alpha\beta\gamma}(r_i) := -\int_{\mathbf{R}^3} \chi_\mu(r)\chi_\nu(r)\left(3\frac{(r_i^\alpha - r^\alpha)\,\delta_{\beta\gamma} + (r_i^\beta - r^\beta)\,\delta_{\alpha\gamma} + (r_i^\gamma - r^\gamma)\,\delta_{\alpha\beta}}{|r_i - r|^5} - 15\frac{(r_i^\alpha - r^\alpha)(r_i^\beta - r^\beta)(r_i^\gamma - r^\gamma)}{|r_i - r|^7}\right)\mathrm{d}^3 r. \quad \text{(III.5)}$$

The derivatives for the electrostatic energy can now be concisely written as

$$\frac{\partial \mathcal{E}_{\text{coup}}^{\text{el}}}{\partial r_i^\alpha}(D) = q(\mathrm{E}_{\text{QM}})^\alpha(D) + \mu_{\text{stat}}^\beta(\mathsf{G}_{\text{QM}})^{\alpha\beta}(D) + \Theta^{\beta\gamma}(\mathsf{O}_{\text{QM}})^{\alpha\beta\gamma}(D). \quad \text{(III.6)}$$

We note that in TINKER, there is a subtlety due to the definitions of the dipoles and quadrupoles: the quantities are given with respect to local coordinates on the molecules. Hence, when deriving the electrostatics contributions with respect to classical particles, we have to also account for these artificial forces.

Finally, it remains to evaluate the derivatives of the polarisation energy

$$\frac{\partial \tilde{\mathcal{E}}^{\text{pol}}}{\partial r_i^\alpha}(D,\mu) = \frac{\partial \mathcal{E}_{\text{AMOEBA}}^{\text{pol}}}{\partial r_i^\alpha}(\mu) - \frac{1}{2}(\mu_d^\gamma + \mu_p^\gamma)(\mathsf{G}_{\text{QM}})^{\alpha\gamma}(D), \quad \text{(III.7)}$$

where the first part of the sum is unchanged from classical polarisable computations.

We refer the reader to Fig. III.1 for a workflow of the implementation for molecular dynamics in Gaussian and TINKER. A Bash driver was developed to launch successively Gaussian and TINKER. The choice to use the two pieces of software and not only Gaussian was to simplify the implementation, by not having to redo all the work of Ponder in implementing anew the AMOEBA force field. The method was successfully used for molecular dynamics.

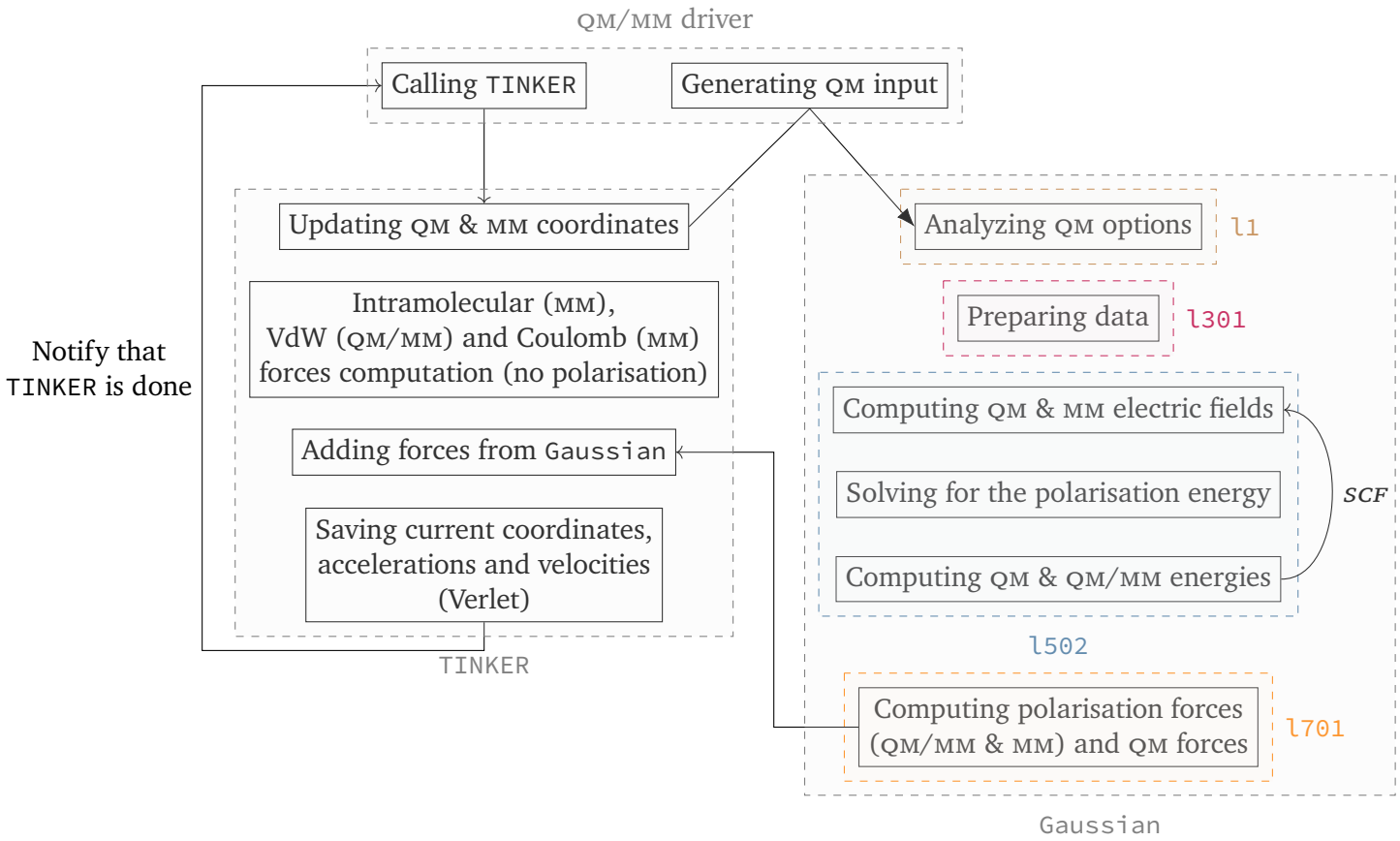

Figure III.1: Workflow for the quantum mechanics/molecular mechanics molecular dynamics. The inner boxes in `Gaussian` represent subprograms in which the developments was done.

JCTC Journal of Chemical Theory and Computation
Article
pubs.acs.org/JCTC

A QM/MM Approach Using the AMOEBA Polarizable Embedding: From Ground State Energies to Electronic Excitations

Daniele Loco,[†] Étienne Polack,[‡,§] Stefano Caprasecca,[†] Louis Lagardère,[∥,‡] Filippo Lipparini,*[,⊥] Jean-Philip Piquemal,*[,‡,#,▽] and Benedetta Mennucci*[,†]

[†]Dipartimento di Chimica e Chimica Industriale, Università di Pisa, via G. Moruzzi 13, I-56124 Pisa, Italy
[‡]Sorbonne Universités, UPMC Univ. Paris 06, UMR 7616, Laboratoire de Chimie Théorique, F-75005, Paris, France
[§]Sorbonne Universités, UPMC Univ. Paris 06, UMR 7598, Laboratoire Jacques-Louis Lions, F-75005, Paris, France
[∥]Sorbonne Universités, UPMC Univ. Paris 06, Institut du Calcul et de la Simulation, F-75005, Paris, France
[⊥]Institut für Physikalische Chemie, Universität Mainz, Duesbergweg 10-14, D-55128 Mainz, Germany
[#]CNRS, UMR 7598 and 7616, F-75005, Paris, France
[▽]Department of Biomedical Engineering, The University of Texas at Austin, Austin, Texas 78712, USA

Supporting Information

ABSTRACT: A fully polarizable implementation of the hybrid quantum mechanics/molecular mechanics approach is presented, where the classical environment is described through the AMOEBA polarizable force field. A variational formalism, offering a self-consistent relaxation of both the MM induced dipoles and the QM electronic density, is used for ground state energies and extended to electronic excitations in the framework of time-dependent density functional theory combined with a state specific response of the classical part. An application to the calculation of the solvatochromism of the pyridinium *N*-phenolate betaine dye used to define the solvent $E_T(30)$ scale is presented. The results show that the QM/AMOEBA model not only properly describes specific and bulk effects in the ground state but it also correctly responds to the large change in the solute electronic charge distribution upon excitation.

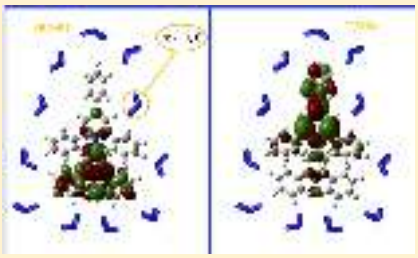

1. INTRODUCTION

The idea of studying an intrinsically quantum-mechanical (QM) process taking place in a complex environment by partitioning the whole system into a (smaller) subsystem (*S*) and the environment (*E*) has a long history in quantum chemistry. Within this framework, *S* is identified as the minimal subunit where the process occurs, and is described using an accurate albeit expensive level of theory, typically QM, whereas the environment is treated at a much lower detail but sufficient to properly describe its effects on the process under study. Two alternative strategies are most commonly followed: one can either model the environment as a polarizable continuum[1,2] or employ an atomistic description of *E* by introducing a molecular mechanics (MM) force field (FF).[3−7] The latter class of approaches is commonly referred to as QM/MM, and is widely used, particularly when electronic processes in complex environments are studied.

Since the first formulations, different QM/MM approaches have been proposed; in most of them, the *effective* Hamiltonian defining the electronic properties of the QM subsystem in the presence of the MM system is divided into a term describing the isolated *S* and a term taking into account its electrostatic interaction with the classical environment through point charges centered on the MM atoms. This formulation, known as "electrostatic embedding", is nowadays the most common QM/MM formulation: it in fact allows one to include the effects of the classical subsystem in the determination of the QM electronic density and all its related properties. What, however, this approach still misses is the possibility for *E* to polarize in response to the charge density (and its eventual changes) of the *S* subsystem. To include such a mutual polarization effect, an extension of the QM/MM formulation beyond the electrostatic embedding is necessary and different alternative strategies have been proposed so far.[8−20] In this work, we will illustrate the theoretical development and the computational implementation of a novel polarizable QM/MM approach, based on the AMOEBA polarizable FF,[21−23] which we will refer to as QM/AMOEBA. Within this framework, the environment polarization is achieved through the use of atomic point dipoles, which are induced as a response to the electric field generated by the *S* system as well as the same MM sites bearing distributed multipoles up to quadrupoles. An approach to couple AMOEBA to a QM package has been recently proposed[24] in the framework of a non-self-consistent procedure. In this contribution, for the first time in the context

Received: April 16, 2016
Published: June 24, 2016

DOI: 10.1021/acs.jctc.6b00385
J. Chem. Theory Comput. 2016, 12, 3654−3661

Journal of Chemical Theory and Computation Article

of AMOEBA, the global relaxation of the mutual QM/MM polarization is achieved by solving the QM/AMOEBA equations in a self-consistent manner, without approximations.

The implementation is further extended to describe electronically excited states. As a matter of fact, nonpolarizable QM/MM formulations can be easily extended to excited states, as the "new" operator has a one-electron nature. When a polarizable embedding like AMOEBA is used instead, a difficulty appears when a linear response (LR) approach like that commonly used in the time-dependent density functional theory (TD-DFT) is used. In the LR formulation, in fact, the whole spectrum of the excitations of interest is determined in a single step calculation by solving for the poles of the proper response function. When the same problem is formulated within a polarizable embedding, an additional contribution has to be taken into account, namely, the dynamic response of the *E* subsystem. In the standard formulation of polarizable models (both in their continuum and MM formulations), such a response is calculated through the transition densities corresponding to the different excitations: the oscillating transition density of the *S* subsystem induces an oscillating polarization in the *E* subsystem which creates an in-phase response acting back to the transition density.[25,26] This LR formulation has been shown to properly describe the dynamic environment effect in excitations involving bright states characterized by a large transition dipole moment.[27] The same formulation, however, lacks the capability of describing the relaxation of the environment in response to the changes in the QM density upon excitation: it is therefore not suitable to model excitations involving large changes such as charge-transfer (CT) like excitations. To overcome this shortcoming, various models have been introduced to recover a state-specific (SS) description of the response both within a continuum[28−30] or an MM formulation.[20] Here we adopt a perturbative correction which is exactly equivalent to the so-called corrected linear response (c-LR) scheme originally developed for polarizable continuum models.[28] Within this framework, a relaxed density matrix is calculated for the excited state of interest and the corresponding excitation energy is corrected for the interaction with the proper induced dipole moments within the environment.

To show the potentialities of the method, we have selected a very well-known solvatochromic probe, namely, the pyridinium *N*-phenolate betaine dye (or "betaine-30"). Due to its large negative solvatochromism combined with a high solubility in many different solvents, it was proposed as a solvatochromic indicator for the determination of the solvent polarity, through an empirical scale called $E_T(30)$.[31,32] From a computational point of view, this molecule is really challenging for at least two reasons: (i) it is zwitterionic in its ground state and (ii) the excitation is related to an intramolecular charge transfer (CT) between the pyrimidine and phenolate moieties which acts to reduce the zwitterionic character. For such a kind of excitation, the solvation model not only needs to be able to properly describe both specific and bulk effects in the ground state, but it also has to correctly respond to the large change in the electronic charge distribution from the ground to the excited state. We will show that both of these requirements are fully satisfied by our implementation of the QM/AMOEBA.

2. THEORY AND IMPLEMENTATION

2.1. The AMOEBA Force Field. One of the main characteristics of AMOEBA is the improved description of the electrostatics through atomic multipoles, up to the quadrupoles, placed on each classical atom. Polarization effects are included by using an induced point-dipole model within the smeared Thole damping interaction scheme.[33] This is achieved by also providing the classical atoms with atomic polarizabilities. In general, the polarizability $\boldsymbol{\alpha}_i$ is a symmetric matrix; in practice, the scalar isotropic polarizabilities $\langle\alpha_i\rangle \equiv \frac{1}{3}\,\mathrm{tr}(\boldsymbol{\alpha}_i)$ are used instead.

In a purely classical framework, at each polarizable site *i*, the static multipolar distribution generates an electric field $\vec{E}_i$ that induces an electric point-dipole moment, $\vec{\mu}_i$. The set $\{\vec{\mu}_i\}_{i=1}^{N_{\mathrm{Pol}}}$ is the unknown of the polarization problem and the minimizer of the functional[34]

$$\mathcal{E}^{\mathrm{Pol}} = -\sum_{i=1}^{N_{\mathrm{Pol}}} E_i^{\alpha}\mu_i^{\alpha} + \frac{1}{2}\sum_{i=1}^{N_{\mathrm{Pol}}} (\boldsymbol{\alpha}_i^{-1})^{\alpha\beta}\mu_i^{\alpha}\mu_i^{\beta} + \frac{1}{2}\sum_{i=1}^{N_{\mathrm{Pol}}}\sum_{j\neq i}^{N_{\mathrm{Pol}}} \boldsymbol{\mathcal{T}}_{ij}^{\alpha\beta}\mu_i^{\alpha}\mu_j^{\beta} \tag{1}$$

where indexes α and β generally indicate Cartesian components, for which the Einstein summation convention is assumed; E_i and μ_i are the electric field and the induced dipole, both at atom site *i*. Note that we will generally assume that, while all the classical sites are characterized by multipole moments, not all of them will be polarizable, i.e., associated with a polarizability. The number of classical and polarizable sites are indicated as N_{MM} and N_{Pol}, respectively, with $N_{\mathrm{MM}} \geq N_{\mathrm{Pol}}$. Further details can be found in previous works on the force field;[23,34] here, we only recall the expression for the (damped) dipole interaction tensor:

$$\boldsymbol{\mathcal{T}}_{ij}^{\alpha\beta} = -\frac{\delta_{\alpha\beta}}{|\vec{r}_i - \vec{r}_j|^3}\lambda_3(u_{ij}) + 3\frac{|\vec{r}_i - \vec{r}_j|^{\alpha}|\vec{r}_i - \vec{r}_j|^{\beta}}{|\vec{r}_i - \vec{r}_j|^5}\lambda_5(u_{ij}) \tag{2}$$

Several damping schemes to avoid the well-known *polarization catastrophe* can be found in the literature.[33,35−37] The scheme employed in AMOEBA makes use of an exponential damping

$$\begin{cases} \lambda_3(u_{ij}) = 1 - \mathrm{e}^{-au_{ij}^3} \\ \lambda_5(u_{ij}) = 1 - (1 + \mathrm{e}^{-au_{ij}^3})\mathrm{e}^{-au_{ij}^3} \end{cases} \tag{3}$$

where $u_{ij} = r_{ij}/(\langle\alpha_i\rangle\langle\alpha_j\rangle)^{1/6}$ is the *effective distance* between two polarizable sites *i* and *j*.

In a more compact notation, $\boldsymbol{E} = (\vec{E}_1^T, \vec{E}_2^T, ..., \vec{E}_{N_{\mathrm{Pol}}}^T)^T$ and $\boldsymbol{\mu} = (\vec{\mu}_1^T, \vec{\mu}_2^T, ..., \vec{\mu}_{N_{\mathrm{Pol}}}^T)^T$ are the collections of the electric field and induced point dipoles at each polarizable site, while the symmetric, positive definite matrix $\boldsymbol{T}$, the size of which is $3N_{\mathrm{Pol}} \times 3N_{\mathrm{Pol}}$ and which is usually called the polarization or interaction matrix, is defined as in eq 4, where $(\boldsymbol{\mathcal{T}})_{ij}$ is the 3×3 matrix defined as in eq 2.

$$\boldsymbol{T} = \begin{pmatrix} \boldsymbol{\alpha}_1^{-1} & \boldsymbol{\mathcal{T}}_{12} & \cdots & \boldsymbol{\mathcal{T}}_{1N_{\mathrm{Pol}}} \\ \boldsymbol{\mathcal{T}}_{21} & \boldsymbol{\alpha}_2^{-1} & \cdots & \boldsymbol{\mathcal{T}}_{2N_{\mathrm{Pol}}} \\ \vdots & \vdots & \ddots & \vdots \\ \boldsymbol{\mathcal{T}}_{N_{\mathrm{Pol}}1} & \boldsymbol{\mathcal{T}}_{N_{\mathrm{Pol}}2} & \cdots & \boldsymbol{\alpha}_{N_{\mathrm{Pol}}}^{-1} \end{pmatrix} \tag{4}$$

Equation 1 can now be rewritten in matrix form as

DOI: 10.1021/acs.jctc.6b00385
J. Chem. Theory Comput. 2016, 12, 3654−3661

Journal of Chemical Theory and Computation Article

$$\mathcal{E}^{\mathrm{Pol}} = \frac{1}{2}\boldsymbol{\mu}^{\dagger}\boldsymbol{T}\boldsymbol{\mu} - \boldsymbol{\mu}^{\dagger}\boldsymbol{E} \tag{5}$$

It is possible to find the polarization energy as the minimum of $\mathcal{E}^{\mathrm{Pol}}$ with respect to the induced point dipoles,[34] which corresponds to the solution to the linear system

$$\frac{\partial \mathcal{E}^{\mathrm{Pol}}}{\partial \boldsymbol{\mu}} = \boldsymbol{T}\boldsymbol{\mu} - \boldsymbol{E} = 0 \tag{6}$$

This is the general formulation of the polarization problem, and is clearly variational. In the case of AMOEBA, however, the polarization energy is no longer a variational functional of the induced dipoles. This is due to the fact that two sets of induced dipoles are generated by two electric fields, differing for the scaling of the local interactions. Particularly, one set of dipoles, indicated as $\boldsymbol{\mu}_{\mathrm{d}}$, is due to the so-called "direct field" $\boldsymbol{E}_{\mathrm{d}}$, which is produced by multipoles placed on all the other classical sites. The other set, indicated as $\boldsymbol{\mu}_{\mathrm{p}}$, is induced by a "polarization field" $\boldsymbol{E}_{\mathrm{p}}$, where the contribution of the $1-n$ (where $n = 2,3,4,5$) neighbors is scaled. A more detailed treatment on this point can be found in other works of some of us.[38] Here it suffices to say that the previous expression can be recast taking into account the different fields and induced dipoles. We recall that

$$\mathcal{E}_{\mathrm{A}}^{\mathrm{Pol}} = -\frac{1}{2}\boldsymbol{\mu}_{\mathrm{d}}^{\dagger}\boldsymbol{E}_{\mathrm{p}} \tag{7}$$

is the proper expression for the AMOEBA polarization energy. Imposing the stationarity conditions for both sets of dipoles

$$\begin{cases} \boldsymbol{T}\boldsymbol{\mu}_{\mathrm{d}} = \boldsymbol{E}_{\mathrm{d}} \\ \boldsymbol{T}\boldsymbol{\mu}_{\mathrm{p}} = \boldsymbol{E}_{\mathrm{p}} \end{cases} \tag{8}$$

where each set of induced dipoles is the variational minimizer of the corresponding energy functional, it is possible to reformulate the AMOEBA polarization energy as the combination of three variational expressions, finally obtaining

$$\mathcal{E}_{\mathrm{A}}^{\mathrm{Pol}}(\boldsymbol{\mu}_{\mathrm{d}}, \boldsymbol{\mu}_{\mathrm{p}}) = \frac{1}{2}\boldsymbol{\mu}_{\mathrm{d}}^{\dagger}\boldsymbol{T}\boldsymbol{\mu}_{\mathrm{p}} - \frac{1}{2}(\boldsymbol{\mu}_{\mathrm{p}}^{\dagger}\boldsymbol{E}_{\mathrm{d}} + \boldsymbol{\mu}_{\mathrm{d}}^{\dagger}\boldsymbol{E}_{\mathrm{p}}) \tag{9}$$

2.2. An SCF-QM/AMOEBA Formulation. The coupling of a classical description of the environment with SCF-based methods has already been discussed, especially for polarizable continuum solvation models in a variational scheme.[39,40] Generalizing those formulations to the QM/AMOEBA approach, the global variational energy functional can be written as the sum of three terms: (i) a purely QM energy functional, i.e., the SCF energy functional $\mathcal{E}^{\mathrm{QM}}$; (ii) a purely MM term given by the sum of the bonding, dispersion/repulsion, electrostatic, and polarization terms according to their definition within the AMOEBA FF; and (iii) a coupling term; namely, we have

$$\begin{aligned} \mathcal{E}(\mathbf{P}, \boldsymbol{\mu}) &= \mathcal{E}^{\mathrm{QM}}(\mathbf{P}) + \mathcal{E}^{\mathrm{MM}}(\boldsymbol{\mu}) + \mathcal{E}^{\mathrm{Coup}}(\mathbf{P}, \boldsymbol{\mu}) \\ &= \mathcal{E}^{\mathrm{QM}}(\mathbf{P}) + \mathcal{E}^{\mathrm{Env}}(\mathbf{P}, \boldsymbol{\mu}) \end{aligned} \tag{10}$$

where in the RHS of the equation we added together the coupling and MM energy functionals in $\mathcal{E}^{\mathrm{Env}}$. Notice how the variational strategy, by introducing the global energy functional in eq 10, automatically takes into account the mutual polarization effects between the QM density and the induced dipoles.[39,41]

The variational environment term, $\mathcal{E}^{\mathrm{Env}}$, can be written as the sum of a constant MM contribution $\mathcal{E}^{\mathrm{FF}}$ which does not depend on either the electronic density or the induced dipoles, a polarization energy, and a QM/MM coupling part. For the following manipulations, it is convenient to write separately the interaction of the QM density with the static multipoles as $\mathcal{E}^{\mathrm{QM/MM}}(\mathbf{P})$, and to add the interaction between the induced dipoles and the QM density to the polarization energy, from now on named $\tilde{\mathcal{E}}^{\mathrm{Pol}}(\mathbf{P}, \boldsymbol{\mu})$; the resulting expressions of the various terms are

$$\mathcal{E}^{\mathrm{Env}}(\boldsymbol{P}, \boldsymbol{\mu}) = \mathcal{E}^{\mathrm{FF}} + \tilde{\mathcal{E}}^{\mathrm{Pol}}(\mathbf{P}, \boldsymbol{\mu}) + \mathcal{E}^{\mathrm{QM/MM}}(\boldsymbol{P}) \tag{11}$$

$$\begin{aligned} \tilde{\mathcal{E}}^{\mathrm{Pol}}(\boldsymbol{P}, \boldsymbol{\mu}) = \frac{1}{2}\boldsymbol{\mu}_{\mathrm{d}}^{\dagger}\boldsymbol{T}\boldsymbol{\mu}_{\mathrm{p}} - \frac{1}{2}(\boldsymbol{\mu}_{\mathrm{p}}^{\dagger}\boldsymbol{E}_{\mathrm{d}} + \boldsymbol{\mu}_{\mathrm{d}}^{\dagger}\boldsymbol{E}_{\mathrm{p}}) \\ - \frac{1}{2}(\boldsymbol{\mu}_{\mathrm{p}} + \boldsymbol{\mu}_{\mathrm{d}})^{\dagger}\mathbf{E}^{\mathrm{QM}}(\mathbf{P}) \end{aligned} \tag{12}$$

$$\mathcal{E}^{\mathrm{QM/MM}}(\boldsymbol{P}) = \boldsymbol{q}^{\dagger}\boldsymbol{V}^{\mathrm{QM}}(\boldsymbol{P}) - \boldsymbol{\mu}_{\mathrm{s}}^{\dagger}\mathbf{E}^{\mathrm{QM}}(\boldsymbol{P}) - \boldsymbol{\Theta}^{\dagger}\nabla\boldsymbol{E}^{\mathrm{QM}}(\boldsymbol{P}) \tag{13}$$

where q_i, $\vec{\mu}_{\mathrm{s},i}$, and $\boldsymbol{\Theta}_i$ are the fixed charges, dipoles, and quadrupoles, respectively.

The electronic terms of $\mathcal{E}^{\mathrm{QM/MM}}$ in eq 13 can be expressed as functions of the one-particle electron density matrix elements

$$\begin{cases} V^{\mathrm{QM}}(\vec{r}_i; \boldsymbol{P}) = \sum_{\mu\nu}^{N_{\mathrm{b}}} P_{\mu\nu} V_{\mu\nu}(\vec{r}_i) \\ \qquad = -\sum_{\mu\nu}^{N_{\mathrm{b}}} P_{\mu\nu} \int_{\mathbb{R}^3} \frac{\chi_\mu(\vec{r})\chi_\nu(\vec{r})}{|\vec{r} - \vec{r}_i|}\, \mathrm{d}^3 r \\ \vec{E}^{\mathrm{QM}}(\vec{r}_i; \boldsymbol{P}) = \sum_{\mu\nu}^{N_{\mathrm{b}}} P_{\mu\nu} E_{\mu\nu}(\vec{r}_i) \\ \qquad = \sum_{\mu\nu}^{N_{\mathrm{b}}} P_{\mu\nu} \int_{\mathbb{R}^3} \frac{\chi_\mu(\vec{r})\chi_\nu(\vec{r})(\vec{r} - \vec{r}_i)}{|\vec{r} - \vec{r}_i|^3}\, \mathrm{d}^3 r \\ \vec{\nabla}\vec{E}^{\mathrm{QM}}(\vec{r}_i; \boldsymbol{P}) = \sum_{\mu\nu}^{N_{\mathrm{b}}} P_{\mu\nu} G_{\mu\nu}(\vec{r}_i) \\ \qquad = \sum_{\mu\nu}^{N_{\mathrm{b}}} P_{\mu\nu} \int_{\mathbb{R}^3} \chi_\mu(\vec{r})\chi_\nu(\vec{r}) \mathcal{J}\vec{E}(\vec{r}_i)\, \mathrm{d}^3 r \end{cases} \tag{14}$$

where the electron density $\boldsymbol{P}$ has been expanded in a basis of atomic orbitals and $\mathcal{J}$ is the Jacobian of the electric field with elements $(\mathcal{J}\vec{E})_{\alpha\beta}(\vec{r}) = \frac{\partial E^{\alpha}(\vec{r})}{\partial r_\beta}$, with α and β being generic Cartesian components. The corresponding terms induced by the nuclear distribution are trivial and are not reported.

Imposing the stationarity conditions for the global functional in eq 10, taking into account the constraints on the electronic density matrices, gives the coupled QM/AMOEBA equations.

The QM/AMOEBA Fock matrix $\tilde{\boldsymbol{F}}$ is obtained by differentiating eq 10 with respect to the density matrix:

$$\begin{aligned} \tilde{\boldsymbol{F}} &= \frac{\partial \mathcal{E}(\boldsymbol{P}, \boldsymbol{\mu})}{\partial \boldsymbol{P}} \\ &= \frac{\partial \mathcal{E}^{\mathrm{QM}}(\boldsymbol{P})}{\partial \boldsymbol{P}} + \frac{\partial \mathcal{E}^{\mathrm{Env}}(\boldsymbol{P}, \mu)}{\partial \boldsymbol{P}} \\ &= \boldsymbol{F}^{(0)} + \boldsymbol{F}^{\mathrm{Env}} \end{aligned} \tag{15}$$

DOI: 10.1021/acs.jctc.6b00385
J. Chem. Theory Comput. 2016, 12, 3654−3661

Journal of Chemical Theory and Computation Article

where the term $\boldsymbol{F}^{(0)}$ of eq 15 corresponds to the Fock matrix of the pure QM electronic problem, while $\boldsymbol{F}^{\mathrm{Env}}$ is the contribution to $\tilde{\boldsymbol{F}}$ from the classical environment. The elements of the latter can be written as

$$F^{\mathrm{Env}}_{\mu\nu} = \boldsymbol{q}^{\dagger}\boldsymbol{V}_{\mu\nu} - \boldsymbol{\mu}_{\mathrm{s}}^{\dagger}\boldsymbol{E}_{\mu\nu} - \boldsymbol{\Theta}^{\dagger}\boldsymbol{G}_{\mu\nu} - \frac{1}{2}(\boldsymbol{\mu}_{\mathrm{p}} + \boldsymbol{\mu}_{\mathrm{d}})^{\dagger}\boldsymbol{E}_{\mu\nu} \tag{16}$$

where the matrices $\boldsymbol{V}_{\mu\nu}$, $\boldsymbol{E}_{\mu\nu}$, and $\boldsymbol{G}_{\mu\nu}$ are those appearing in eq 14. Note that the $E_{\mu\nu}$ elements involved in the second term on the RHS of eq 16 are formally identical to those appearing in the first one but are computed over a different set of atomic sites (the polarizable ones only).

The linear equations for the dipoles are obtained by setting the derivatives of eq 10 with respect to both sets of dipoles to zero:

$$\begin{aligned} \boldsymbol{T}\boldsymbol{\mu}_{\mathrm{p}} &= \boldsymbol{E}_{\mathrm{p}} + \boldsymbol{E}^{\mathrm{QM}}(\boldsymbol{P}) \\ \boldsymbol{T}\boldsymbol{\mu}_{\mathrm{d}} &= \boldsymbol{E}_{\mathrm{d}} + \boldsymbol{E}^{\mathrm{QM}}(\boldsymbol{P}) \end{aligned} \tag{17}$$

Notice that the Fock matrix depends on the induced dipoles and that the RHSs of the dipole equations depend on the density matrix: the two sets of equations are therefore coupled, accounting correctly for the mutual polarization of the QM and classical charge densities. The coupled equations need to be solved iteratively, which is not a problem in practice, as the SCF equations are already solved with an iterative algorithm. We note that the matrix $\boldsymbol{T}$ depends only on geometrical parameters, and can be computed and inverted at the first SCF cycle, thus reducing the computational requirements at the following steps. Alternatively, this problem can also be efficiently solved with an iterative procedure (see section 2.4 for more details).

2.3. Extension to Electronic Excitations. The discussion so far has involved the energies and properties of the electronic ground state. To extend the treatment to excited states, we follow a linear response theory for SCF methods. A complete derivation of the polarizable QM/MM LR response equations can be found elsewhere;[14,41] here it suffices to say that the electronic transition energies ω_K and densities $\mathbf{X}_K$, $\mathbf{Y}_K$ are found by solving the modified Casida equations[42]

$$\begin{pmatrix} \tilde{\boldsymbol{A}} & \tilde{\boldsymbol{B}} \\ \tilde{\boldsymbol{B}} & \tilde{\boldsymbol{A}} \end{pmatrix}\begin{pmatrix} \boldsymbol{X}_K \\ \boldsymbol{Y}_K \end{pmatrix} = \omega_K \begin{pmatrix} \mathbf{1} & \mathbf{0} \\ \mathbf{0} & -\mathbf{1} \end{pmatrix}\begin{pmatrix} \boldsymbol{X}_K \\ \boldsymbol{Y}_K \end{pmatrix} \tag{18}$$

The matrices $\tilde{\boldsymbol{A}}$ and $\tilde{\boldsymbol{B}}$ are defined as

$$\begin{aligned} \tilde{A}_{ai,bj} &= \delta_{ab}\delta_{ij}(\epsilon_a - \epsilon_i) + (ai|bj) - c_x(ab|ij) + c_l f^{xc}_{ai,bj} \\ &\quad + C^{\mathrm{Pol}}_{ai,bj} \\ \tilde{B}_{ai,bj} &= (ai|bj) - c_x(aj|ib) + C^{\mathrm{Pol}}_{ai,bj} \end{aligned} \tag{19}$$

where ϵ are the orbital energies, $(pq|rs)$ are two-electron integrals in Mulliken notation, and we assume that the orbitals are real and the coefficients c_x and c_l define whether we are considering the Hartree–Fock theory ($c_x = 1$, $c_l = 0$), pure DFT ($c_x = 0$, $c_l = 1$), or hybrid DFT. The elements of matrix $\boldsymbol{C}^{\mathrm{Pol}}$ are due to the environment polarization:

$$C^{\mathrm{Pol}}_{ai,bj} = -\sum_{P}^{N_{\mathrm{Pol}}}\left(\int_{\mathbb{R}^3}\phi_a(\vec{r})\frac{(\vec{r}-\vec{r}_{\mathrm{p}})}{|\vec{r}-\vec{r}_{\mathrm{p}}|^3}\phi_i(\vec{r})\,\mathrm{d}\vec{r}\right)\cdot\vec{\mu}_P^{\,T}(\phi_b, \phi_j) \tag{20}$$

The matrix $\mathrm{C}^{\mathrm{Pol}}$ depends on the dipoles $\boldsymbol{\mu}^T$ induced by the transition density $\mathbf{P}^T_K = \mathbf{X}_K + \mathbf{Y}_K$, which are obtained by solving, for each couple of transition vectors $\mathbf{X}_K$, $\mathbf{Y}_K$, the response linear equations

$$\mathbf{T}\boldsymbol{\mu}^T = \mathbf{E}(\mathbf{P}^T_K) \tag{21}$$

where

$$\vec{E}(\mathbf{P}^T_K) = \sum_{ai}\mathbf{P}^T_{K,ai}\int_{\mathbb{R}^3}\phi_a(\vec{r})\frac{(\vec{r}-\vec{r}_{\mathrm{p}})}{|\vec{r}-\vec{r}_{\mathrm{p}}|^3}\phi_i(\vec{r})\,\mathrm{d}\vec{r} \tag{22}$$

Notice that in the right-hand side of eq 21 only the electric field due to the transition density appears: as the classical multipoles do not contribute to the transition dipoles, the p and d response dipoles introduced in section 2.1 are identical. Again, the modified Casida equations depend (linearly) on the transition induced dipoles, which in turn depend (linearly) on the transition vectors $\mathbf{X}$, $\mathbf{Y}$: although the coupling is linear, it is still convenient to solve the couple equations iteratively, by solving the transition dipole equations at each step of the iterative procedure used to solve the Casida equations.

The great advantage of the LR scheme is that it allows one to obtain a whole spectrum of transition energies at once. If the system is isolated, it provides the same results as state specific (SS) approaches, where instead the wave function of each excited state is explicitly computed. By contrast, the introduction in the Hamiltonian of a nonlinear term due to the presence of a polarizable environment results in a formal difference between the two approaches.[25,43] For this reason, a correction to the LR scheme (called *corrected* linear response, c-LR) has been proposed.[28] The difference between the two approaches (LR and c-LR) can be depicted by a two-step process for excitation in solution: First, the molecule in its ground state, in equilibrium with the solvent, is excited to the state K in the presence of a solvent response frozen to the one of the solute ground state. The description for this step of the process is the same in both of the approaches. In the second step, the fast electronic degrees of freedom of the solvent equilibrate with the electron density of the solute excited state, and in this part of the process, the LR framework lacks in taking explicitly into account the energy variation accompanying this relaxation, whereas it accounts for a correction which, being originated by the dynamic solute–solvent interactions, can be classified as a part of dispersion. The working equation, namely,

$$\omega^{\text{c-LR}}_K = \omega^0_K - \frac{1}{2}\sum_{P}^{N_{\mathrm{Pol}}}\vec{\mu}_P(\vec{r}_P;\,\mathbf{P}^{\Delta}_K)\vec{E}(\vec{r}_P,\,\mathbf{P}^{\Delta}_K) \tag{23}$$

corresponds to the expression of the c-LR transition energy for the Kth excited state. In this formulation, ω^0_K represents the response of the system in a solvent frozen in its initial configuration (corresponding to the system in its ground state), and it is the solution of a non-Hermitian eigensystem as in eq 18, where $C^{\mathrm{Pol}}_{ai,bj} = 0$ but the orbitals and their corresponding energies, employed to build the A and B matrices have been obtained by solving the SCF equation for the solvated system. $\mathbf{P}^{\Delta}_K$ is the so-called *relaxed-density matrix*, computed through the so-called **Z**-vector approach[44] as

$$\mathbf{P}^{\Delta}_K = \mathbf{P}^T_K + \mathbf{Z}_K \tag{24}$$

where $\mathbf{P}^T_K$ is the unrelaxed density matrix with elements given in terms of the transition vectors $|\boldsymbol{X}_K, \boldsymbol{Y}_K\rangle$, and the **Z**-vector contribution $\mathbf{Z}_K$ accounts for orbital relaxation effects.

2.4. Implementation. The hybrid QM/AMOEBA method has been implemented in a development version of the

DOI: 10.1021/acs.jctc.6b00385
J. Chem. Theory Comput. 2016, 12, 3654–3661

Gaussian software.[45] In the present implementation, the program computes all the terms that depend on the QM density, including the sets of induced dipoles. The $\mathcal{E}^{FF} + \mathcal{E}^{(0)}$ energy terms depend neither on the QM density nor on the induced dipoles and, in a static picture, are constant.

In order to compute the induced dipoles, both an inversion approach and an iterative one have been implemented. In the former case, the polarization matrix (eq 4) is computed and inverted only once during the first step of the SCF and then stored and multiplied for the appropriate field to obtain the solutions to the polarization problem. At each SCF cycle, only two matrix-vector products (one per set of dipoles) need to be performed, concentrating the computational effort almost entirely in the first SCF step.

By contrast, in the iterative approach, the polarization equations are solved iteratively at each SCF step or at each step of the iterative solution of the Casida equations, using as a guess the induced dipoles of a previous step, when available. Two algorithms have been implemented: Jacobi iterations coupled with direct inversion in the iterative subspace (JI/DIIS) and the preconditioned conjugate gradient (PCG).[34,46] Both are available for the ground and LR excited state problems.

The advantage of the inversion approach is that the most expensive part of the procedure, i.e., the matrix inversion, needs only be performed once. However, the computational cost of such an operation grows with the cube of the number of polarizable sites: for large systems, iterative alternatives become mandatory. Furthermore, iterative methods can be easily combined with fast summation techniques, such as the fast multipole method,[46,47] in order to achieve linear scaling in computational cost for the solution of the polarization equations. We here present the relative time requirements for the computation of the induced dipoles in the whole SCF procedure, using the inversion and iterative algorithms. The calculations have been performed on the test system whose results will be discussed in section 3. The dimension of the polarization problem has been artificially varied, by considering various polarization cutoffs, i.e., by including a different number of induced dipoles. The dimensions of the QM system, as well as that of the nonpolarizable classical environment, have been kept fixed. Figure 1 reports the dependence of the relative times on the number of induced dipoles.

From the plots reported in the figure, it is clear that the iterative procedures are more convenient than the inversion one. This becomes more evident as the size of the problem increases, since both JI and PCG algorithms scale quadratically with the number of induced dipoles, while the inversion algorithm, LU decomposition, is characterized by a cubic scaling. In particular, when the polarization radius is increased from 7 to 20 Å (number of dipoles increasing by ∼10× from 765 to 7338), the inversion algorithm increases by ∼300×. For both JI and PCG algorithms, the relative increase is ∼60×.

Furthermore, when the number of polarizable dipoles is small (polarization radius 7 Å, 765 dipoles), even if the JI/PCG methods are faster than the inversion one, the choice of the solution scheme does not really matter, since the relative time to solve for the induced dipoles with respect to the total time is, for each of the three cases, less than 0.1%. This is no longer true in the most expensive case (polarization radius 20 Å, 7338 dipoles), where almost 16.5% of the time for the calculation is spent in computing the induced dipoles with the inversion method (the iterative solutions take less than 1% of the total time).

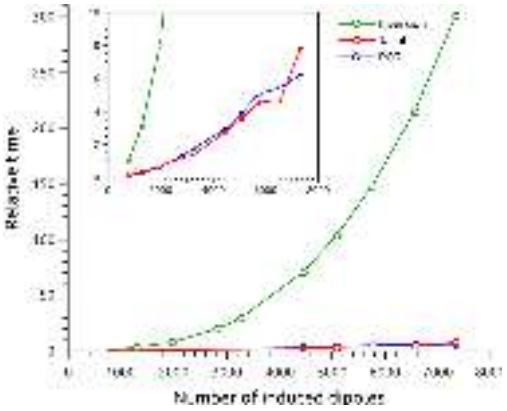

Figure 1. Relative times needed to solve for the induced dipoles, using different methods. Green line, inversion; red line, Jacobi iterations; blue line, preconditioned conjugate gradient. The times are cumulative and refer to the sum of all SCF cycles until convergence is reached. The number of SCF cycles considered is the average one across the various structures considered. The values have been normalized for comparison with respect to the time required to solve the smallest polarization problem (7 Å polarization radius, 765 induced dipoles) with the inversion procedure.

3. A TEST CASE: THE SOLVATOCHROMISM OF BETAINE-30

In this section, we present an application of the QM/AMOEBA implementation to the simulation of the excitation energies of a well-known solvatochromic probe, the pyridinium *N*-phenolate betaine dye, from now on indicated as "betaine-30" (see Figure 2). The solvent we selected for this test case is water, since it constitutes one of the most interesting cases due to its high polarity combined with a hydrogen-bonding character. In particular, we will try to dissect these two components of the solvent effect by comparing QM/AMOEBA with a continuum description using the polarizable continuum model (PCM) within its integral equation formalism (IEF).[48] We recall that this model describes the environment as a structureless continuum, characterized by its macroscopic dielectric function. A cavity containing the solute is built around it, and the solvent polarization as a response to the solute charge density is represented by an induced surface charge distribution on the cavity.

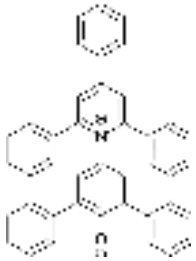

Figure 2. Betaine dye studied.

DOI: 10.1021/acs.jctc.6b00385
J. Chem. Theory Comput. 2016, 12, 3654−3661

In order to obtain a realistic sampling of the solute−solvent interaction, a well-established procedure has been applied, which makes use of snapshots extracted from a classical molecular dynamics (MD) simulation with the AMBER general force field for organic molecules. An optimized geometry of the dye was solvated with a cubic box containing 11380 water molecules, described at the TIP3P level,[49] with dimensions of 74 × 72 × 78 Å^3. The system was heated from 0 to 300 K for 100 ps with a 2 fs time step, employing the SHAKE algorithm[50] as in all the following steps. The Berendsen thermostat[51] was used to control the temperatue. A 200 ps equilibration in the NVT ensemble was then performed. Before the actual production, the system was further equilibrated in the NPT ensamble at 1 atm for 5 ns. Here, the Monte Carlo barostat implemented in Amber14[52] was employed. In the 30 ns long MD simulation, the betaine-30 was kept frozen in its ground state equilibrium geometry (computed at the QM/PCM level). A set of 100 uncorrelated snapshots was extracted, on which the QM/AMOEBA calculations were performed. Since the effect of polarization is short-ranged, and the computational cost increases markedly with the number of induced dipoles, only the classical atoms within a certain radius (the *polarization radius*, R_{pol}) were allowed to polarize. The optimal value of the radius was chosen after performing a convergence test, where the first three excited states of the solvated betaine dye were computed at increasing values of R_{pol}. The results, reported in Figure 3, show that convergence can be observed starting from 10−12 Å. A safe value of R_{pol} = 15 Å was chosen and employed in all of the calculations presented.

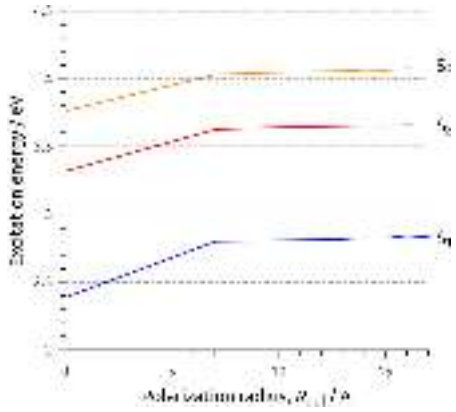

Figure 3. Lowest three excitation energies of betaine-30 as functions of the polarization radius, R_{pol}, with the total radius for the inclusion of classical environment fixed at 25 Å. Blue, red, and yellow curves refer to the first, second, and third excited states, respectively, calculated on one snapshot at the TDDFT level, within the linear response approach. A value of R_{pol} = 0 indicates that all of the solvent molecules are nonpolarizable, and are only described in terms of fixed multipoles.

All calculations (geometry optimizations and excitation energies) have been performed at the (TD)DFT level of theory using the CAM-B3LYP exchange-correlation functional[53] together with the 6-31+G(d,p) Gaussian basis set. We particularly focused on the properties of the lowest (bright) excitation, on which the E_T(30) scale is based. The excitation shows a strong charge-transfer character, and for this reason, the corrected linear response (c-LR) approach[28] is expected to give a more accurate picture than the standard LR.

The results obtained with the three different QM/AMOEBA responses described in section 2.3 (namely, ω_0, LR, and c-LR) are summarized in Figure 4.

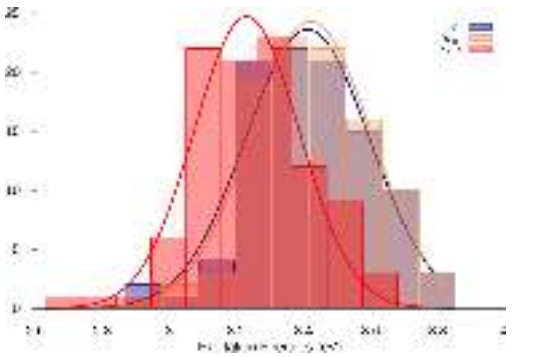

Figure 4. Distributions of the lowest (bright) excitation of betaine-30 calculated with the three different QM/AMOEBA responses (LR, blue line; ω_0, yellow line; c-LR, red line). The curves are Gaussian fits of the histograms.

From the comparison, it is evident that the effects of the relaxation of the solvent, which we include through a c-LR formulation, play an important role, as a significant redshift (of about 0.2 eV) is observed with respect to the frozen solvent approximation (ω_0). As expected due to the CT character of the excitation, the LR formulation does not change the ω_0 value, as it cannot account for the effects of the rearrangement of electron density undergone by the dye upon excitation.

The comparison with experimental data is, however, the most interesting test. In order to be able to provide an analysis which is not biased by systematic errors in the excitation energies due to the QM level of theory, we compare the computed and experimental gas-to-water solvatochromic shifts instead of the absolute excitation energies. To better elucidate the various effects that determine the observed solvatochromic shift, i.e., short-range and specific interactions and the bulk effects, it is useful to compare with two different solvation models. The first, QM/PCM, employs a purely continuum description of the solvent, whereas the second, QM(ME)/PCM, includes a "minimal environment" in the QM system, i.e., the two water molecules hydrogen-bonded to the oxygen of the dye, while the rest of the solvent is still treated at the PCM level. The latter model should better describe the combination of short-range specific and bulk interaction with respect to the QM/PCM analogue. In the QM(ME)/PCM calculation, the configuration of the QM water molecules has been optimized at CAM-B3LYP/6-31+G(d,p). The results are reported in Table 1 (all data refer to c-LR calculations).

As expected, the QM/PCM model markedly underestimates the solvatochromic shift with respect to the two other models (and to experiments). This clearly shows that including an atomistic description of the most strongly interacting water molecules is fundamental to account for the differential solvation effects in the ground and excited states of the betaine-30. However, it is worth noting that the inclusion of the two hydrogen bonded water molecules in the QM region in combination with a continuum description (through the

DOI: 10.1021/acs.jctc.6b00385
J. Chem. Theory Comput. 2016, 12, 3654−3661

Table 1. Gas-to-Water Solvatochromic Shift (in eV) for the Lowest (Bright) Excitation of Betaine-30, Computed with Different Solvation Models[a]

QM/PCM	0.79
QM(ME)/PCM	1.17
QM/AMOEBA	1.58 ± 0.02
Exp[54]	1.56

[a]The QM/AMOEBA value is obtained from the average over 100 snapshots extracted from the MD. The confidence interval is indicated. All calculations were performed at the TDCAM-B3LYP/6-31+G(d,p) level.

QM(ME)/PCM model) still fails to recover a large portion of the observed solvatochromic effects (namely, 0.4 eV are still missing to reproduce the experiments). The inclusion of a larger number of explicit solvent molecules with AMOEBA instead leads to a solvatochromic shift which is almost exactly equivalent to the experiments. Such an excellent agreement might be fortuitous due to the many approximations introduced in the comparison, such as the use of a calculated vertical excitation and an experimental band maximum, and the extrapolated value used for the experimental gas-phase value. However, the additional +0.4 eV shift obtained going from the QM(ME)/PCM to the QM/AMOEBA model clearly suggests that the strong hydrogen-bonding effect is not the only source of differences with respect to a purely bulk description. Looking more deeply into the results, it is interesting to point out that the difference between QM/AMOEBA and QM(ME)/PCM solvatochromic shifts is already present at the ω_0 level, which means that the addition of the c-LR response is almost equally described by the two models. We can thus speculate that the zwitterionic nature of the betaine-30 ground state has a large, specific, long-range effect in orienting the water molecules and this leads to a final solvation effect that cannot be accurately described with a pure continuum or a partial atomistic/continuum approach.

4. CONCLUSIONS

We presented here the theoretical development and the computational implementation of a polarizable embedding QM/MM within the AMOEBA framework. The implementation accounts for a fully relaxed evaluation of the QM/MM energy for both ground and excited states, in the framework of a DFT/TD-DFT theory. In particular for the excited state, a state-specific (SS) formulation of the response of the classical part of the system has been used following the c-LR approach originally developed within continuum models.[28] The test case of betaine-30 is presented and discussed in comparison with purely continuum and mixed atomistic/continuum models: the obtained results in the simulation of the large gas-to-water solvatochromism of this dye show that the QM/AMOEBA approach can describe with equal accuracy the effect of water on the zwitterionic ground state and the modification induced by the excitation.

This work represents the first step of a series of new developments toward a high-performance, parallel implementation of polarizable QM/MM molecular dynamics, which stems from the recent developments in the implementation of AMOEBA for classical MD simulations in the newly developed Tinker-HP[34,55−57] code and with the implementation of a versatile and transparent Tinker HP/Gaussian interface for energy, gradients, and properties. The implementation of analytical gradients for the QM/AMOEBA model and the development of the Gaussian/AMOEBA interface will allow us to exploit not only parallelism but also linear scaling techniques[46] in order to further reduce the overall computational cost due to the polarizable embedding. The addition of a further layer to the model, namely, of a polarizable continuum solvation model, will finally allow one to deal with long-range, bulk effects while, at the same time, reducing the portion of environment to be treated explicitly. An innovative, parallel, linear-scaling implementation of the conductor-like screening model[38,58,59] has already been coupled to AMOEBA for classical MD simulations[38] and to the MMpol dipole-based polarizable force field for QM/MM calculations:[46] the combination of all the aforementioned developments will result in a powerful and efficient tool to investigate dynamic properties and reactivity in complex environments.

■ ASSOCIATED CONTENT

Supporting Information

The Supporting Information is available free of charge on the ACS Publications website at DOI: 10.1021/acs.jctc.6b00385.

Cartesian coordinates of all the snapshots used for the QM/AMOEBA calculations (ZIP)

■ AUTHOR INFORMATION

Corresponding Authors

*E-mail: flippari@uni-mainz.de.
*E-mail: jpp@lct.jussieu.fr.
*E-mail: benedetta.mennucci@unipi.it.

Funding

This work was supported in part by French state funds managed by CalSimLab and the ANR within the Investissements d'Avenir program under reference ANR-11-IDEX-0004-02. F.L. gratefully acknowledges the Alexander von Humboldt foundation for funding. E.P. and J.-P.P. are grateful for support by the Direction Generale de l'Armement (DGA) - Maitrise NRBC of the French Ministry of Defense. S.C. and B.M. acknowledge the European Research Council (ERC) for financial support in the framework of the Starting Grant (EnLight-277755).

Notes

The authors declare no competing financial interest.

■ REFERENCES

(1) Cramer, C.; Truhlar, D. *Chem. Rev.* **1999**, *99*, 2161−2200.
(2) Tomasi, J.; Mennucci, B.; Cammi, R. *Chem. Rev.* **2005**, *105*, 2999−3093.
(3) Warshel, A.; Levitt, M. *J. Mol. Biol.* **1976**, *103*, 227−249.
(4) Gao, J.; Xia, X. *Science* **1992**, *258*, 631−635.
(5) Maseras, F.; Morokuma, K. *J. Comput. Chem.* **1995**, *16*, 1170−1179.
(6) Lin, H.; Truhlar, D. G. *Theor. Chem. Acc.* **2007**, *117*, 185−199.
(7) Senn, H. M.; Thiel, W. *Angew. Chem., Int. Ed.* **2009**, *48*, 1198−1229.
(8) Thompson, M. A.; Schenter, G. K. *J. Phys. Chem.* **1995**, *99*, 6374−6386.
(9) Bryce, R. A.; Buesnel, R.; Hillier, I. H.; Burton, N. A. *Chem. Phys. Lett.* **1997**, *279*, 367−371.
(10) Gordon, M. S.; Freitag, M. A.; Bandyopadhyay, P.; Jensen, J. H.; Kairys, V.; Stevens, W. J. *J. Phys. Chem. A* **2001**, *105*, 293−307.
(11) Jensen, L.; van Duijnen, P. T.; Snijders, J. G. *J. Chem. Phys.* **2003**, *119*, 3800−3809.

DOI: 10.1021/acs.jctc.6b00385
J. Chem. Theory Comput. 2016, 12, 3654−3661

(12) Nielsen, C. B.; Christiansen, O.; Mikkelsen, K. V.; Kongsted, J. *J. Chem. Phys.* **2007**, *126*, 154112−154118.
(13) Illingworth, C. J. R.; Parkes, K. E. B.; Snell, C. R.; Ferenczy, G. G.; Reynolds, C. A. *J. Phys. Chem. A* **2008**, *112*, 12151−12156.
(14) Curutchet, C.; Muñoz-Losa, A.; Monti, S.; Kongsted, J.; Scholes, G. D.; Mennucci, B. *J. Chem. Theory Comput.* **2009**, *5*, 1838−1848.
(15) Lipparini, F.; Barone, V. *J. Chem. Theory Comput.* **2011**, *7*, 3711−3724.
(16) Steindal, A. H.; Ruud, K.; Frediani, L.; Aidas, K.; Kongsted, J. *J. Phys. Chem. B* **2011**, *115*, 3027−3037.
(17) Boulanger, E.; Thiel, W. *J. Chem. Theory Comput.* **2012**, *8*, 4527−4538.
(18) Gordon, M. S.; Fedorov, D. G.; Pruitt, S. R.; Slipchenko, L. V. *Chem. Rev.* **2012**, *112*, 632−672.
(19) Gao, J.; Truhlar, D. G.; Wang, Y.; Mazack, M. J. M.; Löffler, P.; Provorse, M. R.; Rehak, P. *Acc. Chem. Res.* **2014**, *47*, 2837−2845.
(20) Zeng, Q.; Liang, W. *J. Chem. Phys.* **2015**, *143*, 134104−134119.
(21) Ren, P.; Ponder, J. W. *J. Phys. Chem. B* **2003**, *107*, 5933−5947.
(22) Grossfield, A.; Ren, P.; Ponder, J. W. *J. Am. Chem. Soc.* **2003**, *125*, 15671−15682.
(23) Ponder, J. W.; Wu, C.; Ren, P.; Pande, V. S.; Chodera, J. D.; Schnieders, M. J.; Haque, I.; Mobley, D. L.; Lambrecht, D. S.; DiStasio, R. A., Jr; Head-Gordon, M.; Clark, G. N. I.; Johnson, M. E.; Head-Gordon, T. *J. Phys. Chem. B* **2010**, *114*, 2549−2564.
(24) Kratz, E. G.; Walker, A. R.; Lagardère, L.; Lipparini, F.; Piquemal, J.-P.; Andrés Cisneros, G. *J. Comput. Chem.* **2016**, *37*, 1019−1029.
(25) Corni, S.; Cammi, R.; Mennucci, B.; Tomasi, J. *J. Chem. Phys.* **2005**, *123*, 134512−134522.
(26) Cupellini, L.; Amovilli, C.; Mennucci, B. *J. Phys. Chem. B* **2015**, *119*, 8984−8991.
(27) Guido, C. A.; Jacquemin, D.; Adamo, C.; Mennucci, B. *J. Chem. Theory Comput.* **2015**, *11*, 5782−5790.
(28) Caricato, M.; Mennucci, B.; Tomasi, J.; Ingrosso, F.; Cammi, R.; Corni, S.; Scalmani, G. *J. Chem. Phys.* **2006**, *124*, 124520−124533.
(29) Improta, R.; Barone, V.; Scalmani, G.; Frisch, M. J. *J. Chem. Phys.* **2006**, *125*, 054103−054112.
(30) Marenich, A. V.; Cramer, C. J.; Truhlar, D. G.; Guido, C. A.; Mennucci, B.; Scalmani, G.; Frisch, M. *J. Chem. Sci.* **2011**, *2*, 2143−2161.
(31) Reichardt, C. *Chem. Rev.* **1994**, *94*, 2319−2358.
(32) Machado, V. G.; Stock, R. I.; Reichardt, C. *Chem. Rev.* **2014**, *114*, 10429−10475.
(33) Thole, B. T. *Chem. Phys.* **1981**, *59*, 341−350.
(34) Lipparini, F.; Lagardère, L.; Stamm, B.; Cancès, E.; Schnieders, M.; Ren, P.; Maday, Y.; Piquemal, J.-P. *J. Chem. Theory Comput.* **2014**, *10*, 1638−1651.
(35) van Duijnen, P. T.; Swart, M. *J. Phys. Chem. A* **1998**, *102*, 2399−2407.
(36) Wang, J.; Cieplak, P.; Li, J.; Wang, J.; Cai, Q.; Hsieh, M.; Lei, H.; Luo, R.; Duan, Y. *J. Phys. Chem. B* **2011**, *115*, 3100−3111.
(37) Sala, J.; Guàrdia, E.; Masia, M. *J. Chem. Phys.* **2010**, *133*, 234101−234115.
(38) Lipparini, F.; Lagardère, L.; Raynaud, C.; Stamm, B.; Cancès, E.; Mennucci, B.; Schnieders, M.; Ren, P.; Maday, Y.; Piquemal, J. P. *J. Chem. Theory Comput.* **2015**, *11*, 623−634.
(39) Lipparini, F.; Scalmani, G.; Mennucci, B.; Cancès, E.; Caricato, M.; Frisch, M. J. *J. Chem. Phys.* **2010**, *133*, 014106−014117.
(40) Lipparini, F.; Scalmani, G.; Mennucci, B.; Frisch, M. J. *J. Chem. Theory Comput.* **2011**, *7*, 610−617.
(41) Lipparini, F.; Cappelli, C.; Barone, V. *J. Chem. Theory Comput.* **2012**, *8*, 4153−4165.
(42) Casida, M. E.; Jamorski, C.; Casida, K. C.; Salahub, D. R. *J. Chem. Phys.* **1998**, *108*, 4439−4449.
(43) Cammi, R.; Corni, S.; Mennucci, B.; Tomasi, J. *J. Chem. Phys.* **2005**, *122*, 104513−104525.
(44) Handy, N. C.; Schaefer, H. F. *J. Chem. Phys.* **1984**, *81*, 5031−5033.
(45) Frisch, M. J.; Trucks, G. W.; Schlegel, H. B.; Scuseria, G. E.; Robb, M. A.; Cheeseman, J. R.; Scalmani, G.; Barone, V.; Mennucci, B.; Petersson, G. A.; Nakatsuji, H.; Caricato, M.; Li, X.; Hratchian, H. P.; Izmaylov, A. F.; Bloino, J.; Zheng, G.; Sonnenberg, J. L.; Hada, M.; Ehara, M.; Toyota, K.; Fukuda, R.; Hasegawa, J.; Ishida, M.; Nakajima, T.; Honda, Y.; Kitao, O.; Nakai, H.; Vreven, T.; Montgomery, J. A., Jr.; Peralta, J. E.; Ogliaro, F.; Bearpark, M.; Heyd, J. J.; Brothers, E.; Kudin, K. N.; Staroverov, V. N.; Kobayashi, R.; Normand, J.; Raghavachari, K.; Rendell, A.; Burant, J. C.; Iyengar, S. S.; Tomasi, J.; Cossi, M.; Rega, N.; Millam, J. M.; Klene, M.; Knox, J. E.; Cross, J. B.; Bakken, V.; Adamo, C.; Jaramillo, J.; Gomperts, R.; Stratmann, R. E.; Yazyev, O.; Austin, A. J.; Cammi, R.; Pomelli, C.; Ochterski, J. W.; Martin, R. L.; Morokuma, K.; Zakrzewski, V. G.; Voth, G. A.; Salvador, P.; Dannenberg, J. J.; Dapprich, S.; Daniels, A. D.; Farkas, O.; Foresman, J. B.; Ortiz, J. V.; Cioslowski, J.; Fox, D. J. *Gaussian 09*, revision A.1; Gaussian, Inc.: Wallingford, CT, 2009; www.Gaussian.com.
(46) Caprasecca, S.; Jurinovich, S.; Lagardère, L.; Stamm, B.; Lipparini, F. *J. Chem. Theory Comput.* **2015**, *11*, 694−704.
(47) Greengard, L.; Rokhlin, V. *J. Comput. Phys.* **1987**, *73*, 325−348.
(48) Cancès, E.; Mennucci, B.; Tomasi, J. *J. Chem. Phys.* **1997**, *107*, 3032−3041.
(49) Jorgensen, W. L.; Chandrasekhar, J.; Madura, J. D.; Impey, R. W.; Klein, M. L. *J. Chem. Phys.* **1983**, *79*, 926−935.
(50) Ryckaert, J.-P.; Ciccotti, G.; Berendsen, H. J. *J. Comput. Phys.* **1977**, *23*, 327−341.
(51) Berendsen, H. J. C.; Postma, J. P. M.; van Gunsteren, W. F.; DiNola, A.; Haak, J. R. *J. Chem. Phys.* **1984**, *81*, 3684−3690.
(52) Case, D. A.; Babin, V.; Berryman, J. T.; Betz, R. M.; Cai, Q.; Cerutti, D. S., Cheatham, T. E., III; Darden, T. A.; Duke, R. E.; Gohlke, H.; Goetz, A. W.; Gusarov, S.; Homeyer, N.; Janowski, P.; Kaus, J.; Kolossváry, I.; Kovalenko, A.; Lee, T. S.; LeGrand, S.; Luchko, T.; Luo, R.; Madej, B.; Merz, K. M.; Paesani, F.; Roe, D. R.; Roitberg, A.; Sagui, C.; Salomon-Ferrer, R.; Seabra, G.; Simmerling, C. L.; Smith, W.; Swails, J.; Walker, R. C.; Wang, J.; Wolf, R. M.; Wu, X.; Kollman, P. A. *AMBER 14*; University of California: San Francisco, CA, 2014; http://ambermd.org/.
(53) Yanai, T.; Tew, D. P.; Handy, N. C. *Chem. Phys. Lett.* **2004**, *393*, 51−57.
(54) Reichardt, C.; Welton, T. *Solvents and Solvent Effects in Organic Chemistry*, 4th ed.; Wiley-VCH: Weinheim, Germany, 2011.
(55) Lagardère, L.; Lipparini, F.; Stamm, B.; Polack, E.; Jolly, L.; Narth, C.; Kratz, E.; Cisneros, G.; Schnieders, M.; Darden, T.; Gresh, N.; Maday, Y.; Ponder, J.; Ren, P.; Piquemal, J.-P. *TINKER-HP*; Sorbonne Universitè, UPMC Univ. Paris 06: 2016.
(56) Lagardère, L.; Lipparini, F.; Polack, E.; Stamm, B.; Cancès, E.; Schnieders, M.; Ren, P.; Maday, Y.; Piquemal, J.-P. *J. Chem. Theory Comput.* **2015**, *11*, 2589−2599.
(57) Narth, C.; Lagardère, L.; Polack, E.; Gresh, N.; Wang, Q.; Bell, D. R.; Rackers, J. A.; W, P. J.; Ren, P.; Piquemal, J.-P. *J. Comput. Chem.* **2016**, *37*, 494−506.
(58) Klamt, A.; Schuurmann, G. *J. Chem. Soc., Perkin Trans. 2* **1993**, 799−805.
(59) Lipparini, F.; Stamm, B.; Cancès, E.; Maday, Y.; Mennucci, B. *J. Chem. Theory Comput.* **2013**, *9*, 3637−3648.

DOI: 10.1021/acs.jctc.6b00385
J. Chem. Theory Comput. 2016, 12, 3654−3661

III.E References

[Amo+98] Amovilli, Claudio et al. "Recent Advances in the Description of Solvent Effects with the Polarizable Continuum Model". In: *Advances in Quantum Chemistry*. Ed. by Löwdin, Per-Olov. Vol. 32. Academic Press, Jan. 1, 1998, pp. 227–261 (cit. on pp. 5, 69).

[CBM06] Cancès, Eric, Bris, Claude Le, and Maday, Yvon. "Méthodes Mathématiques En Chimie Quantique. Une Introduction". Mathématiques et Applications. Berlin Heidelberg: Springer-Verlag, 2006. ISBN: 978-3-540-30996-3 (cit. on pp. 6, 68).

[CCM12] Caprasecca, Stefano, Curutchet, Carles, and Mennucci, Benedetta. "Toward a Unified Modeling of Environment and Bridge-Mediated Contributions to Electronic Energy Transfer: A Fully Polarizable QM/MM/PCM Approach". In: *Journal of Chemical Theory and Computation* 8.11 (Nov. 13, 2012), pp. 4462–4473. ISSN: 1549-9618 (cit. on p. 69).

[Cur+09] Curutchet, Carles et al. "Electronic Energy Transfer in Condensed Phase Studied by a Polarizable QM/MM Model". In: *Journal of Chemical Theory and Computation* 5.7 (July 14, 2009), pp. 1838–1848. ISSN: 1549-9618 (cit. on p. 69).

[Fri+09] Frisch, M. J. et al. "Gaussian 09". 2009 (cit. on p. 71).

[Kar14] Karplus, Martin. "Development of Multiscale Models for Complex Chemical Systems: From H+H2 to Biomolecules (Nobel Lecture)". In: *Angewandte Chemie International Edition* 53.38 (2014), pp. 9992–10005. ISSN: 1521-3773 (cit. on pp. 2, 69).

[Lev14] Levitt, Michael. "Birth and Future of Multiscale Modeling for Macromolecular Systems (Nobel Lecture)". In: *Angewandte Chemie International Edition* 53.38 (2014), pp. 10006–10018. ISSN: 1521-3773 (cit. on pp. 2, 69).

[Loc+16] Loco, Daniele et al. "A QM/MM Approach Using the AMOEBA Polarizable Embedding: From Ground State Energies to Electronic Excitations". In: *Journal of Chemical Theory and Computation* 12.8 (Aug. 9, 2016), pp. 3654–3661. ISSN: 1549-9618 (cit. on pp. 68, 75, 77, 79, 81).

[PC03] Ponder, Jay W. and Case, David A. "Force Fields for Protein Simulations". In: *Protein Simulations*. Ed. by Daggett, Valerie. Vol. 66. Advances in Protein Chemistry. Academic Press, 2003, pp. 27–85 (cit. on pp. 16, 19, 57, 69).

[Pon+10] Ponder, Jay W. et al. "Current Status of the AMOEBA Polarizable Force Field". In: *Journal of Physical Chemistry B* 114.8 (2010), pp. 2549–2564 (cit. on pp. 13, 16, 71, 93).

[TCS04] Toulouse, Julien, Colonna, François, and Savin, Andreas. "Long-Range–Short-Range Separation of the Electron-Electron Interaction in Density-Functional Theory". In: *Physical Review A* 70.6 (Dec. 17, 2004), p. 062505 (cit. on p. 69).

[War14] Warshel, Arieh. "Multiscale Modeling of Biological Functions: From Enzymes to Molecular Machines (Nobel Lecture)". In: *Angewandte Chemie International Edition* 53.38 (2014), pp. 10020–10031. ISSN: 1521-3773 (cit. on pp. 2, 69).

[WR84] Warshel, Arieh and Russell, Stephen T. "Calculations of Electrostatic Interactions in Biological Systems and in Solutions". In: *Quarterly Reviews of Biophysics* 17.3 (Aug. 1984), pp. 283–422. ISSN: 0033-5835 (cit. on pp. 57, 69).

Chapter IV

Scalable linear scaling method for polarisable molecular dynamics: The fast multipole method

Overview

Programming languages • C • C++ • Fortran • Matlab • Bash • Lua • R

APIs • OpenMP • MPI

Modified software • ScalFMM • TINKER

Used software ddPCM

Visits

- Centre INRIA Bordeaux (Bordeaux, two days, Nov. 2015) with Bérenger Bramas and Pierre Blanchard
- RWTH Aachen University (Aachen, ten days, May 2017) with Benjamin Stamm and Paolo Gatto

Paper

[Lin+18] Lindgren, Eric B. et al. "An Integral Equation Approach to Calculate Electrostatic Interactions in Many-Body Dielectric Systems". In: *Journal of Computational Physics* 371 (Oct. 15, 2018), pp. 712–731. ISSN: 0021-9991

Collaborators • Pierre Blanchard • Bérenger Bramas • Louis Lagardère • Benjamin Stamm

IV.A Problem statement

In this chapter, we present a high-performance linear scaling method for the computation of polarisable molecular dynamics in direct space. The method has hence better scalability than the $\mathcal{O}(N \log N)$ methods that use Ewald's summation presented in Chapter II; which we recall is due to the use of fast Fourier transform. The method is based on a generalisation of the spherical harmonics kernel of the fast multipole method for possibly any order point multipoles distribution of particles. We provide a framework for force fields that use point multipoles up to quadrupoles with explicit or implicit solvent. We discuss the accuracy, speed and scalability of our method which are underlined by molecular dynamics simulations.

A brief introduction to the AMOEBA force field has been given in Section I.E.2 and to the ddCOSMO method in Section I.F. We will first provide a summary of the fast multipole method as well as the formulæ needed to generalise the method for the AMOEBA force field. These theoretical parts will be the building blocks of the developments presented in Section IV.D.

We refer to the work of Fortin [For06], from which we follow the notation, for a detailed description of the fast multipole method method. For a nice graphical explanation of the method, we refer the reader to the first figure in [YB11], authors of another fast multipole method software, ExaFMM.

IV.A.1 Fast multipole method

The fast multipole method [GR97] is a linear scaling method that gives the solution to arbitrary precision to N-body problems, in particular for the interaction involving a $1/r$ kernel such as electrostatic interaction that is considered here.

Typically, the problem setting considered is the following: Let there be N point charges located at r_i and of charge M_{0i} be given. Then, one would like to evaluate the electric potential $\phi_i(r_i)$ created by those charges and optionally also the electric field, the forces generated or the interaction energy. All these quantities can be computed using the fast multipole method in an approximate manner that scales like $\mathcal{O}(N)$ with an additional part scaling like $\mathcal{O}(N \log N)$ for creating some initial data-structure that is however often negligible for the values of N considered in practice.

The case we are interested in, where we have point multipoles instead of point charges to describe the electrostatic charges, goes beyond the classical framework of the fast multipole method. We are looking to compute the same physical quantities presented above, but for densities generated by point multipoles used in the description of the AMOEBA force field.

In this case, the input of the method will be the set of nuclear positions r_i and an associated generic multipole operator from $\mathbf{R}$ to $\mathbf{R}$ of the form

$$\hat{\mathrm{L}}_i := \mathrm{M}_{0i} + \mathrm{M}_{1i} \cdot \mathrm{D}_i + \mathrm{M}_{2i} \cdot \mathrm{D}_i^2, \tag{I.1}$$

where the quantities M_{mi} are the multipoles that characterise the nuclei of the molecular system, and the differential operators D_i^m are the gradient for $m = 1$ and the Hessian for $m = 2$. This framework covers the static point multipoles presented in Section I.E.2 and the induced point dipoles with $\{\mathrm{M}_{0i} \equiv 0,\ \mathrm{M}_{1i} \equiv \mu_i,\ \mathrm{M}_{2i} \equiv 0\}$.

IV.A.2 Objectives

We wish to compute the potential and some associated quantities due to the COULOMB energy of a distribution of particles in three dimensions using the fast multipole method.

The particles are characterised by point multipoles, instead of the more usual point charges for which the fast multipole method is usually applied. That is, for a set of N particles at positions $(r_i)_{1 \leq i \leq N}$, we associate a multipolar operator $\hat{\mathrm{L}}_i$ defined by

$$\hat{\mathrm{L}}_i := \sum_{m=0}^{M} \mathrm{M}_{mi} \cdot \mathrm{D}_i^m. \tag{I.2}$$

For the AMOEBA force field, we are only interested in multipoles up to order two ($M = 2$); that is charges, dipoles and quadrupoles.

For any $r \in \mathbf{R}^3$ we then have a charge density due to point multipoles $\hat{\mathrm{L}}_i$

$$\rho_i(r) := \hat{\mathrm{L}}_i \delta(r - r_i), \tag{I.3}$$

where δ is the DIRAC function. This generalises the point charge density $q_i \delta(r - r_i)$.

For all $r \in \mathbf{R}^3$, the electrostatic potential obtained from the point multipole $\hat{\mathrm{L}}_i$ is then

$$\phi_i(r) := \hat{\mathrm{L}}_i \left(\frac{1}{|r - r_i|} \right). \tag{I.4}$$

We can rewrite this potential for all $r \in \mathbf{R}^3$, using an expansion in spherical harmonics, as

$$\phi_i(r) = \sum_{\ell=0}^{\ell_{\max}} \sum_{m=-\ell}^{\ell} [S_i]_\ell^m \frac{1}{|r - r_i|^{\ell+1}} Y_\ell^m \left(\frac{r - r_i}{|r - r_i|} \right), \tag{I.5}$$

where $\ell_{\max}$ is the highest order of the point multipole we consider, and the spherical harmonics Y_ℓ^m are defined below.

We want to numerically evaluate the potential due to $N \gg 1$ point multipoles

$$\sum_{1 \leq i \leq N} \phi_i(r), \tag{I.6}$$

in a large number of points r in a simulation box, as well as the energy of the system

$$\mathcal{E} := \frac{1}{2} \sum_{\substack{1 \leq i,j \leq N \\ i \neq j}} \hat{\mathrm{L}}_j \phi_i(r_j) = \frac{1}{2} \sum_{\substack{1 \leq i,j \leq N \\ i \neq j}} \hat{\mathrm{L}}_j \hat{\mathrm{L}}_j \left(\frac{1}{|r_j - r_j|} \right), \tag{I.7}$$

and the forces exerted by the particles j

$$\mathrm{F}_j(r) := -\mathrm{D}_r \left(\hat{\mathrm{L}}_j \sum_{1 \leq i \leq N} \phi_i(r) \right), \tag{I.8}$$

for $j \in [\![1 \,..\, N]\!]$ and $r \in \mathbf{R}^3$.

IV.B Formulas for spherical harmonics

To be able to use the molecular mechanics for the AMOEBA force field, we will first need a few definitions and properties regarding LEGENDRE polynomials and spherical harmonics.

IV.B.1 LEGENDRE polynomials

Definition IV.B.1 (LEGENDRE polynomials). — Let ℓ be a natural number. We define the ℓ-th LEGENDRE polynomial — using RODRIGUES' formula, as the ℓ-th degree polynomial associated to the function

$$\mathbf{R} \ni x \mapsto P_\ell(x) := \frac{1}{2^\ell} \frac{\mathrm{d}^\ell}{\mathrm{d}x^\ell} (x^2 - 1)^\ell. \tag{II.1}$$

Definition IV.B.2 (Associated LEGENDRE polynomials). — Let $\ell \in \mathbf{N}$ and $|m| \leq \ell$, then the associated LEGENDRE polynomial of degree ℓ and order m is the polynomial defined by the associated polynomial function

$$\mathbf{R} \ni x \mapsto P_\ell^m(x) := (-1)^m (1 - x^2)^{m/2} \frac{\mathrm{d}^m}{\mathrm{d}x^m} P_\ell(x). \tag{II.2}$$

We will also need the following relation for the computation of derivatives of spherical harmonics.

Proposition IV.B.1. — Let $\ell \in \mathbf{N}$ and $|m| \leq \ell$, then we have the identity

$$\frac{\mathrm{d}}{\mathrm{d}\theta} P_\ell^m(\cos\theta) = \begin{cases} \dfrac{\ell \cos(\theta) P_\ell^m(\cos\theta) - (\ell + m) P_{\ell-1}^m(\cos\theta)}{\sin\theta} & \text{if } m \neq \ell \\ \dfrac{\ell \cos(\theta) P_\ell^m(\cos\theta)}{\sin\theta} & \text{if } m = \ell \end{cases}. \tag{II.3}$$

ADMITTED PROOF: This is a classical result, see [Col21c] for example. □

IV.B.2 Spherical harmonics

There are several ways to define the spherical harmonics: either real or complex and with different normalisation factors.

In practice, the convention may be imposed by the tools that we use. For example, to use the ddPCM software [GLS17] along with the `ScalFMM` library [Bla+15], it is more natural for the latter to use a convention with real spherical harmonics, while for the former to use a convention for the complex spherical harmonics. To couple `ScalFMM` with the AMOEBA force field however we use only real spherical harmonics; with the supplementary step of converting Cartesian quantities to spherical harmonics. Hence, in the following, we will present these two conventions.

Definitions

Definition IV.B.3 (Complex spherical harmonics). — Let $(\theta, \varphi) \in [0\,;\pi] \times [0\,;2\pi[$, then for each $\ell \in \mathbf{N}$ and $|m| \leq \ell$,

$$Y_\ell^m(\theta,\varphi) := (-1)^m \sqrt{\frac{(\ell-|m|)!}{(\ell+|m|)!}} P_\ell^{|m|}(\cos\theta)\exp(im\varphi). \tag{II.4}$$

Definition IV.B.4 (Real spherical harmonics). — Let $(\theta, \varphi) \in [0\,;\pi]\times[0\,;2\pi[$, then for all $\ell \in \mathbf{N}$ and $|m| \leq \ell$, we have

$$\hat{Y}_\ell^m(\theta,\varphi) := \begin{cases} (-1)^m\sqrt{2}\sqrt{\dfrac{2\ell+1}{4\pi}}\sqrt{\dfrac{(\ell-|m|)!}{(\ell+|m|)!}}P_\ell^{|m|}(\cos\theta)\sin(|m|\varphi) & \text{if } m<0 \\ \sqrt{\dfrac{2\ell+1}{4\pi}}P_\ell^{|m|}(\cos\theta) & \text{if } m=0\,\cdot \\ (-1)^m\sqrt{2}\sqrt{\dfrac{2\ell+1}{4\pi}}\sqrt{\dfrac{(\ell-|m|)!}{(\ell+|m|)!}}P_\ell^{|m|}(\cos\theta)\cos(|m|\varphi) & \text{if } m>0 \end{cases} \tag{II.5}$$

Transformations between real and complex spherical harmonics

To convert between real and complex spherical harmonics, we need the following propositions.

Proposition IV.B.2 (Complex to real spherical harmonics transformation). — For any $\ell \in \mathbf{N}$ and $|m| \leq \ell$, we have with $(\theta, \varphi) \in [0\,;\pi] \times [0\,;2\pi[$

$$\hat{Y}_\ell^m(\theta,\varphi) = \begin{cases} \sqrt{2}\sqrt{\dfrac{2\ell+1}{4\pi}}\operatorname{Re} Y_\ell^m(\theta,\varphi) & \text{if } \ell>0 \text{ and } m>0 \\ \sqrt{\dfrac{2\ell+1}{4\pi}}Y_\ell^m(\theta,\varphi) & \text{if } \ell\geq 0 \text{ and } m=0\,\cdot \\ \sqrt{2}\sqrt{\dfrac{2\ell+1}{4\pi}}\operatorname{Im} Y_\ell^m(\theta,\varphi) & \text{if } \ell>0 \text{ and } m<0 \end{cases} \tag{II.6}$$

In particular, for any $\ell \in \mathbf{N}$ we have

$$Y_\ell^0(\theta,\varphi) = P_\ell(\cos\theta) \in \mathbf{R}. \tag{II.7}$$

Proof: The result is immediate using the definitions, once we notice that

$$-\operatorname{Im} Y_\ell^{-m}(\theta,\varphi) = \operatorname{Im} Y_\ell^m(\theta,\varphi). \tag{II.8}$$

■

Proposition IV.B.3 (Real to Complex spherical harmonics transformation)**.—** For any $\ell \in \mathbf{N}$ and $|m| \leq \ell$, we have with $(\theta,\varphi) \in [0\,;\pi] \times [0\,;2\pi[$

$$Y_\ell^m(\theta,\varphi) = \begin{cases} \dfrac{1}{\sqrt{2}}\sqrt{\dfrac{4\pi}{2\ell+1}}(\hat{Y}_\ell^m + i\hat{Y}_\ell^{-m}) & \text{if } m > 0 \\ \sqrt{\dfrac{4\pi}{2\ell+1}}\hat{Y}_\ell^m(\theta,\varphi) & \text{if } m = 0\,\cdot \\ \dfrac{1}{\sqrt{2}}\sqrt{\dfrac{4\pi}{2\ell+1}}(\hat{Y}_\ell^m - i\hat{Y}_\ell^{-m}) & \text{if } m < 0 \end{cases} \tag{II.9}$$

In particular, for all $\ell \in \mathbf{N}$ and $|m| \leq \ell$ we have

$$Y_\ell^{-m}(\theta,\varphi) = \overline{Y_\ell^m}(\theta,\varphi). \tag{II.10}$$

Proof: The result is immediate using definitions. ■

To have a closed formula for the coefficients, we will use the following lemma.

Lemma IV.B.1.— Let $\ell \in \mathbf{N}$. Then, if

$$\sum_{|m|\leq\ell} [S]_\ell^m Y_\ell^m(\theta,\varphi) \in \mathbf{R}, \tag{II.11}$$

we have the identity

$$[S]_\ell^{-m} = \overline{[S]_\ell^m}. \tag{II.12}$$

Proof: Let $\ell \in \mathbf{N}$.

$$\begin{aligned} \sum_{|m|\leq\ell} [S]_\ell^m Y_\ell^m(\theta,\varphi) \in \mathbf{R} \Leftrightarrow & \quad \sum_{|m|\leq\ell} \overline{[S]_\ell^m} \cdot \overline{Y_\ell^m}(\theta,\varphi) = \sum_{|m|\leq\ell} [S]_\ell^m Y_\ell^m(\theta,\varphi) \\ \Leftrightarrow & \quad \sum_{|m|\leq\ell} \overline{[S]_\ell^m} Y_\ell^{-m}(\theta,\varphi) = \sum_{|m|\leq\ell} [S]_\ell^m Y_\ell^m(\theta,\varphi) \\ \Leftrightarrow & \quad \sum_{|m|\leq\ell} \overline{[S]_\ell^{-m}} Y_\ell^m(\theta,\varphi) = \sum_{|m|\leq\ell} [S]_\ell^m Y_\ell^m(\theta,\varphi). \end{aligned} \tag{II.13}$$

We thus have the identity as the spherical harmonics are linearly independent. ■

Finally we have the desired property.

Proposition IV.B.4.— We assume that the coefficients of the complex spherical harmonics $[S]_\ell^m$ are given for all $\ell \in \mathbf{N}$ and $|m| \leq \ell$. Then the coefficients of the real spherical

harmonics $[\hat{S}]_\ell^m$ are

$$[\hat{S}]_\ell^m = \begin{cases} \sqrt{2}\sqrt{\dfrac{4\pi}{2\ell+1}}\,\mathrm{Re}[S]_\ell^m & \text{if } m > 0 \\ \sqrt{\dfrac{4\pi}{2\ell+1}}[S]_\ell^m & \text{if } m = 0\,. \\ \sqrt{2}\sqrt{\dfrac{4\pi}{2\ell+1}}\,\mathrm{Im}[S]_\ell^m & \text{if } m < 0 \end{cases} \tag{II.14}$$

Proof: By expanding the development in complex spherical harmonics, we find that

$$\begin{aligned}
\mathbf{R} \ni \sum_{|m|\le\ell} [S]_\ell^m Y_\ell^m(\theta,\varphi) &= [S]_\ell^0 Y_\ell^0(\theta,\varphi) + \sum_{m=1}^{\ell} \left([S]_\ell^m Y_\ell^m(\theta,\varphi) + [S]_\ell^{-m} Y_\ell^{-m}(\theta,\varphi)\right) \\
&= [S]_\ell^0 Y_\ell^0(\theta,\varphi) + \sum_{m=1}^{\ell} \left([S]_\ell^m Y_\ell^m(\theta,\varphi) + \overline{[S]_\ell^m Y_\ell^m}(\theta,\varphi)\right) \quad \text{(by Lem. IV.B.1 and Prop. IV.B.3)} \\
&= [S]_\ell^0 Y_\ell^0(\theta,\varphi) + 2\sum_{m=1}^{\ell} \mathrm{Re}\left([S]_\ell^m Y_\ell^m(\theta,\varphi)\right) \\
&= [S]_\ell^0 Y_\ell^0(\theta,\varphi) + 2\sum_{m=1}^{\ell} \left(\mathrm{Re}[S]_\ell^m \,\mathrm{Re}\, Y_\ell^m(\theta,\varphi) - \mathrm{Im}[S]_\ell^m \,\mathrm{Im}\, Y_\ell^m(\theta,\varphi)\right) \\
&= [S]_\ell^0 \sqrt{\frac{4\pi}{2\ell+1}} \hat{Y}_\ell^0(\theta,\varphi) + \sqrt{2}\sqrt{\frac{4\pi}{2\ell+1}} \left(\sum_{m=1}^{\ell} \mathrm{Re}[S]_\ell^m \hat{Y}_\ell^m(\theta,\varphi) \; - \sum_{m=-\ell}^{-1} \mathrm{Im}[S]_\ell^{-m} \hat{Y}_\ell^m(\theta,\varphi) \right).
\end{aligned}$$

Finally, using the identity

$$-\mathrm{Im}[S]_\ell^{-m} = -\,\mathrm{Im}\,\overline{[S]_\ell^m} = \mathrm{Im}[S]_\ell^m, \tag{II.15}$$

we can identify the coefficients from the equality

$$\sum_{|m|\le\ell} [S]_\ell^m Y_\ell^m(\theta,\varphi) = \sum_{|m|\le\ell} [\hat{S}]_\ell^m \hat{Y}_\ell^m(\theta,\varphi), \tag{II.16}$$

which gives us the desired result. ∎

IV.C Generalisation of the fast multipole method

We describe the changes with respect to an implementation of the fast multipole method that only uses point charges with a so-called spherical harmonics kernel in $r \mapsto 1/r$. If other conventions are used, then the results must be adapted; however the underling idea of what is presented remains.

One of the main ideas of the fast multipole method is to approximate the interaction between well-separated particles collectively by means of so-called local and multipole developments. This requires the introduction of boxes and all charges residing in each box are replaced by one multipole development located at the centre of the box creating approximatively the same potential as the set of charges for points sufficiently far away of the box (in the so-called far-field). This procedure is known as the particle-to-moment operator.

If the point charges are now replaced by multipoles $\{\mathrm{M}_{0i}, \mathrm{M}_{1i}, \mathrm{M}_{2i}\}$, the particle-to-moment operator should be replaced by a so-called moment-to-moment operator as we seek a multipole

development in the centre of each box creating the same potential in the far-field as the sum of the given multipoles residing in the box. Since this multipole-approximation is only valid on regions sufficiently far away from each box, the interaction of closely located particle (in the so-called near-field) are taken exactly into account by evaluating the needed quantities of Eq. (I.4). The fact that one deals with multipoles instead of point charges can be easily taken into account by adapting the formula. These computations are collected in the so-called particle-to-particle operator. This is the second operator in the fast multipole method methodology that needs to be adapted to our purpose.

Finally, we have to evaluate at each site the quantities of interests or the functionals as introduced above (potential, field, etc.) due to boxes in the far-field. This is the role of the local-to-particle operator. That is we have to compute the derivatives of the analytical formulae of the far field potential at those sites.

All the other operators (moment-to-moment, moment-to-local, local-to-local) are not affected and the rest of the algorithm remains the same. This also implies that the algorithmic complexity of the method stays the same, as the modifications have only local influence.

To sum up, to generalise the fast multipole method to consider multipoles, we need to modify the computations of the operators:

(I) particle-to-moment, to take into account the multipolar density;

(II) local-to-particle, to compute the potential and forces due to long-range particles exerted to point multipoles;

(III) particle-to-particle, to compute short-range interactions exactly.

IV.C.1 Inner and outer functions

To lighten notation, we introduce the outer and inner functions.

The outer functions enable us to write the potential due to point charges outside a sphere at points inside it, while the inner functions let us express the potential exerted by points inside a sphere to points outside it.

Definition IV.C.1. — Let $\ell \in \mathbf{N}$, $|m| \leq \ell$ and $(\rho, \theta, \varphi) \in \mathbf{R}_+ \times [0\,;\pi] \times [0\,;2\pi[$ a point in space, then we define the outer function as

$$O_\ell^m(\rho, \theta, \varphi) := \frac{i^{-|m|}(\ell - |m|)!}{\rho^{\ell+1}} P_\ell^{|m|}(\cos\theta) \exp(im\varphi), \tag{III.1}$$

and the inner function as

$$I_\ell^m(\rho, \theta, \varphi) := (-1)^\ell \frac{i^{|m|}\rho^\ell}{(\ell + |m|)!} P_\ell^{|m|}(\cos\theta) \exp(im\varphi). \tag{III.2}$$

IV.C.2 P2M operator

To generalise the particle-to-moment operator to multipoles, when we know the development of the potential in a basis of spherical harmonics, it is sufficient to replace the routine by a the same kind of computations done by the moment-to-moment routine.

Indeed, we can rewrite the real spherical harmonics using outer functions by identifying the coefficients $(M_\ell^m)_{\ell\in\mathbf{N},|m|\leq\ell}$ in the identity

$$\sum_{\ell=0}^{\ell_{\max}} \sum_{m=-\ell}^{\ell} [S_j]_\ell^m \frac{1}{|z_j - z_c|^{\ell+1}} Y_\ell^m \left(\frac{z_j - z_c}{|z_j - z_c|} \right) = \sum_{\ell=0}^{\infty} \sum_{m=-\ell}^{\ell} M_\ell^m O_\ell^{-m}(\rho_j, \theta_j, \varphi_j), \tag{III.3}$$

where z_c is the point at which we want to get the multipolar development, z_j is the position of the particle, and $(\rho_j, \theta_j, \varphi_j)$ are the spherical coordinates of the point $z_j - z_c$.

Hence, we use the coefficients

$$M_\ell^{-m} = \frac{(-i)^{|m|}[S_j]_\ell^m}{\sqrt{(\ell+|m|)!(\ell-|m|)!}}, \quad \text{that is} \quad M_\ell^m = \frac{(-i)^{|m|}\overline{[S_j]_\ell^m}}{\sqrt{(\ell+|m|)!(\ell-|m|)!}}. \tag{III.4}$$

IV.C.3 L2P operator

We want the local-to-particle operator to be able to give us physical quantities of interest, namely • the potential; • the gradient of the potential (to compute the energy of dipoles); • the Hessian of the potential (for the energy of the quadrupoles); • the third-order partial derivatives of the potential (for the forces up to quadrupoles).

Proposition IV.C.1 (Local development of the potential)**.—** Let $(L_\ell^m)_{\ell\in\mathbf{N},|m|\leq\ell}$ be the coefficients of the local development centred around z_c. Then

$$\phi(z) = \sum_{\ell=0}^{+\infty}\sum_{m=-\ell}^{\ell} L_\ell^m I_\ell^m(\rho,\theta,\varphi) = \sum_{\ell=0}^{m}\left(L_\ell^0 I_\ell^0(r,\theta,\varphi) + 2\,\mathrm{Re}\sum_{m=1}^{\ell} L_\ell^m I_\ell^m(\rho,\theta,\varphi)\right), \tag{III.5}$$

where (ρ,θ,φ) are the spherical coordinates of the point $z - z_c$.

Admitted proof. □

Proposition IV.C.2 (First-order partial spherical derivatives of the potential)**.—** Using the same notation as in the previous proposition, we have

$$\begin{aligned}\frac{\partial\phi}{\partial\rho}(z) &= \sum_{\ell=1}^{+\infty}\sum_{m=-\ell}^{\ell}\frac{\ell}{\rho}L_\ell^m I_\ell^m(\rho,\theta,\varphi)\\ &= \sum_{\ell=1}^{+\infty}\frac{\ell}{\rho}\left(L_\ell^0 I_\ell^0(\rho,\theta,\varphi) + 2\,\mathrm{Re}\sum_{m=1}^{\ell} L_\ell^m I_\ell^m(\rho,\theta,\varphi)\right),\end{aligned} \tag{III.6a}$$

$$\begin{aligned}\frac{\partial\phi}{\partial\theta}(z) &= \sum_{\ell=1}^{+\infty}\sum_{m=-\ell}^{\ell}\frac{\partial I_\ell^m}{\partial\theta}(\rho,\theta,\varphi)\\ &= \sum_{\ell=1}^{+\infty}\left(L_\ell^0\frac{\partial I_\ell^0}{\partial\theta}(\rho,\theta,\varphi) + 2\,\mathrm{Re}\sum_{m=1}^{\ell} L_\ell^m\frac{\partial I_\ell^m}{\partial\theta}(\rho,\theta,\varphi)\right),\end{aligned} \tag{III.6b}$$

$$\begin{aligned}\frac{\partial\phi}{\partial\varphi}(z) &= \sum_{\ell=1}^{+\infty}\sum_{\substack{m=-\ell\\ \ell\neq 0}}^{\ell} imL_\ell^m I_\ell^m(\rho,\theta,\varphi)\\ &= -2\sum_{\ell=1}^{+\infty}\mathrm{Im}\sum_{m=1}^{\ell} mL_\ell^m I_\ell^m(\rho,\theta,\varphi).\end{aligned} \tag{III.6c}$$

Proof: The calculation is straightforward, as it is a direct derivation of Proposition IV.C.1. ■

Proposition IV.C.3 (Second-order partial spherical derivatives of the potential)**.** — Still with the same notation, we have

$$\begin{aligned}\frac{\partial^2\phi}{\partial\rho^2}(z) &= \sum_{\ell=2}^{+\infty}\sum_{m=-\ell}^{\ell}\frac{\ell(\ell-1)}{\rho^2}L_\ell^m I_\ell^m(\rho,\theta,\varphi)\\ &= \sum_{\ell=2}^{+\infty}\frac{\ell(\ell-1)}{\rho^2}\left(L_\ell^0 I_\ell^0(\rho,\theta,\varphi)+2\,\mathrm{Re}\sum_{m=1}^{\ell}L_\ell^m I_\ell^m(\rho,\theta,\varphi)\right),\end{aligned} \tag{III.7a}$$

$$\begin{aligned}\frac{\partial^2\phi}{\partial r\,\partial\theta}(z) &= \sum_{\ell=1}^{+\infty}\sum_{m=-\ell}^{\ell}\frac{\ell}{\rho}L_\ell^m\frac{\partial I_\ell^m}{\partial\theta}(\rho,\theta,\varphi)\\ &= \sum_{\ell=1}^{+\infty}\frac{\ell}{\rho}\left(L_\ell^0\frac{\partial I_\ell^0}{\partial\theta}(\rho,\theta,\varphi)+2\,\mathrm{Re}\sum_{m=1}^{\ell}L_\ell^m\frac{\partial I_\ell^m}{\partial\theta}(\rho,\theta,\varphi)\right),\end{aligned} \tag{III.7b}$$

$$\begin{aligned}\frac{\partial^2\phi}{\partial\rho\,\partial\varphi}(z) &= \sum_{\ell=1}^{+\infty}\sum_{\substack{m=-\ell\\ \ell\neq 0}}^{\ell}\frac{\ell}{\rho}imL_\ell^m I_\ell^m(\rho,\theta,\varphi)\\ &= -2\sum_{\ell=1}^{+\infty}\frac{\ell}{\rho}\,\mathrm{Im}\sum_{m=1}^{\ell}mL_\ell^m I_\ell^m(\rho,\theta,\varphi),\end{aligned} \tag{III.7c}$$

$$\begin{aligned}\frac{\partial^2\phi}{\partial\theta^2}(z) &= \sum_{\ell=1}^{+\infty}\sum_{m=-\ell}^{\ell}\frac{\partial^2 I_\ell^m}{\partial\theta^2}(\rho,\theta,\varphi)\\ &= \sum_{\ell=1}^{+\infty}\left(L_\ell^0\frac{\partial^2 I_\ell^0}{\partial\theta^2}(\rho,\theta,\varphi)+2\,\mathrm{Re}\sum_{m=1}^{\ell}L_\ell^m\frac{\partial^2 I_\ell^m}{\partial\theta^2}(\rho,\theta,\varphi)\right),\end{aligned} \tag{III.7d}$$

$$\begin{aligned}\frac{\partial^2\phi}{\partial\theta\,\partial\varphi}(z) &= \sum_{\ell=1}^{+\infty}\sum_{\substack{m=-\ell\\ \ell\neq 0}}^{\ell}imL_\ell^m\frac{\partial I_\ell^m}{\partial\theta}(\rho,\theta,\varphi)\\ &= -2\sum_{\ell=1}^{+\infty}\mathrm{Im}\sum_{m=1}^{\ell}mL_\ell^m\frac{\partial I_\ell^m}{\partial\theta}(\rho,\theta,\varphi),\end{aligned} \tag{III.7e}$$

$$\begin{aligned}\frac{\partial^2\phi}{\partial\varphi^2}(z) &= -\sum_{\ell=1}^{+\infty}\sum_{\substack{m=-\ell\\ \ell\neq 0}}^{\ell}m^2L_\ell^m I_\ell^m(\rho,\theta,\varphi)\\ &= 2\sum_{\ell=1}^{+\infty}\mathrm{Re}\sum_{m=1}^{\ell}m^2L_\ell^m I_\ell^m(\rho,\theta,\varphi).\end{aligned} \tag{III.7f}$$

Proof: The calculation is straightforward, as it is a direct derivation of Proposition IV.C.2. ■

The third-order partial spherical derivatives of the potential is more tedious but as straightforward to compute. We will omit the proposition. For this, the only new quantities that we need compared to the computation of the potential are the partial derivatives with respect to θ of the inner function.

IV.C.4 P2P operator

The modifications that have to be done are very close to the ones to do for the local-to-particle method, with the difference that the calculations have to be done in the complex spherical harmonics basis and not with inner functions.

In practice, the main difference is that instead of having to differentiate the function $r \mapsto r^\ell$ for a natural integer ℓ, we have to differentiate the function $r \mapsto r^{-(\ell+1)}$. Hence we will omit the formulæ.

IV.D Software implementation for the AMOEBA force field

In this part, we describe in more details the developed implementation to use the fast multipole method with the AMOEBA force field. We did other implementations of the method to apply the fast multipole method to other problems — in particular for the paper [Lin+18], but what we present here is the more general case we looked at.

The fast multipole method computations were externalised to `ScalFMM` [Bla+15], which is a general C++ library. Our modifications were introduced through its add-on system. The AMOEBA simulations were done with the `Fortran` molecular mechanics software `TINKER` [Pon+10]. Every computation that is quadratic in the number of particles was modified so that `ScalFMM` performs the computations.

For the communication between these two software (`ScalFMM` and `TINKER`), we created a `C` interface to `ScalFMM`, and used `Fortran`'s compilers ability of calling `C` functions (foreign function interface).

This is done to limit the cost of an increased complexity in the maintenance and evolution of the implementation. We would expect faster timings if all the computations were done within a single code.

In Table IV.1, we give an overview of what we are able to compute using the described method. To obtain the energy for 2^n poles — and thus the forces of 2^{n-1} poles, we derived the equations by hand. This is straightforward, albeit tedious, work.

Table IV.1: Status of the implementation in `ScalFMM`

Terms	Potential	Energy	Forces
Charges	✓	✓	✓
Dipoles	✓	✓	✓
Quadrupoles	✓	✓	✓
General multipoles	✓	✗	✗

For a general framework, we would need a closed formula for the derivatives of the LEGENDRE polynomials with respect to the angular variable.

IV.D.1 Integration for polarisable classical molecular dynamics

In this section, we look at how to convert between Cartesian and spherical harmonics representation of multipoles, as the former description is often used in molecular dynamics software.

We will need the following propositions to convert Cartesian quantities to real spherical harmonics. The notation for the multipoles are changed to use ones that are more common in chemistry: $q_i \in \mathbf{R}$, $\mu_i \in \mathbf{R}^3$ and $\Theta_i \in \mathbf{R}^{3\times 3}$ representing respectively the charges, dipoles and quadrupoles, while ∇_i and $\nabla_i\nabla_i$ represent respectively the differential operators D_i and D_i^2.

Proposition IV.D.1 (Cartesian to real spherical harmonics). — Let

$$\hat{\mathrm{L}}_i = q_i + \mu_i \cdot \nabla_i + \Theta_i \colon \nabla_i \nabla_i \tag{IV.1}$$

be the multipolar density operator associated to a point $r_i \in \mathbf{R}^3$.

Then, the coefficients for this multipole in a real spherical harmonics basis are

$$[\hat{S}_i]_0^0 = \sqrt{4\pi} q_i, \tag{IV.2a}$$

$$[\hat{S}_i]_1^{-1} = \sqrt{\frac{4\pi}{3}} \mu_{i,y}, \quad [\hat{S}_i]_1^0 = \sqrt{\frac{4\pi}{3}} \mu_{i,z}, \quad [\hat{S}_i]_1^1 = \sqrt{\frac{4\pi}{3}} \mu_{i,x}, \tag{IV.2b}$$

$$\begin{aligned} [\hat{S}_i]_2^{-2} &= 6\sqrt{\frac{4\pi}{15}} \Theta_{i,xy}, \quad [\hat{S}_i]_2^{-1} = 6\sqrt{\frac{4\pi}{15}}, \Theta_{i,yz}, \\ [\hat{S}_i]_2^0 &= -6\sqrt{\frac{\pi}{15}} (\Theta_{i,xx} + \Theta_{i,yy}), \\ [\hat{S}_i]_2^1 &= 6\sqrt{\frac{4\pi}{15}} \Theta_{i,xz}, \quad [\hat{S}_i]_2^2 = 6\sqrt{\frac{\pi}{15}} (\Theta_{i,xx} - \Theta_{i,yy}). \end{aligned} \tag{IV.2c}$$

Proof: The potential exerted by a multipolar operator $\hat{\mathrm{L}}_i$ is given in Cartesian coordinates by

$$\phi_i(r) = \hat{\mathrm{L}}_i \left(\frac{1}{|r - r_i|} \right) = \frac{q_i}{|r - r_i|} + \sum_\gamma \frac{\mu_{i,\gamma} (r - r_i)_\gamma}{|r - r_i|^3} + \sum_\gamma \sum_{\gamma'} 3 \frac{(r - r_i)_\gamma \Theta_{\gamma\gamma'} (r - r_i)_{\gamma'}}{|r - r_i|^5}, \tag{IV.3}$$

where γ and γ' go through the coordinates $\{x, y, z\}$.

However, this same potential is written in real spherical harmonics basis as

$$\phi_i(r) = \sum_{\ell=0}^{2} \sum_{m=-\ell}^{\ell} [\hat{S}_i]_{\ell,m} \frac{1}{|r - r_i|^{\ell+1}} \hat{Y}_\ell^m \left(\frac{r - r_i}{|r - r_i|} \right) \tag{IV.4}$$

We can identify the coefficients by hand, using the fact that the Cartesian coordinates can be written in spherical coordinates as

$$\begin{cases} r_x = \sin(\theta) \cos(\varphi) \\ r_y = \sin(\theta) \sin(\varphi) \\ r_z = \cos(\theta) \end{cases}, \tag{IV.5}$$

that the first associated Legendre polynomials are

$$\begin{aligned} P_0^0(\cos\theta) &= 1, \\ P_1^0(\cos\theta) = \cos\theta, \quad P_1^1(\cos\theta) &= -\sin\theta, \\ P_2^0(\cos\theta) = \frac{3\cos^2\theta - 1}{2}, \quad P_2^1(\cos\theta) &= -3\cos\theta\sin\theta, \quad P_2^2(\cos\theta) = 3\sin^2\theta; \end{aligned} \tag{IV.6}$$

and finally that, by convention, the trace of the trace of quadrupoles matrices is zero

$$\Theta_{xx} + \Theta_{yy} + \Theta_{zz} = 0. \tag{IV.7}$$

By denoting θ and φ the angles given by the projection on the unit sphere of the vector $r - r_i$, we then find

$$\hat{Y}_0^0(\theta,\varphi) = \frac{1}{\sqrt{4\pi}}, \tag{IV.8a}$$

$$\begin{gathered}\hat{Y}_1^{-1}(\theta,\varphi) = \sqrt{\frac{3}{4\pi}}\cdot\frac{(r-r_i)_y}{|r-r_i|}, \quad \hat{Y}_1^0(\theta,\varphi) = \sqrt{\frac{3}{4\pi}}\cdot\frac{(r-r_i)_z}{|r-r_i|}, \\ \hat{Y}_1^1(\theta,\varphi) = \sqrt{\frac{3}{4\pi}}\cdot\frac{(r-r_i)_x}{|r-r_i|},\end{gathered} \tag{IV.8b}$$

$$\begin{gathered}\hat{Y}_2^{-2}(\theta,\varphi) = \sqrt{\frac{15}{4\pi}}\cdot\frac{(r-r_i)_x(r-r_i)_y}{|r-r_i|^2}, \quad \hat{Y}_2^{-1}(\theta,\varphi) = \sqrt{\frac{15}{4\pi}}\cdot\frac{(r-r_i)_y(r-r_i)_z}{|r-r_i|^2}, \\ \hat{Y}_2^0(\theta,\varphi) = \frac{1}{2}\sqrt{\frac{5}{4\pi}}\cdot\frac{2(r-r_i)_z^2-(r-r_i)_x^2-(r-r_i)_y^2}{|r-r_i|^2}, \\ \hat{Y}_2^1(\theta,\varphi) = \sqrt{\frac{15}{4\pi}}\cdot\frac{(r-r_i)_z(r-r_i)_x}{|r-r_i|^2}, \quad \hat{Y}_2^2(\theta,\varphi) = \frac{1}{2}\sqrt{\frac{15}{4\pi}}\cdot\frac{(r-r_i)_x^2-(r-r_i)_y^2}{|r-r_i|^2}.\end{gathered} \tag{IV.8c}$$

It is then straightforward to identify the coefficients. ■

IV.D.2 Dealing with scalings in the fast multipole method

We saw in Chapter I that some interactions have to be modified for the AMOEBA force field: Some of them have to be screened (in the static electrostatic energy computation), while other have to be damped by the THOLE damping scheme (in the polarisation energy computation). However, the screening and damping are local in the sense that the interaction is modified only for particles that are close to each other.

Screening terms

As the interactions to be scaled are some neighbours (in the sense of bonding) of each atoms, this means that we can store the list of neighbours in some arrays that are computed only once. This enables us to compute the full, non-screened, interactions with the fast multipole method, while removing the quantities in excess directly in the molecular mechanics software after calling the external fast multipole method library. Some interactions are thus computed twice, which adds some overhead to the computations. However as the arrays are of a fixed-size this does not change the algorithmic complexity. Practical experience shows that the time spent computing the corrections is negligible with respect to the time spent in the fast multipole method. Moreover, this has the advantage of making the fast multipole method software oblivious to this peculiarity of the computations.

Damping terms

For the THOLE damping the same trick could be used in principle, but since no topological considerations are made it can be directly integrated into the fast multipole method code without communicating topological neighbor lists. Since the THOLE damping scheme is such that modifications appear only in the near-field, only the particle-to-particle part of the algorithm has to be modified; all the far-field computations remaining untouched.

IV.E Results

IV.E.I Calibration

The fast multipole method has two degrees of freedom: the expansion order ℓ of the spherical harmonics and the height LV of the octree. The height of the octree has to be chosen with respect to the size of the system: As the first level exactly encloses the system, should the height remain constant, then the bigger the system, the more particles would be in the smallest boxes (leaves). In consequence, the near-field interaction would scale quadratically and start to dominate the total cost after a certain number of particles. One way to adapt the height with respect to the system is to use the fact that particles tends not to be arbitrarily close to each other. We can therefore fix the edge length B of the smallest box of the octree. Then the height will be the smallest integer LV such that the cube of edge length LV × B contains all particles. We then use the integer LV as parameter for the octree and LV × B for the size of simulation box. We refer to Fig. IV.1 for a schematic description.

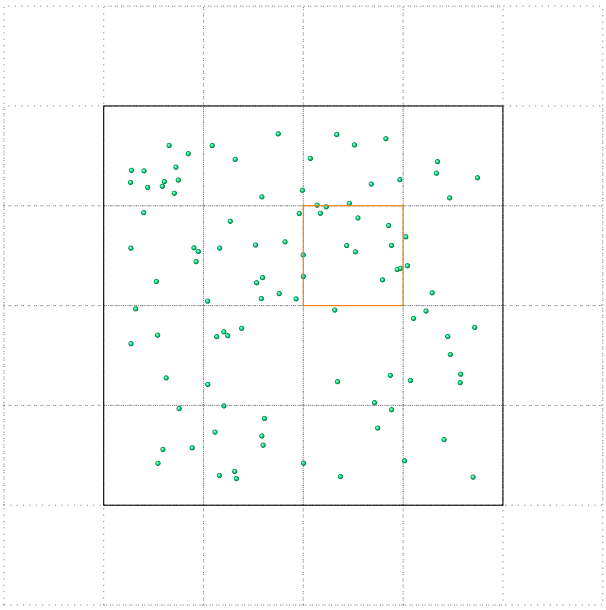

Figure IV.1: Schematic description for the minimum box size B. For a minimum box size of one unit (in orange), we have an associated depth of three for the fast multipole method tree: If we have three levels, then all particles are included in the full simulation box (in black).

To choose the parameters, we tested several of them for different systems and looked at the error on the potential created by the charges with respect to the exact computation using the naive — but exact — double loop method of quadratic computational complexity. The results are reported in Tables IV.2 to IV.4. The systems had between 2000 and 12 000 particles, with steps of 2000 particles, randomly inside a box of fixed size and the charges were arbitrarily fixed to some value. To lighten the tables, we omitted results for 4000, 6000 and 10 000 particles. We note that we did the same kind of tests for multipoles up to quadrupoles, but the results were similar and hence are not reported. Moreover, as point multipoles were arbitrarily fixed for calibration and had no particular physical meaning, we rather tried to chose *optimal* parameter only for point charges, and validate them for test-cases on real molecular systems later on.

The potential was evaluated at every particles' positions. The rightmost column indicate if the computation was faster or slower than with the reference method. Are also reported the

spherical harmonics expansion order ℓ, the minimum box size B of the fast multipole method tree, in ångströms and its associated height LV of the fast multipole method tree, the time that was the computations took, the root-mean-square on the potential and the maximum of the error MAX on the potential.

Table IV.2: Precision results for 2000 point charges

ℓ	B	LV	TIME	RMS	MAX	
6	4.0	5	0.0125	1.94×10^{-4}	1.29×10^{-3}	✗
6	8.0	4	0.0102	1.76×10^{-4}	1.31×10^{-3}	✗
6	12.0	4	0.0140	1.18×10^{-4}	7.96×10^{-4}	✗
6	16.0	3	0.0189	1.36×10^{-4}	1.43×10^{-3}	✗
6	20.0	3	0.0216	2.09×10^{-5}	5.30×10^{-4}	✗
8	4.0	5	0.0213	5.22×10^{-5}	4.60×10^{-4}	✗
8	8.0	4	0.0124	4.74×10^{-5}	4.94×10^{-4}	✗
8	12.0	4	0.0156	2.88×10^{-5}	2.95×10^{-4}	✗
8	16.0	3	0.0202	3.57×10^{-5}	5.25×10^{-4}	✗
8	20.0	3	0.0230	6.03×10^{-6}	2.25×10^{-4}	✗
10	4.0	5	0.0358	2.21×10^{-5}	2.23×10^{-4}	✗
10	8.0	4	0.0172	1.99×10^{-5}	2.28×10^{-4}	✗
10	12.0	4	0.0170	1.25×10^{-5}	1.43×10^{-4}	✗
10	16.0	3	0.0229	1.40×10^{-5}	2.02×10^{-4}	✗
10	20.0	3	0.0244	1.31×10^{-6}	3.53×10^{-5}	✗
12	4.0	5	0.0565	6.66×10^{-6}	9.14×10^{-5}	✗
12	8.0	4	0.0181	6.11×10^{-6}	9.08×10^{-5}	✗
12	12.0	4	0.0188	3.48×10^{-6}	4.47×10^{-5}	✗
12	16.0	3	0.0232	4.98×10^{-6}	9.69×10^{-5}	✗
12	20.0	3	0.0255	4.83×10^{-7}	1.30×10^{-5}	✗
	Ref.		0.0076			

Table IV.3: Precision results for 8000 point charges

ℓ	B	LV	TIME	RMS	MAX	
6	4.0	6	0.0581	2.81×10^{-4}	2.27×10^{-3}	✓
6	8.0	5	0.0378	2.64×10^{-4}	2.29×10^{-3}	✓
6	12.0	5	0.0809	4.09×10^{-4}	4.38×10^{-3}	✓
6	16.0	4	0.1301	2.37×10^{-4}	2.31×10^{-3}	✗
6	20.0	4	0.1648	3.62×10^{-4}	4.51×10^{-3}	✗
8	4.0	6	0.1087	6.90×10^{-5}	5.19×10^{-4}	✓
8	8.0	5	0.0491	6.32×10^{-5}	5.27×10^{-4}	✓
8	12.0	5	0.0853	1.08×10^{-4}	1.07×10^{-3}	✓
8	16.0	4	0.1290	5.23×10^{-5}	5.08×10^{-4}	✗
8	20.0	4	0.1684	8.63×10^{-5}	1.14×10^{-3}	✗
10	4.0	6	0.1838	3.14×10^{-5}	3.81×10^{-4}	✗
10	8.0	5	0.0636	2.92×10^{-5}	3.53×10^{-4}	✓
10	12.0	5	0.0911	4.72×10^{-5}	5.37×10^{-4}	✓
10	16.0	4	0.1336	2.32×10^{-5}	3.12×10^{-4}	✗
10	20.0	4	0.1730	3.57×10^{-5}	4.73×10^{-4}	✗
12	4.0	6	0.2968	8.49×10^{-6}	1.04×10^{-4}	✗
12	8.0	5	0.0821	7.58×10^{-6}	1.05×10^{-4}	✓
	Ref.		0.1196			

Table IV.3: (continued)

ℓ	B	LV	TIME	RMS	MAX	
12	12.0	5	0.1032	1.39×10^{-5}	2.52×10^{-4}	✓
12	16.0	4	0.1388	5.94×10^{-6}	1.02×10^{-4}	✗
12	20.0	4	0.1791	1.02×10^{-5}	2.24×10^{-4}	✗
	Ref.		0.1196			

Table IV.4: Precision results for 12 000 point charges

ℓ	B	LV	TIME	RMS	MAX	
6	4.0	6	0.0955	3.13×10^{-4}	3.34×10^{-3}	✓
6	8.0	5	0.0624	2.96×10^{-4}	3.00×10^{-3}	✓
6	12.0	5	0.1363	4.33×10^{-4}	7.85×10^{-3}	✓
6	16.0	4	0.2322	2.69×10^{-4}	3.05×10^{-3}	✓
6	20.0	4	0.3247	3.85×10^{-4}	5.26×10^{-3}	✗
8	4.0	6	0.1789	7.68×10^{-5}	8.27×10^{-4}	✓
8	8.0	5	0.0740	7.23×10^{-5}	8.83×10^{-4}	✓
8	12.0	5	0.1413	1.11×10^{-4}	1.01×10^{-3}	✓
8	16.0	4	0.2316	6.22×10^{-5}	8.23×10^{-4}	✓
8	20.0	4	0.3276	9.21×10^{-5}	1.04×10^{-3}	✗
10	4.0	6	0.3019	3.68×10^{-5}	4.35×10^{-4}	✗
10	8.0	5	0.0896	3.49×10^{-5}	3.69×10^{-4}	✓
10	12.0	5	0.1501	5.10×10^{-5}	6.95×10^{-4}	✓
10	16.0	4	0.2381	2.87×10^{-5}	3.65×10^{-4}	✓
10	20.0	4	0.3341	4.19×10^{-5}	5.48×10^{-4}	✗
12	4.0	6	0.4756	9.34×10^{-6}	1.35×10^{-4}	✗
12	8.0	5	0.1187	8.44×10^{-6}	1.28×10^{-4}	✓
12	12.0	5	0.1623	1.45×10^{-5}	3.68×10^{-4}	✓
12	16.0	4	0.2450	7.17×10^{-6}	1.08×10^{-4}	✓
12	20.0	4	0.3404	1.11×10^{-5}	1.78×10^{-4}	✗
	Ref.		0.2681			

We remark that in general, the time increases and the errors decrease as the box length increases. This is consistent with the fact that the number of interactions that are exactly computed increases. The time actually decreases between using a box length of 4.0 and 6.0; this can be explained by the increase of work that has to be done having to use an octree with a depth of six levels instead of five. This glitch is not present for other change of depth. We also remark that time increases with the expansion order ℓ, while the error decreases.

Based on the above observations, we have selected the parameters (ℓ, B) to be $(6, 12.0)$ or $(8, 8.0)$ as they seem to represent a good trade-off between accuracy and speed. We notice that the latter parameters are both more precise and faster than the former parameters.

IV.E.2 Performance results

For the remaining of this section on the analysis of the scalability, we did computations for a single time-step of a molecular dynamic simulation on homogeneous water boxes of different sizes. The AMOEBA force field was used for the parameterisation of the multipoles up to quadrupoles. Computations were done with and without the inclusion of the polarisation term. When polarisation is active, we used a convergence parameter of 10^{-5} on the residual.

Linear scaling

We first analyse the scaling of the computational time when the number of atoms increases on a fixed number of 216 cores. In Fig. IV.2, we report the total execution time for performing one time-step of AMOEBA polarisable molecular dynamics using our integration of TINKER with ScalFMM, as well the average time to run a single call to the fast multipole method method. We observe that the scaling is indeed linear, as expected, as the size of the system increases. The computations using the parameters (ℓ, B) of $(8, 8.0)$ are faster than for $(6, 12.0)$, which is in accordance with the observation of the calibration results.

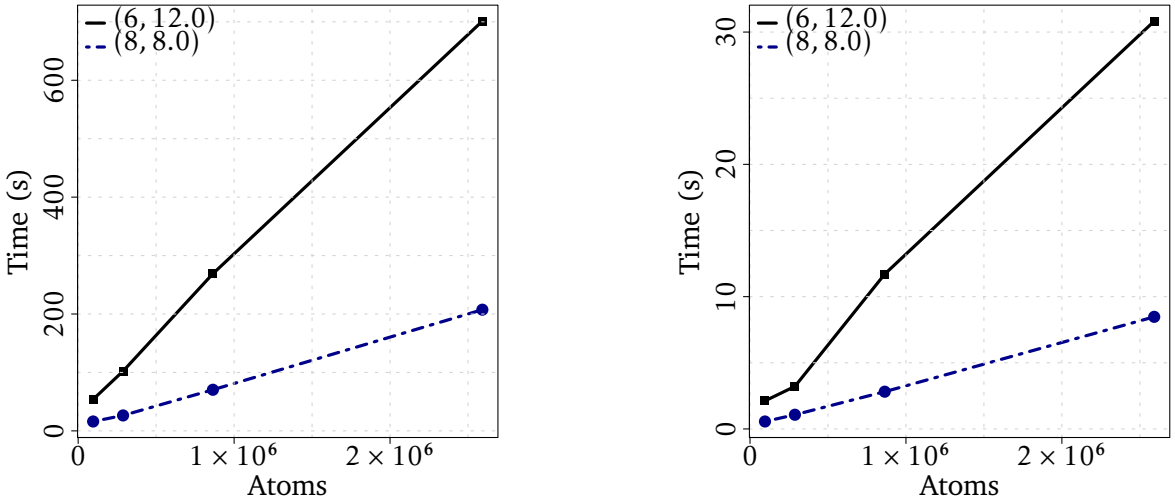

(a) Total execution time of TINKER for one time-step

(b) Average time per fast multipole method call

Figure IV.2: Timings for one time-step of AMOEBA polarisable molecular dynamics on different sizes of homogeneous water boxes

Weak and strong scalability

In this section, we look at strong and weak scalability results where we have chose an order of expansion $\ell = 8$ and a minimum box size of $B = 8$.

Strong scalability In Fig. IV.3, we analyse the strong scalability of the method: We look at the computational time when we increase the number of processors while fixing every other parameters.

First, we note that the scaling is roughly the same whether or not we use polarisation, as can be seen in Fig. IV.3a for a water box of around 100 000 atoms. As it is significantly faster to do computations without polarisation, the remaining comparisons within this section will not discuss it, and computations should be assumed to use the AMOEBA force field without polarisation.

To have a baseline for the scalability, we have also reported the scaling of the double loop algorithm (with polarisation) implemented in TINKER. The results are similar.

In Fig. IV.3b, we compare the speedup for three different water boxes of between 1.0×10^5 and 2.5×10^6 atoms. We can observe that the scalability is better with the largest boxes that we used. This can be explained by the fact that the work to be done by every processor is more homogeneous. However, we are far from optimal scaling, which can be explained by some lack of homogeneity in the distribution of particles for each processor; in particular for processors

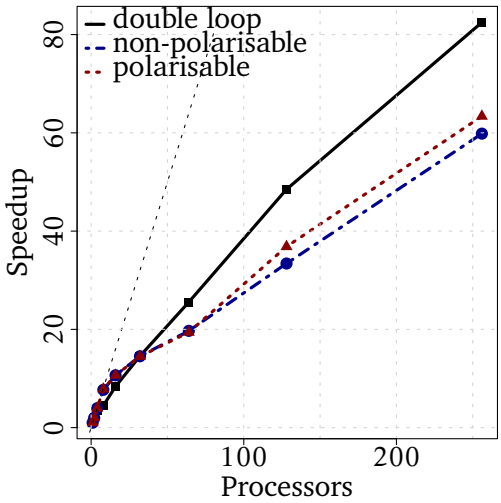

(a) Comparison of the scaling with and without polarisation for a system of 96 000 atoms

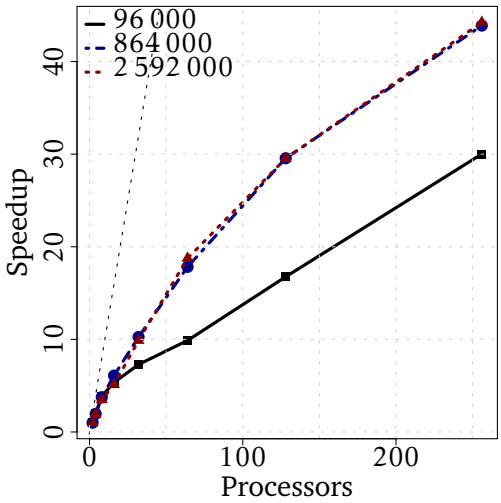

(b) Total time speedup for one time-step with fixed minimum fast multipole method box size

Figure IV.3: Strong scalability results with water boxes of different sizes for $(\ell, B) = (8, 8.0)$. The dashed curve represents optimal scaling.

attached to particles at the border of the system. It can also be explained by some overhead of the implementation, as we recreate the data structure (which scales as $N \log N$) at every new time-step.

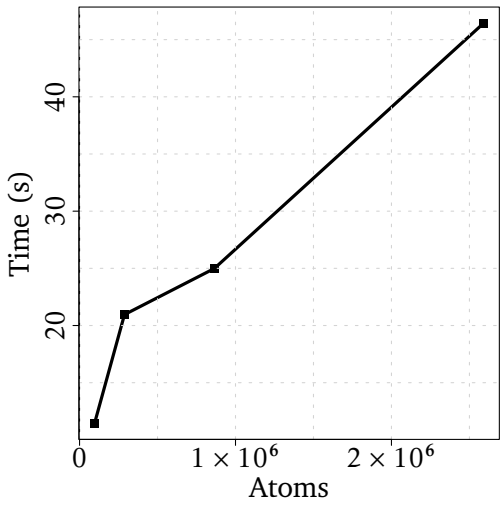

Figure IV.4: Weak scalability without polarisation for different water boxes of sizes between 96 000 and 3 million atoms

Weak scalability Finally, in Fig. IV.4 we triple the number of processors as we roughly triple the number of atoms in the box, starting with eight processors. The trends show that we can keep a linear increase in the cost of doing the molecular dynamics as we increase the number of atoms by jointly increasing the number of processors. We note that we were limited by using existing water boxes, which were only approximately increasing by multiples of three; which can explain the glitch for the second point. However, we are confident of the weak scaling due to the linear

trend for systems that had atoms varying by orders of magnitude.

IV.E.3 Energy conservation

To validate the choice of parameters we have made in Section IV.E.1 for a possibly long-running molecular dynamics, we look at the conservation of energy for small proteins of different sizes.

As we look at energy conservation, we will use notions of short-term fluctuations and long-term drift for the energy. The former is computed by averaging the root-mean-square of the energy fluctuations every 50 femtoseconds; while the latter is by looking at the slope of linear curves that fit the energies with respect to the time in picoseconds. Depending on whether the system was first *stabilised* with canonical ensemble molecular dynamics, we may discard some of the first time-steps, to prevent accounting for natural fluctuations at the beginning. We will state when this is the case.

The reader should be aware that for figures that we will present, panels may not be directly comparable to one another. Indeed, some computations have different initial geometries, which can be spotted by the shift in energy on the ordinate, or the different time-steps.

Dihydrofolate reductase protein

In Figs. IV.5 and IV.6 we report results for the dihydrofolate reductase (DHFR) [Ban88], which has 2489 atoms. We used the configuration available in TINKER, which we prepared by heating it to 300 kelvins using the BERNSTEIN thermostat with the full AMOEBA force field for 20 picoseconds. This molecule was used as it is small enough to be able to compare the energy drift with the *exact* computations using the double loop method.

To only account for the approximations due to the use of the fast multipole method, we ran a molecular dynamics of a couple of hundred picoseconds with 0.1 femtosecond time-steps and without polarisation. With the double loop method, which is not reported, the energy varies by around 1.0×10^{-1} kcal/mol for a 250 picoseconds molecular dynamics. We tested for point charges only and multipoles up to quadrupoles. The results with the fast multipole method are reported in figure Fig. IV.5, and are similar in both cases.

No energy drift is really noticeable on the figure for parameters $(\ell, B) = (6, 12.0)$, and are similar, although a bit higher than the reference using the double loop method. For parameters $(\ell, B) = (8, 8.0)$, a drift is present, but reasonable in view of the length of the molecular dynamics. We notice that compared to the calibration results of Section IV.E.1, the former parameters now seem to give the more accurate results, which can be explained by the bigger box in which the interactions are exactly computed. We do not report the timings, but we note that the latter parameters still give the fastest timings.

In Fig. IV.6, we ran the simulation on the same molecule, but with polarisation, after doing a canonical molecular dynamics for 20 picoseconds. The time-steps were chosen as 0.25 femtosecond and 1.0 femtosecond for the canonical and micro-canonical ensembles molecular dynamics. We used a conservative convergence parameter for polarisation of 10^{-8}, to prevent an energy drift due to that parameter. We do not observe an energy drift in either case, although the fluctuations are more important — but expected — with the larger time-step.

We also report in Table IV.5 the results for the short-term fluctuations and long-term drift, which confirm these observations. We note that the simulation times reported there are longer than the one in the figure. It is because we only show simulations for the same number of time-steps in each panel.

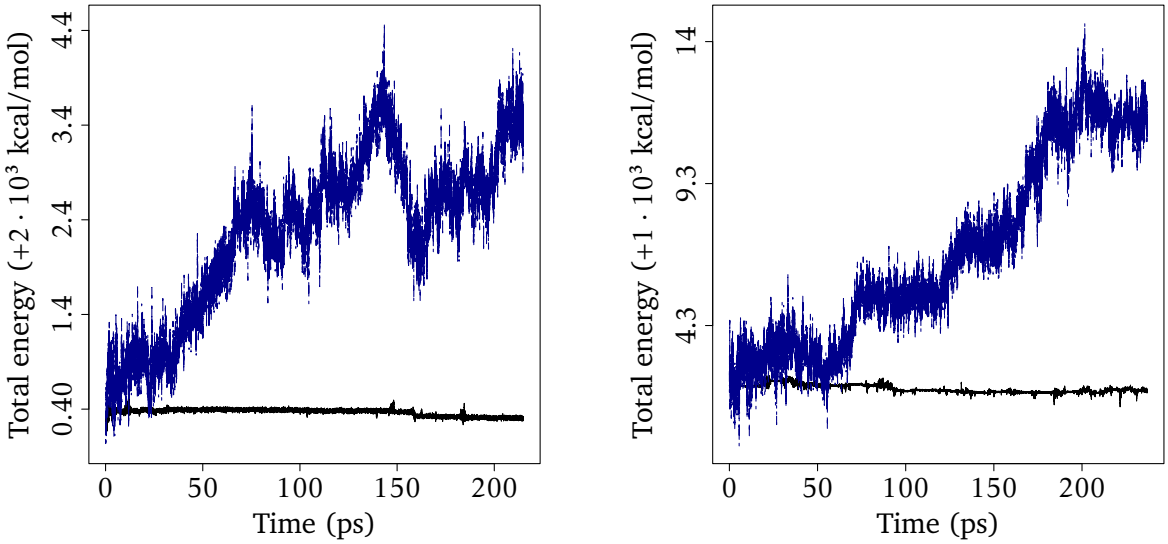

(a) Molecular dynamics using only point charges

(b) Molecular dynamics using multipoles up to quadrupoles

Figure IV.5: DHFR without polarisation and with 0.1 femtosecond time-steps. The curve in black is with parameters $(\ell, B) = (6, 12.0)$ and in blue with $(8, 8.0)$. We extracted the energy every 100 steps.

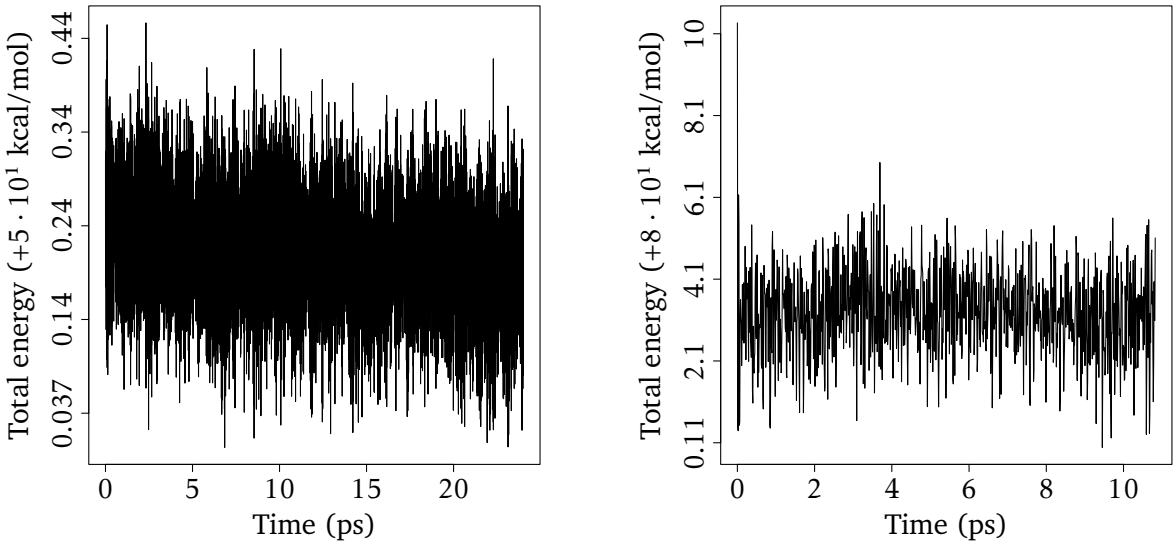

(a) Molecular dynamics with 0.25 femtosecond time-steps

(b) Molecular dynamics with 1.0 femtosecond time-steps

Figure IV.6: Energy conservation for DHFR with the full AMOEBA force field and fast multipole method parameters $(\ell, B) = (6, 12.0)$. Polarisation convergence was set to 10^{-8} and the computations were done on 24 processors. We extracted the energy every 100 steps.

Table IV.5: Short-term fluctuations and long-term drift in kcal/mol for the total energy of DHFR with associated simulation length in picoseconds and time-steps in femtoseconds

CASE	PARAMETERS	STF	LTD	LENGTH	TIME-STEP
charges (IV.5a)	(6, 12.0)	1.4×10^{-3}	-4.2×10^{-4}	265	0.10
	(8, 8.0)	1.6×10^{-2}	1.1×10^{-2}	215	0.10
multipoles (IV.5b)	(6, 12.0)	3.1×10^{-3}	-1.5×10^{-3}	237	0.10
	(8, 8.0)	4.5×10^{-2}	4.4×10^{-2}	399	0.10
AMOEBA (IV.6a)	(6, 12.0)	1.7×10^{-2}	-2.1×10^{-3}	24	0.25
AMOEBA (IV.6b)	(6, 12.0)	1.1×10^{0}	-1.6×10^{-2}	10	1.0

Dronpa protein

We now look at the conservation of energy for the first picosecond with systems of different sizes with polarisation. We prepared the systems by first minimising its energies and then heated them to 300 K using the BERNSTEIN thermostat and time-steps of 1.0 femtosecond for a picosecond using the full AMOEBA force field. We extracted different sections of the dronpa protein [Ban06]. The molecule was not solvated and computations were performed on 24 cores. The sections are of respective sizes 3783 atoms, 7723 atoms, 11 728 atoms, 15 580 atoms and 19 663 atoms. The results were similar in all cases, with higher fluctuations as the number of atoms increased. We only report figures for the first and fifth sections in Figs. IV.7a and IV.7b.

We report in Table IV.6 the results for the short-term fluctuations and long-term drift. The numbers are higher than for DHFR which can be explained by the use of polarisation and the fact that the molecule was from the Proteins Data Bank and not from a system in TINKER, which may be less suitable for molecular dynamics. However, the results show that we can obtain similar conservation results as the DHFR protein, even for a random system in the Proteins Data Bank, which shows some robustness of the fast multipole method.

Table IV.6: Short-term fluctuations and long-term drift in kcal/mol for the total energy for different sections of the dronpa protein with polarisation for 1.0 picosecond molecular dynamics with 0.1 femtosecond time-steps

SYSTEM	PARAMETERS	STF	LTD
First section (IV.7a)	(6, 12.0)	1.5	-3.8×10^{-2}
	(8, 8.0)	1.5	-6.5×10^{-3}
Second section	(6, 12.0)	2.4	-8.7×10^{-1}
	(8, 8.0)	2.4	-5.7×10^{-1}
Third section	(6, 12.0)	3.0	2.2×10^{-1}
	(8, 8.0)	3.0	1.6×10^{0}
Fourth section	(6, 12.0)	3.5	1.2×10^{0}
	(8, 8.0)	3.6	-6.1×10^{-1}
Fifth section (IV.7b)	(6, 12.0)	3.3	-8.8×10^{-1}
	(8, 8.0)	3.3	6.1×10^{-1}

IV.E.4 Solvated molecular systems

Finally, we look at results where a solvent, in this case water, is used. First, with explicit water molecules that are treated as any other atoms, using the AMOEBA force field; and next with implicit

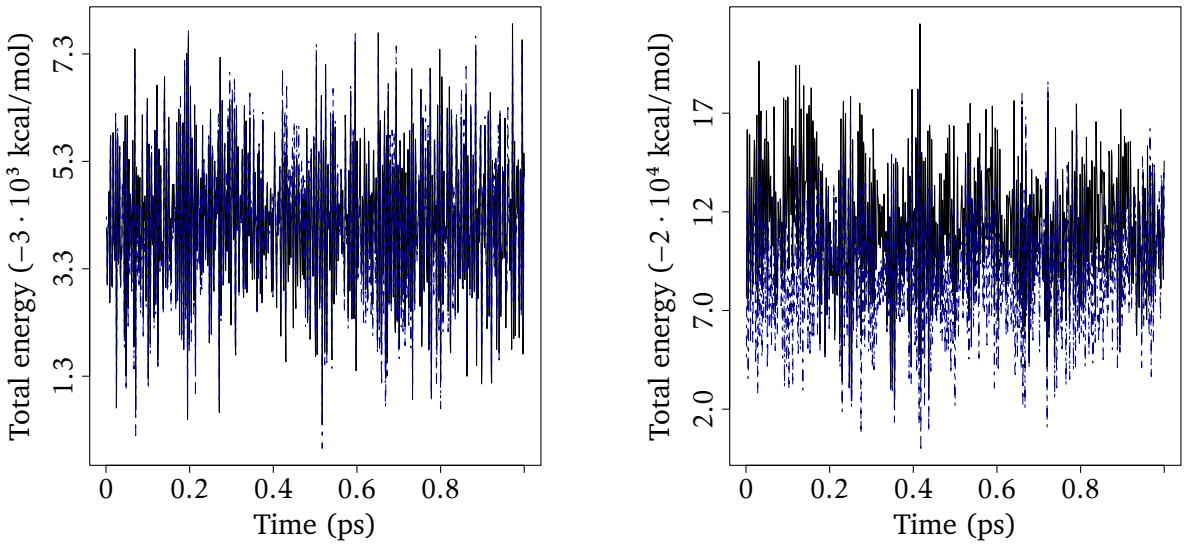

(a) Energy conservation for the first section of the dronpa protein

(b) Energy conservation for the fifth section of the dronpa protein

Figure IV.7: Energy conservation for the first (left) and fifth (right) sections of the dronpa protein with polarisation and with 0.1 femtosecond time-steps. The curve in black is with parameters $(\ell, B) = (6, 12.0)$ and in blue with $(8, 8.0)$.

water molecules using ddCOSMO [CMS13]. Both descriptions have thus a linear computational complexity, as ddCOSMO is a linear implementation of the COSMO [KS93] method.

Molecular dynamics with explicit solvent

In Fig. IV.8, we present results of a molecular dynamics for the solvated DHFR protein. It is solvated with 7023 water molecules, which amount to a system of 23 558 atoms in total. We chose two different tolerance parameters of 10^{-5} and 10^{-8} for polarisation with 0.25 femtosecond time-steps. To prevent the water molecules from *going away*, we used a spherical droplet restraint between atoms of 100 ångströms.

For parameters $(\ell, B) = (8, 8.0)$, as we expect the system to have a drift, as it was already the case when DHFR was not solvated, we first heated it to 300 kelvins for 10 picoseconds. The geometry for parameters $(\ell, B) = (6, 12.0)$ was the one given in TINKER, hence the large fluctuations at the beginning of the simulation, which are due to the increase of temperature at the beginning. The short-term fluctuations and long-term drift for the energy are also reported in Table IV.7.

There is a clear drift that is present in every cases. However, as it did not exist when DHFR was not solvated for $(\ell, B) = (6, 12.0)$ we think it is mostly due a system that is not well behaved.

Molecular dynamics with implict solvent

To obtain physical properties from a molecular dynamics, we have to sample enough configurations of the molecular system of interest. However, explicit solvent means that lots of dynamic steps will only serve to sample the solvent. Implicit solvation may decrease the simulation time necessary to obtain physical quantities by making use of collective variables for the solvent. As a proof of concept, we used this method for the first section of the dronpa protein, which is shown in Fig. IV.9 for an order $\ell = 8$ using the COSMO model and 1.0 femtosecond time-steps. Even though

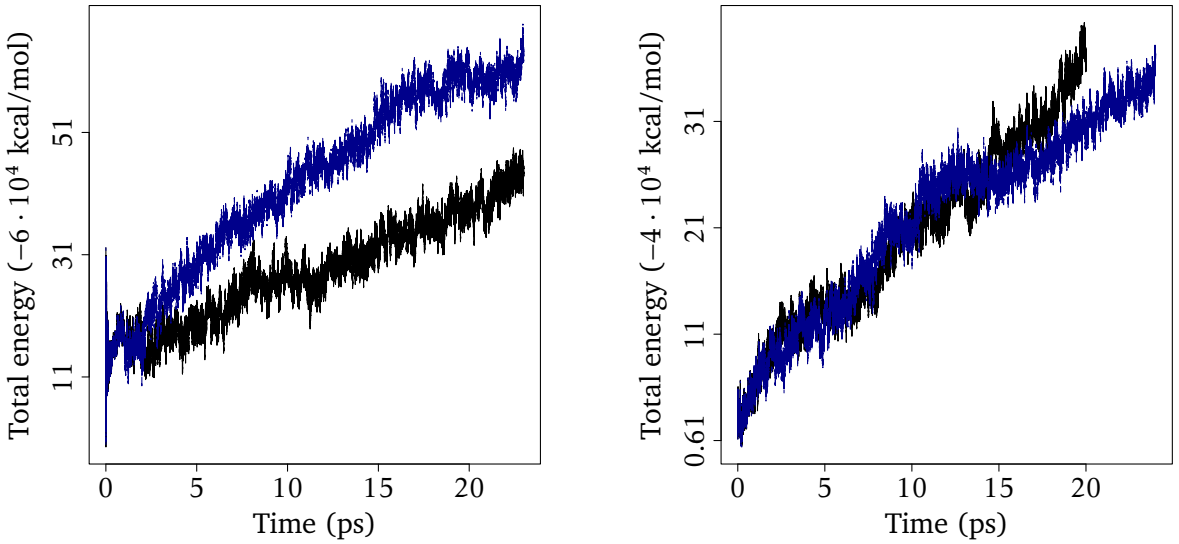

(a) Parameters $(\ell, B) = (6, 12.0)$ and 0.25 femtosecond time-steps

(b) Parameters $(\ell, B) = (8, 8.0)$ and 0.25 femtosecond time-steps.

Figure IV.8: Solvated DHFR with polarisation. The computation was done on 48 processors using a spherical droplet restraint between atoms of size 100 ångströms. The curves in black are for a convergence for polarisation of 10^{-8} and the ones in blue for 10^{-5}.

Table IV.7: Short-term fluctuations and long-term drift in kcal/mol for the total energy of solvated DHFR for molecular dynamics with 0.25 femtosecond time-steps

TOLERANCE	PARAMETERS	STF	LTD	LENGTH
10^{-5} (IV.8a)†	$(6, 12.0)$	3.4×10^{-1}	1.8	29
10^{-8} (IV.8a)†	$(6, 12.0)$	3.4×10^{-1}	1.3	23
10^{-5} (IV.8b)	$(8, 8.0)$	2.1×10^{-1}	1.2	24
10^{-8} (IV.8b)	$(8, 8.0)$	2.1×10^{-1}	1.5	20

†Due to fluctuations, we do not account for the first picosecond of computations.

its complexity is linear in the number of particles, the computations are slow to perform. Hence, we did not use a box size as before, but we fixed the height of the hierarchical tree to five, to be able to use more computer nodes. We see that there is a clear drift in the energy, which may be due to the use of a fixed level which cannot take into account particles' densities, or even to a deficiency of the preparation of the molecule. For example, the minimisation and canonical ensemble molecular dynamics were not performed using implicit solvent, and as we took directly the dronpa protein from the Proteins Data Bank, the molecule may have needed more preparation. Moreover, at the time of the computations, the COSMO model used in `TINKER` had no particular parameterisation; hence its use as a proof of concept.

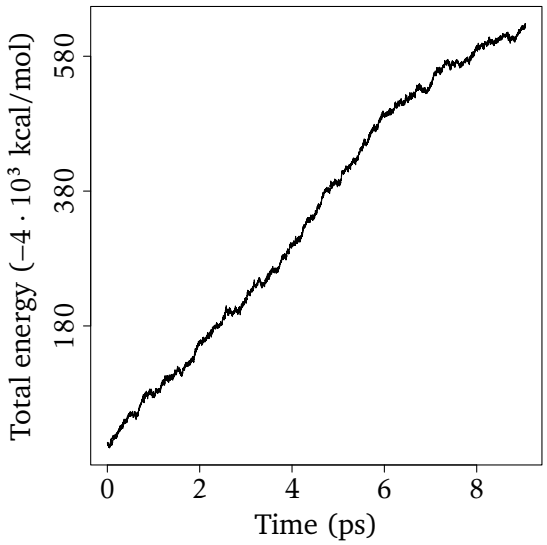

Figure IV.9: Energy drift for the first section of the dronpa protein with polarisable continuum model for parameters $(\ell, \text{LV}) = (6, 5)$ with 1.0 femtosecond time-steps

In this chapter, we have shown that the fast multipole method should be sufficiently robust to be used for molecular dynamics of molecular systems. Depending on the need for accuracy, some fixed parameters for the expansion order and box size seem to give similar results for different systems, which limits the effort to tune them. Hence, it is an alternative worth considering with respect to particle mesh EWALD. This is especially true for very large simulations, where the higher than linear computational complexity of particle mesh EWALD in $N \log N$ may start to impair results. However, more research should be done to compare the physics that can be obtain when using fast multipole method, as the particle mesh EWALD can take advantage the side-effect of modelling a *larger* amount of solvent due to its periodic boundary conditions.

IV.F References

[Ban06] Bank, RCSB Protein Data. "Crystal Structural and Functional Analysis of GFP-like Fluorescent Protein Dronpa". May 8, 2006. URL: https://www.rcsb.org/structure/2GX2 (cit. on p. 103).

[Ban88] Bank, RCSB Protein Data. "Crystal Structure of Unliganded Escherichia Coli Dihydrofolate Reductase. Ligand-induced Conformational Changes and Cooperativity in Binding." Oct. 21, 1988. URL: https://www.rcsb.org/structure/5DFR (cit. on p. 101).

[Bla+15] Blanchard, Pierre et al. "ScalFMM: A Generic Parallel Fast Multipole Library". In: *SIAM Conference on Computational Science and Engineering (CSE15)*. SIAM Conference on Computational Science and Engineering (SIAM CSE 2015). Mar. 14, 2015 (cit. on pp. 87, 93).

[CMS13] Cancès, Eric, Maday, Yvon, and Stamm, Benjamin. "Domain Decomposition for Implicit Solvation Models". In: *The Journal of Chemical Physics* 139.5 (2013), p. 054111 (cit. on pp. 20, 104).

[Col21c] Collective. *Legendre Polynomials*. In: *Wikipedia*. Ed. by Wikipedia. Feb. 21, 2021 (cit. on p. 86).

[For06] Fortin, Pierre. "Algorithmique hiérarchique parallèle haute performance pour les problèmes à N-corps". PhD thesis. Université Sciences et Technologies - Bordeaux I, Nov. 27, 2006 (cit. on p. 84).

[GLS17] Gatto, Paolo, Lipparini, Filippo, and Stamm, Benjamin. "Computation of Forces Arising from the Polarizable Continuum Model within the Domain-Decomposition Paradigm". In: *The Journal of Chemical Physics* 147.22 (Dec. 12, 2017), p. 224108. ISSN: 0021-9606 (cit. on p. 87).

[GR97] Greengard, L. and Rokhlin, V. "A Fast Algorithm for Particle Simulations". In: *Journal of Computational Physics* 135.2 (1997), pp. 280–292. ISSN: 0021-9991 (cit. on p. 84).

[KS93] Klamt, A. and Schuurmann, G. "COSMO: A New Approach to Dielectric Screening in Solvents with Explicit Expressions for the Screening Energy and Its Gradient". In: *Journal of the Chemical Society, Perkin Transactions 2* 5 (1993), pp. 799–805 (cit. on pp. 20, 104).

[Lin+18] Lindgren, Eric B. et al. "An Integral Equation Approach to Calculate Electrostatic Interactions in Many-Body Dielectric Systems". In: *Journal of Computational Physics* 371 (Oct. 15, 2018), pp. 712–731. ISSN: 0021-9991 (cit. on pp. 84, 93).

[Pon+10] Ponder, Jay W. et al. "Current Status of the AMOEBA Polarizable Force Field". In: *Journal of Physical Chemistry B* 114.8 (2010), pp. 2549–2564 (cit. on pp. 13, 16, 71, 93).

[YB11] Yokota, Rio and Barba, Lorena A. "Chapter 9 - Treecode and Fast Multipole Method for N-Body Simulation with CUDA". In: *GPU Computing Gems Emerald Edition*. Ed. by Hwu, Wen-mei W. Applications of GPU Computing Series. Boston: Morgan Kaufmann, Jan. 1, 2011, pp. 113–132. ISBN: 978-0-12-384988-5 (cit. on p. 84).

Face B

Extrapolation techniques for quantum mechanics problems

Chapter V

Extrapolation using the magic points method: Application to computational chemistry

Overview

Programming languages • C • Fortran • Julia • Mathematica • R

API OpenMP

Used software Molpro

Paper

[PMS21] Polack, Étienne, Maday, Yvon, and Savin, Andreas. "FLEIM: A Stable, Accurate and Robust Extrapolation Method at Infinity for Computing the Ground State of Electronic Hamiltonians". Dec. 24, 2021

Collaborators • Yvon Maday • Andeas Savin

v.a Problem setting

In this chapter, we consider a system with M nuclei and N electrons described by a linear Hamiltonian

$$\mathcal{H} = \mathcal{T} + \mathcal{V}, \tag{1.1}$$

where $\mathcal{T}$ is the kinetics energy operator and $\mathcal{V}$ is the Coulomb operator.

The operator $\mathcal{V}$ can be split into an interaction operator between nuclei and electrons and one between electrons $\mathcal{V} = \mathcal{V}_{\text{ne}} + \mathcal{V}_{\text{ee}}$, which gives

$$\mathcal{H} = \mathcal{T} + \mathcal{V}_{\text{ne}} + \mathcal{V}_{\text{ee}}. \tag{1.2}$$

If we use the Born–Oppenheimer [MH09] approximation, that is that we consider the nuclei to be classical particles, the problem is then transformed into the following eigenvalue problem

$$\mathcal{H}\psi(r_1, \dots, r_N) = E_0\psi(r_1, \dots, r_N), \tag{1.3}$$

where E_0 is the lowest eigenvalue, called the *ground state energy* (see Section I.D.1).

Due to the cusp of the Coulombic potential, this problem is in general expensive to solve numerically as we may have to use a large basis set to have accurate results. However, if we model the interactions between electrons with the operator

$$\mathcal{V}_{\text{ee}}(\mu) = \sum_{1 \le i < j \le N} \frac{\operatorname{erf}(\mu |r_{ij}|)}{|r_{ij}|}, \tag{1.4}$$

then, the problem can be solved with a smaller basis set for small enough values of $\mu > 0$. When μ tends toward infinity, we have the original problem.

The aim of this work is to explore the use of the empirical interpolation method on the family of operators with multiple values of μ

$$\mathcal{H}(\mu) = \mathcal{T} + \mathcal{V}_{\text{ne}} + \mathcal{V}_{\text{ee}}(\mu), \tag{1.5}$$

which gives us a set $(E(\mu))_\mu$ of eigenvalues.

The empirical interpolation method was introduced by Barrault et al. [Bar+04] as a way to efficiently find a reduced basis if a so-called Kolmogorov n-width is small (see Section VI.A.3 for more details). The method is empirical in the sense that it gives good results, but cannot be

proven *a priori* for most problems. The points at which to do the interpolation are quasi-optimal and are referred as magic points, [Mad+09]. They are quasi-optimal in the sens that empirically, the interpolant should be close to the best results if we hose had the knowledge to choose optimal interpolation points.

In the supporting article Page 114, we have looked at how to extrapolate the values for the energy at $\mu \equiv \infty$ from small values of μ for small molecular systems of two electrons using a modification of the empirical interpolation method more suitable for our problem. We have obtained accurate results using simple analytic basis for the extrapolation.

A contribution to the Proceedings of the
Workshop on Density Functionals for Many-Particle Systems
2–29 September 2019, Singapore

FLEIM:
A stable, accurate and robust extrapolation method at infinity for computing the ground state of electronic Hamiltonians

Étienne Polack
Université Bourgogne Franche-Comté and CNRS,
Laboratoire de Mathématiques de Besançon, F-25030 Besançon, France
etienne.polack@math.cnrs.fr

Yvon Maday
Sorbonne Université, CNRS, Université de Paris,
Laboratoire Jacques-Louis Lions (LJLL), F-75005 Paris,
and Institut Universitaire de France
yvon.maday@sorbonne-universite.fr

Andreas Savin
CNRS and Sorbonne Université,
Laboratoire de Chimie Théorique (LCT), F-75005 Paris, France
andreas.savin@lct.jussieu.fr

The Kohn–Sham method uses a single model system, and corrects it by a density functional the exact user friendly expression of which is not known and is replaced by an approximated, usable, model. We propose to use instead more than one model system, and use a greedy extrapolation method to correct the results of the model systems. Evidently, there is a higher price to pay for it. However, there are also gains: within the same paradigm, e.g., excited states and physical properties can be obtained.

1. Introduction

1.1. *Motivation*

Density functional theory (DFT) has a weak point: its approximations (DFAs). First, the Hohenberg–Kohn theorem tells us that there is a density functional for electronic systems, $F[\rho]$, that is universal (that is, indepen-

dent of the potential of the nuclei), but does not give us a hint on how systematic approximations can be constructed. In practice, models are produced to be fast in computations, typically by transferring properties from other systems, like the uniform electron gas. Second, the most successful approximations are using the Kohn–Sham method (introducing a fermionic wave function) that decomposes $F[\rho]$ into the kinetic energy, the Hartree energy and an exchange-correlation energy contribution although the question of how and what part of $F[\rho]$ should be approximated is, in principle, open.

In the present contribution we totally change the paradigm in the following way still led by the issue of universality. Let us start with a physical consideration. When electrons are close, the Coulomb repulsion is so strong that some of its features dominate over the effect of the external potential. This is also reflected mathematically in the short-range behavior of the wave function, as present in the Kato cusp condition [1, 2, 3, 4], and in higher-order terms [5, 6]. We further note that approximating numerically the short-range part of the wave function needs special care, due to the singularity of the Coulomb interaction when the electrons are close.

The considerations above and the independence of the interaction between electrons from that between them and the external potential provides a basis for constructing approximations. Thus, we propose to solve accurately a Schrödinger equation with a Hamiltonian that is modified to eliminate the short-range part of the interaction between the electrons which is one of the difficult parts in the numerical simulations. The way to do it is not unique, and we try to turn this to our advantage: we use several models, and from them we try to extrapolate to the physical system [7]. In other words, we follow an "adiabatic connection" (see [8]), without ever constructing a density functional. This new paradigm thus explores the possibility to replace the use of DFAs by mathematically controlled approximations: we make density functional theory "without density functionals."

Our approach has introduced an additional difficulty nonexistent in the Kohn–Sham method: the long-range part of the interaction has to be treated accurately, and not only its electrostatic component. One may ask whether this additional effort is justified, and whether one gains anything with respect to a calculation where the physical (Coulomb) interaction is used. For a single calculation, the gain is due to the lack of singularity in the interaction expressed by a weak interaction potential allowing for simplified treatments, such as perturbation theory. However, as the extrapolation to the physical system needs more than one point, it is essential that the number of points stays very small, and the interaction weak.

1.2. *Objective and structure of the paper*

We first choose, in Sec.2.1, a family of model (parameter dependent) Hamiltonians that are more flexible than using only the Kohn–Sham (noninteracting) Hamiltonian.* This is followed by a description of how universality is introduced, namely by analyzing how a nonsingular interaction approaches the Coulomb one, and not by transfer from other systems, as usually done in DFAs. The physical system of interest is one among the parameter dependent models corresponding to some precise value of the parameter; in Sec. 2.2 its solution is extrapolated from the solutions to the models for other values of the parameter, expected that these solutions are more simple to be approximated. This extrapolation is efficiently handled in the general framework of the model reduction methods and more precisely referring to a variation of the *Empirical Interpolation Method* [9].

We believe that such an approach can not only discuss what DFAs are really doing, but can evolve to being used in applications. Some argument supporting this statement is given. However, in this paper numerical examples (gathered in Sec. 3) are only presented for two-electron systems that are numerically (and sometimes even analytically) easily accessible: the harmonium, the hydrogen anion, H^-, and the hydrogen molecule, H_2 in the ground state, at the equilibrium distance.

As we do not use the Hohenberg–Kohn theorem, the technique can be applied without modification also to excited states. We provide in Sec. 3.5, as an example, the first excited state of the same symmetry as the ground state.

Some conclusions and perspectives are presented in Sec. 4. Finally, in order to facilitate reading the manuscript, various details are given in Appendices A–E that follow Sec. 4.

2. Approach

2.1. *The model Schrödinger equation*

We study a family of Schrödinger equations,

$$H(\mu)\Psi(\mu) = E(\mu)\Psi(\mu), \tag{2.1}$$

*Note however that this is at the prize of working in $\mathbb{R}^{3N}$ instead of $\mathbb{R}^3$, and thus requiring accurate many-body, e.g., configuration interaction calculations.

where μ is some nonnegative parameter. More precisely, in this paper, we use

$$H(\mu) = T + V + W(\mu), \tag{2.2}$$

where T is the operator for the kinetic energy, V is the external potential (in particular that of the interaction between nuclei and electrons) and $W(\mu)$ represents the interaction between electrons. Although not required by the general theory, in this paper we introduce the dependence on μ only by modifying the interaction between electrons,

$$W(\mu) = \sum_{i<j} w(r_{ij}, \mu), \tag{2.3}$$

choosing

$$w(r_{ij}, \mu) = \frac{\operatorname{erf}(\mu r_{ij})}{r_{ij}} \tag{2.4}$$

where $r_{ij} = |\boldsymbol{r}_i - \boldsymbol{r}_j|$ is the distance between electron i (at position $\boldsymbol{r}_i$) and electron j (at position $\boldsymbol{r}_j$). Finally, the external potential V is written like

$$V = \sum_{i=1}^{N} v(\boldsymbol{r}_i). \tag{2.5}$$

where v is the local one particle operator. Note that the N-particle operators are denoted by upper case letters, while the one-particle operators are denoted by lower case letters.

Note also that for $\mu = 0$ we have a trivial noninteracting system, while for $\mu = \infty$ we recover the Coulomb system. The operator w is long-ranged: as μ increases, the Coulomb interaction $1/r_{12}$ starts being recovered from large distances. The first reason for this choice is that, as mentioned above, we expect a universal character for short range (this is related to the difficulty of common DFAs to correctly describe long-range contributions, cf. Appendix A). The second reason is that the solution of Eq. (2.1) is converging more rapidly with (conventional) basis set size when the interaction has no singularity at $r_{12} = 0$.

In principle, introducing a dependence of the one-particle operators (T and V) on μ makes the formulas a bit more clumsy, but does not introduce important difficulties in its application. Using such a dependence might improve the results, but it is not discussed in this contribution. In the following, in order to simplify notation, we drop the argument μ, when $\mu = \infty$, e.g., $E = E(\mu = \infty)$.

2.2. *The correction to the model*

2.2.1. *Using a basis set*

Of course, solving the Schrödinger equation for the model, Eq. (2.1) with finite μs, does not provide the desired solution, i.e., the one that is obtained for $\mu = \infty$. We thus need to estimate the difference in eigenvalues:

$$\bar{E}(\mu) = E - E(\mu). \tag{2.6}$$

Since $\bar{E}(\mu)$ tends to zero at infinity, the idea is to first expand this difference $\bar{E}(\mu)$ in a basis (of functions that tend to zero at infinity), retaining M terms,

$$\bar{E}(\mu) \approx \bar{E}_M(\mu) = \sum_{j=1}^{M} c_j \chi_j(\mu), \tag{2.7}$$

leading to

$$E(\mu) \approx E - \sum_{j=1}^{M} c_j \chi_j(\mu),$$

or, more precisely since E is not known, we replace it by an approximation denoted as E_M,

$$E(\mu) \approx E_M - \sum_{j=1}^{M} c_j \chi_j(\mu). \tag{2.8}$$

The idea then proceeds by determining the unknown E_M values and the coefficients c_i from $M+1$ values of $E(\mu_m)$, for $m = 0, \ldots, M$ for an appropriate choice of the parameter values μ_m. Finally, taking into account that the functions χ_j tend to zero at infinity, the proposed approximation for E is E_M. Of course, this extrapolation approach often fails if care is not enough taken in the choice of the functions $\chi_j, 1 \leq j \leq M$, and the values μ_m, for $m = 0, \ldots, M$.

First, one has to decide about their form. Second, one has to find a way to keep M as small as possible to reduce computational cost while preserving a good accuracy.

2.2.2. *Approaching the Coulomb interaction*

As recalled above, we derive from the leading term of the Coulomb interaction between the electrons that, to leading order, the solutions of differential

equations are determined at short range by the singularities. The interaction w in Eq. (2.4) has no singularity at $r_{12} = 0$, for any finite μ. However, as the parameter μ increases, $w(\cdot, \mu)$ approaches the singular Coulomb potential.

In order to see how this limit is approached, let us perturb the exact solution. To first order, the perturbation correction to the energy is given by

$$\bar{E}(\mu) = \big\langle \Psi \big| \big(W - W(\mu)\big) \big| \Psi \big\rangle, \quad \text{for } \mu \to \infty. \tag{2.9}$$

By changing the integration variables $\boldsymbol{r}_i$ to $\mu \boldsymbol{r}_i$ we see that

$$\bar{E}(\mu) \propto \mu^{-2} \quad \text{as } \mu \to \infty, \tag{2.10}$$

providing a leading behavior that we want the basis functions χ_i to reflect. It is possible to continue this analysis for higher order terms. In fact, the next term (in μ^{-3}) has a coefficient proportional to that of μ^{-2}, the proportionality coefficient being determined by the nature of the Coulomb singularity [10].

2.2.3. *Choice of the basis functions*

In the main part of this contribution we use a simple ansatz,

$$\tilde{\chi}_j(\mu) = 1 - j\ \mu(1 + j^2\ \mu^2)^{-1/2}, \quad j = 1, \ldots, M, \tag{2.11}$$

that respects indeed the condition of Eq. (2.10). The motivation for this specific choice, that is arbitrary to a certain degree, as well as some results obtained with other choices of basis functions, is given in Appendix B.

The first functions of this basis set are presented in Fig. 1, together with an example of a function it has to approximate. It illustrates that the function we want to describe is between basis function $\tilde{\chi}_2$ — for small μ — and basis function $\tilde{\chi}_3$ —for large μ. However, a simple linear combination between these (only) two surrounding basis functions from the family in Eq. (2.11) does not improve much the accuracy, but of course, more (and more appropriate) functions in the family can (and should) be called.

2.2.4. *Reducing the basis set*

Using a large set of χ_j (a large M) can rapidly become computationally prohibitive (because it requires a large number of evaluations of $E(\mu_m)$, for $m = 0, \ldots, M$) and numerically unstable (because it is classically much more difficult to stabilize extrapolation than interpolation). In order to

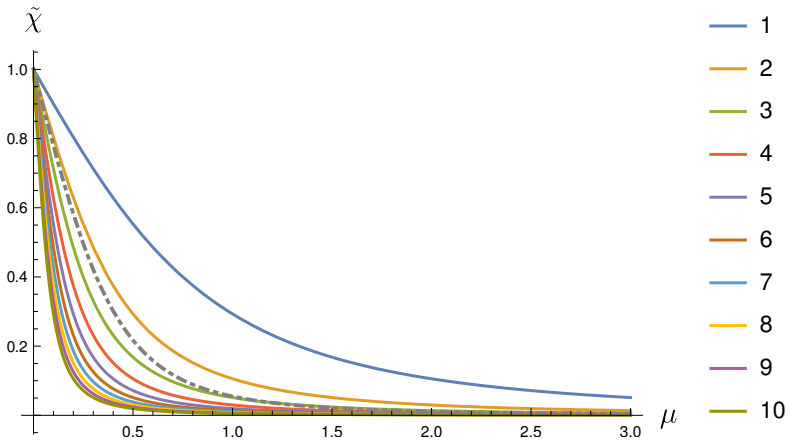

Fig. 1. Basis functions $\tilde{\chi}_j$ of Eq. (2.11), continuous curves with the color corresponding to j; and an (unknown) function to be approximated by linear combination on this basis (dot-dashed, gray). The unknown function in this figure is proportional to $\bar{E}(\mu)$ of harmonium.

reduce their number and increase the stability of the extrapolation, we use a greedy (iterative) method, as in the *Empirical Interpolation Method* (EIM) leading to proper choices of μ_m, for $m = 0, \ldots, M$ known as "magic points."

In the Kth iteration of EIM, one starts from a set of $K-1$ basis functions (for us, $\tilde{\chi}_j$) and $K-1$ points (for us, $\tilde{\mu}_j$ belonging to some (discretized) interval, say, close to zero, to benefit at most of the regularization of the erf function). One then chooses the Kth function $\tilde{\chi}_{K-1}$ (among the remaining $M-K$ basis functions) as being the one that is most poorly approximated by the current interpolation (based on the $K-1$ basis functions and the $K-1$ points) in a sense dedicated to the final goal we want to achieve (that can be uniform error, error on some part of the domain, or even at some value) and the Kth point $\tilde{\mu}_{K-1}$ that, in the admissible set, brings the more information. In this contribution, as we are only interested at extrapolating the value of μ at infinity, so we chose the error as the absolute value of difference between the Kth basis function and its interpolant at infinity as the final goal we want to achieve.

Note that the procedure selecting the next point and function does not make any use of the function to be approximated (here $\bar{E}$). It is thus a cheap step compared with the calculation of $E(\tilde{\mu}_m)$ on the system of interest.

To improve the results for the extrapolation, we have modified the EIM algorithm into what we call the *Forward Looking* EIM (FLEIM). While EIM tries to get the maximal improvement through a sequential choice of, first the new basis function, then the new point of interpolation, FLEIM tries to get the best pair for improvement in the selected goal. The method is explained in more detail in Appendix C. In what follows, we present the results of FLEIM as they are better and more stable than those of EIM, as is illustrated in App D.1.

2.3. *Computing other physical properties*

FLEIM can be used to approximate other physical properties, i.e., correct expectation values of operators $A \neq H$ obtained with the model wave functions, $\Psi(\mu)$,

$$A(\mu) = \langle \Psi(\mu)|A|\Psi(\mu)\rangle. \tag{2.12}$$

This can be seen immediately by noting that the derivation in Sec. 2.2.1 is not specific for correcting $E(\mu)$, but can also be applied to $A(\mu)$.

For the choice of the basis functions, we point out that properties are obtained by perturbing the Hamiltonian with the appropriate operator, say, A,

$$H \to H(\lambda) = H + \lambda A. \tag{2.13}$$

The expectation value of A can be obtained as the derivative of $E(\lambda)$ w.r.t. λ, at $\lambda = 0$. Of course, this procedure can be applied to model Hamiltonians, yielding $E(\lambda, \mu)$ and

$$\langle \Psi(\mu)|A|\Psi(\mu)\rangle = \partial_\lambda E(\lambda, \mu)\big|_{\lambda=0} \tag{2.14}$$

Thus, in this contribution, we use the same type of basis functions for $A(\mu)$ as for $E(\mu)$; see the results in Sec. 3.4. Note that computing $\langle \Psi(\mu)|A|\Psi(\mu)\rangle$ is not possible in DFT, without having a property-specific density functional [11].

3. Numerical results

3.1. *Guidelines*

The quality of the corrections using Eqs. (2.7) and (2.11) is explored numerically. Technical details on the calculations are given in Appendix D.

The plots show the errors done by the approximations in the estimate of the energy: we choose a model, $\mu \mapsto E(\mu)$, and let the empirical interpolation method choose which easier models (with weaker interactions) to extrapolate and get an approximation for $E = E(\mu = \infty)$. The plots show the error in the estimate of E made when considering approximations that use information only for $\tilde{\mu}_m \leq \mu$. From the plots, we read off how small μ can be and still have "reasonable" accuracy. In thermochemistry, $\mathrm{kcal\,mol^{-1}}$ is a commonly considered unit, and is often considered as "chemical accuracy." For electronic excitations, one often uses eV units, and one often indicates it with one decimal place. "Chemical accuracy" is marked in the plots by horizontal dotted lines. The plots show the errors in the range of $\pm 0.1\,\mathrm{eV} \approx 2.3\,\mathrm{kcal\,mol^{-1}}$.

We consider approximations using up to four points (thus chosen in $[0, \mu]$). The first point μ_0 is always the value chosen $\mu_0 = \mu$ shown on the x-axis of the plots, and the basis function associated to it is $\tilde{\chi}_0$, the constant function; note that using only this pair (χ_0, μ_0) corresponds to choosing $E \simeq E(\mu_0)$= the value provided by the model, i.e., no correction is applied. When the number of points is increased, further values of $E(\tilde{\mu}_m)$, chosen by the algorithm, are used with $\tilde{\mu}_m < \mu$.

The (maximal) parameter μ is considered between 0 and $3\,\mathrm{bohr^{-1}}$. The model without correction (blue curve) reaches chemical accuracy for $\mu \approx 3\,\mathrm{bohr^{-1}}$ for H^- and harmonium, but only at $\mu \approx 5\,\mathrm{bohr^{-1}}$ for H_2 in its ground state.

3.2. *General behavior of errors*

The plots in Fig. 2 for harmonium, H_2, and H^- have similar features and are discussed together. As the number of points used increases, the smallest value of μ for which the good accuracy is reached decreases. Note that FLEIM produces very small errors for values of μ larger than 2. However, with the chosen basis set, the algorithm presented in this contribution has difficulties correcting the errors for μ smaller than 1.

3.3. *Possibility of error estimates*

Some tests can be done to estimate the quality of the approximation. For example, we can compare how the approximations change when increasing the number of basis functions, K, in our approximation and consider $|E_K - E_{K-1}|$ as an *asymptotically* valid error estimate for E_{K-1}. One can notice in the above figures that, when the difference between, say, the 2-

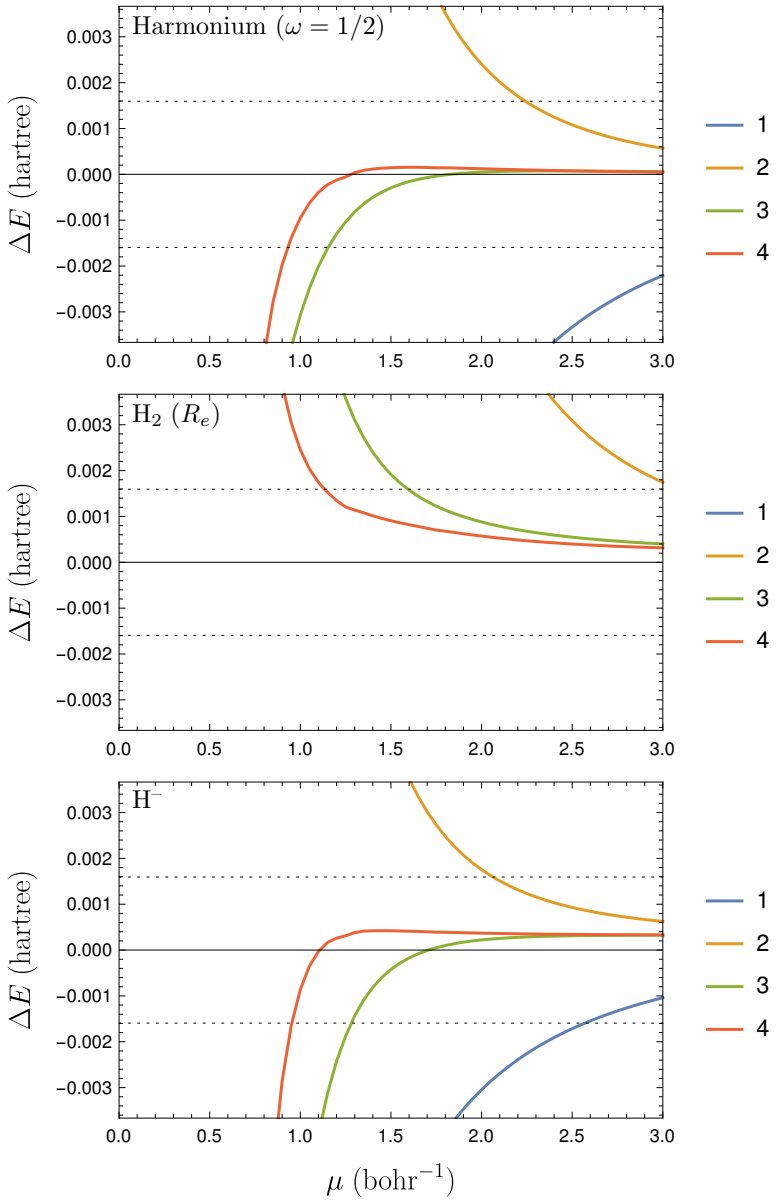

Fig. 2. Errors for harmonium (top), H_2 (middle), and H^- (bottom) using FLEIM with one to four points (1: blue curve, 2: brown curve, 3: green curve, 4: red curve). The abscissa represents the biggest μ allowed for use in the FLEIM algorithm. The error of the model without correction (blue curve) does not show up in the figure for the H_2 molecule because it is larger than the domain covered by the plot.

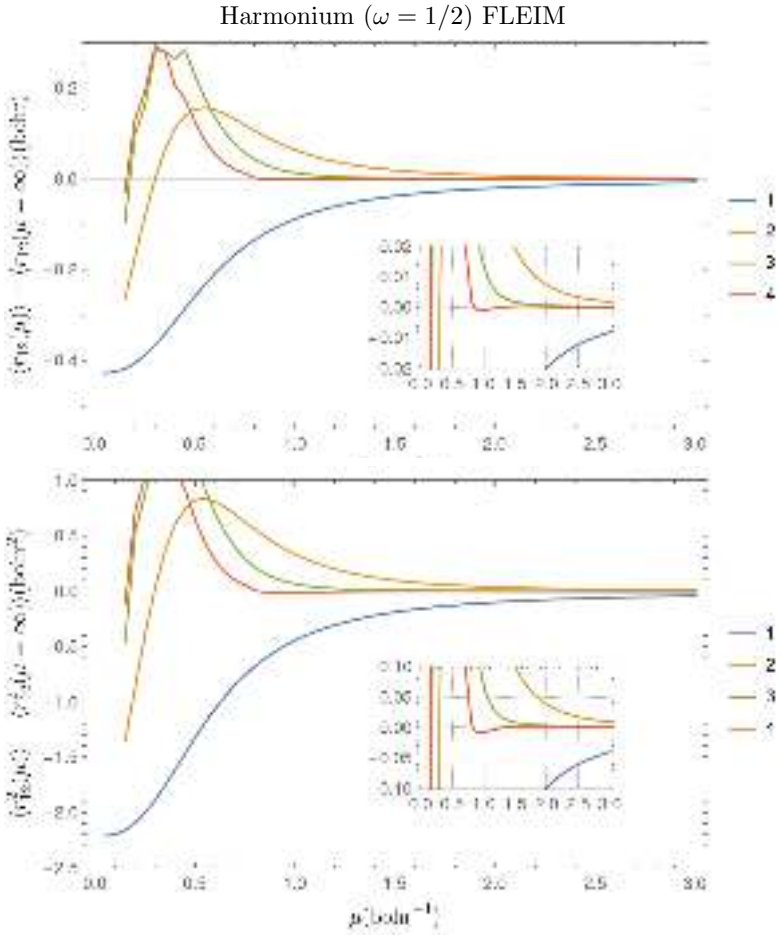

Fig. 3. Errors made for the expectation value of the distance between electrons (top) and the distance squared (bottom) for harmonium, by using a model wave function, $\Psi(\mu)$, and after correcting with FLEIM (the different curves correspond to the number of points used). The insets zooms in.

and the 3-point approximation error is larger than "chemical accuracy," so is the error in the 2-point approximation.

3.4. *Expectation values with FLEIM: $\langle r_{12} \rangle$ and $\langle r_{12}^2 \rangle$ for harmonium*

We look at the average distance between the electrons in harmonium. Figure 3(top) shows the error made by using $\Psi(\mu)$ instead of $\Psi(\mu = \infty)$ in computing the expectation value of r_{12}, as well as the correction that can be achieved with FLEIM, using the same basis set as above (2.11). The inset in Figure 3(top) concentrates on the errors made in the region that could be considered chemically relevant (1 pm $\approx$ 0.02 bohr). We note the similarity with the behavior of in correcting $E(\mu)$.

Let us now examine the average square distance between the electrons, $\langle r_{12}^2 \rangle$, in harmonium. While for computing the energy we explored correcting the missing short-range part of the interaction, we now ask whether it is possible to correct the error of using the model wave function, $\Psi(\mu)$ for the expectation value of an operator that is important at long range.

For $\omega = 1/2$, we know the exact values of the expectation value of r_{12}^2 at $\mu = 0$ and $\mu = \infty$; they are 6 and $(42\sqrt{\pi} + 64)/(5\sqrt{\pi} + 8) \approx 8.21$, respectively (see, e.g., Ref. [12]). Note the large effect of the model wave function, $\Psi(\mu)$, in computing $\langle r_{12}^2 \rangle$. Figure 3(bottom) shows the error made by using $\Psi(\mu)$ instead of $\Psi(\mu = \infty)$ in computing the expectation value of r_{12}^2, as well as the effect of the correction that can be achieved with FLEIM, using the same basis set (2.11) as above. We note again the similarity with the behavior of in correcting $E(\mu)$ or the expectation value of the distance between electrons.

The expectation value $\langle r_{12}^2 \rangle$ also illustrates another aspect: the effect of a change of the external potential on the energy. At first sight this may seem surprising, as the external potential is a one-particle operator, while r_{12}^2 is a two-particle operator. However, changing the one-particle operator also modifies the wave function and this affects the value of $\langle r_{12}^2 \rangle$. In the case of harmonium, this can be shown analytically. Changing $\boldsymbol{r}_1$ and $\boldsymbol{r}_2$ to center-of-mass, $\boldsymbol{R}$, and inter-particle distance, $\boldsymbol{r}_{12}$, cf. Appendix E, allows us to see explicitly that a modification of ω^2, the parameter that specifies the external potential, affects the Schödinger equation in $\boldsymbol{r}_{12}$. It introduces a term proportional to $\omega^2 r_{12}^2$. The first order change in the energy when we change the external potential (ω^2) is thus proportional to $\langle r_{12}^2 \rangle$. Our results in Fig. 3(bottom) show that our conclusions on model corrections are not modified by small changes in the external potential. Note that the center-of-mass Schrödinger equation also depends on ω^2, but it is independent of μ and thus does not affect our discussion on model correction.

3.5. *Comparison with DFAs*

Instead of using extrapolation with FLEIM, one can use DFAs. While up to now the external potential did not change with μ, in DFA calculations a one particle potential that depends on μ is added in order to correct the density.

We consider here two DFAs, the local density approximation, LDA [13, 14], and one that reproduces that of Perdew, Burke and Ernzerhof (PBE) [15, 16] at $\mu = 0$. Both approximations are modified to be μ-dependent. In particular, they vanish at $\mu = \infty$.

As shown in Fig. 4(top) for harmonium, DFAs are clearly much better at small μ. However, they are not good enough. The figure suggests the range of μ for which DFAs are within chemical accuracy is similar to that obtained with the 3-point FLEIM. This is confirmed when comparing the results with DFAs and for the H_2; see Fig. 4(middle). Note that with FLEIM the errors at large μ are smaller.

Note also that the curves obtained with extrapolation are significantly *flatter* at large μ than those obtained with DFAs. This should not be surprising: DFAs transfer the large μ behavior, while extrapolation extracts it from information available for the system under study.

Furthermore, using ground-state DFAs for excited states does not only pose a problem of principle (questions its validity, as the Hohenberg–Kohn theorem is proven for the ground state), but can also show a deterioration of quality. However, there is no question of principle from the perspective of this contribution (of using a model and correcting it by extrapolation). Also, the error in the excited state seems comparable to that in the ground state, as seen in the example of the H_2 molecule, in the first excited state of the same symmetry as the ground state; see Fig. 4(bottom).

4. Conclusion and perspectives

In this contribution we have illustrated with a few models how to simplify the Hamiltonians by smoothly getting rid of the singularities in the system and thus have more numerically tractable problems. This simplification is obtained by introducing a parameter that, when it is equal to infinity, it corresponds to the original, plain Hamiltonian. After numerically solving a few simplified problems, the solution of interest is obtained by extrapolation.

We present a new (in the field) method for extrapolating the quantities of interest from few finite values (hence easy to solve) of the parameter by a technique borrowed from reduced basis paradigm: the empirical interpo-

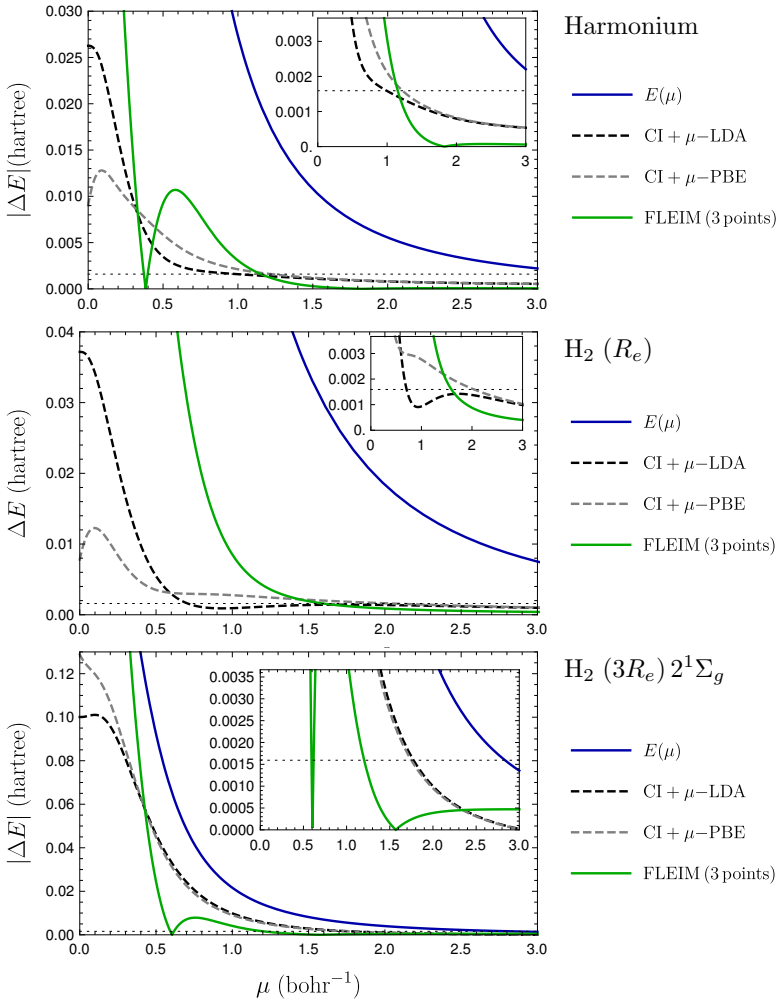

Fig. 4. Absolute errors for the harmonium molecule at equilibrium distance (top), for the H_2 molecule at equilibrium distance (middle), and in the first excited state of the same symmetry as the ground state (bottom): a μ-dependent LDA (black dashed curve), combined with the a μ-dependent Perdew–Burke–Ernzerhof approximation (PBE, gray dashed curve), FLEIM (3 points) (green curve), combined with a μ-dependent local density approximation. The abscissa represents the biggest μ allowed for use in the FLEIM algorithm. The insets zoom into the regions of small errors, the dotted line corresponding to the value of "chemical accuracy." Note the different ranges for ΔE.

lation method. In contrast to DFAs, no parameters are fitted, no transfer from different system are made: only extrapolation is used. Note that in contrast to DFAs, improvement can be envisaged by either adding further points or using more appropriate basis functions and error estimates are asymptotically accessible.

Appendices

A. On density functional approximations

In DFT, the existence of a universal functional of the density, $F[\rho]$, i.e., the Hohenberg–Kohn theorem [17], is rigorously proven [18, 19]. However, obtaining accurately the value of F for a given density $\rho(\boldsymbol{r})$, while possible (see, e.g., Ref. [20]), is exceedingly time-consuming. Computationally convenient DFAs exploit the knowledge of the density around a given point $\boldsymbol{r}$ in space. Typically,

$$F[\rho] \approx \int_{\mathbb{R}^3} f\left(\rho(\boldsymbol{r}), |\boldsymbol{\nabla}\rho(\boldsymbol{r})|, \dots\right) \mathrm{d}\boldsymbol{r}. \tag{A.1}$$

The limitation of such an approach can be seen for a simple density functional, the Hartree term of the energy,*

$$E_H[\rho] = \int_{\mathbb{R}^6} \frac{\rho(\boldsymbol{r}_1)\rho(\boldsymbol{r}_2)}{|\boldsymbol{r}_1 - \boldsymbol{r}_2|} \tag{A.2}$$

when $\rho(\boldsymbol{r}) = \rho_A(\boldsymbol{r}) + \rho_B(\boldsymbol{r})$ and $\rho_A(\boldsymbol{r})\rho_B(\boldsymbol{r}) \approx 0$ (i.e., ρ_A and ρ_B are spatially separated; their overlap decreases much faster than $1/|\boldsymbol{r}_1 - \boldsymbol{r}_2|$). Hohenberg and Kohn recognized the difficulty of approximating E_H by expressions of the type given in Eq. (A.1) and suggested separating it from $F[\rho]$. However, this does not fundamentally solve the problem, as one can immediately see in one-electron systems, where E_H has to be canceled by another term commonly expressed in DFAs by an ansatz of the forms given in Eq. (A.1). Note, that the problem would not exist for interactions that are not Coulomb (long-ranged), but short-ranged. For instance, if the interaction is Dirac's $\delta(\boldsymbol{r}_1 - \boldsymbol{r}_2)$ function, E_H becomes exactly of the form of Eq. (A.1). For other short-range interactions one can approach such a form by using Taylor expansions. In recent years it has become popular to compensate for the limitation of the ansatz in Eq. (A.1) by adding "empirical" energy corrections to describe long-range effects.

*The volume elements $\mathrm{d}\boldsymbol{r}_1\,\mathrm{d}\boldsymbol{r}_2$ are omitted when the context is unambiguous.

Another problem is that the antisymmetry of the electronic wave function is hidden in $F[\rho]$. As the most important effect of the antisymmetry is the Pauli repulsion, Kohn and Sham [21] proposed to consider the variational principle for a model in which particles do not interact. However, DFAs following the pattern of Eq. (A.1) are still in use. In fact, further separating terms from $F[\rho]$ may even lead (for degenerate cases) to the question whether the limit of a noninteracting system is well-defined (see, e.g., Sec. 3.5 in [13]).

B. Basis functions

In order to get an idea how the leading term of the correction behaves, we consider the missing part of the Hartree term,

$$\big\langle \Psi(\mu) \big| \big(W - W(\mu)\big) \big| \Psi(\mu) \big\rangle = \frac{1}{2} \int_{\mathbb{R}^6} \rho(\boldsymbol{r}_1)\rho(\boldsymbol{r}_2) \left(\frac{1}{r_{12}} - w(r_{12}, \mu) \right). \quad \text{(B.1)}$$

Separating the Hartree part from $F[\rho]$ was already proposed by Hohenberg and Kohn [17], and it is also the dominant part in $\bar{E}(\mu)$. Most molecular codes use Gaussian one-particle basis functions, so ρ is a linear combination of Gaussian functions. We consider a generic term,

$$\int_{\mathbb{R}^6} e^{-\alpha r_1^2} e^{-\alpha r_2^2} \left(\frac{1}{r_{12}} - w(r_{12}, \mu) \right). \quad \text{(B.2)}$$

This integral is easily computed, e.g., by using Fourier transforms, and one obtains an expression that is proportional to the form of the basis function $\tilde{\chi}_j$ in Eq. (2.11), after arbitrarily relating $1/\alpha^2$ to the basis index j.

Let us now consider another basis set, constructed from the requirement that the functions decay as μ^{-2} and are finite at the origin.

$$\tilde{\chi}_{1,j}(\mu) = \big(1 + (j\,\mu)^2\big)^{-1} \quad \text{(B.3)}$$

where we choose again $j = 1, 2, \ldots, 10$. The results are only slightly worse than those obtained when using the basis set of Eq. (2.11), compare Fig. 2(top) and Fig. 5(top).

Let us consider

$$\tilde{\chi}_{2,j}(\mu) = a_j \mu \big(1 + (a_j\,\mu)^3\big)^{-1} \quad \text{(B.4)}$$

where we choose $a_j = 2^{j/2}$. The result for harmonium is shown in Fig. 5(bottom). We note a slight improvement of the results for the 2- and 3-point approximations, as well as a change of sign of the error in the 4-point approximation. This direction of investigation deserves to be pursued.

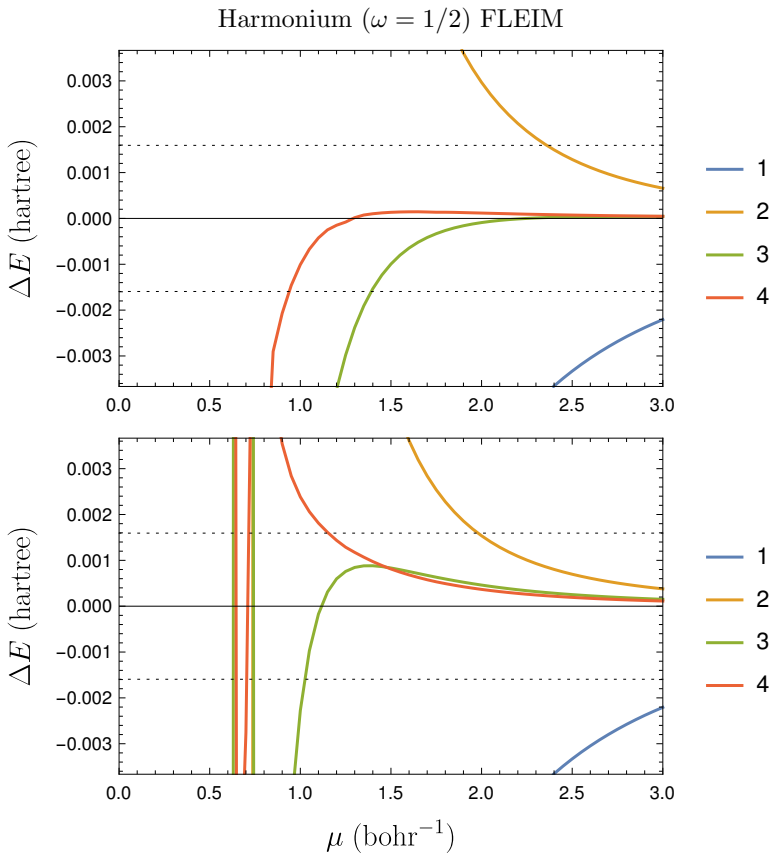

Fig. 5. Errors for harmonium using FLEIM with up to four points (1: blue curve, 2: brown curve, 3: green curve, 4: red curve), using the basis sets given in (B.3) (top) and (B.4) (bottom). The abscissa represents the biggest μ allowed for use in the FLEIM algorithm.

C. The empirical interpolation method

The empirical interpolation method is a model-order reduction method introduced in [9] as a way to efficiently find a reduced basis and approximate one particular function within a manifold of parameter dependent functions. The points at which to do the interpolation are referred as magic points [22].

For a family of basis functions χ_i, $i \in I$ with discrete points μ_j, $j \in J$ chosen on a regular grid close to zero (see Appendix D.2 for an analy-

sis of the influence of the choice of the grid), we want to find a family of K functions and interpolation points with which to interpolate a test function $f \in \mathrm{Span}\{\chi_i, i \in I\}$.

C.1. *Algorithm for EIM*

We assume that we have chosen some cost function $\mathcal{C}$, e.g., a norm $\mathcal{C}[\cdot] \equiv \|\cdot\|$, or, if we are, as in this contribution, only interested in correctly approximating the value for $\mu \equiv \infty$, we choose the cost function as the absolute value at that extrapolation point $\mathcal{C}[\varphi] = |\varphi(\infty)| = \lim_{\mu\to\infty} |\varphi(\mu)|$.

First, select one of the basis functions. We can choose to add the constant function χ_0,

$$\tilde{\chi}_0 \coloneqq \chi_0. \tag{C.1}$$

We then select the first interpolation point as the largest admissible μ available,

$$\tilde{\mu}_0 \coloneqq \max_{j\in J} \mu_j. \tag{C.2}$$

We can then define the first normalized interpolation function as

$$q_0 \coloneqq \frac{\tilde{\chi}_0}{\tilde{\chi}_0(\tilde{\mu}_0)}. \tag{C.3}$$

We can then create the first approximation with an interpolation scheme, for instance Lagrangian interpolation as

$$\mathcal{I}_0[f] \coloneqq f(\tilde{\mu}_0) q_0. \tag{C.4}$$

We now assume to have chosen $K-1$ functions $\tilde{\chi}_k$, normalized functions q_k. Let us also assume that we have selected $K-1$ interpolation points $\tilde{\mu}_k$, $k = 0, \ldots, K-2$. We define the $\mathcal{I}_{K-2}$ Lagrangian interpolation function as

$$\mathcal{I}_{K-2}[f] \coloneqq \sum_{k=0}^{K-2} \beta_k q_k, \tag{C.5}$$

where the coefficients β_k are determined by solving the system

$$\sum_{k=0}^{K-2} \beta_k q_k(\tilde{\mu}_\ell) = f(\tilde{\mu}_\ell) \quad \text{for } \ell = 0, \ldots, K-2. \tag{C.6}$$

If we denote $\tilde{I}$ as the set of indices of remaining basis functions and $\tilde{J}$ as the set of indices of remaining interpolation points, we choose the next function as

$$\tilde{\chi}_{K-1} \coloneqq \arg\max_{\chi_i,\, i\in\tilde{I}} \big\{ \mathcal{C}\big[\chi_i - \mathcal{I}_{K-2}[\chi_i]\big] \big\}, \tag{C.7}$$

and the next interpolation point as

$$\tilde{\mu}_{K-1} \coloneqq \underset{\mu_j,\, j\in\tilde{J}}{\arg\max}\big\{\big|\tilde{\chi}_{K-1}(\mu_j) - \mathcal{I}_{K-2}[\tilde{\chi}_{K-1}](\mu_j)\big|\big\}. \tag{C.8}$$

We can then define the Kth normalised interpolation function as

$$q_{K-1} \coloneqq \frac{\tilde{\chi}_{K-1} - \mathcal{I}_{K-2}[\tilde{\chi}_{K-1}]}{\tilde{\chi}_{K-1}(\tilde{\mu}_{K-1}) - \mathcal{I}_{K-2}[\tilde{\chi}_{K-1}](\tilde{\mu}_K)}. \tag{C.9}$$

This system is represented by a lower triangular matrix with ones on the diagonal, and hence has a unique solution. The algorithm ends when the desired target accuracy is reached.

C.2. *The forward looking empirical interpolation method (FLEIM)*

To better adapt the method for extrapolation, we propose a double loop alternative: Instead of selecting sequentially first for a new basis function and then a new interpolation point — Eqs. (C.7) and (C.8) — we select the best pair

$$(\tilde{\chi}_{K-1}, \tilde{\mu}_{K-1}) \coloneqq \underset{\chi_i,\, i\in\tilde{I}}{\arg\max}\ \underset{\mu_j,\, j\in\tilde{J}}{\arg\min}\big\{\mathcal{C}\big[\chi_i(\mu_j) - \mathcal{I}_{K-2}[\chi_i](\mu_j)\big]\big\}. \tag{C.10}$$

D. Numerical details of the calculations

D.1. *Testing EIM and FLEIM with $E(\mu) = 1 + \chi_j(\mu)$*

In this subsection, we compare on a simple function, the behaviour of EIM and FLEIM on a analytic test function $E(\mu)$ behaves like $1 + \chi_j(\mu)$. The results for EIM are given in Fig. 6, and for FLEIM, in Fig. 7.

First, we note that FLEIM provides better approximation together with more stable results when μ varies. Second, we note that the "wall" for $j > 1$ at small μ is also imporved. At large μ, all χ_j have the same decay at large μ: this makes both methods fit to work in this regime.

D.2. *Discretization for FLEIM*

The interval between 0 and the value of μ under study was divided in 10 equal intervals (producing 11 points). FLEIM was used to select $K(\leq 4)$ points and basis functions on which $E(\mu)$ was calculated.

We now investigate the effect of changing the grid of μ and use, for comparison a fixed finer grid of values of $\mu_1, \mu_2, \ldots$ ranging from 0 to the

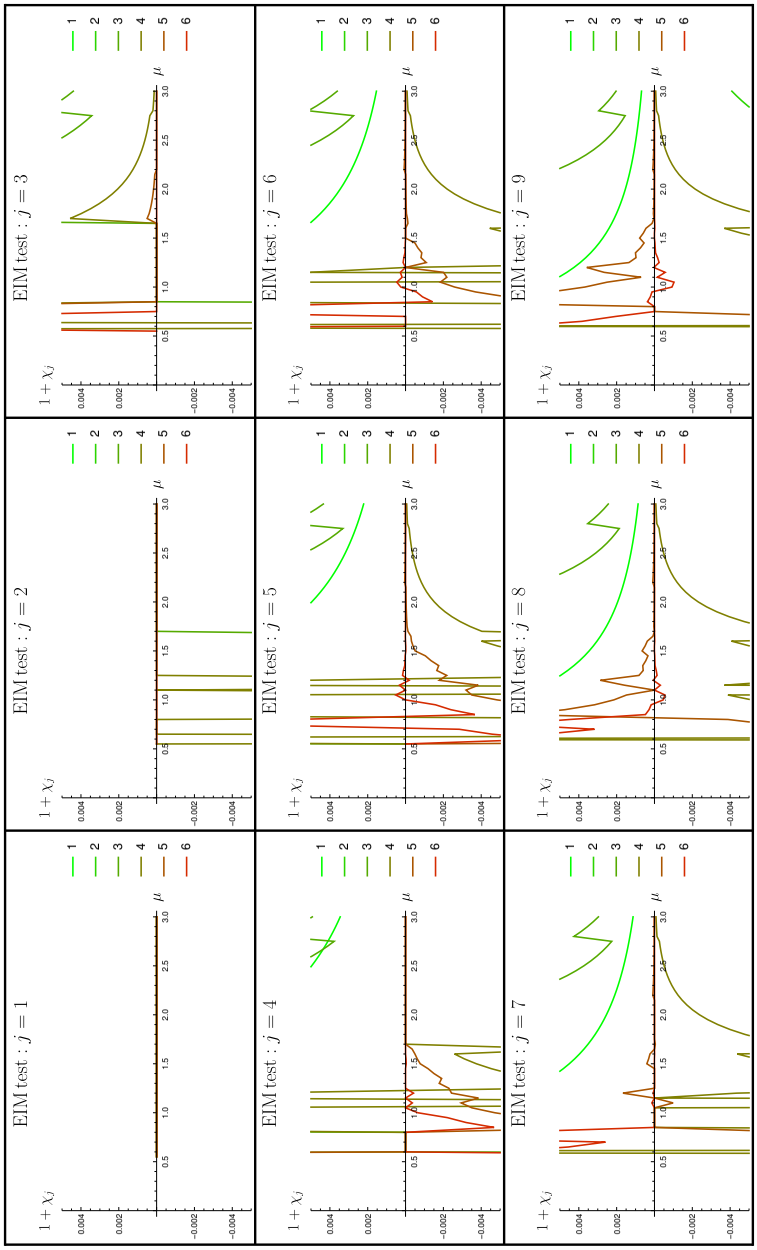

Fig. 6. Test of EIM using model $E(\mu) = 1 + \chi_j(\mu)$.

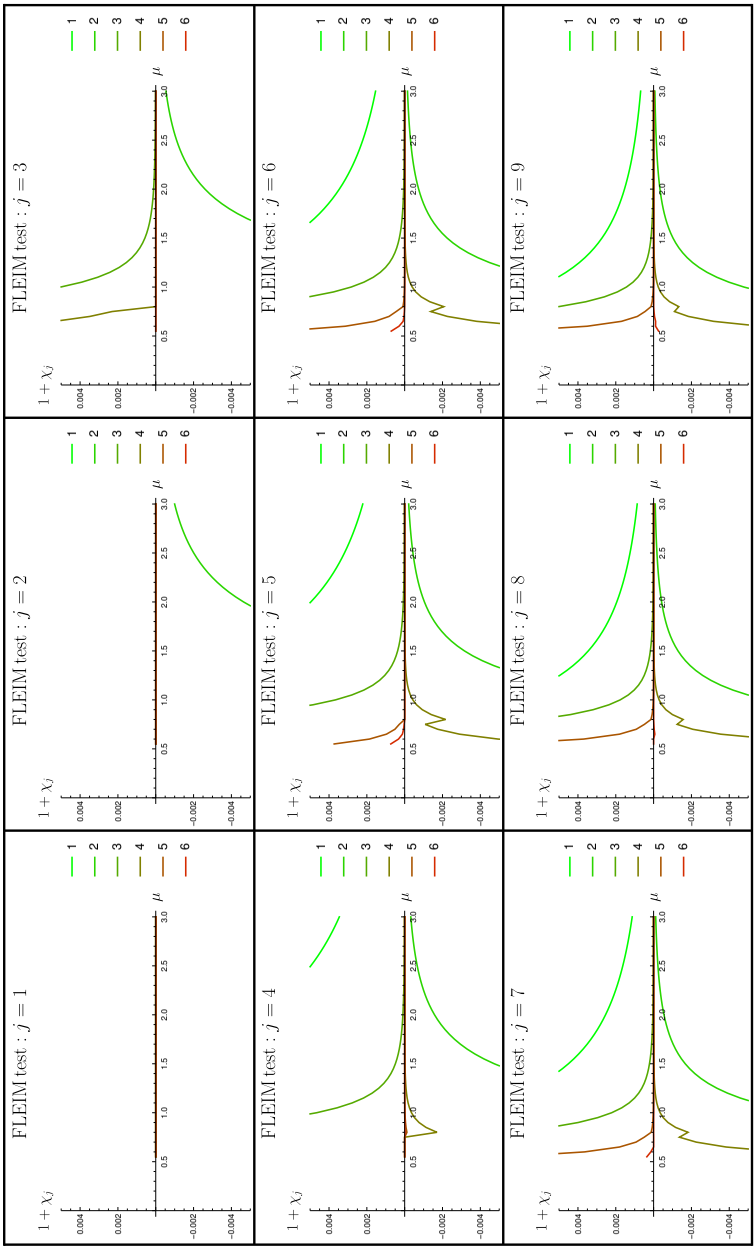

Fig. 7. Test of FLEIM using model $E(\mu) = 1 + \chi_j(\mu)$.

value μ indicated in the plots, with a step of $0.01\,\mathrm{bohr}^{-1}$, the FLEIM results are only slightly changed, as shown in Fig. 8.

D.3. *Systems*

Two-electron systems studied are

(1) harmonium, having

$$v(\boldsymbol{r}) = \frac{1}{2}\omega^2 r^2 \tag{D.1}$$

where for $\omega = 1/2$ the exact energy is known ($E = 2\,\mathrm{hartree}$);

(2) H^- anion,

$$v(\boldsymbol{r}) = -\frac{1}{r}; \tag{D.2}$$

(3) H_2 molecule,

$$v(\boldsymbol{r}) = -\frac{1}{|\boldsymbol{r} - \boldsymbol{R}_A|} - \frac{1}{|\boldsymbol{r} - \boldsymbol{R}_B|} \tag{D.3}$$

where the nuclei are in the equilibrium position, $\boldsymbol{R}_A = -\boldsymbol{R}_B$ with $|\boldsymbol{R}_A| = 0.7\,\mathrm{bohr}$.

D.4. *Obtaining the model energy*

In order to simplify the test of FLEIM, $E(\mu)$ was pre-calculated for a dense range of values μ and interpolated. The values for $E(\mu)$ were obtained with the program Molpro [23] for H^- and H_2. This program was also used for the density functional calculations.

For harmonium, it is possible to separate the variables in the Schrödinger equation. The center-of-mass equation can be solved exactly. The equation in r_{12} was solved by discretization on a grid of 10^4 points between 0 and 10 bohr.

For H_2 the V5Z basis set of [24] was used; for H^- the aug-V5Z basis set of [25]. (The error in the energy of H^- is too large if we do not augment the V5Z basis set with a diffuse basis function.) The aug-V5Z basis set was also used for the excited state of H_2, as it has an important contribution of ionic states ($H^+ \cdots H^-$). For H_2 the equilibrium distance of 1.4 bohr was chosen for the ground state. For the excited state, the distance of 4.2 bohr was chosen. It is close to a minimum of the potential energy curve. Furthermore, this value can be compared with the accurate calculation of Ref. [26].

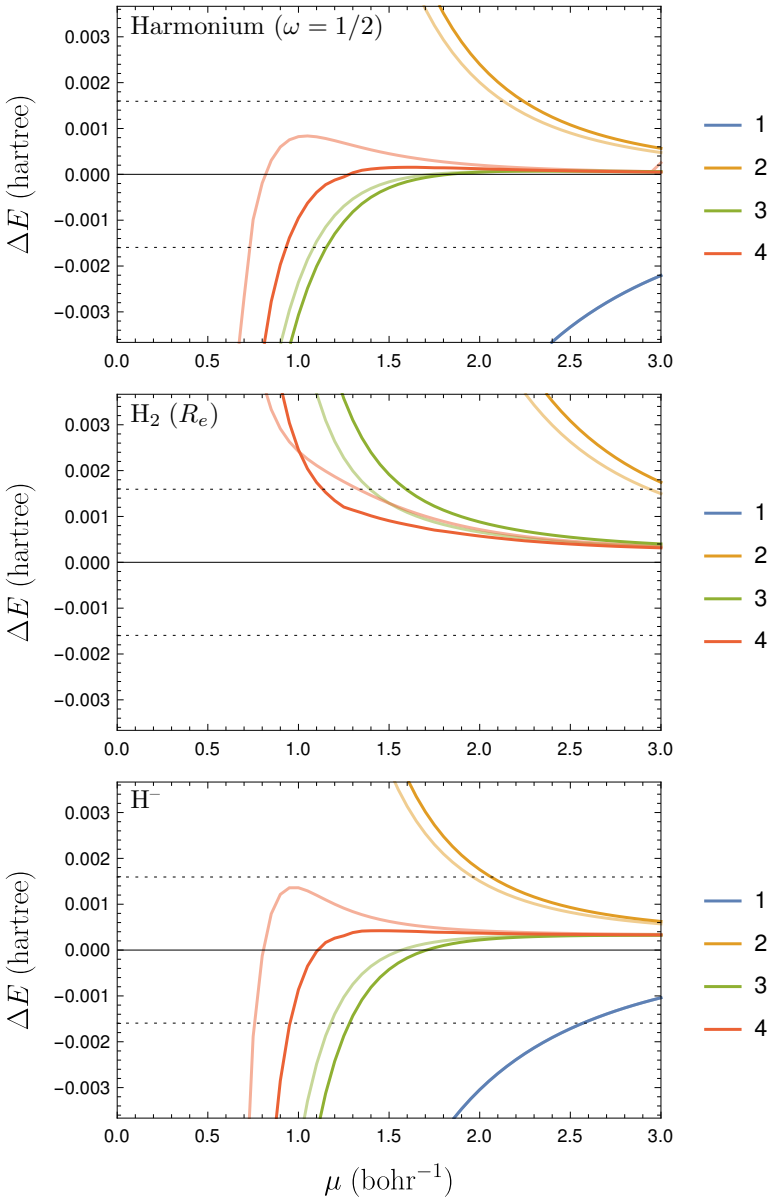

Fig. 8. Results using a denser grid (lighter colors), for harmonium, H_2 at equilibrium distance, and H^-; the curves obtained with the denser grid are shown in lighter colors. The error of the model without correction (blue curve) does not show up in the figure for the H_2 molecule because it is larger than the domain covered by the plot.

E. Change of coordinates in harmonium

Harmonium is characterized by the external potential given by Eq. (D.1). For two particles the variables $\boldsymbol{r}_1, \boldsymbol{r}_2$ can be changed to those corresponding to the center of mass and the distance between particles,

$$\begin{aligned} \boldsymbol{R} &= \frac{1}{2}\left(\boldsymbol{r}_1 + \boldsymbol{r}_2\right), \\ \boldsymbol{r}_{12} &= \left(\boldsymbol{r}_1 - \boldsymbol{r}_2\right) \end{aligned} \tag{E.1}$$

yielding for the potential energy

$$\frac{1}{2}\omega^2\left(\boldsymbol{r}_1^1 + \boldsymbol{r}_2^2\right) = \omega^2\left(\boldsymbol{R}^2 + \frac{1}{4}\boldsymbol{r}_{12}^2\right) \tag{E.2}$$

The transformation of variables can be done also for the kinetic energy, and makes the model Schrödinger equation separable into a part (in $\boldsymbol{R}$) that is independent of the model, and one (in $\boldsymbol{r}_{12}$) that through 2.4 depends on the model (μ).

Note that $\langle\Psi(\mu)|r_{12}^2|\Psi(\mu)\rangle$ is also measuring the error due to the change of density with μ, for harmonium

$$H(\mu) = T + \frac{1}{2}\omega^2(r_1^2 + r_2^2) + \frac{\operatorname{erf}(\mu r_{12})}{r_{12}} \tag{E.3}$$

Indeed, by using the Hellmann–Feynman theorem,

$$\begin{aligned} \frac{\partial}{\partial\omega^2}\langle\Psi(\mu)|H(\mu)|\Psi(\mu)\rangle &= \langle\Psi(\mu)|\frac{1}{2}(r_1^2 + r_2^2)|\Psi(\mu)\rangle \\ &= \langle\Psi(\mu)|(R^2 + \frac{1}{4}r_{12}^2)|\Psi(\mu)\rangle \end{aligned} \tag{E.4}$$

where $\boldsymbol{R} = (\boldsymbol{r}_1 + \boldsymbol{r}_2)/2$. As it is possible to separate variables $\boldsymbol{R}$ and $\boldsymbol{r}_{12}$ in the Schrödinger equation,

$$\Psi(\mu) = \Psi(\boldsymbol{R}, \boldsymbol{r}_{12}, \mu) = \Phi(\boldsymbol{R})\phi(\boldsymbol{r}_{12}, \mu) \tag{E.5}$$

Φ and ϕ both normalized to one, and

$$\langle\Psi(\mu)|\frac{1}{2}(r_1^2 + r_2^2)|\Psi(\mu)\rangle = \int_{\mathbb{R}^3}\rho(\boldsymbol{r}, \mu)r^2\,\mathrm{d}\boldsymbol{r} \tag{E.6}$$

where $\rho(\boldsymbol{r}, \mu)$ is the density of the model system, we have

$$\frac{1}{4}\langle\Psi(\mu)|r_{12}^2|\Psi(\mu)\rangle = \int_{\mathbb{R}^3}\rho(\boldsymbol{r}, \mu)\,r^2\,\mathrm{d}\boldsymbol{r} - \int_{\mathbb{R}^3}|\Phi(\boldsymbol{R})|^2R^2\,\mathrm{d}\boldsymbol{R} \tag{E.7}$$

Note that the change of $\langle r_{12}^2\rangle$ with μ is only due to the change of the density with μ. Thus, the difference between $\frac{1}{4}\langle\Psi(\mu)|r_{12}^2|\Psi(\mu)\rangle$ and $\frac{1}{4}\langle\Psi|r_{12}^2|\Psi\rangle$ also indicates how much the density is affected by the model.

Funding

Part of this work was supported by the French "Investissements d'Avenir" program, project ISITE-BFC (contract ANR15-IDEX-0003) (ÉP). This work has also received funding from the European Research Council (ERC) under the European Union's Horizon 2020 research and innovation program (grant agreement No 810367–project EMC2) (YM & AS).

References

1. T. Kato, "On the eigenfunctions of many-particle systems in quantum mechanics", *Commun. Pure Appl. Math.* **10**, 151–177 (1957).
2. S. Fournais, M. Hoffmann-Ostenof, T. Hoffmann-Ostenhof, and T. O. Sorensen, "Analytic Structure of Many-Body Coulombic Wave Functions", *Comm. Math. Phys.* **289**, 291 (2009).
3. H. Yserentant, *Regularity and Approximability of Electronic Wave Functions*, Springer, Heidelberg, 2010.
4. H.-J. Flad, G. Flad-Harutyunyan, and B.-W. Schulze, "Explicit Green operators for quantum mechanical Hamiltonians. II. Edge-type singularities of the helium atom", *Asian-Eur. J. Math.* **13**, 2050122 (2020).
5. V. A. Rassolov and D. M. Chipman, "Behavior of electronic wave functions near cusps", *J. Chem. Phys.* **104**, 9908 (1996).
6. Y. I. Kurokawa, H. Nakashima, and H. Nakatsuji, "General coalescence conditions for the exact wave functions: Higher-order relations for coulombic and non-coulombic systems", *Adv. Quantum Chem.* **73**, 59 (2016).
7. A. Savin, "Correcting model energies by numerically integrating along an adiabatic connection and a link to density functional approximations", *J. Chem. Phys.* **134**, 214108 (2011).
8. J. Harris and R. O. Jones, "The surface energy of a bounded electron gas-solid", *J. Phys. F: Met. Phys.* **4**, 1170–1186 (1974).
9. M. Barrault, Y. Maday, N. C. Nguyen, and A. T. Patera, "An 'empirical interpolation' method: Application to efficient reduced-basis discretization of partial differential equations", *Compt. Rend. Math.* **339**, 667–672 (2004).
10. E. Goll, H.-J. Werner, H. Stoll, T. Leininger, P. Gori-Giorgi, and A. Savin, "A short-range gradient-corrected spin density functional in combination with long-range coupled-cluster methods: Application to alkali-metal rare-gas dimers", *Chem. Phys.* **329**, 276–282 (2006).
11. G. E. W. Bauer, "General operator ground-state expectation values in the Hohenberg–Kohn–Sham density-functional formalism", *Phys. Rev. B* **27**, 5912 (1983).
12. H. F. King, "The electron correlation cusp", *Theor. Chim. Acta* **94**, 345–381 (1996).
13. A. Savin, "On degeneracy, near-degeneracy and density functional theory", pp. 227–357 in: J. M. Seminario (ed.), *Theoretical and Computational Chemistry*, volume 4 of *Recent Developments and Applications of Modern Density Functional Theory*, Elsevier, Amsterdam, 1996.

14. S. Paziani, S. Moroni, P. Gori-Giorgi, and G. B. Bachelet, "Local-spin-density functional for multideterminant density functional theory", *Phys. Rev. B* **73**, 155111 (2006).
15. E. Goll, H.-J. Werner, and H. Stoll, "A short-range gradient-corrected density functional in long-range coupled-cluster calculations for rare gas dimers", *Phys. Chem. Chem. Phys.* **7**, 3917–3923 (2005).
16. E. Goll, T. Leininger, F. R. Manby, A. Mitrushchenkov, H.-J. Werner, and H. Stoll, "Local and density fitting approximations within the short-range/long-range hybrid scheme: application to large non-bonded complexes", *Phys. Chem. Chem. Phys.* **10**, 3353–3357 (2008).
17. P. Hohenberg and W. Kohn, "Inhomogeneous Electron Gas", *Phys. Rev.* **136**, B864–B871 (1964).
18. M. Levy, "Universal variational functionals of electron densities, first-order density matrices, and natural spin-orbitals and solution of the v-representability problem", *Proc. Nat. Acad. Sci. USA* **76**, 6062–6065 (1979).
19. E. H. Lieb, "Density functionals for Coulomb systems", *Int. J. Quantum Chem.* **24**, 243–277 (1983).
20. F. Colonna and A. Savin, "Correlation energies for some two- and four-electron systems along the adiabatic connection in density functional theory", *J. Chem. Phys.* **110**, 2828–2835 (1999).
21. W. Kohn and L. J. Sham, "Self-Consistent Equations Including Exchange and Correlation Effects", *Phys. Rev.* **140**, A1133–A1138 (1965).
22. Y. Maday, N. C. Nguyen, A. T. Patera, and S. H. Pau, "A general multipurpose interpolation procedure: The magic points", *Comm. Pure Appl. Analysis* **8**, 383–404 (2009).
23. R. D. Amos, A. Bernhardsson, A. Berning, P. Celani, D. L. Cooper, M. J. O. Deegan, A. J. Dobbyn, F. Eckert, C. Hampel, G. Hetzer, P. J. Knowles, T. Korona, R. Lindh, A. W. Lloyd, S. J. McNicholas, F. R. Manby, W. Meyer, M. E. Mura, A. Nicklass, P. Palmieri, R. Pitzer, G. Rauhut, M. Schütz, U. Schumann, H. Stoll, A. J. Stone, R. Tarroni, T. Thorsteinsson, and H.-J. Werner, "Molpro, a package of ab initio programs designed by H.-J. Werner and P. J. Knowles, version 2002.2" (2002).
24. T. H. Dunning Jr., "Gaussian basis sets for use in correlated molecular calculations. I. The atoms boron through neon and hydrogen", *J. Chem. Phys.* **90**, 1007–1023 (1989).
25. D. E. Woon and T. H. Dunning Jr., "Gaussian basis sets for use in correlated molecular calculations. IV. Calculation of static electrical response properties", *J. Chem. Phys.* **100**, 2975–2988 (1994).
26. H. Nakashima and H. Nakatsuji, "Solving the Schrödinger equation of hydrogen molecule with the free complement–local Schrödinger equation method: Potential energy curves of the ground and singly excited singlet and triplet states, Σ, Π, Δ, and Φ", *J. Chem. Phys.* **149**, 244116 (2018).

v.c References

[Bar+04] Barrault, Maxime et al. "An 'Empirical Interpolation' Method: Application to Efficient Reduced-Basis Discretization of Partial Differential Equations". In: *Comptes Rendus Mathematique* 339.9 (Nov. 1, 2004), pp. 667–672. ISSN: 1631-073X (cit. on p. 112).

[Mad+09] Maday, Yvon et al. "A General Multipurpose Interpolation Procedure: The Magic Points". In: *Communications on Pure & Applied Analysis* 8.1 (2009), p. 383 (cit. on p. 113).

[MH09] Marx, Dominik and Hutter, Jürg. "Ab Initio Molecular Dynamics: Basic Theory and Advanced Methods". Cambridge: Cambridge University Press, 2009. ISBN: 978-0-521-89863-8 (cit. on pp. 6, 112).

[PMS21] Polack, Étienne, Maday, Yvon, and Savin, Andreas. "FLEIM: A Stable, Accurate and Robust Extrapolation Method at Infinity for Computing the Ground State of Electronic Hamiltonians". Dec. 24, 2021 (cit. on pp. 112, 115, 117, 119, 121, 123, 125, 127, 129, 131, 133, 135, 137, 139).

Chapter VI

Density matrices extrapolation

Overview

Programming languages • `Fortran` • `Julia` • `Python` • `R`

Modified software • `PySCF` • `TINKER`

Used software • `CFOUR` • `Gaussian`

Visit RWTH Aachen University (Aachen, three days, Jan. 2020) with Benjamin Stamm and Aleksandr Mikhalev

Presentations

- New horizons in density functional theory, Faraday Discussion (lighting poster session, online, Sep. 2020)
- Modelling, Analysis and Simulation of Molecular Systems (MOANSI) Workshop (talk, online, Sep. 2020)

Paper

- [Pol+20] Polack, Étienne et al. "An Approximation Strategy to Compute Accurate Initial Density Matrices for Repeated Self-Consistent Field Calculations at Different Geometries". In: *Molecular Physics* 118.19-20 (Oct. 17, 2020), e1779834. ISSN: 0026-8976
- [Pol+21] Polack, Étienne et al. "Grassmann Extrapolation of Density Matrices for Born–Oppenheimer Molecular Dynamics". In: *Journal of Chemical Theory and Computation* 17.11 (Nov. 9, 2021), pp. 6965–6973. ISSN: 1549-9618

Collaborators • Geneviève Dusson • Filippo Lipparini • Yvon Maday • Aleksandr Mikhalev • Benjamin Stamm

VI.A Problem statement

In this chapter, we look for accurate and efficient ways to compute the quantum mechanics density of a chosen chemical system that depends on some parameters. For example, we can consider normal modes of a molecule, positions of its atoms or time during a molecular dynamics simulation or a geometry optimisation process. This is of interest because often, quantum mechanics computations are done for same molecular system, but at different geometries. As it is the case for molecular dynamics or geometry optimisation.

Articles such as ones from Cancès et al. [Can+07] and Maday and Razafison [MR08] hint that the Kolmogorov n-width of a family of densities for a chemical system may be small when considering its positions as parameters (see Section VI.A.3 for a brief description). We should thus be able to find a *smallish* reduced basis which will span the space of density matrices of interest up to some desired numerical accuracy. We also want a method that cheaply evaluates density matrices for new parameters.

To gain insight in the objects we are studying and to reduce the complexity of the work, we have looked at the self-consistent field method that arises when doing density functional theory or Hartree–Fock quantum mechanics computations. The main advantage of this point of view is that densities that will be obtained by the methods we develop can be used as an initial guess to the self-consistent field algorithm. Thus, we keep usable accuracy to chemists, while decreasing

the cost of the self-consistent field method if the guesses are close to the final density. The longer goal is to be able to bypass the self-consistent field algorithm altogether and provide *directly correct* density matrices, or even physical properties.

We will present the method for HARTREE–FOCK computations using a linear combination of atomic orbitals basis set, but everything in this chapter can be used when doing density functional theory.

We first present a short reminder about the restricted HARTREE–FOCK method that we introduced in Section I.D.4. Then, we show two applications of the developed method, which enabled us to reduce the number of self-consistent field iterations.

VI.A.1 Discrete HARTREE–FOCK method

We consider the electronic SCHRÖDINGER problem for N electrons and M nuclei. The nuclear positions $r \in \mathbf{R}^{3M}$ are parameterised by an implicit (and non-linear) map $\mathbb{P} \ni \mu \mapsto r(\mu) \in \mathbf{R}^{3M}$. We refer to the bounded domain $\mathbb{P} \in \mathbf{R}^P$ as the parameter domain.

We consider the HARTREE–FOCK equations. Using a given basis set of dimension $\mathcal{N}$ within the linear combination of atomic orbitals framework, the discrete HARTREE–FOCK energy of the N electrons system can be written as finding the minimum of a functional

$$C_\mu = \operatorname*{arg\,min}_{C \in \mathcal{M}(\mu)} \mathcal{E}_\mu^{\mathrm{HF}}(C) = \min_{C \in \mathcal{M}(\mu)} \operatorname{Tr}\left(C^\mathsf{T} h_\mu C + \frac{1}{2} C^\mathsf{T} G_\mu(CC^\mathsf{T})C\right), \tag{I.1}$$

where h_μ and G_μ are the customary one- and two-electron operators with respect to the linear combination of atomic orbitals basis set for the parameter value μ, C is the matrix of occupied orbitals, $D := CC^\mathsf{T}$ is the density matrix and

$$\mathcal{M}(\mu) := \left\{C \in \mathbf{R}^{\mathcal{N}\times N} \;\middle|\; C^\mathsf{T} S_\mu C = \mathrm{Id}_N\right\}, \tag{I.2}$$

with S_μ the overlap matrix. We will drop the superscript $\cdot^{\mathrm{HF}}$ when there is no possible confusion. We note that G_μ is a non-linear map.

If we introduce the FOCK operator (see Section I.D)

$$F_\mu(\cdot) := h_\mu + G_\mu(\cdot), \tag{I.3}$$

then the HARTREE–FOCK method is often rewritten to find the matrix of occupied orbitals $C \in \mathcal{M}(\mu)$ that minimises the energy

$$\mathcal{E}_\mu(C) = \operatorname{Tr}\left(\left(h_\mu + \frac{1}{2} F_\mu(CC^\mathsf{T})\right) CC^\mathsf{T}\right), \tag{I.4}$$

or to find the density matrix $D \in \tilde{\mathcal{P}}_N := \{D \in \mathbf{R}^{N_b \times N_b} \mid D^\mathsf{T} = D,\ DSD = D,\ \operatorname{Tr}(SD) = N\}$ that minimises

$$\tilde{\mathcal{E}}_\mu(D) := \operatorname{Tr}\left(h_\mu \cdot D + \frac{1}{2} F_\mu(D) \cdot D\right). \tag{I.5}$$

We will drop the tilde of the energy and use the same notation for energy functional $\mathcal{E}$ applied either to density matrix or occupied molecular orbitals when there is no possible confusion.

VI.A.2 Self-consistent field method for HARTREE–FOCK

The self-consistent field method is a class of iterative algorithms used to find the minimum of the HARTREE–FOCK energy. The outline of the algorithm is as follow. By writing the EULER–LAGRANGE

equation, this means trying to find $C_\mu \in \mathcal{M}(\mu)$ and $E_\mu \in \mathbf{R}^{N\times N}$ that solve the system

$$\begin{cases} F_\mu(D_\mu)C_\mu = S_\mu C_\mu E_\mu \\ C_\mu^\intercal S_\mu C_\mu = \mathrm{Id}_N \\ D_\mu = C_\mu^\intercal C_\mu \end{cases}. \tag{I.6}$$

We can use a simplified form of the fixed-point algorithm used to solve the system as: First, choose some C_μ^0 such that $C_\mu^{0\intercal} S_\mu C_\mu^0 = \mathrm{Id}_N$ and construct a sequence $\left(C_\mu^n\right)_{n\in\mathbf{N}}$ that satisfies

$$\begin{cases} F_\mu(D_\mu^{n-1})C_\mu^n = S_\mu C_\mu^n E_\mu^n \\ C_\mu^{n\intercal} S_\mu C_\mu^n = \mathrm{Id}_N \\ D_\mu^n = C_\mu^{n\intercal} C_\mu^n \end{cases}, \quad \text{for all } n \in \mathbf{N}. \tag{I.7}$$

The algorithms stops when the residual $|C_\mu^n - C_\mu^{n-1}|$ is smaller than a desired tolerance.

For chemical systems, the bottleneck of this method is the evaluation of the Fock matrices. The first line of the system, the diagonalisation of the Fock matrix, has often a cost that is negligible compared to it. We note that this still may be true for density functional theory, depending on the choice for so-called exchange–correlation functional.

Thus, providing an accurate guess to the self-consistent field method can dramatically decrease the cost to find solutions to the Hartree–Fock problem.

As we have already written, most of the time, this algorithm has to be run sequentially for the same molecular system, but for a lot of different geometries. However, although much has been done to develop convergence acceleration techniques for the self-consistent field procedure, less is known on how to efficiently exploit the abundance of information generated by previous computations to provide the self-consistent field with a good initial guess.

For example, for geometry optimisation, we may use the density of the precedent step as a guess. And for molecular dynamics we may do extrapolations on the time-steps for a few previous positions, or use the Lagrangian extended method, or direct inversion in the iterative subspace. But those methods never use more than a few consecutive points in the history.

We note that depending on the software that is used, the constrain that $C_\mu^\intercal S_\mu C_\mu = \mathrm{Id}_N$ may not be imposed at all for the initial guess, or may be partially checked, such as only verifying that the trace is correct.

VI.A.3 Geometric interpretation

We would like a method that is oblivious to crossings of eigenvalues, as long as no crossing occurs between occupied and non-occupied orbitals. That is because the pre-processing needed to take care of those case may considerably slow algorithms, as was the case for [MR08].

Density matrices seem to be good objects to look at with respect to those constraints. Moreover the property that up to normalisation by $S_\mu^{1/2}$,

$$S_\mu^{1/2} D_\mu S_\mu^{1/2} \in \mathcal{G}r(N, \mathcal{N}), \tag{I.8}$$

where

$$\mathcal{G}r(N, \mathcal{N}) = \left\{ D \in \mathbf{R}^{\mathcal{N}\times\mathcal{N}} \;\middle|\; D^2 = D,\ D^\intercal = D,\ \mathrm{Tr}\, D = N \right\} \tag{I.9}$$

means that density matrices can be seen as object on a smooth manifold, the Grassmannian $\mathcal{G}r(N, \mathcal{N})$, as will be explained below. This implies locally the existence of a diffeomorphism that transforms the manifold into an affine space, the tangent space, and back. The maps are known as the Grassmannian exponential and logarithm. This allows us to apply well-known

methods to approximate the elements in the tangent space, and then map back the results to the manifold. This way, we are assured that the final result is indeed still a density matrix, see Fig. VI.1 for a schematic description.

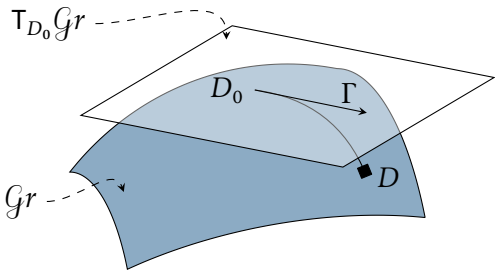

Figure VI.1: Schematic illustration of the geometrical setting. We illustrate by the blue hypersurface the Grassmann manifold $\mathcal{G}r$ and by the transparent plane the tangent space $\mathsf{T}_{D_0}\mathcal{G}r$ to $\mathcal{G}r$ at D_0. We illustrate the one-to-one relationship between a close density matrix $D \in \mathcal{G}r$ and the corresponding vector $\Gamma = \mathrm{Log}_{\mathcal{G}r,0} D$ in the tangent space.

Definitions and properties

We suppose the reader has some notions about differential manifolds. However it is not fully needed to understand the gist of the method. Most of the definitions and properties can be found in texts of Edelman, Arias, and Smith [EAS98], Absil, Mahony, and Sepulchre [AMS08], and Zimmermann [Zim19]. We first start with a few definitions.

Definition VI.A.1 (Grassmann manifold)**.—** The Grassmann manifold (or Grassmannian) $\mathcal{G}r(k,n)$ is the set of all k-dimensional linear subspaces in $\mathbf{R}^n$

$$\mathcal{G}r(k,n) := \Big\{ \mathrm{Span}(V) \,\Big|\, V \in \mathbf{R}^{n\times k},\ \dim(V) = k \Big\} = \Big\{ \mathrm{Span}(V) \,\Big|\, V \in \mathbf{R}^{n\times k},\ V^{\mathsf{T}}V = \mathrm{Id}_k \Big\}. \tag{I.10}$$

Definition VI.A.2 (Stiefel manifold (compact))**.—** The (compact) Stiefel manifold $\mathcal{S}t(k,n)$ is the set of all k-tuples of orthonormal vectors of $\mathbf{R}^n$

$$\mathcal{S}t(k,n) := \Big\{ V \in \mathbf{R}^{n\times k} \,\Big|\, V^{\mathsf{T}}V = \mathrm{Id}_k \Big\}. \tag{I.11}$$

Definition VI.A.3 (non-compact Stiefel manifold)**.—** The non-compact Stiefel manifold $\widetilde{\mathcal{S}t}(k,n)$ is the set of all k-tuples of linearly independent vectors of $\mathbf{R}^n$

$$\widetilde{\mathcal{S}t}(k,n) := \Big\{ V \in \mathbf{R}^{n\times k} \,\Big|\, \dim(V) = k \Big\}. \tag{I.12}$$

The following properties are interesting to have a better understanding of the objects we manipulate.

Property VI.A.1.— We can identify the Stiefel $\mathcal{S}t(k,n)$ with the quotient of two orthogonal groups

$$\mathcal{S}t(k,n) \cong \mathrm{O}(n) \Big/ \mathrm{O}(n-k)\,. \tag{I.13}$$

Admitted proof. □

Property VI.A.2. — We can identify the non-compact Stiefel $\widetilde{\mathcal{S}t}(k,n)$ with the quotient of two general linear groups

$$\widetilde{\mathcal{S}t}(k,n) \cong \mathrm{GL}(n)\Big/\mathrm{GL}(n-k)\,. \tag{I.14}$$

Admitted proof. □

Property VI.A.3. — We can identify the Grassmannian $\mathcal{G}r(k,n)$ with the quotient of the non-compact Stiefel $\widetilde{\mathcal{S}t}(k,n)$ by

$$\mathcal{G}r(k,n) \cong \widetilde{\mathcal{S}t}(k,n)\Big/\mathrm{GL}(k) \cong \mathrm{GL}(n)\Big/\mathrm{GL}(n-k)\times\mathrm{GL}(k)\,, \tag{I.15}$$

or with the quotient of the Stiefel $\mathcal{S}t(k,n)$ by

$$\mathcal{G}r(k,n) \cong \mathcal{S}t(k,n)\Big/\mathrm{O}(k) \cong \mathrm{O}(n)\Big/\mathrm{O}(n-k)\times\mathrm{O}(k)\,. \tag{I.16}$$

Admitted proof. □

Using the last proposition, for an element $C \in \mathcal{S}t(k,n)$, we will denote elements of the Grassmannian $\mathcal{G}r(k,n)$ as $[C]$, and always work with Stiefel elements. In the case of the Grassmannian, for $C, C' \in \mathcal{S}t(k,n)$,

$$[C] = [C'] \quad \text{when} \quad \operatorname{Span} C = \operatorname{Span} C'. \tag{I.17}$$

The collection of N electrons is characterised by the density matrix $D = \sum_{i=1}^{N} |\psi_i\rangle\langle\psi_i|$. This matrix can be seen as the projection on the eigenspace generated by orthonormal functions ψ_i, $i \in [\![1\,..\,N]\!]$, *i.e.*, $\operatorname{Span}\left(\{\psi_i\}_{i=1}^{N}\right)$. This eigenspace characterises a plane of dimension N in the space of dimension $\mathcal{N}$. Hence the density matrices can be associated to objects living on the Grassmannian $\mathcal{G}r(N,\mathcal{N})$.

Property VI.A.4. — We can identify the Grassmannian $\mathcal{G}r(k,n)$ with the set of rank k projectors

$$\mathcal{G}r(k,n) \cong \mathcal{P}(k,n). \tag{I.18}$$

Admitted proof. □

We note that given a density matrix, and up to normalisation with the overlap matrix, the tuple of its eigenvectors is an element of the Stiefel. Moreover, for any element Φ of the Stiefel $\mathcal{S}t(k,n)$, $\Phi\Phi^{\mathsf{T}}$ is a projector of rank k. Intuitively, the fact that the eigenvectors are in the Stiefel and that we have an invariance by the orthogonal group gives us that we are interested in elements of the Grassmannian $\mathcal{G}r(N,\mathcal{N})$ by the last property.

Formulas

The Grassmannian is a smooth manifold. Thus there exists local diffeomorphisms between neighbourhoods of any points on the Grassmannian and some affine spaces, their tangent spaces. This will enable us to do linear approximations in the affine space and map back the results on the manifold. The map from the Grassmannian to the tangent space is known as the exponential map and its inverse as the logarithmic map.

Proposition – Definition VI.A.1 (Grassmannian exponential)**.—** Let $[C_0] \in \mathcal{G}r(k,n)$ and $\Gamma \in \mathsf{T}_{[C_0]}\mathcal{G}r(k,n)$ an element of its tangent space. Then the Grassmannian exponential of the tangent element Γ to the point $[C_0]$ is

$$\begin{aligned} \mathrm{Exp}_{\mathcal{G}r,[C_0]} : \mathsf{T}_{[C_0]}\mathcal{G}r(k,n) &\longrightarrow \mathcal{G}r(k,n) \\ \Gamma &\longmapsto [C_0 V \cos(\Sigma) + U \sin(\Sigma)] \end{aligned}, \tag{I.19}$$

where the quantities are computed from the (thin) singular value decomposition of Γ

$$U\Sigma V^\mathsf{T} := \Gamma. \tag{I.20}$$

The cosinus and sinus functions only act on the diagonal elements of the matrix Σ.

Admitted proof. □

In the following, we will often omit using equivalence classes when no confusion is possible.

Proposition – Definition VI.A.2 (Grassmannian logarithm)**.—** Let $[C_0], [C] \in \mathcal{G}r(k,n)$. Then the Grassmannian logarithm of the element $[C]$ with respect to point $[C_0]$ is

$$\begin{aligned} \mathrm{Log}_{\mathcal{G}r,[C_0]} : \mathcal{G}r(k,n) &\longrightarrow \mathsf{T}_{[C_0]}\mathcal{G}r(k,n) \\ [C] &\longmapsto V \arctan(\Sigma) U^\mathsf{T} \end{aligned}, \tag{I.21}$$

where the quantities are computed from the (thin) singular value decomposition of L

$$U\Sigma V^\mathsf{T} := L, \tag{I.22}$$

where

$$L = (C^\mathsf{T} C_0)^{-1} C^\mathsf{T} - C_0^\mathsf{T}. \tag{I.23}$$

The arctangent function only acts on the diagonal elements of the matrix Σ.

Admitted proof. □

Density matrices can thus be approached by Grassmannian exponentials of linear combinations of elements in the tangent space

$$D_\mu \approx C C^\mathsf{T}, \quad \text{where} \quad C := \mathrm{Exp}_{\mathcal{G}r,0}\left(\sum_i c_{\mu,i}\Gamma_i\right). \tag{I.24}$$

Intuition behind the method

As we recall, works from Cancès et al. [Can+07] and Maday and Razafison [MR08] seem to show that density matrices are a set of points with a small Kolmogorov n-width. We want to take advantage of this property in the tangent space, with the hope that the transformation does not increase (too much) the width.

Definition VI.A.4 (Kolmogorov n-width)**.—** Let $\mathcal{X}$ be a normed linear space, $\mathcal{S}$ be a subset of $\mathcal{X}$ and $\mathcal{X}_n$ be a generic n-dimensional subspace of $\mathcal{X}_n$. The deviation of $\mathcal{S}$ from $\mathcal{X}_n$ is given by

$$E(\mathcal{S}, \mathcal{X}_n) := \sup_{u \in \mathcal{S}} \inf_{v_n \in \mathcal{X}_n} |u - v_n|_{\mathcal{X}}. \tag{I.25}$$

The Kolmogorov n-width of $\mathcal{S}$ is defined by

$$d_n(\mathcal{S}, \mathcal{X}) := \inf_{\mathcal{X}_n} \sup_{u \in \mathcal{S}} \inf_{v_n \in \mathcal{X}_n} |u - v_n|_{\mathcal{X}}. \tag{I.26}$$

It measures how well $\mathcal{S}$ can be approximated by an n-dimensional subspace of $\mathcal{X}$. A schematic representation is shown in shown in the right panel of Fig. VI.2.

If the Kolmogorov n-width is small, then there exists a small reduce basis on which we can approximate any parameter values. However this is a theoretical results, and does not give a way to construct the basis.

We expect that for all $i \in [\![1 \,..\, N_\mu]\!]$, the tangent elements

$$\Gamma_i := \mathrm{Log}_{\mathcal{G}r,0}(D_i) \in \mathsf{T}_{D_0}\mathcal{G}r \tag{I.27}$$

are highly linearly dependant. So there exists a low dimensional basis ($n \ll N_\mu$)

$$\{\Theta_1, \dots, \Theta_n\} \in \mathsf{T}_{D_0}\mathcal{G}r \tag{I.28}$$

such that

$$\mathcal{D}_{0,\mathsf{T}} := \left\{\Gamma_\mu \,\middle|\, \mu \in \mathbb{P}\right\} \subseteq \mathsf{T}_{D_0}\mathcal{G}r \tag{I.29}$$

can be well approximated by elements of the n-dimensional space

$$\mathbb{V}_{\mathrm{rb}} := \mathrm{Span}\,\{\Theta_1, \dots, \Theta_n\} \subseteq \mathsf{T}_{D_0}\mathcal{G}r. \tag{I.30}$$

In Fig. VI.2, we give a schematic representation, as well as a link between this and the Kolmogorov n-width.

VI.B Application to normal modes

We have used the previous results to be able to provide good initial guesses for the self-consistent field method of Hartree–Fock or density functional theory. First, we will develop this to a case where the nuclear coordinates are changed along a few user-specified collective variables. We choose to look at displacements along molecular normal modes of vibration. This has the advantage of providing *real-case* displacements while having the possibility to have a few degrees of freedom that we know explicitly. For more detail on this method, we refer the reader to an article we have published [Pol+20] and an overview of the results Page 161.

The vibrational normal modes of a molecular system are obtained by diagonalisation of the mass-weighted Hessian matrix of the energy at a local minimum of energy. The eigenvalues correspond to the square of the normal mode vibrational frequencies, and the eigenvectors to

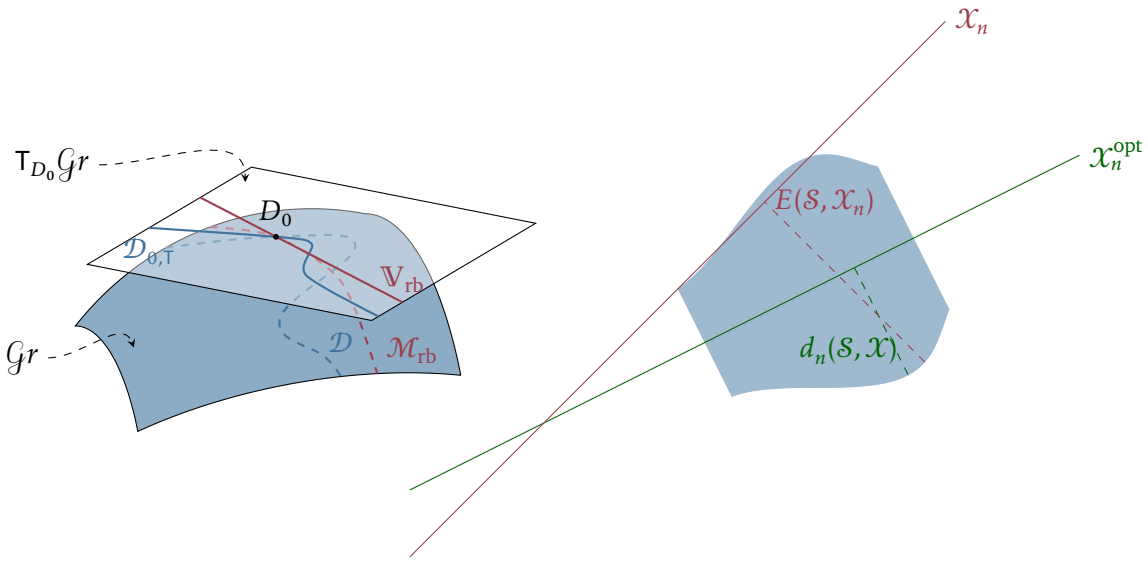

Figure VI.2: On the left is a schematic illustration of the geometrical setting. We illustrate by the blue hypersurface the Grassmann manifold $\mathcal{G}r$ and by the transparent plane the tangent space $\mathsf{T}_{D_0}\mathcal{G}r$ to $\mathcal{G}r$ at D_0. We schematically illustrate the notions of $\mathcal{D}_{0,\mathsf{T}}$ and $\mathbb{V}_{\mathrm{rb}}$, as well as their equivalent sets $\mathcal{D} = \left\{D_\mu \,\middle|\, \mu \in \mathbb{P}\right\}$ and $\mathcal{M}_{\mathrm{rb}} = \mathrm{Exp}_{\mathcal{G}r,0}(\mathbb{V}_{\mathrm{rb}})$ on $\mathcal{G}r$. On the right is a link between the representations of the Kolmogorov n-width and the objects of the Grassmannian. We can identify $\mathcal{S} \cong \mathcal{D}_{0,\mathsf{T}}$ and $\mathcal{X}_n \cong \mathbb{V}_{\mathrm{rb}}$.

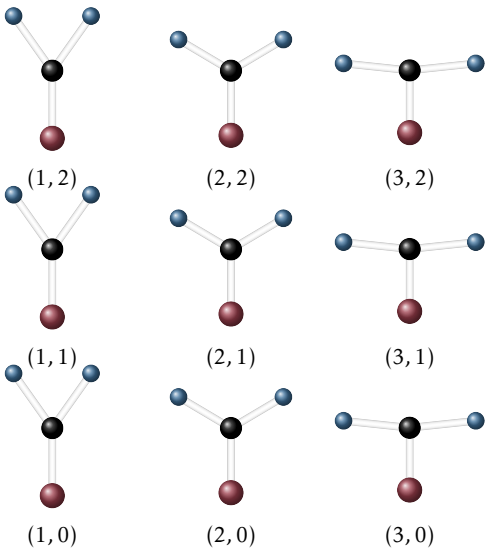

Figure VI.3: Schematic representation of the parameter space along two normal modes for the formaldehyde (H_2CO). The positions of the atoms are projected on two axes.

the amplitude of displacements along normalised coordinates. For all our example we chose a normal mode corresponding to the carbonyl C–O stretching (one- and two-dimensional case) and optionally a second corresponding to a low-frequency collective vibration (two-dimensional case). We refer to Fig. VI.3 for a schematic representation.

In this case, we will allow a large computational cost for data generation of some collective variables that can be stored, as long as the on-the-fly cost for evaluating new variables is negligible compared to the self-consistent field computations. We want the method to be robust with respect to change of basis set, and to work for a large range of displacements in the self-consistent field energy.

VI.B.1 One-dimensional case

For the one-dimensional case, we developed a basic scheme. A number N_g of displacements along one normal mode gives us N_g points in the tangent space of one of the density matrices, which we can choose arbitrarily. From these snapshots, we select the ones to be chosen as a basis for a Lagrangian interpolation in a greedy way: we add functions that are approximated the worst by the current interpolant Γ^n_{app}

$$\Gamma_{n+1} = \arg\max_{\Gamma_i} \left|\Gamma_i - \Gamma^n_{\text{app}}(\mu_i)\right|. \tag{II.1}$$

.

VI.B.2 Two-dimensional case

We assume to have a two-dimensional grid of $N_g \times N_g$ elements in the tangent space of one of the density matrices. We want to find a function $L_i \colon \mathbb{P} \to \mathbf{R}$ and a reduced basis $\{\Theta_1, \dots, \Theta_n\}$ such that

$$\Gamma_{\text{app}}(\mu) := \sum_{i=1}^{n} L_i(\mu)\Theta_i \tag{II.2}$$

is a good approximation of $\Gamma(\mu) := \text{Log}_{\mathcal{G}r,0}(D_\mu)$ for all $\mu \in \mathbb{P}$.

Below is the outline of the steps for the method.

1. Create a matrix of monomes P of size $N_p \times d$.
2. Extract d lines from this matrix to create a square matrix $\hat{P} \in \mathbf{R}^{d\times d}$.
3. We can form the matrix
$$\tilde{\Gamma}_{\text{app}} := \sum_{i=1}^{d} \lambda_i(\mu)\Gamma(\mu_{\sigma(i)}). \tag{II.3}$$
Note that $\lambda_i(\mu) := P(\mu)\hat{P}^{-1}$. Hence it is an interpolation of Γ at points $\mu_{\sigma(i)}$, $i \in [\![1 \,..\, d]\!]$: if μ has been chosen as a line for P, then $P(\mu)\hat{P}^{-1} = (0, \dots, 0, 1, \dots, 0)$, where 1 corresponds to the matrix $\Gamma_{\sigma(i)}$.
4. We do an SVD of $\Gamma(\mu_{\sigma(i)})$ to form the Θ_i.

In the case where we have only one normal mode, then P is the Vandermonde matrix, which inverse is a matrix of Lagrange polynomials, similarly as in the 1D case.

We did not consider dimensions higher than the two-dimensional case; however we think that the method we describe here should be applicable up to half a dozen normal modes. At which point we expect the curse of dimensionality to bite us due to a large amount of data to consider, such as to correctly sample the parameter space.

VI.C Application to molecular dynamics

The results of the previous paragraph are interesting, but the applications are quite narrow. We would like to be able to predict density matrices for any conformation of the molecules. For such a general case, we may want to look at molecular dynamics, where the number of degrees of freedom is the cube of the number of atoms. If we consider conformations near a local minimum, we may hope that each successive conformation during time are not completely random, but may follow a path with some regularity.

The obvious set of parameters available when doing molecular dynamics are the time-steps and the positions of the atoms. In the supporting article Page 152, we have developed such a method using a simple least-squares method on molecular descriptors — functions that depends on atomic positions. Schematically, the density matrices D_i for $i \in [\![1 \,..\, N_t]\!]$ are first projected on tangent space of some reference matrix D_0, using the logarithm function

$$\Gamma_i = \mathrm{Log}_{D_0}(D_i). \tag{III.1}$$

Then, by using the coefficients c_i from the least-squares, we can do a linear combination on the tangent space, and retract it on the Grassmann manifold to have the guess

$$D_{\mathrm{app}} := \mathrm{Exp}_{D_0}\left(\sum_{i=1}^{N_t} c_i \Gamma_i\right). \tag{III.2}$$

The results on real test-cases are encouraging, as we were able to decrease by in some cases more than a third the number of self-consistent field iterations needed to have a desired accuracy when compared to using the extended Lagrangian method of Niklasson [Nik08]. A natural next step would be to implement that method for geometry optimisation.

JCTC Journal of Chemical Theory and Computation

pubs.acs.org/JCTC Article

Grassmann Extrapolation of Density Matrices for Born−Oppenheimer Molecular Dynamics

Étienne Polack, Geneviève Dusson, Benjamin Stamm, and Filippo Lipparini*

Cite This: J. Chem. Theory Comput. 2021, 17, 6965−6973 Read Online

ACCESS | Metrics & More | Article Recommendations | Supporting Information

ABSTRACT: Born−Oppenheimer molecular dynamics (BOMD) is a powerful but expensive technique. The main bottleneck in a density functional theory BOMD calculation is the solution to the Kohn−Sham (KS) equations that requires an iterative procedure that starts from a guess for the density matrix. Converged densities from previous points in the trajectory can be used to extrapolate a new guess; however, the nonlinear constraint that an idempotent density needs to satisfy makes the direct use of standard linear extrapolation techniques not possible. In this contribution, we introduce a locally bijective map between the manifold where the density is defined and its tangent space so that linear extrapolation can be performed in a vector space while, at the same time, retaining the correct physical properties of the extrapolated density using molecular descriptors. We apply the method to real-life, multiscale, polarizable QM/MM BOMD simulations, showing that sizeable performance gains can be achieved, especially when a tighter convergence to the KS equations is required.

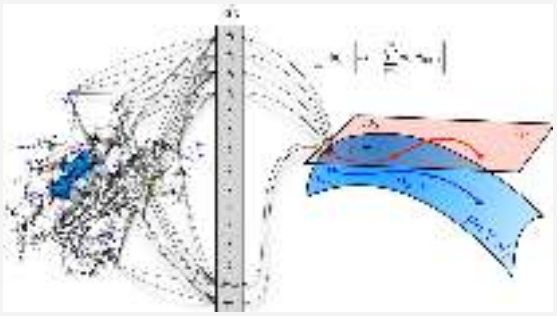

1. INTRODUCTION

Ab initio Born−Oppenheimer molecular dynamics (BOMD) is one of the most powerful and versatile techniques in computational chemistry, but its computational cost represents a big limitation to its routine use in quantum chemistry. To perform a BOMD simulation, one needs to solve the quantum mechanics (QM) equations, usually Kohn−Sham (KS) density functional theory (DFT), at each step, before computing the forces and propagating the trajectory of the nuclei. The iterative self-consistent field (SCF) procedure is expensive, as it requires to build, at each iteration, the KS matrix and to diagonalize it. Convergence can require tens of iterations, making the overall procedure, which has to be repeated a very large number of times, very expensive. To reduce the cost of BOMD simulations, it is therefore paramount to be able to perform as little iterations as possible while, at the same time, obtaining an SCF solution accurate enough to afford stable dynamics. From a conceptual point of view, at each step of a BOMD simulation, a map is built from the molecular geometry to the SCF density and then to the energy and forces. The former map, in practice, requires the solution to the SCF problem and is not only very complex but also highly nonlinear. However, the propagation of the molecular dynamics (MD) trajectory uses short, finite time steps so that the converged densities at previous steps, and thus at similar geometries, are available. As a consequence, the geometry to the density map can be in principle approximated by extrapolating the available densities at previous steps. The formulation of effective extrapolation schemes has been the object of several previous works.[1] Among the proposed strategies, one for density matrix extrapolation was developed by Alfè,[2] as a generalization of the wavefunction extrapolation method by Arias et al.,[3] which is based on a least-squares regression on a few previous atomic positions. The main difficulty in performing an extrapolation of the density matrix stems from the nonlinearity of the problem. In other words, a linear combination of idempotent density matrices is not an idempotent density matrix, as density matrices are elements of a manifold and not of a vector space. To circumvent this problem, strategies that extrapolate the Fock or KS matrix[4,5] or that use orbital transformation methods[6−8] have been proposed.

A completely different strategy has been proposed by Niklasson and co-workers.[9−11] In the extended Lagrangian Born-Oppenheimer (XLBO) method, an auxiliary density is propagated in a time-reversible fashion and then used as a guess for the SCF procedure. The strategy is particularly successful, as it combines an accurate guess with excellent stability properties. In particular, the XLBO method allows one to perform accurate simulations converging the SCF to average

Received: July 27, 2021
Published: October 8, 2021

values [for instance, 10^{-5} in the root-mean-square (RMS) norm of the density increment], which are usually insufficient to compute accurate forces. An XLBO-based BOMD strategy has been recently developed by some of us in the context of polarizable multiscale BOMD simulations of both ground and excited states.[12−15] Multiscale strategies can be efficiently combined, in a focused model spirit, to BOMD simulations to extend the size of treatable systems. Using a polarizable embedding allows one to achieve good accuracy in the description of environmental effects, especially if excited states or molecular properties are to be computed. In such a context, the XLBO guessing strategy allows one to perform stable simulation even using a modest 10^{-5} RMS convergence threshold, which, thanks to the quality of the XLBO guess, typically requires only about four SCF iterations. Recently, SCF-less formulations of the XLBO schemes have also been proposed.[16,17]

Unfortunately, the performances of the XLBO-based BOMD scheme are not so good when a tighter SCF convergence is required, which can be the case when one wants to perform MD simulations using post Hartree−Fock (HF) methods or for excited states described in a time-dependent DFT framework.[14,18] In fact, such methods require the solution to a second set of QM equations which are typically nonvariational, making them more susceptible to numerical errors and instabilities. Computing the forces for non-SCF energies therefore requires a more accurate SCF solution.

The present work builds on all previous methods for density matrix extrapolation and aims at proposing a simple framework to overcome the difficulties associated with the nonlinearity of the problem. The strategy that we propose is based on a differential geometry approach and is particularly simple. First, we introduce a molecular descriptor, that is, a function of the molecular geometry and other molecular parameters that represent the molecular structure in a natural way that respects the invariance properties of the molecule within a vector space. At the $(n + 1)$-th step of an MD trajectory, we fit the new descriptor in a least-square fashion using the descriptors available at a number of previous steps and obtain a new set of coefficients. However, we do not use them to directly extrapolate the density. Instead, we first map the unknown density matrix that we aim to approximate from the manifold where it is defined to its tangent space. We then perform the extrapolation to approximate the representative density matrix in the tangent space, before mapping this approximation back to the manifold in order to obtain an extrapolated density matrix that satisfies the required physical constraints. This geometrical strategy, which has recently been introduced in the context of density matrix approximation by us,[19] allows one to use standard linear extrapolation machinery without worrying about the nonlinear physical constraints on the density matrix, since both the space of descriptors and the tangent space are vector spaces. As the mapping between the manifold and the tangent space is locally bijective, no concerns about redundant degrees of freedom (such as rotations that mix occupied orbitals) arise. The map and its inverse, which are known as Grassmann logarithm and exponential, are easily computed and the implementation of the strategy is straightforward. We shall denote this approach as Grassmann extrapolation (G-Ext).

In this contribution, we choose a simple, yet effective molecular descriptor, and, for the extrapolation, a least square strategy. These are not the only choices. As our strategy allows one to use any linear extrapolation technique, which can be in turn coupled with any choice of molecular descriptor, more advanced strategies can be proposed, including machine learning. Our approach ensures that the extrapolated density, independent of how it is obtained, satisfies all the physical requirements of a density stemming from a single Slater determinant.

The paper is organized as follows. In the upcoming Section 2, we present all necessary theoretical foundations required for the development and implementation of the presented G-Ext approach. Section 3 then presents detailed numerical tests illustrating the performance of the extrapolation scheme, including realistic applications of BOMD within a QM/molecular mechanics (MM) context before we draw the conclusion in Section 4.

2. THEORY

We consider ab initio BOMD simulations where the position vector $\mathbf{R} \in \mathbb{R}^{3M}$ evolves in time according to classical mechanics as

$$M_i \ddot{\mathbf{R}}_i(t) = F_i(t, \mathbf{R}(t)) \tag{1}$$

where $\mathbf{R}_i(t)$, $F_i(t) \in \mathbb{R}^3$ denote the position of the i-th atom with mass M_i, respectively, and the force acting on it at time t. We consider a general QM−MM method, but the setting also trivially applies to pure QM models. The forces at a given time t and position $\mathbf{R}$ of the nuclei arise from different interactions, namely, QM−QM, QM−MM, and MM−MM interactions. The computationally expensive part is to determine the state of the electronic structure, which is modeled here at the DFT level with a given basis set of dimension $\mathcal{N}$. Note that considering HF instead of DFT would not change much in the presentation of the method. It consists of computing the instantaneous nonlinear eigenvalue problem

$$\begin{cases} F_{\mathbf{R}}(D_{\mathbf{R}})C_{\mathbf{R}} = S_{\mathbf{R}}C_{\mathbf{R}}E_{\mathbf{R}} \\ C_{\mathbf{R}}^{\mathrm{T}}S_{\mathbf{R}}C_{\mathbf{R}} = \mathrm{Id}_N \\ D_{\mathbf{R}} = C_{\mathbf{R}}C_{\mathbf{R}}^{\mathrm{T}} \end{cases} \tag{2}$$

where $C_{\mathbf{R}} \in \mathbb{R}^{\mathcal{N}\times N}$ and $D_{\mathbf{R}} \in \mathbb{R}^{\mathcal{N}\times\mathcal{N}}$ denote the coefficients, respectively, of the occupied orbitals and density matrix and $E_{\mathbf{R}} \in \mathbb{R}^{N\times N}$ denotes the diagonal matrix containing the energy levels. Furthermore, $F_{\mathbf{R}}$ denotes the DFT operator acting on the density matrix and $S_{\mathbf{R}}$ denotes the customary overlap matrix.

At this point, it is useful to note that the slightly modified coefficient matrix $\tilde{C}_{\mathbf{R}} := {S_{\mathbf{R}}}^{1/2}C_{\mathbf{R}}$ belongs to the so-called Stiefel manifold defined as follows

$$\mathcal{S}t(N, \mathcal{N}) := \{V \in \mathbb{R}^{\mathcal{N}\times N} | V^{\mathrm{T}}V = \mathrm{Id}_N\} \tag{3}$$

due to the second equation in eq 2. In consequence, the normalized density matrix $\tilde{D}_{\mathbf{R}} = \tilde{C}_{\mathbf{R}}\tilde{C}_{\mathbf{R}}^{\mathrm{T}} = {S_{\mathbf{R}}}^{1/2}D_{\mathbf{R}}{S_{\mathbf{R}}}^{1/2}$ belongs to the following set

$$\mathcal{G}r(N, \mathcal{N}) := \{D \in \mathbb{R}^{\mathcal{N}\times\mathcal{N}} | D^2 = D, D^{\mathrm{T}} = D, \mathrm{Tr}\, D = N\} \tag{4}$$

which can be identified with the Grassmann manifold of N-dimensional subspaces of $\mathbb{R}^{\mathcal{N}}$ by means of the spectral projectors. In the following, we always assume that the density matrix has been orthonormalized and therefore drop the ∼

https://doi.org/10.1021/acs.jctc.1c00751
J. Chem. Theory Comput. 2021, 17, 6965−6973

Journal of Chemical Theory and Computation pubs.acs.org/JCTC Article

from the notation. For any $D \in \mathcal{G}r(N, \mathcal{N})$, one can associate the tangent space $\mathcal{T}_D$ which has the structure of a vector space. The evolution of the electronic structure can therefore be seen as a trajectory $t \to D_{\mathbf{R}(t)}$ on $\mathcal{G}r(N, \mathcal{N})$ where $t \to \mathbf{R}(t)$ denotes the trajectory of the nuclei.

The goal of the present work is to find a good approximation for the electronic density matrix at the next step of MD trajectory by extrapolating the densities at previous steps. More precisely, based on the knowledge of the density matrices $D_i := D_{\mathbf{R}(t_i)}$, $i = n - N_t, ..., n - 1$, at N_t previous times t_i, one aims to compute an accurate guess of the density matrix D_n at time t_n.

Thus, the problem formulation can be seen as an extrapolation problem of the following form: given the set of couples $(\mathbf{R}(t_i), D_i)$ and a new position vector $\mathbf{R}(t_n)$ provide a guess for the solution D_n. Here and in the remaining part of the article, we restrict ourselves on the positions of the QM atoms, that is, with slight abuse of notation, we denote from now on by $\mathbf{R}$ the set of QM positions only, even within a QM−MM context.

In order to approximate the mapping $\mathbf{R} \to D_{\mathbf{R}}$, we split this mapping in several submaps that will be composed as follows

$$\begin{aligned} &\mathbb{R}^{3M} \to \mathcal{M} \to \mathcal{T}_{D_0} \to \mathcal{G}r(N, \mathcal{N}) \\ &\mathbf{R} \to d_{\mathbf{R}} \to \Gamma_{\mathbf{R}} \to D_{\mathbf{R}} = \mathrm{Exp}_{D_0}(\Gamma_{\mathbf{R}}) \end{aligned} \tag{5}$$

where the first line shows the concatenation of maps in terms of spaces and the second in terms of variables. The different mappings will be presented and motivated in the following.

The first map is a mapping of the nuclear coordinates $\mathbf{R} \in \mathbb{R}^{3M}$ to a (possibly high-dimensional) molecular descriptor that accounts for certain symmetries and invariances of the molecule. The last map, known as the Grassmann exponential, is introduced in order to obtain a resulting density matrix belonging to $\mathcal{G}r(N, \mathcal{N})$ and thus to guarantee that the guess fulfils all properties of a density matrix. As $\mathcal{G}r(N, \mathcal{N})$ is a manifold, this is not straightforward. The second mapping is the one that we aim to approximate but before we do that let us first introduce those two special mappings, that is, the molecular descriptor and the Grassmann exponential, in more details.

2.1. Molecular Descriptors. The map $\mathbf{R} \to d_{\mathbf{R}}$ is a map from atomic positions to molecular descriptors. These descriptors are used as fingerprints for the considered molecular configurations. Such molecular descriptors have been widely used in the past decades, for example, to learn potential energy surfaces (PESs)[20−26] or to predict other quantities of interest. Among widely used descriptors, one can find Behler−Parinello symmetry functions,[27] Coulomb matrix,[21] smooth overlap of atomic positions (SOAP),[28] permutationally invariant polynomials,[29] or the atomic cluster expansion (ACE).[30,31] These molecular descriptors are usually designed to retain similar symmetries as the targeted quantities of interest.

In this work, the quantity we are approximating is the density matrix, which is invariant with respect to translations and permutations of like particles. The transformation of the density matrix with respect to a global rotation of the system depends on the implementation, as it is possible to consider either a fixed Cartesian frame or one that moves with respect to the molecular system. In the former case, there is an equivariance with respect to rotations of the molecular system, while in the latter, the density matrix is invariant. We should therefore in principle use a molecular descriptor satisfying those properties.

However, the symmetry properties we will rely on are mostly translation and rotation invariance. Therefore, we will use a simple descriptor in the form of the Coulomb matrix denoted by $d_{\mathbf{R}}$, given by

$$(d_{\mathbf{R}})_{ij} = \begin{cases} 0.5 z_i^{2.4} & \text{if } i = j \\ \dfrac{z_i z_j}{\|\mathbf{R}(t_i) - \mathbf{R}(t_j)\|} & \text{otherwise} \end{cases} \tag{6}$$

Note that such a descriptor is not invariant (nor equivariant) with respect to permutations of identical particles. However, we have found this descriptor to offer a good trade-off between simplicity and efficiency. Note that since we aim to extrapolate the density matrix from previous time steps, permutations of identical particles never occur from one time step to another and we do not need to rely on this property. Nevertheless, we expect that a better description could be achieved using more flexible descriptors, such as ACE polynomials or the SOAP descriptors, where the descriptors themselves can be tuned.

2.2. Grassmann Exponential. We only give a brief overview as the technical details have already been reported elsewhere,[19,32,33] and are recapitulated in the Supporting Information. The set $\mathcal{G}r(N, \mathcal{N})$ is a smooth manifold and thus, at any point, say $D_0 \in \mathcal{G}r(N, \mathcal{N})$ in our application, there exists the tangent space $\mathcal{T}_{D_0}$ such that one can associate nearby points $D \in \mathcal{G}r(N, \mathcal{N})$ to tangent vectors $\Gamma(D) \in \mathcal{T}_{D_0}$. The mapping $D \to \mathrm{Log}_{D_0}(D) = \Gamma(D)$ is known as the Grassmann logarithm and its inverse mapping is known as the Grassmann exponential $\Gamma \to \mathrm{Exp}_{D_0}(\Gamma) = D$. Furthermore, $\mathrm{Log}_{D_0}(D_0) = 0$ and $\mathrm{Exp}_{D_0}(0) = D_0$. These mappings are not only abstract tools from differential geometry but can also be computed by means of performing a singular value decomposition (SVD).[19,32,33] In our application, we use the same reference point D_0 in all cases which brings some computational advantages as will be discussed in more detail in the upcoming Section 2.3.

2.3. Approximation Problem. Since the tangent space $\mathcal{T}_{D_0}$ is a (linear) vector space, we can now aim to approximate the mapped density matrix on the tangent space $\mathcal{T}_{D_0}$. To simplify the presentation, we shift the indices in the following and describe the extrapolation method for the first N_t time steps. In the general setting, we should consider the positions $\mathbf{R}(t_i)$ for $i = n - N_t, ..., n - 1$, to extrapolate the density matrix at position $\mathbf{R}(t_n)$, where n is the current time step of the MD. We look for parameter functions c_i such that, given previous snapshots $\Gamma_i = \mathrm{Log}(D_i)$ for i from 1 to N_t, corresponding to some $\mathbf{R}(t_i)$'s, the approximation of any density matrix on the tangent space is written as

$$\mathbf{R} \to \Gamma_{\mathrm{app}}(\mathbf{R}) = \sum_{i=1}^{N_t} c_{\mathbf{R},i} \Gamma_i \in \mathcal{T}_{D_0} \tag{7}$$

with $\Gamma_i = \Gamma_{\mathbf{R}(t_i)}$.

The question is then how to find these coefficient functions $c_{\mathbf{R},i}$ and we propose to find those via the resolution of a

https://doi.org/10.1021/acs.jctc.1c00751
J. Chem. Theory Comput. 2021, 17, 6965−6973

Algorithm 1: Density extrapolation framework G-Ext

Data: Array desc containing the descriptors for k previous time-steps, p_n the descriptor for the current position, C_{n-1} and S_{n-1} respectively the molecular orbitals and overlap matrices of the previous time-step, and cref the reference point on the Grassmannian

Result: Guess density matrix for time-step $n > 1$

begin

$\texttt{cmat}(:, :, n-1) \leftarrow \texttt{Orthonormalization}(C_{n-1}, S_{n-1})$;
$\texttt{gmat}(:, :, n-1) \leftarrow \texttt{Log}(\texttt{cref}, \texttt{cmat}(:, :, n-1))$;
$\texttt{desc}, p_n \leftarrow \texttt{Stabilization}(\texttt{desc}, p_n)$;
$\texttt{c} \leftarrow \texttt{LeastSquares}(\texttt{desc}, p_n)$;
$\Gamma_{\text{app}} \leftarrow \sum_{i=n-1-k}^{n-1} \texttt{c}(i) \cdot \texttt{gmat}(:, :, i)$;
$C_{\text{app}} \leftarrow \texttt{Exp}(\texttt{cref}, \Gamma_{\text{app}})$;
return $2 \cdot C_{\text{app}} \cdot C_{\text{app}}^{\mathrm{T}}$;

(standard) least-square minimization problem. For a given position $\mathbf{R}$, we look for coefficients that minimize the l^2-error between the descriptor $d_{\mathbf{R}}$ and a linear combination of the previous ones $d_{\mathbf{R}(ti)}$

$$\min_{c_{\mathbf{R}} \in \mathbb{R}^{N_t}} \left\| d_{\mathbf{R}} - \sum_{i=1}^{N_t} c_{\mathbf{R},i} d_{\mathbf{R}(t_i)} \right\|^2 \tag{8}$$

In the matrix form, this simply reads

$$\min_{c_{\mathbf{R}} \in \mathbb{R}^{N_t}} \| d_{\mathbf{R}} - P^{\mathrm{T}} c_{\mathbf{R}} \|^2 \tag{9}$$

where P is the matrix of size $N_t \times N_d$ containing the descriptors $P_{i,j} := (d_{\mathbf{R}(t_i)})_j$. Note that we only fit on the level of the descriptor, that is, the mapping from the position vector $\mathbf{R}$ to the descriptor $d_{\mathbf{R}}$ and that this method is similar to the ones used by Alfè[2] and Arias et al.,[3] where the descriptors they used were the positions of the atoms and only considered the previous three time steps of the MD.

If the system is underdetermined, we select the vector $c_{\mathbf{R}}$ that has the smallest norm. However, in general, the system is overdetermined as we have more descriptors than snapshots. This implies that this formulation verifies the interpolation principle: for every i and j from 1 to N_t, the solution of problem (8) at the positions $\mathbf{R}(t_j)$ satisfies $c_{\mathbf{R}(t_j)i} = \delta_{ji}$.

In principle, should we consider a large amount of previous descriptors, then the system may become undetermined and violate the interpolation principle. To mitigate this, we can use a stabilization scheme, as explained in the upcoming subsection.

Note that once we have computed the coefficients $c_{\mathbf{R}}$ by solving problem (12), one computes the initial guess for the density using the same coefficients in the linear combination on the tangent space as in eq 7 and finally takes the exponential (see eq 5). The rational for this step is that if the second mapping in eq 5, which we denote here by $\mathcal{F}$: $\mathcal{M} \to \mathcal{T}_{D_0}$, was linear, then there would hold

$$\mathcal{F}\left(\sum_{i=1}^{N_t} c_{\mathbf{R},i} d_{\mathbf{R}_i} \right) = \sum_{i=1}^{N_t} c_{\mathbf{R},i} \mathcal{F}(d_{\mathbf{R}_i}) = \sum_{i=1}^{N_t} c_{\mathbf{R},i} \Gamma_i \tag{10}$$

In practice, the mapping is, however, not linear and this approach works well in the test cases we considered. A possible explanation for this is the unfolding of the nuclear coordinates into a high-dimensional descriptor-space $\mathcal{M}$. Indeed, the high-dimensionality of $\mathcal{M}$ seems to allow an accurate approximation of $\mathcal{F}$ by a linear map. Furthermore, if the system is overdetermined, the scheme satisfies the interpolation property $\Gamma_j = \Gamma(\mathbf{R}(t_j))$, and hence, we recover the expected density matrix $D_{\mathbf{R}(t_j)} = \mathrm{Exp}\, P_{D_0}(\Gamma_j)$.

2.3.1. Stabilization. To stabilize the extrapolation by limiting high oscillations of the coefficients, we apply a Tikhonov regularization

$$\min_{c_{\mathbf{R}} \in \mathbb{R}^{N_t}} \left(\left\| d_{\mathbf{R}} - \sum_{i=1}^{N_t} c_{\mathbf{R},i} d_{\mathbf{R}_i} \right\|^2 + \varepsilon \| c_{\mathbf{R}} \|^2 \right) \tag{11}$$

for some choice of ε. This problem is always well-posed and corresponds to solving the following problem

$$\min_{c_{\mathbf{R}} \in \mathbb{R}^{N_t}} \| \tilde{d}_{\mathbf{R}} - \tilde{P}^{\mathrm{T}} c_{\mathbf{R}} \|^2 \tag{12}$$

where $\tilde{d}_{\mathbf{R}} \in \mathbb{R}^{N_d + N_t}$ is the vector $d_{\mathbf{R}}$ padded with N_t zeroes and $\tilde{P} \in \mathbb{R}^{N_t} \times \mathbb{R}^{N_d + N_t}$ is the P matrix padded with the square diagonal matrix $\varepsilon \mathrm{Id}_{N_t}$. We observe in practice that using such a stabilization makes possible to use more previous points without degradation of the initial guess.

2.4. Final Algorithm. Given previous density matrices $D_{\mathbf{R}(t_j)}$ for $j = 1, \ldots, N_t$, the initial guess is computed following Algorithm 1. That is, we start by computing the logarithms of the density matrices $D_{\mathbf{R}(t_j)}$, from the coefficients $C_{\mathbf{R}(t_j)}$ that are first orthonormalized by performing $\tilde{C}_{\mathbf{R}} = S_{\mathbf{R}}^{1/2} C_{\mathbf{R}}$. Here, we remark that we assume that the density matrices $D_{\mathbf{R}(t_j)}$ have been previously Löwdin orthonormalized.

We then compute the descriptors needed to build the $\tilde{P}$ matrix and solve problem (12). This provides the coefficients in the linear combination of the Γ_i's on the tangent space. Finally, we compute the exponential of the linear combination in order to obtain the predicted density matrix.

Note that the reference point D_0 is chosen once and for all, which makes the computations of these logarithms lighter, even though there is no theoretical justification for keeping a single point D_0 as a reference. Indeed, it is known that the formulae are only correct locally (around D_0) on the manifold. However, in practice, we have never observed the need to change the reference point. This enables us to compute only one logarithmic map per time step and hence, only two SVDs in total per time step. To have a robust algorithm that will work even in this edge case, it will be sufficient to check that the exponential and logarithmic maps are still inverse of one another.

Finally, to be on the safe side with respect to the computations of the exponential, we have added a check on the orthogonality of the matrix that is obtained: if the residue is

https://doi.org/10.1021/acs.jctc.1c00751
J. Chem. Theory Comput. 2021, 17, 6965−6973

higher than a certain threshold, we then perform an orthogonalization of the result.

3. NUMERICAL TESTS

In this section, we present a series of numerical tests of the newly developed strategy. We test our method on four different systems. All the systems have been an object of a previous or current study by some of us and can therefore be considered representative of real-life applications.

The first system is 3-hydroxyflavone (3HF) in acetonitrile.[18] Two systems (OCP and APPA) are chromophores embedded in a biological matrix—namely, a carotenoid in the orange carotenoid protein (OCP) and avine in acid phosphatase (APPA), a blue light-using flavine photoreceptor.[34−36] The fourth system is dimethylaminobenzonitrile (DMABN) in methanol.[14] The main characteristics of the systems used for testing are recapitulated in Table 1.

Table 1. Overview of the System Size in Terms of Number of QM Atoms (N_{QM}), Number of MM Atoms (N_{MM}), and the Total Number of QM Basis Functions ($\mathcal{N}$)

system	N_{QM}	N_{MM}	$\mathcal{N}$
OCP	129	4915	1038
APPA	31	16,449	309
DMABN	21	6843	185
3HF	28	15,018	290

The systems used for testing include a quite large QM chromophore, the OCP, and three medium-sized systems, embedded in large- (APPA and 3HF) and medium-sized environments (DMABN), and are representative of different possible scenarios.

To test the performances of the new G-Ext strategy, we performed three sets of short (1 ps) multiscale BOMD simulations on OCP, APPA, 3HF, and DMABN. KS density functional theory was used to model the QM subsystem, using the B3LYP[37] hybrid functional and Pople's 6-31G(d) basis set.[38] For the stability and energy conservation of the method, we did a longer and more realistic simulations of 10 ps on 3HF, where the flavone moiety was described using the ωB97X hybrid functional[39] and Pople's 6-31G(d) basis set. In all cases, the environment was modeled using the AMOEBA polarizable force field.[40]

All the simulations have been performed using the Gaussian−Tinker interface previously developed by some of us.[12,13] In particular, we use a locally modified development version of Gaussian[41] to compute the QM, electrostatic, and polarization energy and forces and Tinker[42] to compute all other contributions to the QM/MM energy. We implemented the G-Ext extrapolation scheme in Tinker that acts as the main driver for the MD simulation, being responsible of summing together all the various contributions to the forces and propagating the trajectory. At each MD step, using the GauOpen interface,[43] the density matrix, molecular orbital (MO) coefficients, and overlap matrix produced by Gaussian are retrieved. These are used to compute the extrapolated density, as described in Section 2. The density is then passed back to Gaussian to be used for the next MD step. All the simulations were carried out in the NVE ensemble, using the velocity Verlet integrator and a 0.5 fs time step. Concerning stabilization, we found that good overall results were obtained using a parameter $\varepsilon := 10^3 \times r_{scf}$, where r_{scf} is the tolerance of the SCF algorithm.

3.1. Numerical Results. To assess the performance of the G-Ext guess, we perform 1 ps MD simulations on the four systems described in Section 3 starting from the same exact conditions (positions and initial velocities) and using various strategies to compute the guess density for the SCF solver. We compare various flavors of the G-Ext method with the XLBO extrapolation scheme.[10] Here, we note that the original XLBO method performs a propagation of an auxiliary density matrix, which is then used as a guess. The latter is not idempotent: to restore such a property, we perform a purification step at the beginning of the SCF procedure using McWeeny's algorithm.[44] In the following, we therefore compare our method, where we use 3 to 6 previous points for the fitting and extrapolation, to both the standard XLBO and to XLBO followed by purification (XLBO/MW). We use an SCF convergence threshold of 10^{-5} with respect to the RMS variation of the density.

We report in Table 2, for each method, the average number of SCF iterations performed along the MD simulation together with the associated standard deviation. As the XLBO strategy requires eight previous points, during which a standard SCF is performed, we discard the first points from the evaluation of the aforementioned quantities to have a fairer comparison.

We do not report the total time required to compute the guess, as it is in all cases very small (up to 0.1 s wall clock time for the largest system using the G-Ext(6) guess). This is an important consideration, as the G-Ext method requires one to perform various linear-algebra operations (in particular, thin SVD) that can in principle be expensive. Thanks to the

Table 2. Performances of the G-Ext Method for Different Numbers of Extrapolation Points, Compared with the XLBO Algorithm with and without McWeeny Purification[a]

	OCP		DMABN		APPA		3HF	
method	average	σ	average	σ	average	σ	average	σ
XLBO	3.82	0.66	3.98	0.16	3.00	0.03	4.00	0.14
XLBO/MW	2.95	0.31	3.76	0.56	3.00	0.34	3.96	0.31
G-Ext(3)	2.57	0.84	3.54	0.78	2.95	0.50	3.09	0.41
G-Ext(4)	2.48	0.88	3.14	0.62	2.51	0.50	3.25	0.68
G-Ext(5)	2.25	0.96	3.23	0.75	2.51	0.50	3.30	0.72
G-Ext(6)	2.20	0.96	2.99	0.02	2.51	0.50	3.14	0.56

[a]All the results were obtained using a 10^{-5} convergence threshold for the RMS increment of the density matrix and are derived from a 1 ps long MD simulation, using a 0.5 fs time step. We report the average number of iterations required to converge the SCF, together with the associated standard deviation. Note that the first eight steps were discarded.

https://doi.org/10.1021/acs.jctc.1c00751
J. Chem. Theory Comput. 2021, 17, 6965−6973

Journal of Chemical Theory and Computation pubs.acs.org/JCTC Article

Table 3. Performances of the G-Ext(6) Method Compared with the XLBO Algorithm with McWeeny Purification[a]

	OCP		DMABN		APPA		3HF	
method	average	σ	average	σ	average	σ	average	σ
XLBO/MW	5.02	0.17	7.30	0.64	7.49	0.84	7.47	0.63
G-Ext(6)	3.58	0.79	4.23	0.50	4.39	0.57	6.81	0.78

[a]All the results were obtained using a 10^{-7} convergence threshold for the RMS increment of the density matrix and are derived from a 1 ps long MD simulation, using a 0.5 fs time step. We report the average number of iterations required to converge the SCF, together with the associated standard deviation. Note that the first eight steps were discarded.

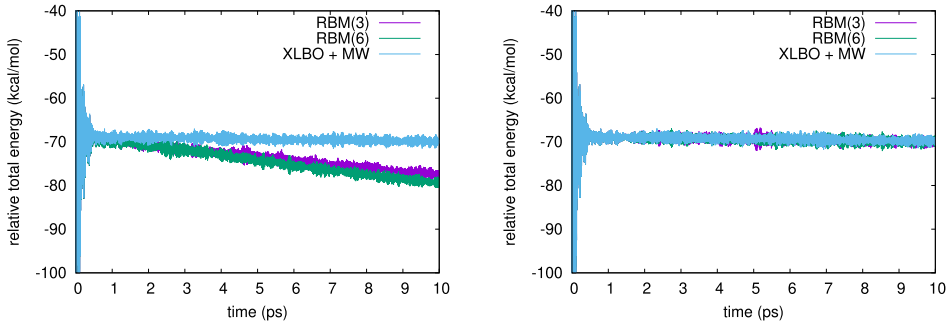

Figure 1. Total energy (kcal/mol) as a function of simulation time (fs) for 3HF comparing G-Ext(3), G-Ext(6), and XLBO with McWeeny purification, using a convergence threshold for the SCF algorithm of 10^{-5} (left panel) and 10^{-7} (right panel). The total energy was shifted to +505,000 kcal/mol for readability.

availability of optimized LAPACK libraries, this is in practice not a problem.

From the results in Table 2, we see that the G-Ext algorithms systematically outperforms the XLBO method. It is interesting to note that the McWeeny purification step has a sizeable effect on the performances of the XLBO method only for the largest system, OCP, where it results in the gain of almost one SCF iteration on average. On the other systems, the purification step has a smaller effect.

In all the systems we tested, the performances of the G-Ext method are systematically better than in XLBO, including McWeeny purification. The effectiveness of the G-Ext extrapolation increases when going from 3 to 6 points but quickly stagnates. We have performed further tests with more than 6 (up to 20) extrapolation points but never noted any further gain.

We observe a reduction in the number of iterations that goes from 0.5 in DMABN to 0.75 in OCP (1.62 when compared to XLBO without McWeeny purification). We remark that these gains, while apparently not so large, are greatly amplified during the MD simulation, due to the large number of steps that need to be performed.

The tests performed with a 10^{-5} convergence threshold are representative of a standard, DFT ground-state BOMD simulation. When performing a more sophisticated quantum mechanical calculation, such as a BOMD on an excited-state PES,[18] such a convergence threshold may not be sufficient to guarantee the stability of the simulation, as the SCF solution is used to set up the linear response equations and the numerical error can be amplified, resulting in poorly accurate forces.

We tested the G-Ext algorithm in its best-performing version, the one that uses six extrapolation points, with a tighter, 10^{-7} threshold, again for the RMS variation of the density. The results are reported in Table 3, where we compare the G-Ext(6) scheme with the XLBO method with McWeeny purification.

The XLBO method is based on the propagation of an auxiliary density, and therefore, the accuracy of the guess it generates depends little on the accuracy of the previous SCF densities. As a consequence, its performances are reduced if a tighter convergence is required. The G-Ext guess, on the other hand, uses previously computed densities as its building blocks and one can expect the accuracy of the resulting guess to be linked to the convergence threshold used during the simulation.

This is exactly what we observe. Using a threshold of 10^{-7}, the G-Ext(6) guess exhibits significantly better performances than XLBO, gaining, on average, from about 0.7 to about 3 SCF iterations on the tested systems.

3.1.1. Stability. The good performances of the G-Ext guess come, however, at a price, namely, the lack of time reversibility. We can thus expect the total energy in an NVE simulation to exhibit a long-time drift (LTD). Time reversibility and long-time energy conservation are, on the other hand, one of the biggest strengths of the XLBO method.

To investigate the stability of BOMD simulations using the G-Ext guess, we build a challenging case, where we start a BOMD simulation far from well-equilibrated conditions. We use the 3HF system as a test case and achieve the noisy starting conditions by starting from a well-equilibrated structure and changing the DFT functional from B3LYP to ωB97XD. This way, we have a physically acceptable structure, with no close atoms or other problematic structural situations, but obtain starting conditions that are far from equilibrium.

We report in Figure 1 the total energy along a 10 ps BOMD simulation of 3HF in acetonitrile using either a 10^{-5} SCF convergence threshold (left panel) or a 10^{-7} one (right panel). The same results for a 10^{-6} threshold are reported in the Supporting Information. We compare the G-Ext(3) and G-Ext(6) methods to the XLBO one including McWeeny purification. As already noted, while in principle the

https://doi.org/10.1021/acs.jctc.1c00751
J. Chem. Theory Comput. 2021, 17, 6965−6973

purification may spoil the time reversibility, this has no noticeable effect in practice.

The very noisy starting conditions are apparent from the energy profiles that exhibit large oscillations in the first couple of hundreds of femtoseconds.

To better estimate the short- and long-time energy stability, we report in Table 4 the average short-time fluctuation (STF) and LTD of the energy. The former is computed by taking the RMS of the energy fluctuation every 50 fs and averaging the results over the trajectory, discarding the first 500 fs, the latter by fitting the energy with a linear function and taking the slope.

Table 4. Short- and Long-Term Stability Analysis of the G-Ext(3) and G-Ext(6) Methods, Compared to the XLBO Algorithm with McWeeny Purification, for the 3HF System[a]

	conv. 10^{-5}		conv. 10^{-6}		conv. 10^{-7}	
method	STF	LTD	STF	LTD	STF	LTD
XLBO/MW	0.55	−0.04	0.55	−0.03	0.57	−0.03
G-Ext(3)	0.55	−0.42	0.57	−0.15	0.53	−0.04
G-Ext(6)	0.56	−0.53	0.52	−0.13	0.57	−0.04

[a]For each method, we report the STF and the LTD and the average number of SCF iterations, for three convergence thresholds of the SCF algorithm.

All methods show comparable short-term stability, which is to be mainly ascribed to the chosen integration time step. On the other hand, from both the results in Table 4 and Figure 1, we observe a clear drift of the energy when the G-Ext method is used. In particular, the system cools of about 10 kcal/mol with either G-Ext(3) or G-Ext(6). The XLBO trajectory, despite the McWeeny purification, exhibits an almost perfect energy conservation.

These results are not surprising but should be taken into account when choosing to use the G-Ext guess, which, if coupled to a 10^{-5} SCF convergence threshold, cannot guarantee long-term energy conservation. The drift is overall not too large and can be handled using a thermostat. Whether or not the trade between performances and energy conservation is acceptable for a production simulation is a decision that ultimately lies with the user.

Increasing the accuracy of the SCF computation improves the overall stability for G-Ext, which is already good at 10^{-6} and becomes virtually identical to the one offered by the XLBO method at 10^{-7}.

4. CONCLUSIONS

In this contribution, we presented an extrapolation scheme to predict initial guesses of the density matrix for the SCF iterations within BOMD. What makes our approach new is that we enforce the idempotency of the density matrix by extrapolating not the densities themselves but their map onto a vector space, which is the tangent plane to the manifold of the physically acceptable densities. Such a map is locally bijective so that after performing the extrapolation, we can map the new density back to the original manifold, providing thus an idempotent density. The main element of novelty of the algorithm is that by working on a tangent space, it allows one to use any linear extrapolation technique, while, at the same time, automatically ensuring the correct geometrical structure of the density matrix. As such, the technique presented in this paper can be seen as a simple case of a more general framework. Such a framework allows one to recast the problem of predicting a guess density by extrapolating information available from previous MD steps as a mapping between two vector spaces, that is, the space of molecular descriptors and the tangent plane. This geometric approach can be seen as an alternative to extrapolating quantities derived from the density, such as the Fock or Kohn−Sham matrix, as proposed by Pulay and Fogarasi[4] and by Herbert and Head-Gordon.[5] However, the framework we developed, using molecular descriptors and a general linear extrapolation technique, can in principle be easily extended to such approaches.

That being said, our choices of both the molecular descriptor and of the extrapolation strategies are far from being unique. In recent years, molecular descriptors gained attraction within the rise of machine-learning (ML) techniques. Our choice, namely, using the Coulomb matrix, is only one of the many possibilities, and while being simple and effective, more advanced descriptors may be used and possibly improve the overall performances of the method. We also used a straightforward (stabilized) least-square interpolation of the descriptors at the previous point to compute the extrapolation coefficients for the densities. This strategy is, again, simple yet effective. However, many other approaches can be used. In particular, ML techniques may not only provide a very accurate approximated map but also benefit of a larger amount of information (i.e., use the densities computed at a large number of previous steps), further improving the accuracy of the guess. Improvements on the descriptors and extrapolation strategies are not the only possible extensions of the proposed method. A natural extension that is under active investigation is the application to the G-Ext guess to geometry optimization, for which the XLBO scheme cannot be used.

Overall, even the simple choices made in this contribution produced an algorithm that exhibits promising performances. In all our tests, the G-Ext method outperformed the well-established XLBO technique, especially for tighter SCF accuracies which may be relevant for post-SCF BOMD computations, including computations on excited-state PES. While we tested the method only for KS DFT, it can also be used for HF or semiempirical calculations. The main disadvantage of the proposed strategy with respect to the XLBO method is, however, the lack of time reversibility, which manifests itself as a lack of long-term energy conservation. In particular, for longer MD simulations, the total energy may exhibit a visible drift, which is something that the user must be aware of. In our test, the observed drift was relatively small and the use of a thermostat should be enough to avoid problems in practical cases; however, this is a clear, and expected, limitation of the proposed approach. We note that using a tighter SCF convergence, which is also the case where the proposed method shows its best performances and produces an energy conserving trajectory, even starting from very noisy conditions. A time-reversible generalization of the G-Ext method is anyways particularly attractive and is at the moment under active investigation.

■ ASSOCIATED CONTENT

Supporting Information

The Supporting Information is available free of charge at https://pubs.acs.org/doi/10.1021/acs.jctc.1c00751.

Julia template of the G-Ext algorithm is available at https://github.com/epolack/GExt.jl, figure representing the total energy computation with an SCF convergence

https://doi.org/10.1021/acs.jctc.1c00751
J. Chem. Theory Comput. 2021, 17, 6965−6973

Journal of Chemical Theory and Computation pubs.acs.org/JCTC Article

threshold of 10^{-6} for the molecule 3HF, and formulae for the exponential and logarithm functions (PDF)

AUTHOR INFORMATION

Corresponding Author

Filippo Lipparini − *Dipartimento di Chimica e Chimica Industriale, Univeristà di Pisa, I-56124 Pisa, Italy;* orcid.org/0000-0002-4947-3912; Email: filippo.lipparini@unipi.it

Authors

Étienne Polack − *Laboratoire de Mathématiques de Besançon, UMR CNRS 6623, Université Bourgogne Franche-Comté, 25030 Besançon, France*

Geneviève Dusson − *Laboratoire de Mathématiques de Besançon, UMR CNRS 6623, Université Bourgogne Franche-Comté, 25030 Besançon, France*

Benjamin Stamm − *Department of Mathematics, RWTH Aachen University, 52062 Aachen, Germany*

Complete contact information is available at: https://pubs.acs.org/10.1021/acs.jctc.1c00751

Funding

Part of this work was supported by the French "Investissements d'Avenir" program, project ISITE-BFC (contract ANR-15-IDEX-0003).

Notes

The authors declare no competing financial interest.

REFERENCES

(1) Fang, J.; Gao, X.; Song, H.; Wang, H. On the Existence of the Optimal Order for Wavefunction Extrapolation in Born-Oppenheimer Molecular Dynamics. *J. Chem. Phys.* **2016**, *144*, 244103.

(2) Alfè, D. Ab Initio Molecular Dynamics, a Simple Algorithm for Charge Extrapolation. *Comput. Phys. Commun.* **1999**, *118*, 31−33.

(3) Arias, T. A.; Payne, M. C.; Joannopoulos, J. D. Ab Initio Molecular-Dynamics Techniques Extended to Large-Length-Scale Systems. *Phys. Rev. B: Condens. Matter Mater. Phys.* **1992**, *45*, 1538−1549.

(4) Pulay, P.; Fogarasi, G. Fock Matrix Dynamics. *Chem. Phys. Lett.* **2004**, *386*, 272−278.

(5) Herbert, J. M.; Head-Gordon, M. Accelerated, Energy-Conserving Born−Oppenheimer Molecular Dynamics via Fock Matrix Extrapolation. *Phys. Chem. Chem. Phys.* **2005**, *7*, 3269−3275.

(6) Hutter, J.; Parrinello, M.; Vogel, S. Exponential Transformation of Molecular Orbitals. *J. Chem. Phys.* **1994**, *101*, 3862−3865.

(7) VandeVondele, J.; Hutter, J. An Efficient Orbital Transformation Method for Electronic Structure Calculations. *J. Chem. Phys.* **2003**, *118*, 4365−4369.

(8) VandeVondele, J.; Krack, M.; Mohamed, F.; Parrinello, M.; Chassaing, T.; Hutter, J. Quickstep: Fast and Accurate Density Functional Calculations Using a Mixed Gaussian and Plane Waves Approach. *Comput. Phys. Commun.* **2005**, *167*, 103−128.

(9) Niklasson, A. M. N.; Tymczak, C. J.; Challacombe, M. Time-Reversible Born-Oppenheimer Molecular Dynamics. *Phys. Rev. Lett.* **2006**, *97*, 123001.

(10) Niklasson, A. M. N. Extended Born-Oppenheimer Molecular Dynamics. *Phys. Rev. Lett.* **2008**, *100*, 123004.

(11) Niklasson, A. M. N.; Steneteg, P.; Odell, A.; Bock, N.; Challacombe, M.; Tymczak, C. J.; Holmström, E.; Zheng, G.; Weber, V. Extended Lagrangian Born−Oppenheimer Molecular Dynamics with Dissipation. *J. Chem. Phys.* **2009**, *130*, 214109.

(12) Loco, D.; Lagardère, L.; Caprasecca, S.; Lipparini, F.; Mennucci, B.; Piquemal, J.-P. Hybrid QM/MM Molecular Dynamics with AMOEBA Polarizable Embedding. *J. Chem. Theory Comput.* **2017**, *13*, 4025−4033.

(13) Loco, D.; Lagardère, L.; Cisneros, G. A.; Scalmani, G.; Frisch, M.; Lipparini, F.; Mennucci, B.; Piquemal, J.-P. Towards large scale hybrid QM/MM dynamics of complex systems with advanced point dipole polarizable embeddings. *Chem. Sci.* **2019**, *10*, 7200−7211.

(14) Nottoli, M.; Mennucci, B.; Lipparini, F. Excited State Born-Oppenheimer Molecular Dynamics through a coupling between Time Dependent DFT and AMOEBA. *Phys. Chem. Chem. Phys.* **2020**, *22*, 19532−19541.

(15) Bondanza, M.; Nottoli, M.; Cupellini, L.; Lipparini, F.; Mennucci, B. Polarizable embedding QM/MM: the future gold standard for complex (bio)systems? *Phys. Chem. Chem. Phys.* **2020**, *22*, 14433−14448.

(16) Niklasson, A. M. N. Next generation extended Lagrangian first principles molecular dynamics. *J. Chem. Phys.* **2017**, *147*, 054103.

(17) Niklasson, A. M. N. Density-Matrix Based Extended Lagrangian Born−Oppenheimer Molecular Dynamics. *J. Chem. Theory Comput.* **2020**, *16*, 3628−3640.

(18) Nottoli, M.; Bondanza, M.; Lipparini, F.; Mennucci, B. An enhanced sampling QM/AMOEBA approach: The case of the excited state intramolecular proton transfer in solvated 3-hydroxyflavone. *J. Chem. Phys.* **2021**, *154*, 184107.

(19) Polack, É.; Mikhalev, A.; Dusson, G.; Stamm, B.; Lipparini, F. An Approximation Strategy to Compute Accurate Initial Density Matrices for Repeated Self-Consistent Field Calculations at Different Geometries. *Mol. Phys.* **2020**, *118*, No. e1779834.

(20) Behler, J. Neural network potential-energy surfaces in chemistry: a tool for large-scale simulations. *Phys. Chem. Chem. Phys.* **2011**, *13*, 17930−17955.

(21) Rupp, M.; Tkatchenko, A.; Müller, K.-R.; von Lilienfeld, O. A. Fast and Accurate Modeling of Molecular Atomization Energies with Machine Learning. *Phys. Rev. Lett.* **2012**, *108*, 058301.

(22) Bartók, A. P.; Gillan, M. J.; Manby, F. R.; Csányi, G. Machine-learning approach for one- and two-body corrections to density functional theory: Applications to molecular and condensed water. *Phys. Rev. B: Condens. Matter Mater. Phys.* **2013**, *88*, 054104.

(23) Behler, J. Constructing high-dimensional neural network potentials: A tutorial review. *Int. J. Quantum Chem.* **2015**, *115*, 1032−1050.

(24) Manzhos, S.; Dawes, R.; Carrington, T. Neural network-based approaches for building high dimensional and quantum dynamics-friendly potential energy surfaces. *Int. J. Quantum Chem.* **2015**, *115*, 1012−1020.

(25) Chmiela, S.; Tkatchenko, A.; Sauceda, H. E.; Poltavsky, I.; Schütt, K. T.; Müller, K.-R. Machine learning of accurate energy-conserving molecular force fields. *Sci. Adv.* **2017**, *3*, No. e1603015.

(26) Chmiela, S.; Sauceda, H. E.; Müller, K.-R.; Tkatchenko, A.; Tkatchenko, A. Towards exact molecular dynamics simulations with machine-learned force fields. *Nat. Commun.* **2018**, *9*, 3887.

(27) Behler, J.; Parrinello, M. Generalized neural-network representation of high-dimensional potential-energy surfaces. *Phys. Rev. Lett.* **2007**, *98*, 146401.

(28) Goscinski, A.; Fraux, G.; Imbalzano, G.; Ceriotti, M. The role of feature space in atomistic learning. *Mach. Learn.: Sci. Technol.* **2021**, *2*, 025028.

(29) Braams, B. J.; Bowman, J. M. Permutationally invariant potential energy surfaces in high dimensionality. *Int. Rev. Phys. Chem.* **2009**, *28*, 577−606.

(30) Drautz, R. Atomic cluster expansion for accurate and transferable interatomic potentials. *Phys. Rev. B* **2019**, *99*, 014104.

(31) Bachmayr, M.; Csanyi, G.; Drautz, R.; Dusson, G.; Etter, S.; van der Oord, C.; Ortner, C. Atomic Cluster Expansion: Completeness, Efficiency and Stability, **2019**. arxiv:1911.03550, https://arxiv.org/abs/1911.03550.

(32) Edelman, A.; Arias, T. A.; Smith, S. T. The Geometry of Algorithms with Orthogonality Constraints. *SIAM J. Matrix Anal. Appl.* **1998**, *20*, 303−353.

(33) Zimmermann, R. Manifold Interpolation and Model Reduction, **2019**. arxiv:1902.06502, http://arxiv.org/abs/1902.06502.
(34) Bondanza, M.; Cupellini, L.; Lipparini, F.; Mennucci, B. The Multiple Roles of the Protein in the Photoactivation of Orange Carotenoid Protein. *Chem* **2020**, *6*, 187−203.
(35) Bondanza, M.; Cupellini, L.; Faccioli, P.; Mennucci, B. Molecular Mechanisms of Activation in the Orange Carotenoid Protein Revealed by Molecular Dynamics. *J. Am. Chem. Soc.* **2020**, *142*, 21829−21841.
(36) Hashem, S.; Macaluso, V.; Nottoli, M.; Lipparini, F.; Cupellini, L.; Mennucci, B. From crystallographic data to the solution structure of photoreceptors: the case of the AppA BLUF domain. *Chem. Sci.* **2021**, DOI: 10.1039/D1SC03000K.
(37) Becke, A. D. Density-functional thermochemistry. III. The role of exact exchange. *J. Chem. Phys.* **1993**, *98*, 5648−5652.
(38) Hehre, W. J.; Ditchfield, R.; Pople, J. A. Self-Consistent Molecular Orbital Methods. XII. Further Extensions of Gaussian-Type Basis Sets for Use in Molecular Orbital Studies of Organic Molecules. *J. Chem. Phys.* **1972**, *56*, 2257−2261.
(39) Chai, J.-D.; Head-Gordon, M. Long-range corrected hybrid density functionals with damped atom-atom dispersion corrections. *Phys. Chem. Chem. Phys.* **2008**, *10*, 6615−6620.
(40) Ponder, J. W.; Wu, C.; Ren, P.; Pande, V. S.; Chodera, J. D.; Schnieders, M. J.; Haque, I.; Mobley, D. L.; Lambrecht, D. S.; DiStasio, R. A.; Head-Gordon, M.; Clark, G. N. I.; Johnson, M. E.; Head-Gordon, T. Current Status of the AMOEBA Polarizable Force Field. *J. Phys. Chem. B* **2010**, *114*, 2549−2564.
(41) Frisch, M. J.; Trucks, G. W.; Schlegel, H. B.; Scuseria, G. E.; Robb, M. A.; Cheeseman, J. R.; Scalmani, G.; Barone, V.; Petersson, G. A.; Nakatsuji, H.; Li, X.; Caricato, M.; Marenich, A. V.; Bloino, J.; Janesko, B. G.; Gomperts, R.; Mennucci, B.; Hratchian, H. P.; Ortiz, J. V.; Izmaylov, A. F.; Sonnenberg, J. L.; Williams-Young, D.; Ding, F.; Lipparini, F.; Egidi, F.; Goings, J.; Peng, B.; Petrone, A.; Henderson, T.; Ranasinghe, D.; Zakrzewski, V. G.; Gao, J.; Rega, N.; Zheng, G.; Liang, W.; Hada, M.; Ehara, M.; Toyota, K.; Fukuda, R.; Hasegawa, J.; Ishida, M.; Nakajima, T.; Honda, Y.; Kitao, O.; Nakai, H.; Vreven, T.; Throssell, K.; Montgomery, J. A., Jr.; Peralta, J. E.; Ogliaro, F.; Bearpark, M. J.; Heyd, J. J.; Brothers, E. N.; Kudin, K. N.; Staroverov, V. N.; Keith, T. A.; Kobayashi, R.; Normand, J.; Raghavachari, K.; Rendell, A. P.; Burant, J. C.; Iyengar, S. S.; Tomasi, J.; Cossi, M.; Millam, J. M.; Klene, M.; Adamo, C.; Cammi, R.; Ochterski, J. W.; Martin, R. L.; Morokuma, K.; Farkas, O.; Foresman, J. B.; Fox, D. J. *Gaussian Development Version*, Revision J.16. 2020; Gaussian, Inc.: Wallingford CT, 2020.
(42) Rackers, J. A.; Wang, Z.; Lu, C.; Laury, M. L.; Lagardère, L.; Schnieders, M. J.; Piquemal, J.-P.; Ren, P.; Ponder, J. W. Tinker 8: Software Tools for Molecular Design. *J. Chem. Theory Comput.* **2018**, *14*, 5273−5289.
(43) Interfacing to Gaussian 16 (v2). https://gaussian.com/interfacing/ (last accessed June 1, 2018).
(44) McWeeny, R. Some Recent Advances in Density Matrix Theory. *Rev. Mod. Phys.* **1960**, *32*, 335−369.

https://doi.org/10.1021/acs.jctc.1c00751
J. Chem. Theory Comput. 2021, 17, 6965−6973

A strategy to compute accurate initial density matrices for repeated self-consistent field calculations

É. Polack [1] A. Mikhalev [2] G. Dusson [1] B. Stamm [2] F. Lipparini [3]

[1]Laboratoire de mathématiques de Besançon, Université de Bourgogne Franche-Comté [2]Center for Computational Engineering Science, RWTH Aachen [3]Dipartimento di Chimica e Chimica Industriale, Univeristà di Pisa

Problem statement

When performing Density Functional Theory or Hartree–Fock calculations, quite a share of the computational time comes from executing the self-consistent field iterations. Often, those calculations have to be done for the same molecular system, but at different geometries, e.g., when running ab-initio molecular dynamics simulations or geometry optimisations.

Although much has been done to develop convergence acceleration techniques for the self-consistent field procedure, less is known on how to efficiently exploit the abundance of information generated during previous computations to provide it with a good guess.

How can we make the most of repeated self-consistent field computations on the same molecular system?

Objectives

We wish to provide an accurate guess to density matrices for the self-consistent field algorithm with localised basis functions and where the nuclear coordinates are changed along a few user-specified collective variables (Figure 1).

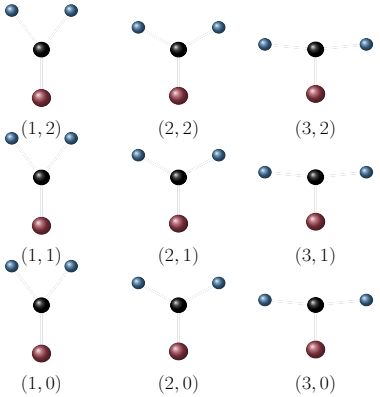

Figure 1. Schematic representation of the parameter space along two normal modes for the formaldehyde. The positions of the atoms are projected on two axes.

We will allow a large computational cost for data generation of some collective variables that can be stored, as long as on-the-fly cost for a new variable is negligible. Moreover, the developed method should not be affected by the choice of basis set and should work for a large range of displacements in the self-consistent field energy.

To validate both the accuracy and robustness of our method, we will try to improve on the number of self-consistent field convergence iterations with Hartree–Fock of the following four amino-acids: alanine, asparagine, phenylalanine and tryptophan (13, 17, 23 and 27 atoms, respectively).

A qualitative estimate of a reference for the number of iterations to improve upon is presented in Table 1. The computations where done using Dunning's cc-pVDZ basis set.

	Alanine	Asparagine	Phenylalanine	Tryptophan
Core	21	21	23	26
Harris	13	14	14	15
Hückel	16	17	17	18
MinAO	15	17	17	17
SAD	16	17	17	17

Table 1. Number of SCF iterations required to achieve convergence (max change in the density smaller than 10^{-6}) using different initial guesses. As the computations were carried out using different packages, that offer different SCF implementations, this cannot be considered an accurate comparison between the various guesses, but only a qualitative estimate of the number of required iterations. Note that all the calculations have been performed using standard DIIS extrapolation.

We would like a method that computes an inexpensive and accurate guess to the self-consistent field algorithm.

Results

With the cc-pVDZ basis set, the energy fluctuates of 9.1, 8.9, 8.5 and 7.6 kcal/mol for alanine, asparagine, phenylalanine, and tryptophan, respectively. For alanine*, that has much larger displacements, it is of well over 1000 kcal/mol. The aug-cc-pVTZ basis set was used for alanine+.

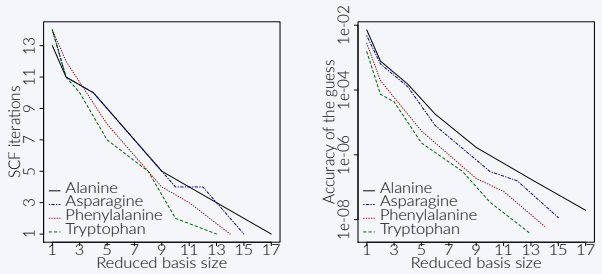

Figure 2. Results for the 2D parameter space. Number of SCF iterations required to achieve convergence (left panel) and Frobenius norm error on the density guess (right panel) as a function of the interpolation order for the various test systems. All the calculations were performed with CFOUR using the following convergence criteria for the increment of the density ΔP: RMS $\Delta P < 10^{-7}$ and max $|\Delta P| < 10^{-6}$.

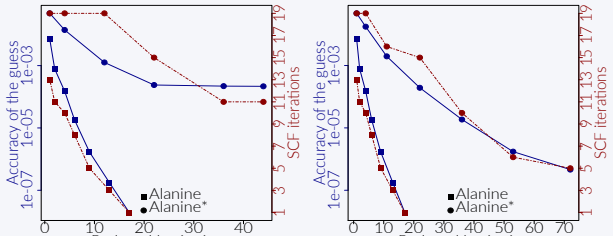

Figure 3. Comparison of alanine and alanine* in the 2D parameter space. Number of SCF iterations required to achieve convergence and Frobenius norm error on the density guess as a function of the interpolation order for $M = 8$ for both systems (left panel) and $M = 8$ for alanine and $M = 14$ for alanine* (right panel). All the calculations were performed with CFOUR using the following convergence criteria for the increment of the density ΔP: RMS $\Delta P < 10^{-7}$ and max $|\Delta P| < 10^{-6}$.

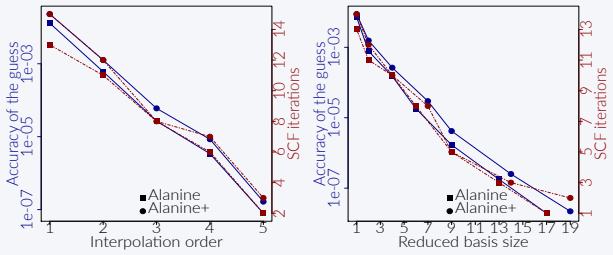

Figure 4. Comparison of alanine and alanine+. Number of SCF iterations required to achieve convergence and Frobenius norm error on the density guess as a function of the interpolation order for the 1D parameter space (left panel) and the 2D parameter space (right panel). All the calculations were performed with CFOUR using the following convergence criteria for the increment of the density ΔP: RMS $\Delta P < 10^{-7}$ and max $|\Delta P| < 10^{-6}$.

We can almost instantly predict the density matrices of all other configurations using only a small number of data.

Methodology

From a mathematical point of view, the density matrices are on a Grassmannian smooth manifold. This imply the existence a diffeomorphism that transforms the manifold into an affine space, the tangent space, and back. The maps are the Grassmannian exponential and logarithm. This allows us to apply well-known methods to approximate the elements in the tangent space, and then map back the results to the manifold. This way we are assured that the final result is indeed still a density matrix. See Figure 5 for a schematic description.

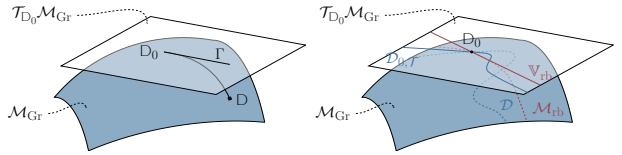

Figure 5. Schematic illustration of the geometrical setting. In both figures, we illustrate by the blue hypersurface the Grassmann manifold $\mathcal{M}_{Gr}$ and by the transparent plane the tangent space $\mathcal{T}_{D_0}\mathcal{M}_{Gr}$ to $\mathcal{M}_{Gr}$ at D_0. On the left, we illustrate the one-to-one relationship between a close density matrix $D \in \mathcal{M}_{Gr}$ and the corresponding vector $\Gamma = \mathrm{Log}_{\mathcal{M}_{Gr},0} D$ in the tangent space. On the right, we further schematically illustrate the notions of $\mathcal{D}_{0,\mathcal{T}}$ and $\mathbb{V}_{rb}$, as well as their equivalent sets $\mathcal{D} = \{D_p | p \in \mathbb{P}\}$ and $\mathcal{M}_{rb} = \mathrm{Exp}_{\mathcal{M}_{Gr},0}(\mathbb{V}_{rb})$ on $\mathcal{M}_{Gr}$.

For example, the formulation of the Grassmannian exponential of some matrix Γ is

$$\mathrm{Exp}_{\mathcal{M}_{Gr},0}(\Gamma) = CC^\top, \qquad C = [C_0 V \cos(\Sigma) + U \sin(\Sigma)]\, V^\top,$$

where the quantities are computed from the singular value decomposition Γ

$$\Gamma = U\Sigma V^\top.$$

Density matrices can then be approached by Grassmannian exponentials of linear combinations of elements in the tangent space

$$D(p) \approx \mathrm{Exp}_{\mathcal{M}_{Gr},0}\left(\sum_i c_i(p)\Gamma_i\right).$$

We have used an offline/online paradigm. We store the density matrices of a few parameter values. Then the knowledge of how the parameters vary makes the computation of the density matrix for a new parameter almost immediately available.

The density matrix that is obtained can then be used as an initial guess to the self-consistent field algorithm to speed-up the calculations.

We use basic properties from differential geometry to approximate density matrices with linear combinations.

Perspectives

Promising results have been obtained when we tested amino-acids and the method seems both accurate and robust.

However, this method is limited in its applications. We are thus exploring how to generalize it when the variations of the parameters is not known. The method could then be used for ab-initio molecular dynamics simulations and geometry optimisations.

We are eager to have a better understanding of the underlying mathematics and to apply this method to a larger class of chemistry problems.

Funding

This work was supported by the French "Investissements d'Avenir" program, project Agence Nationale de la Recherche (ISITE-BFC) (contract ANR-15-IDEX-0003).

References

Absil, P.-A., Mahony, R., and Sepulchre, R. (2008). *Optimization Algorithms on Matrix Manifolds*. Princeton University Press.

Amsallem, D. and Farhat, C. (2008). Interpolation method for adapting reduced-order models and application to aeroelasticity. *AIAA Journal*, 46(7):1803–1813.

Cancès, É., Bris, C. L., Maday, Y., Nguyen, N., Patera, A., and Pau, G. (2007). Feasibility and competitiveness of a reduced basis approach for rapid electronic structure calculations in quantum chemistry. In *CRM Proceedings and Lecture Notes*, volume 41, pages 15–47. American Mathematical Society.

Maday, Y. and Razafison, U. (2008). A reduced basis method applied to the restricted hartree–fock equations. *Comptes Rendus Mathematique*, 346(3-4):243–248.

Polack, É., Mikhalev, A., Dusson, G., Stamm, B., and Lipparini, F. (2020). An approximation strategy to compute accurate initial density matrices for repeated self-consistent field calculations at different geometries. *Molecular Physics*, page e1779834.

Zimmermann, R. (2019). Manifold interpolation and model reduction. *arXiv preprint arXiv:1902.06502*.

VI.F References

[AMS08] Absil, P.-A., Mahony, R., and Sepulchre, R. "Optimization Algorithms on Matrix Manifolds". Princeton, N.J. ; Woodstock: Princeton University Press, 2008. 224 pp. ISBN: 978-0-691-13298-3 (cit. on p. 145).

[Can+07] Cancès, Eric et al. "Feasibility and Competitiveness of a Reduced Basis Approach for Rapid Electronic Structure Calculations in Quantum Chemistry". In: *Proceedings of the Workshop for Highdimensional Partial Differential Equations in Science and Engineering (Montreal)* 41 (June 20, 2007) (cit. on pp. 142, 148).

[EAS98] Edelman, Alan., Arias, Tomás A., and Smith, Steven T. "The Geometry of Algorithms with Orthogonality Constraints". In: *SIAM Journal on Matrix Analysis and Applications* 20.2 (Jan. 1, 1998), pp. 303–353. ISSN: 0895-4798 (cit. on p. 145).

[MR08] Maday, Yvon and Razafison, Ulrich. "A Reduced Basis Method Applied to the Restricted Hartree–Fock Equations". In: *Comptes Rendus Mathematique* 346.3 (Feb. 1, 2008), pp. 243–248. ISSN: 1631-073X (cit. on pp. 142, 144, 148).

[Nik08] Niklasson, Anders M. N. "Extended Born-Oppenheimer Molecular Dynamics". In: *Physical Review Letters* 100.12 (Mar. 25, 2008), p. 123004 (cit. on p. 151).

[Pol+20] Polack, Étienne et al. "An Approximation Strategy to Compute Accurate Initial Density Matrices for Repeated Self-Consistent Field Calculations at Different Geometries". In: *Molecular Physics* 118.19-20 (Oct. 17, 2020), e1779834. ISSN: 0026-8976 (cit. on pp. 142, 148).

[Pol+21] Polack, Étienne et al. "Grassmann Extrapolation of Density Matrices for Born–Oppenheimer Molecular Dynamics". In: *Journal of Chemical Theory and Computation* 17.11 (Nov. 9, 2021), pp. 6965–6973. ISSN: 1549-9618 (cit. on pp. 142, 153, 155, 157, 159).

[Zim19] Zimmermann, Ralf. "Manifold Interpolation and Model Reduction". 2019 (cit. on p. 145).

Back matter

Symbols

$[\![n \,..\, m]\!]$ Set of integers between n and m

$\mathbf{R}$ Field of real numbers

$\mathbf{C}$ Field of complex numbers

$\mathbf{K}$ Field of numbers that often represents either $\mathbf{R}$ or $\mathbf{C}$

$\mathbf{B}^n$ Unit ball of $\mathbf{R}^n$

$\mathbf{S}^n$ Unit sphere of $\mathbf{R}^n$

L^p Space of functions for which the p-th power of absolute value of continuous functions are Lebesgue integrable

$\mathrm{L}^p_{\mathrm{loc}}$ Locally p-Lebesgue integrable functions

$\mathrm{col}_j(M)$ Column j of a matrix M

$\mathrm{row}_i(M)$ Row i of a matrix M

$\mathrm{GL}(n)$ Group of $n \times n$ invertible matrices

$\mathrm{O}(n)$ Group of $n \times n$ orthogonal matrices: $\mathrm{O}(n) := \{Q \in \mathbf{R}^{n\times n} \mid Q^{\mathsf{T}}Q = QQ^{\mathsf{T}} = \mathrm{Id}_n\}$

$\mathcal{G}r$ Grassmann manifold

$\mathcal{S}t$ Stiefel manifold

Index

Acronyms

AIDS acquired immune deficiency syndrome 4

CM continuum mechanics 3, 5, 6, 20

COVID-19 coronavirus disease 2019 4

CS continuum solvation iii, 20, 21, 68, 69

DFT density functional theory 3, 5, 12, 13, 68, 142–144, 148

DIIS direct inversion in the iterative subspace 144

EIM empirical interpolation method 112, 113

FF force field iii, 6, 13–17, 19–21, 30, 31, 34, 51, 53, 57, 68, 69, 72, 84–87, 93, 95, 98, 99, 101–103

FFI foreign function interface 93

FFP fast Fourier–Poisson 51

FFT fast Fourier transform 30, 41, 44–46, 48, 51, 52, 84

FMM fast multipole method 2, 84, 85, 89, 90, 93, 95–97, 99–103, 106

HF Hartree–Fock 3, 7–13, 68, 142–144, 148

HIV-1 human immunodeficiency virus 1 4

L2L local-to-local 90

L2P local-to-particle 90, 91, 93

LCAO linear combination of atomic orbitals 9, 11, 143

LTD long-term drift 101, 103–105

M2L moment-to-local 90

M2M moment-to-moment 89, 90

MD molecular dynamics iii, vii, 3, 5, 6, 12, 13, 21, 39, 44, 46, 48, 50, 51, 57, 68, 69, 71–73, 93, 99–106, 142, 144, 151

MM molecular mechanics iii, vii, 2, 3, 5, 6, 13, 15, 20, 21, 30, 68, 69, 71, 73, 86, 93, 95

NVE micro-canonical 101

NVT canonical 101, 106

P2M particle-to-moment 89, 90

P2P particle-to-particle 90, 95

P^{3}M particle-particle–particle-mesh 45, 46, 52

PBC periodic boundary conditions 15, 30, 31, 37, 41, 106

PCM polarisable continuum model vii, 69, 106

PDB Proteins Data Bank 103, 106

PME particle mesh Ewald 19, 46, 47, 50–52, 106

QM quantum mechanics iii, vii, 2, 3, 5, 6, 13, 15, 20, 21, 68–71, 73, 142, 151

RMS root-mean-square 97, 101

SCF self-consistent field 11, 12, 21, 69, 142–144, 148, 150, 151

SPME smooth particle mesh Ewald 46, 50, 57

STF short-term fluctuations 101, 103–105

SVD singular value decomposition 147

Complete bibliography

[ACF72] Applequist, Jon, Carl, James R., and Fung, Kwok-Kueng. "Atom Dipole Interaction Model for Molecular Polarizability. Application to Polyatomic Molecules and Determination of Atom Polarizabilities". In: *Journal of the American Chemical Society* 94.9 (May 1, 1972), pp. 2952–2960. ISSN: 0002-7863 (cit. on pp. 15, 17).

[AF93] Arnaudiès, Jean-Marie and Fraysse, Henri. "Cours de Mathématiques. Tome 2. Analyse". Dunod, Mar. 1993 (cit. on p. 38).

[Ain+15] Ain, Qurrat Ul et al. "Machine-Learning Scoring Functions to Improve Structure-Based Binding Affinity Prediction and Virtual Screening". In: *WIREs Computational Molecular Science* 5.6 (2015), pp. 405–424. ISSN: 1759-0884 (cit. on p. 5).

[Amo+98] Amovilli, Claudio et al. "Recent Advances in the Description of Solvent Effects with the Polarizable Continuum Model". In: *Advances in Quantum Chemistry*. Ed. by Löwdin, Per-Olov. Vol. 32. Academic Press, Jan. 1, 1998, pp. 227–261 (cit. on pp. 5, 69).

[AMS08] Absil, P.-A., Mahony, R., and Sepulchre, R. "Optimization Algorithms on Matrix Manifolds". Princeton, N.J. ; Woodstock: Princeton University Press, 2008. 224 pp. ISBN: 978-0-691-13298-3 (cit. on p. 145).

[Bal+08] Ballenegger, Vincent et al. "The Optimal P3M Algorithm for Computing Electrostatic Energies in Periodic Systems". In: *Journal of Chemical Physics* 128.3, 034109 (2008), pp. 1–13 (cit. on p. 52).

[Ban06] Bank, RCSB Protein Data. "Crystal Structural and Functional Analysis of GFP-like Fluorescent Protein Dronpa". May 8, 2006. URL: https://www.rcsb.org/structure/2GX2 (cit. on p. 103).

[Ban88] Bank, RCSB Protein Data. "Crystal Structure of Unliganded Escherichia Coli Dihydrofolate Reductase. Ligand-induced Conformational Changes and Cooperativity in Binding." Oct. 21, 1988. URL: https://www.rcsb.org/structure/5DFR (cit. on p. 101).

[Bar+04] Barrault, Maxime et al. "An 'Empirical Interpolation' Method: Application to Efficient Reduced-Basis Discretization of Partial Differential Equations". In: *Comptes Rendus Mathematique* 339.9 (Nov. 1, 2004), pp. 667–672. ISSN: 1631-073X (cit. on p. 112).

[BCH12] Ballenegger, Vincent, Cerdà, Juan J., and Holm, Christian. "How to Convert SPME to P3M: Influence Functions and Error Estimates". In: *Journal of Chemical Theory and Computation* 8.3 (2012), pp. 936–947 (cit. on p. 52).

[BGS87] Berendsen, H. J. C., Grigera, J. R., and Straatsma, T. P. "The Missing Term in Effective Pair Potentials". In: *The Journal of Physical Chemistry* 91.24 (Nov. 1, 1987), pp. 6269–6271. ISSN: 0022-3654 (cit. on p. 18).

[Bla+15] Blanchard, Pierre et al. "ScalFMM: A Generic Parallel Fast Multipole Library". In: *SIAM Conference on Computational Science and Engineering (CSE15)*. SIAM Conference on Computational Science and Engineering (SIAM CSE 2015). Mar. 14, 2015 (cit. on pp. 87, 93).

[Boe11] Boehm, Markus. "Virtual Screening of Chemical Space: From Generic Compound Collections to Tailored Screening Libraries". In: *Virtual Screening*. Ed. by Sotriffer, Christoph. Methods and Principles in Medicinal Chemistry. Weinheim, Germany: John Wiley & Sons, Ltd, 2011, pp. 1–33. isbn: 978-3-527-63332-6 (cit. on p. 5).

[Böt73] Böttcher, Carl Johan Friedrich. "Theory of Electric Polarization, Volume 1: Dielectrics in Static Fields". 2nd ed. Elsevier, Jan. 1973. isbn: 978-0-444-41019-1 (cit. on p. 17).

[BRD13] Barré-Sinoussi, Françoise, Ross, Anna Laura, and Delfraissy, Jean-François. "Past, Present and Future: 30 Years of HIV Research". In: *Nature Reviews Microbiology* 11.12 (12 Dec. 2013), pp. 877–883. issn: 1740-1534 (cit. on p. 4).

[Bro+83] Brooks, Bernard R. et al. "CHARMM: A Program for Macromolecular Energy, Minimization, and Dynamics Calculations". In: *Journal of Computational Chemistry* 4.2 (1983), pp. 187–217. issn: 1096-987X (cit. on p. 13).

[Bur12] Burke, Kieron. "Perspective on Density Functional Theory". In: *The Journal of Chemical Physics* 136.15 (Apr. 21, 2012), p. 150901. issn: 0021-9606 (cit. on p. 5).

[Can+07] Cancès, Eric et al. "Feasibility and Competitiveness of a Reduced Basis Approach for Rapid Electronic Structure Calculations in Quantum Chemistry". In: *Proceedings of the Workshop for Highdimensional Partial Differential Equations in Science and Engineering (Montreal)* 41 (June 20, 2007) (cit. on pp. 142, 148).

[CB00] Cancès, Eric and Bris, Claude Le. "On the Convergence of SCF Algorithms for the Hartree-Fock Equations". In: *ESAIM: Mathematical Modelling and Numerical Analysis* 34.4 (4 July 1, 2000), pp. 749–774. issn: 0764-583X (cit. on p. 11).

[CBM06] Cancès, Eric, Bris, Claude Le, and Maday, Yvon. "Méthodes Mathématiques En Chimie Quantique. Une Introduction". Mathématiques et Applications. Berlin Heidelberg: Springer-Verlag, 2006. isbn: 978-3-540-30996-3 (cit. on pp. 6, 68).

[CCM12] Caprasecca, Stefano, Curutchet, Carles, and Mennucci, Benedetta. "Toward a Unified Modeling of Environment and Bridge-Mediated Contributions to Electronic Energy Transfer: A Fully Polarizable QM/MM/PCM Approach". In: *Journal of Chemical Theory and Computation* 8.11 (Nov. 13, 2012), pp. 4462–4473. issn: 1549-9618 (cit. on p. 69).

[CMS13] Cancès, Eric, Maday, Yvon, and Stamm, Benjamin. "Domain Decomposition for Implicit Solvation Models". In: *The Journal of Chemical Physics* 139.5 (2013), p. 054111 (cit. on pp. 20, 104).

[Col21a] Collective. *Fubini's Theorem*. In: *Wikipedia*. Ed. by Wikipedia. Mar. 3, 2021 (cit. on p. 40).

[Col21b] Collective. *Gamma Function*. In: *Wikipedia*. Ed. by Wikipedia. Apr. 2, 2021 (cit. on p. 39).

[Col21c] Collective. *Legendre Polynomials*. In: *Wikipedia*. Ed. by Wikipedia. Feb. 21, 2021 (cit. on p. 86).

[Cur+09] Curutchet, Carles et al. "Electronic Energy Transfer in Condensed Phase Studied by a Polarizable QM/MM Model". In: *Journal of Chemical Theory and Computation* 5.7 (July 14, 2009), pp. 1838–1848. issn: 1549-9618 (cit. on p. 69).

[Dar08] Darden, Thomas A. "Extensions of the Ewald Method for Coulomb Interactions in Crystals". In: *Reciprocal Space*. Ed. by Shmueli, Uri. 3rd ed. Vol. B. International Tables for Crystallography. John Wiley & Sons, Aug. 2008, pp. 458–481 (cit. on pp. 34, 39, 41, 47, 53).

[dLee+80] De Leeuw, S. W. et al. "Simulation of Electrostatic Systems in Periodic Boundary Conditions. I. Lattice Sums and Dielectric Constants". In: *Proceedings of the Royal Society of London. A. Mathematical and Physical Sciences* 373.1752 (Oct. 31, 1980), pp. 27–56 (cit. on pp. 44, 53).

[DYP93] Darden, Tom, York, Darrin, and Pedersen, Lee. "Particle Mesh Ewald: An N□log(N) Method for Ewald Sums in Large Systems". In: *The Journal of Chemical Physics* 98.12 (June 15, 1993), pp. 10089–10092. ISSN: 0021-9606 (cit. on pp. 46, 52).

[EAS98] Edelman, Alan., Arias, Tomás A., and Smith, Steven T. "The Geometry of Algorithms with Orthogonality Constraints". In: *SIAM Journal on Matrix Analysis and Applications* 20.2 (Jan. 1, 1998), pp. 303–353. ISSN: 0895-4798 (cit. on p. 145).

[EHL79] Eastwood, James W., Hockney, Roger W., and Lawrence, D. N. "P3M3DP – The Three-Dimentional Periodique Particle-Particle/Particle-Mesh Program". In: *Computer Physics Communications* 19 (1979), pp. 215–261 (cit. on pp. 45, 46, 52).

[El +21] El Ahdab, Dina et al. "Interfacial Water Many-Body Effects Drive Structural Dynamics and Allosteric Interactions in SARS-CoV-2 Main Protease Dimerization Interface". In: *The Journal of Physical Chemistry Letters* 12.26 (July 8, 2021), pp. 6218–6226 (cit. on p. 2).

[Ess+95] Essmann, Ulrich et al. "A Smooth Particle Mesh Ewald Method". In: *The Journal of Chemical Physics* 103.19 (Nov. 15, 1995), pp. 8577–8593. ISSN: 0021-9606 (cit. on pp. 39, 46, 50, 51).

[Ewa21] Ewald, P. P. "Die Berechnung Optischer Und Elektrostatischer Gitterpotentiale". In: *Annalen der Physik* 369.3 (1921), pp. 253–287. ISSN: 1521-3889 (cit. on p. 37).

[Fis94] Fischer, Emil. "Synthesen in Der Zuckergruppe II". In: *Berichte der deutschen chemischen Gesellschaft* 27.3 (1894), pp. 3189–3232. ISSN: 1099-0682 (cit. on pp. 4, 5).

[For06] Fortin, Pierre. "Algorithmique hiérarchique parallèle haute performance pour les problèmes à N-corps". PhD thesis. Université Sciences et Technologies - Bordeaux I, Nov. 27, 2006 (cit. on p. 84).

[Fri+09] Frisch, M. J. et al. "Gaussian 09". 2009 (cit. on p. 71).

[GLS17] Gatto, Paolo, Lipparini, Filippo, and Stamm, Benjamin. "Computation of Forces Arising from the Polarizable Continuum Model within the Domain-Decomposition Paradigm". In: *The Journal of Chemical Physics* 147.22 (Dec. 12, 2017), p. 224108. ISSN: 0021-9606 (cit. on p. 87).

[God01] Godement, Roger. "Analyse Mathématique III. Fonctions Analytiques, Différentielles et Variétés, Surfaces de Riemann". Springer, Nov. 2001 (cit. on p. 32).

[GR97] Greengard, L. and Rokhlin, V. "A Fast Algorithm for Particle Simulations". In: *Journal of Computational Physics* 135.2 (1997), pp. 280–292. ISSN: 0021-9991 (cit. on p. 84).

[Hal92] Halgren, Thomas A. "The Representation of van Der Waals (vdW) Interactions in Molecular Mechanics Force Fields: Potential Form, Combination Rules, and vdW Parameters". In: *Journal of the American Chemical Society* 114.20 (Sept. 1992), pp. 7827–7843. ISSN: 0002-7863 (cit. on p. 15).

[Har75] Harris, Frank E. "Hartree-Fock Studies of Electronic Structures of Crystalline Solids*". In: *Theoretical Chemistry*. Ed. by Eyring, HENRY and Henderson, DOUGLAS. Vol. 1. Theoretical Chemistry. Elsevier, Jan. 1, 1975, pp. 147–218 (cit. on p. 58).

[HE88] Hockney, Roger W. and Eastwood, James W. "Computer Simulation Using Particles". Adam Higler, 1988. ISBN: 978-0-85274-392-8 (cit. on pp. 37, 45).

[HGE73] Hockney, Roger W., Goel, S. P., and Eastwood, James W. "A 10000 Particle Molecular Dynamics Model with Long Range Forces". In: *Chemical Physics Letters* 21.3 (1973), pp. 589–591 (cit. on p. 45).

[HJO00] Helgaker, Trygve, Jørgensen, Poul, and Olsen, Jeppe. "Molecular Electronic-Structure Theory". John Wiley & Sons, Aug. 2000. ISBN: 978-0-471-96755-2 (cit. on pp. 3, 6).

[HK64] Hohenberg, P. and Kohn, W. "Inhomogeneous Electron Gas". In: *Physical Review* 136 (3B Nov. 9, 1964), B864–B871. ISSN: 0031-899X (cit. on p. 12).

[Kar14] Karplus, Martin. "Development of Multiscale Models for Complex Chemical Systems: From H+H2 to Biomolecules (Nobel Lecture)". In: *Angewandte Chemie International Edition* 53.38 (2014), pp. 9992–10005. ISSN: 1521-3773 (cit. on pp. 2, 69).

[Kit95] Kittel, Charles. "Introduction to Solid State Physics". 7th ed. John Wiley & Sons, Aug. 1995. ISBN: 978-0-471-11181-8 (cit. on p. 17).

[KP92] Kolafa, Jiří and Perram, John W. "Cutoff Errors in the Ewald Summation Formulae for Point Charge Systems". In: *Molecular Simulation* 9.5 (1992), pp. 351–368 (cit. on p. 44).

[KS65] Kohn, W. and Sham, L. J. "Self-Consistent Equations Including Exchange and Correlation Effects". In: *Physical Review* 140 (4A Nov. 15, 1965), A1133–A1138 (cit. on p. 13).

[KS93] Klamt, A. and Schuurmann, G. "COSMO: A New Approach to Dielectric Screening in Solvents with Explicit Expressions for the Screening Energy and Its Gradient". In: *Journal of the Chemical Society, Perkin Transactions 2* 5 (1993), pp. 799–805 (cit. on pp. 20, 104).

[Lag+15] Lagardère, Louis et al. "Scalable Evaluation of Polarization Energy and Associated Forces in Polarizable Molecular Dynamics: II. Toward Massively Parallel Computations Using Smooth Particle Mesh Ewald". In: *Journal of Chemical Theory and Computation* 11.6 (June 9, 2015), pp. 2589–2599. ISSN: 1549-9618 (cit. on p. 30).

[Lee+20] Leermakers, Frans A. M. et al. "Turning Autophobic Wetting on Biomimetic Surfaces into Complete Wetting by Wetting Additives". In: *Soft Matter* 16.20 (May 27, 2020), pp. 4823–4839. ISSN: 1744-6848 (cit. on p. 3).

[Lev14] Levitt, Michael. "Birth and Future of Multiscale Modeling for Macromolecular Systems (Nobel Lecture)". In: *Angewandte Chemie International Edition* 53.38 (2014), pp. 10006–10018. ISSN: 1521-3773 (cit. on pp. 2, 69).

[Lie83] Lieb, Elliott H. "Density Functionals for Coulomb Systems". In: *International Journal of Quantum Chemistry* 24.3 (1983), pp. 243–277. ISSN: 1097-461X (cit. on p. 12).

[Lin+18] Lindgren, Eric B. et al. "An Integral Equation Approach to Calculate Electrostatic Interactions in Many-Body Dielectric Systems". In: *Journal of Computational Physics* 371 (Oct. 15, 2018), pp. 712–731. ISSN: 0021-9991 (cit. on pp. 84, 93).

[Lip+15] Lipparini, Filippo et al. "Polarizable Molecular Dynamics in a Polarizable Continuum Solvent". In: *Journal of Chemical Theory and Computation* 11.2 (Feb. 10, 2015), pp. 623–634. ISSN: 1549-9618 (cit. on pp. 20, 21).

[Loc+16] Loco, Daniele et al. "A QM/MM Approach Using the AMOEBA Polarizable Embedding: From Ground State Energies to Electronic Excitations". In: *Journal of Chemical Theory and Computation* 12.8 (Aug. 9, 2016), pp. 3654–3661. ISSN: 1549-9618 (cit. on pp. 68, 75, 77, 79, 81).

[LR03] Lamoureux, Guillaume and Roux, Benoît. "Modeling Induced Polarization with Classical Drude Oscillators: Theory and Molecular Dynamics Simulation Algorithm". In: *The Journal of Chemical Physics* 119.6 (July 24, 2003), pp. 3025–3039. ISSN: 0021-9606 (cit. on p. 15).

[Mad+09] Maday, Yvon et al. "A General Multipurpose Interpolation Procedure: The Magic Points". In: *Communications on Pure & Applied Analysis* 8.1 (2009), p. 383 (cit. on p. 113).

[MH09] Marx, Dominik and Hutter, Jürg. "Ab Initio Molecular Dynamics: Basic Theory and Advanced Methods". Cambridge: Cambridge University Press, 2009. ISBN: 978-0-521-89863-8 (cit. on pp. 6, 112).

[MR08] Maday, Yvon and Razafison, Ulrich. "A Reduced Basis Method Applied to the Restricted Hartree–Fock Equations". In: *Comptes Rendus Mathematique* 346.3 (Feb. 1, 2008), pp. 243–248. ISSN: 1631-073X (cit. on pp. 142, 144, 148).

[Nar+16] Narth, Christophe et al. "Scalable Improvement of SPME Multipolar Electrostatics in Anisotropic Polarizable Molecular Mechanics Using a General Short-Range Penetration Correction up to Quadrupoles". In: *Journal of Computational Chemistry* 37.5 (2016), pp. 494–506. ISSN: 1096-987X (cit. on p. 30).

[Nik08] Niklasson, Anders M. N. "Extended Born-Oppenheimer Molecular Dynamics". In: *Physical Review Letters* 100.12 (Mar. 25, 2008), p. 123004 (cit. on p. 151).

[NL00] Nymand, Thomas M. and Linse, Per. "Ewald Summation and Reaction Field Methods for Potentials with Atomic Charges, Dipoles, and Polarizabilities". In: *The Journal of Chemical Physics* 112.14 (Mar. 30, 2000), pp. 6152–6160. ISSN: 0021-9606 (cit. on p. 19).

[PC03] Ponder, Jay W. and Case, David A. "Force Fields for Protein Simulations". In: *Protein Simulations*. Ed. by Daggett, Valerie. Vol. 66. Advances in Protein Chemistry. Academic Press, 2003, pp. 27–85 (cit. on pp. 16, 19, 57, 69).

[PCF01] Pérez, José-Philippe, Carles, Robert, and Fleckinger, Robert. "Électromagnétisme, Fondements et Applications". 4th ed. Dunod, Nov. 2001. ISBN: 978-2-10-005574-6 (cit. on pp. 17, 31).

[PG96] Pollock, E. L. and Glosli, Jim. "Comments on P3M, FMM, and the Ewald Method for Large Periodic Coulombic Systems". In: *Computer Physics Communications* 95.2–3 (1996), pp. 93–110 (cit. on p. 46).

[PMS21] Polack, Étienne, Maday, Yvon, and Savin, Andreas. "FLEIM: A Stable, Accurate and Robust Extrapolation Method at Infinity for Computing the Ground State of Electronic Hamiltonians". Dec. 24, 2021 (cit. on pp. 112, 115, 117, 119, 121, 123, 125, 127, 129, 131, 133, 135, 137, 139).

[Pol+20] Polack, Étienne et al. "An Approximation Strategy to Compute Accurate Initial Density Matrices for Repeated Self-Consistent Field Calculations at Different Geometries". In: *Molecular Physics* 118.19-20 (Oct. 17, 2020), e1779834. ISSN: 0026-8976 (cit. on pp. 142, 148).

[Pol+21] Polack, Étienne et al. "Grassmann Extrapolation of Density Matrices for Born–Oppenheimer Molecular Dynamics". In: *Journal of Chemical Theory and Computation* 17.11 (Nov. 9, 2021), pp. 6965–6973. ISSN: 1549-9618 (cit. on pp. 142, 153, 155, 157, 159).

[Pon+10] Ponder, Jay W. et al. "Current Status of the AMOEBA Polarizable Force Field". In: *Journal of Physical Chemistry B* 114.8 (2010), pp. 2549–2564 (cit. on pp. 13, 16, 71, 93).

[Pon12] Ponnusamy, S. "Foundations of Mathematical Analysis". Boston, MA: Birkhäuser Boston, 2012. ISBN: 978-0-8176-8292-7 (cit. on p. 36).

[PPD88] Perram, John W., Petersen, Henrik G., and De Leeuw, Simon W. "An Algorithm for the Simulation of Condensed Matter Which Grows as the 3/2 Power of the Number of Particles". In: *Molecular Physics* 65.4 (Nov. 1, 1988), pp. 875–893. ISSN: 0026-8976 (cit. on p. 44).

[RG91] Rappe, Anthony K. and Goddard, William A. "Charge Equilibration for Molecular Dynamics Simulations". In: *The Journal of Physical Chemistry* 95.8 (Apr. 1, 1991), pp. 3358–3363. ISSN: 0022-3654 (cit. on p. 15).

[Rog11] Rognan, Didier. "Docking Methods for Virtual Screening: Principles and Recent Advances". In: *Virtual Screening*. Ed. by Sotriffer, Christoph. Methods and Principles in Medicinal Chemistry. Weinheim, Germany: John Wiley & Sons, Ltd, 2011, pp. 153–176. ISBN: 978-3-527-63332-6 (cit. on p. 5).

[Roo51] Roothaan, C. C. J. "New Developments in Molecular Orbital Theory". In: *Reviews of Modern Physics* 23.2 (Apr. 1, 1951), pp. 69–89 (cit. on p. 11).

[RP03] Ren, Pengyu and Ponder, Jay W. "Polarizable Atomic Multipole Water Model for Molecular Mechanics Simulation". In: *The Journal of Physical Chemistry B* 107.24 (2003), pp. 5933–5947 (cit. on p. 31).

[RS81] Reed, Michael and Simon, Barry. "I: Functional Analysis". Academic Press, Feb. 23, 1981. 417 pp. ISBN: 978-0-08-057048-8 (cit. on p. 9).

[Sau+92] Saunders, V.r. et al. "On the Electrostatic Potential in Crystalline Systems Where the Charge Density Is Expanded in Gaussian Functions". In: *Molecular Physics* 77.4 (Nov. 1, 1992), pp. 629–665. ISSN: 0026-8976 (cit. on pp. 44, 58).

[SD99] Sagui, Celeste and Darden, Thomas A. "P3M and PME: A Comparison of the Two Methods". In: *Simulation and Theory of Electrostatic Interactions in Solution*. Ed. by Proceedings, AIP Conference. Vol. 492. 1999, pp. 104–113 (cit. on p. 52).

[Sen+20] Senior, Andrew W. et al. "Improved Protein Structure Prediction Using Potentials from Deep Learning". In: *Nature* 577.7792 (7792 Jan. 2020), pp. 706–710. ISSN: 1476-4687 (cit. on p. 4).

[SH73] Saunders, V. R. and Hillier, I. H. "A "Level–Shifting" Method for Converging Closed Shell Hartree–Fock Wave Functions". In: *International Journal of Quantum Chemistry* 7.4 (1973), pp. 699–705. ISSN: 1097-461X (cit. on p. 11).

[Sim+14] Simmonett, Andrew C. et al. "An Efficient Algorithm for Multipole Energies and Derivatives Based on Spherical Harmonics and Extensions to Particle Mesh Ewald". In: *Journal of Chemical Physics* 140.18, 184101 (2014), pp. 1–7 (cit. on p. 57).

[Smi81] Smith, E. R. "Electrostatic Energy in Ionic Crystals". In: *Proceedings of the Royal Society of London. A. Mathematical and Physical Sciences* 375.1763 (Apr. 13, 1981), pp. 475–505 (cit. on pp. 39, 41, 53).

[Smi94] Smith, Edgar R. "Calculating the Pressure in Simulations Using Periodic Boundary Conditions". In: *Journal of Statistical Physics* 77.1–2 (1994), pp. 449–472 (cit. on pp. 55, 56).

[Smi98] Smith, W. "Point Multipoles in the Ewald Summation (Revisited)". In: *ccp5 Newsletter* 46 (1998), pp. 18–30 (cit. on pp. 57, 60).

[Sny+05] Snyder, David A. et al. "Comparisons of NMR Spectral Quality and Success in Crystallization Demonstrate That NMR and X-ray Crystallography Are Complementary Methods for Small Protein Structure Determination". In: *Journal of the American Chemical Society* 127.47 (Nov. 30, 2005), pp. 16505–16511. ISSN: 0002-7863 (cit. on p. 4).

[SPD04] Sagui, Celeste, Pedersen, Lee G., and Darden, Thomas A. "Towards an Accurate Representation of Electrostatics in Classical Force Fields: Efficient Implementation of Multipolar Interactions in Biomolecular Simulations". In: *The Journal of Chemical Physics* 120.1 (Jan. 1, 2004), pp. 73–87. ISSN: 0021-9606 (cit. on p. 57).

[TCS04] Toulouse, Julien, Colonna, François, and Savin, Andreas. "Long-Range–Short-Range Separation of the Electron-Electron Interaction in Density-Functional Theory". In: *Physical Review A* 70.6 (Dec. 17, 2004), p. 062505 (cit. on p. 69).

[Tho81] Thole, B. T. "Molecular Polarizabilities Calculated with a Modified Dipole Interaction". In: *Chemical Physics* 59.3 (Aug. 1, 1981), pp. 341–350. ISSN: 0301-0104 (cit. on p. 19).

[Tou+00] Toukmaji, Abdulnour et al. "Efficient Particle-Mesh Ewald Based Approach to Fixed and Induced Dipolar Interactions". In: *The Journal of Chemical Physics* 113.24 (Dec. 13, 2000), pp. 10913–10927. ISSN: 0021-9606 (cit. on p. 19).

[TP94] Tomasi, Jacopo and Persico, Maurizio. "Molecular Interactions in Solution: An Overview of Methods Based on Continuous Distributions of the Solvent". In: *Chemical Reviews* 94.7 (Nov. 1994), pp. 2027–2094. ISSN: 0009-2665 (cit. on pp. 5, 20).

[vEK97] Van Eijck, Bouke .P. and Kroon, Jan. "Coulomb Energy of Polar Crystals". In: *Journal of Physical Chemistry B* 101.6 (1997), pp. 1096–1100 (cit. on p. 53).

[War14] Warshel, Arieh. "Multiscale Modeling of Biological Functions: From Enzymes to Molecular Machines (Nobel Lecture)". In: *Angewandte Chemie International Edition* 53.38 (2014), pp. 10020–10031. ISSN: 1521-3773 (cit. on pp. 2, 69).

[WK81] Weiner, Paul K. and Kollman, Peter A. "AMBER: Assisted Model Building with Energy Refinement. A General Program for Modeling Molecules and Their Interactions". In: *Journal of Computational Chemistry* 2.3 (1981), pp. 287–303. ISSN: 1096-987X (cit. on p. 13).

[Wol+99] Wolf, D. et al. "Exact Method for the Simulation of Coulombic Systems by Spherically Truncated, Pairwise R−1 Summation". In: *The Journal of Chemical Physics* 110.17 (Apr. 22, 1999), pp. 8254–8282. ISSN: 0021-9606 (cit. on p. 36).

[WR84] Warshel, Arieh and Russell, Stephen T. "Calculations of Electrostatic Interactions in Biological Systems and in Solutions". In: *Quarterly Reviews of Biophysics* 17.3 (Aug. 1984), pp. 283–422. ISSN: 0033-5835 (cit. on pp. 57, 69).

[WS05] Wang, Wei and Skeel, Robert D. "Fast Evaluation of Polarizable Forces". In: *The Journal of Chemical Physics* 123.16 (Oct. 22, 2005), p. 164107. ISSN: 0021-9606 (cit. on p. 19).

[YB11] Yokota, Rio and Barba, Lorena A. "Chapter 9 - Treecode and Fast Multipole Method for N-Body Simulation with CUDA". In: *GPU Computing Gems Emerald Edition*. Ed. by Hwu, Wen-mei W. Applications of GPU Computing Series. Boston: Morgan Kaufmann, Jan. 1, 2011, pp. 113–132. ISBN: 978-0-12-384988-5 (cit. on p. 84).

[Yee+05] Yee, Adelinda A. et al. "NMR and X-ray Crystallography, Complementary Tools in Structural Proteomics of Small Proteins". In: *Journal of the American Chemical Society* 127.47 (Nov. 30, 2005), pp. 16512–16517. ISSN: 0002-7863 (cit. on p. 4).

[Yor+94] York, D. M. et al. "Atomic-Level Accuracy in Simulations of Large Protein Crystals". In: *Proceedings of the National Academy of Sciences* 91.18 (Aug. 30, 1994), pp. 8715–8718. ISSN: 0027-8424 (cit. on p. 30).

[YY94] York, Darrin M. and Yang, Weitao. "The Fast Fourier Poisson Method for Calculating Ewald Sums". In: *Journal of Chemical Physics* 101.4 (1994), pp. 3298–3300 (cit. on p. 51).

[ZH79] Zerner, Michael C. and Hehenberger, Michael. "A Dynamical Damping Scheme for Converging Molecular Scf Calculations". In: *Chemical Physics Letters* 62.3 (Apr. 15, 1979), pp. 550–554. ISSN: 0009-2614 (cit. on p. 11).

[Zim19] Zimmermann, Ralf. "Manifold Interpolation and Model Reduction". 2019 (cit. on p. 145).

Authored publications

[Lag+15] Lagardère, Louis et al. "Scalable Evaluation of Polarization Energy and Associated Forces in Polarizable Molecular Dynamics: II. Toward Massively Parallel Computations Using Smooth Particle Mesh Ewald". In: *Journal of Chemical Theory and Computation* 11.6 (June 9, 2015), pp. 2589–2599. ISSN: 1549-9618 (cit. on p. 30).

[Lin+18] Lindgren, Eric B. et al. "An Integral Equation Approach to Calculate Electrostatic Interactions in Many-Body Dielectric Systems". In: *Journal of Computational Physics* 371 (Oct. 15, 2018), pp. 712–731. ISSN: 0021-9991 (cit. on pp. 84, 93).

[Loc+16] Loco, Daniele et al. "A QM/MM Approach Using the AMOEBA Polarizable Embedding: From Ground State Energies to Electronic Excitations". In: *Journal of Chemical Theory and Computation* 12.8 (Aug. 9, 2016), pp. 3654–3661. ISSN: 1549-9618 (cit. on pp. 68, 75, 77, 79, 81).

[Nar+16] Narth, Christophe et al. "Scalable Improvement of SPME Multipolar Electrostatics in Anisotropic Polarizable Molecular Mechanics Using a General Short-Range Penetration Correction up to Quadrupoles". In: *Journal of Computational Chemistry* 37.5 (2016), pp. 494–506. ISSN: 1096-987X (cit. on p. 30).

[PMS21] Polack, Étienne, Maday, Yvon, and Savin, Andreas. "FLEIM: A Stable, Accurate and Robust Extrapolation Method at Infinity for Computing the Ground State of Electronic Hamiltonians". Dec. 24, 2021 (cit. on pp. 112, 115, 117, 119, 121, 123, 125, 127, 129, 131, 133, 135, 137, 139).

[Pol+20] Polack, Étienne et al. "An Approximation Strategy to Compute Accurate Initial Density Matrices for Repeated Self-Consistent Field Calculations at Different Geometries". In: *Molecular Physics* 118.19-20 (Oct. 17, 2020), e1779834. ISSN: 0026-8976 (cit. on pp. 142, 148).

[Pol+21] Polack, Étienne et al. "Grassmann Extrapolation of Density Matrices for Born–Oppenheimer Molecular Dynamics". In: *Journal of Chemical Theory and Computation* 17.11 (Nov. 9, 2021), pp. 6965–6973. ISSN: 1549-9618 (cit. on pp. 142, 153, 155, 157, 159).

Detailed table of contents